Final Report

Post-oil Global Airliner

AE3200: Design Synthesis
Group 29

Student Number	Student Name
5974747	Attila Kristóf Behán
5963281	Filip Boekema
5922194	Wu-Ji Kao
5996740	Caelan Kort
5907667	Giorgia Malacarne
5948673	Luna Martin Gonzalez
5925827	Adrian Robinson
6001351	Artem Savchenko
5936624	Ivo Wehsely
5906229	Yu Xu

Tutor: Nan Yue
Coaches: Daniel Cisneros Acevedo
Andrea Bettini

Project Duration: April, 2026 - June, 2026
Faculty: Faculty of Aerospace Engineering, Delft

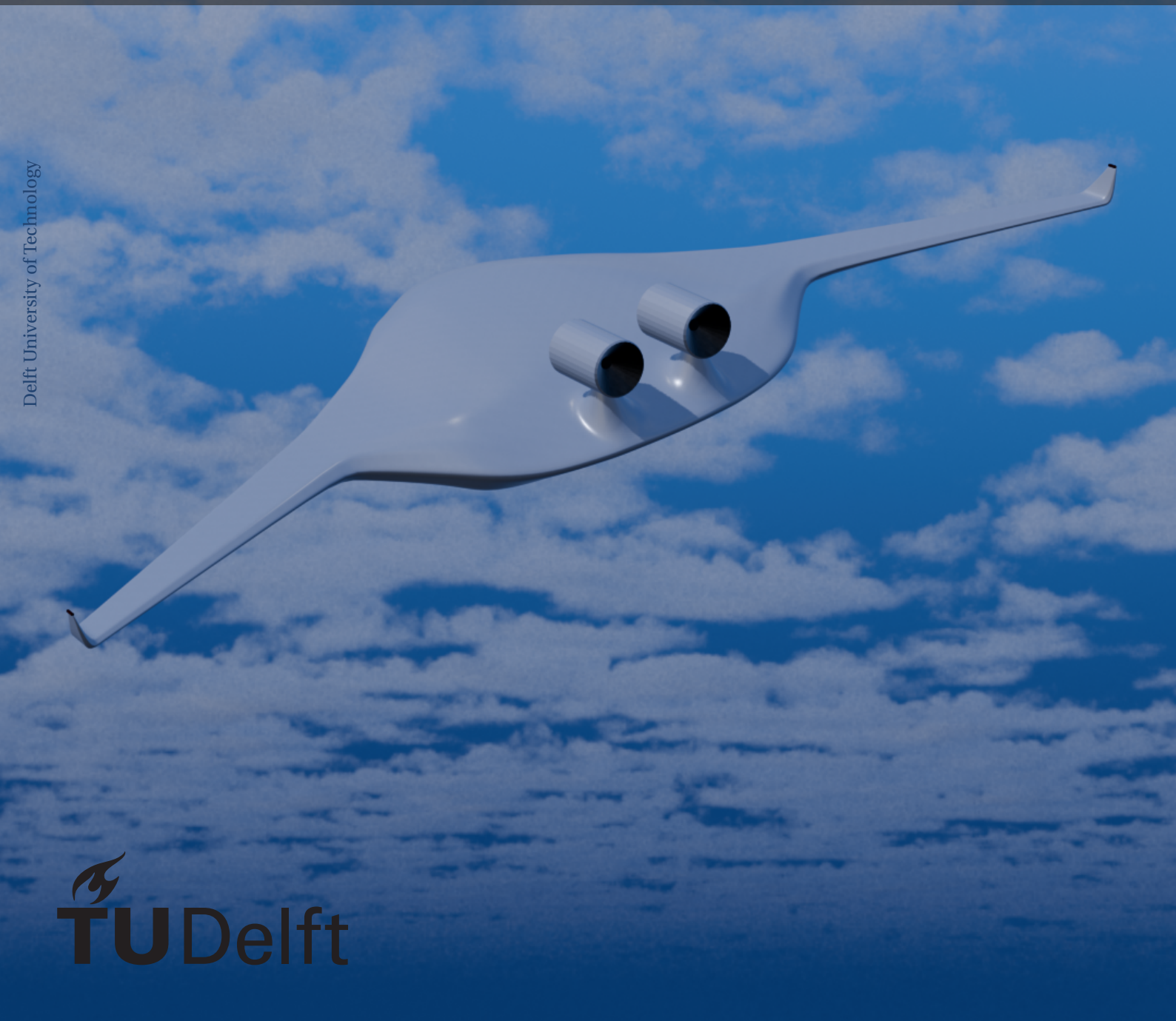

Delft University of Technology

TU Delft

Executive Summary

The aviation industry is at a critical crossroad. Aviation accounts for approximately 2.5% of global anthropogenic CO_2 emissions [1], and the sector remains exceedingly reliant on petroleum-based fuels regarding both the propulsion and airframe materials. In order to meet the ICAO and United Nations net-zero carbon target by 2050[1] [2], a fundamental redesign of intercontinental airliners is required. This final report presents the preliminary design phase for the Post-Oil Global Airliner (POGA), a 120-passenger intercontinental airliner designed to operate without any petroleum-based fuel, and with minimised petroleum-based materials, and a target entry into service in 2035.

This project is conducted by Group 29, which consists of ten students from the Faculty of Aerospace Engineering at Delft University of Technology, as part of the AE3200 Design Synthesis Exercise. The project spans ten weeks, and has a development budget of €50 billion. The objective of this mission is to design a non-kerosene passenger airliner capable of transporting at least 120 passengers over a minimum one-leg distance of 3,000 km, with an intercontinental capability of at least 6,000 km, within a 24-hour operational cycle. To meet the project's sustainability goal, the design must not utilise any petroleum-based fuel, and minimise the use of petroleum-derived materials. It is intended to be operational by 2035, with a first flight target set to 2031.

Building on the selected design established in the midterm report, this final report presents the results of the preliminary design phase, culminating in a converged preliminary design. First, the design option tree pruning and trade-off process is briefly recapped, before the selected Blended Wing Body concept is introduced. The preliminary design is then developed through a Multidisciplinary Design Analysis and Optimisation (MDAO) framework, covering geometry and layout, aerodynamics, weight estimation, power and propulsion, structural analysis, and stability and control. This is followed by a business analysis establishing the commercial and regulatory context, before assessments of reliability, availability, maintainability and safety, technical risk, sustainable development, and a production plan are presented. The report concludes with an outlook on the next design phase.

Requirements

There are two top-level requirements which are treated as absolute: the aircraft shall not be powered with petroleum-based fuels, and its range shall be a minimum of 6,000 km over a 24-hour operational period, and a minimum one-leg distance of 3,000 km. Additionally, the minimisation of petroleum-derived materials is also to be prioritised. These translate directly into two sustainability Key Performance Indicators (KPIs), which track the design throughout its development:

- **Petroleum Fuel Share (%)**: The percentage of total fuel consumption (by mass or energy) that is derived from petroleum-based sources. The target is to have a Petroleum Fuel Share of 0%.
- **Sustainable Material Share (%)**: The percentage of the total structural weight composed of materials that are not derived from petroleum. The target is to maximise the Sustainable Material Share.

Table 1: Driver requirements.

ID	Requirement
8.01	The aircraft shall have a minimum flight range of 3000 km.
8.02	The aircraft shall be capable of covering 6000 km within 24 hours.
8.03	The aircraft shall accommodate a minimum of 120 passengers in TBD configuration.
8.04	Conditions at aircraft level that can lead to a catastrophic event shall be identified.
8.05	The fuel shall not be petroleum-derived.
8.06	The aircraft should use a minimum percentage of TBD petroleum derived materials.
8.07	The first flight shall take place by 2031.
8.08	The aircraft shall be operable by 2035.
8.09	The maximum development cost shall be no more than 50 billion euros.

The driver requirements, directly derived from the investor stakeholder group, are summarised in Table 1, and represent the non-negotiable constraints from which all other requirements are derived.

Concept Development and Selected Design

By translating the design option tree into Python and applying the killer requirements, Technology Readiness Level-based feasibility limits, and Infrastructure Readiness Level (IRL) assessments, the generated total of 421,120 design concepts was reduced to 124 for a first flight by 2031, and 1,459 by 2035, as visualised in Figure 1. Subsequently, each surviving option was assessed across a holistic set of sub-criteria covering mission performance, technical feasibility and performance, operations, risk, sustainability, materials, and safety. As mentioned above, three trade-off strategies

[1] URL `https://www.un.org/en/climatechange/net-zero-coalition` [Cited 23 April 2026]

optimising for market niche, sustainability, and performance were defined, each driving the design by means of differently weighted criteria. This trade-off was conducted by means of a Python program developed by Group 29, and validated through 94 unit tests, a Monte Carlo sensitivity study across 5,000 weight perturbations, and a leave-one-out category analysis, as well as a sensitivity study, computing scores for both 2031 and 2035 first flight horizons.

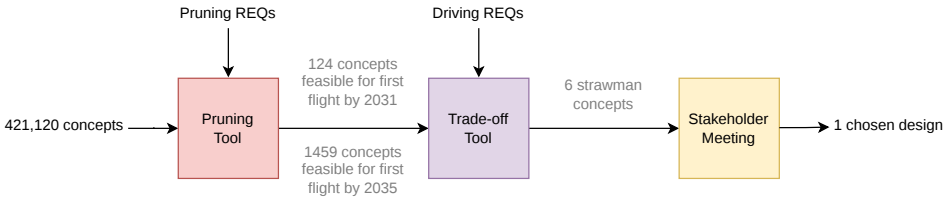

Figure 1: Overall Conceptual Design Process

The selected concept, chosen under Strategy 1, which optimises for market niche for the 2031 first flight timeline, is a Blended Wing Body (BWB) aircraft powered by above-body high-bypass turbofans running on bio-SAF alone, with load-bearing fuel tanks integrated into the airframe structure. Primary and secondary structures use conventional carbon-fibre and glass-fibre with conventional epoxy, selected to meet the 2035 certification timeline while still maintaining structural performance. A retrofitting strategy is in place to progressively increase the Sustainable Material Share over the aircraft's service life as bio-based materials reach commercial maturity.

Preliminary Design

The preliminary design phase, as documented in this final report, established a converged aircraft configuration through a Multidisciplinary Design Analysis and Optimisation (MDAO) framework implemented in OpenMDAO [3].

Geometry and Layout

The BWB centrebody is sized to accommodate 120 business-class passengers at 2.5 m^2 per passenger, resulting in a cabin planform with a maximum width and length of 18.72 m and 19.68 m, respectively. The fuselage airfoil was optimised using Class Shape Transformation based on the MH82 reflexed profile to minimise chord length while fitting the pressurised cabin, resulting in the MH82-AR variant. The outer wing uses the NASA SC(2)-0714 supercritical airfoil, selected for its high lift-to-drag ratio and favourable pitching-moment characteristics in the transonic regime. The outer wing has an aspect ratio and leading-edge sweep angle sized to achieve the design cruise Mach number of 0.79 at 35,000 ft.

Aerodynamics

The aerodynamic analysis was performed using the Athena Vortex Lattice (AVL) solver, supplemented with profile drag, wave drag, and engine drag corrections following the Okonkwo method [4]. The clean configuration achieves a cruise lift-to-drag ratio, L/D of 17.35, with the addition of 4 m winglets increasing this to 17.84. A cross-check using AeroSandbox VLM3 yields a cruise L/D of 19.21 without winglets, giving a bracketed estimate. The SWOT analysis uses the AeroSandbox figure of 19.4 as the representative upper bound for market positioning. The take-off angle of attack of 10.69° and landing angle of attack of 4.90° confirm aerodynamic feasibility of the design at low-speed conditions.

Weight Estimation

The Class I weight estimation follows the van Dommelen–Vos methodology adapted for BWB configurations [5], while the Class II weight estimation combines the Howe BWB airframe method with the Roskam/General Dynamics method for operational items, instruments, and furnishings [6–8]. The design iterates on the Maximum Take-Off Weight (MTOW), with Class I and Class II weight estimation modules surrounding the full analysis chain. The converged design yields an MTOW of 131,554 kg, an Operating Empty Weight (OEW) of 77,187 kg, and a Zero Fuel Weight (ZFW) of 95,188 kg.

Power & Propulsion

Engines are sized to satisfy the CS-25 take-off path requirements, including the One Engine Inoperative (OEI) climb gradients of CS-25.121(a) and CS-25.121(b), as well as the take-off field length requirement of CS-25.113 [9]. The engines shall generate a minimum sea-level static thrust of 288.5 kN and achieve a cruise thrust-specific fuel consumption not exceeding 15 mg/Ns. Fuel mass is computed segment by segment from the mission profile using the thermodynamic efficiency model, with a Lower Heating Value of 44 MJ/kg for bio-SAF. The converged mission fuel load is 35,667 kg of bio-SAF, representing approximately 26.7% of MTOW.

Structural Analysis

The structural analysis sizes three primary components of the BWB centrebody: the outer aerodynamic contour, the multibubble pressure shell, and the internal trapezoidal cabin structure. All components are manufactured from aluminium-lithium alloy (Airware 2198-T8), selected for its low density and high specific strength relative to petroleum-derived CFRP, reducing the use of petroleum-derived structural materials in the centrebody. The critical longitudinal bending moment of 19,246 kNm (LC03, negative manoeuvre at 80% fuel) drives the outer contour to a required equivalent thickness of 4.70 mm. Pressure shell sizing yields a maximum required thickness of 5.08 mm for the top-side arc. The trapezoidal cabin structure, which transfers wing-induced loads and cabin pressurisation into the centrebody, gives an estimated primary structural mass of 18,634 kg for the internal trapezoid alone.

Stability & Control

Due to the unconventional nature of the BWB, stability and control analysis required dedicated methods. The CG range was determined to span from $x_{\text{cg,fwd}} = 12.477$ m (MTOW) to $x_{\text{cg,aft}} = 16.242$ m (ZFW), giving a CG excursion of approximately 1.01 m. The loading diagram confirms all loading sequences remain within the CG envelope, while longitudinal static stability analysis confirms that the BWB exhibits a positive $C_{m\alpha}$ (pitch-up instability) at most CG positions, as is typical for tailless configurations; a fly-by-wire stability augmentation system is therefore assumed throughout. Lateral-directional static stability is evaluated against CS-25.237 (crosswind) and CS-25.149 (OEI yaw control), with split drag-rudder winglets providing directional control authority. Dynamic stability modes (phugoid, short period, Dutch roll, roll, spiral) are analysed at the loiter condition.

Control surface sizing identifies six candidate configurations evaluated for pitch, roll, and yaw authority. The selected configuration provides a pitch authority margin $\xi_{\text{pitch}} \geq 1$, a roll rate exceeding the 15 °/s target, and an OEI yaw authority margin $\xi_{\text{yaw}} \geq 1$. Landing gear positioning was solved iteratively with the CG range, yielding a converged layout with a nose landing gear at $x_{\text{NLG}} = 1.530$ m, main landing gear at $x_{\text{MLG}} = 16.024$ m, and a full track width of 8.676 m, satisfying the 55° turnover angle limit across all loading cases.

Business Analysis

The business analysis validates the commercial feasibility of the 120-seat, all-business-class Blended Wing Body aircraft operating on 100% bio-SAF. The target market capitalizes on a regulatory gap created by ReFuelEU, EU ETS, and CSRD Scope 3 reporting obligations, capturing high-yield intercontinental routes in the 3,500–6,000 km range. Driven by a projected 4.0% CAGR in premium passenger traffic, the Serviceable Obtainable Market (SOM) forecasts 75 deliveries in the base scenario over a 20-year production life.

Financially, the program strictly sticks to the €50 billion development constraint. Utilizing the DAPCA IV model, the total development cost for the base scenario is €28.65 billion, resulting in a unit acquisition cost of €660.7 million. Applying a 25% profit margin establishes a market selling price of €825.8 million per aircraft. Although the Direct Operating Cost (DOC) is 29.96 cents/ASK, the premium revenue per available seat kilometer (RASK) comfortably offsets this metric. The program reaches break-even at 47 deliveries, generating a projected total profit of €12.38 billion at a low-volume production rate of 3.8 aircraft per year. A SWOT analysis confirms this structurally favorable position, leveraging the BWB's high aerodynamic efficiency and zero-petroleum compliance to overcome the high amortized RDT&E costs typical of niche production runs.

Reliability, Availability, Maintainability and Safety (RAMS) Characteristics

RAMS characteristics are evaluated to assess the design's robustness and structure the technical risk analysis for operational and certification standards. Regarding reliability, the BWB's inherent instability places high demands on redundant flight control laws, avionics, and fault-detection sensors, alongside stringent fuel system monitoring to prevent engine failure.

For availability, the primary challenges involve extensive inspection downtime for load-bearing fuel tanks, coordinating early supplier availability for structural components, and ensuring reliable bio-SAF logistics along planned routes.

Maintainability focuses on establishing clear inspection access routes and sensor monitoring for the integrated fuel tanks, multibubble pressure shell junctions, and above-body engines to avoid major disassembly.

Regarding safety, critical considerations address the structural integrity of the multibubble pressure shell, fire protection for integrated fuel tanks, and certifying crashworthiness and rapid passenger evacuation for the wide centrebody.

Technical Risk Analysis

Technical risks are assessed across two phases. During the preliminary design phase, seven risks were identified and mitigated, evaluated using likelihood, consequence and detectability scales. Mitigation actions reduced the majority of risks to an acceptable level: mission performance risk (TR-01) was fully mitigated, with the final design achieving a

direct one-leg range of 5,530 km and 24-hour route coverage of 16,000 km. Turnaround and ground operations (TR-06), fuel-tank maintenance (TR-07) and diversion compatibility (TR-16) were reduced through representative operational and maintenance concept definitions. Three risks remain only partly mitigated and are carried forward: stability and control (TR-02), evacuation compliance with the 90-second CS-25 requirement (TR-11), and pressurisation structural integrity of the multi-bubble pressure shell (TR-12).

For the post-DSE phases, 25 future risks are identified and evaluated. After mitigation, no risk remains in the high-likelihood, high-consequence region; however, nine risks retain catastrophic consequence and require continued monitoring, primarily concerning pressure shell integrity, crashworthiness, emergency access and evacuation, fire protection, avionics, flight control and certification. Sixteen risk-derived requirements are documented to ensure the most critical items are addressed before design freeze.

Sustainability Development Strategy

Sustainability is embedded into the project at the requirement level, tracked via a 0% Petroleum Fuel Share and a maximised Sustainable Material Share. The design pairs a highly aerodynamic BWB with high-bypass turbofans running exclusively on bio-SAF, sourced from lowest-risk domestic feedstocks (agricultural residues, municipal solid waste, used cooking oil) that avoid competition with food or feed markets, though the achievable climate benefit is lower than headline figures suggest once non-CO_2 effects and land-use risks are accounted for [10]. As bio-based structural materials are not yet mature for 2035, conventional composites are retained and progressively retrofitted during heavy maintenance under a "Design for Upgradability" framework, transitioning to direct forward-fit production once these materials reach full maturity; the pace of this transition scales with fleet size. A Cradle-to-Cradle Life Cycle Assessment ties these elements together across material acquisition, manufacturing, operations, and end-of-life recovery.

Manufacturing, Assembly and Integration

The manufacturing plan assigns primary metallic structure (Airware 2198-T8 Al–Li) to a three-tier European supplier network led by voestalpine Böhler aerospace (machining of Alu - Li), Premium AEROTEC (outer BWB shell), Aernnova (pressure shell and movables), and Leonardo Aerostructures (wingbox and integration). Key manufacturing processes include 5-axis Computer Numerical Control (CNC) machining of fuselage and wing panels, stretch-forming of large curved skins, and mechanical assembly of the three-bubble pressure module with pressure testing at module level. The conservative estimate for prototype manufacturing, assembly and integration is on the order of 6–12 months from material availability to a flight-ready article. In serial production, assuming an 80% learning curve, the manufacturing time per airplane is expected to reduce to three months.

Budget Breakdown

The budget breakdown covers mass, volume, electrical power , and cost. Margins are applied to all technical resource budgets to account for uncertainty at the current preliminary phase, and are expected to decrease regressively as the design matures. For the mass, a margin of 35% is applied for all categories except payload. This was done to account for the inherent mass growth of aerospace projects. The payload was kept to 6% to keep in accordance with EASA standard passenger masses. For volume, budgets range from 35-66% to account for mass growth, as well as keeping an acceptable Net Design Volume (NDV) [11]. The electrical power budget only has margins of 15%, as this would insure 99% operability [12]. The cost budgets margins range from 5-35%, this mainly stems from the inaccuracy of the DAPCA IV method.

Including the margins, the final design then gets a final MTOW of 172379 kg, which is 31% higher than the calculated mass. The electrical power budget is estimated at 1184 kW, a value obtained from Figure 19.1 in Chapter 19 which includes margins and covers aircraft systems. This is higher than the total generated power (1132 kW), but this wont be an issue as not all systems operate at their peak at the same time. The volume breakdown caps the volume of the components at 1976.5 of the total 2124.5 m^3, to account for a large enough NDV [11].

The research and development cost budget is capped at €50 billion. After the application of margins to the base case in the cost analysis, the cost will not exceed €29 billion. The acquisition cost per aircraft is estimated at about €840 million. Due to the early stages of the design, these values are estimates derived from parametric cost models and historical programme benchmarks, and are explained in further detail in Section 21.3. Regarding the operating costs, a direct operating cost has been calculated of €24297 per block hour. The Systems Engineer holds responsibility for monitoring all budget lines and approving any reallocation between subsystems.

Project Design and Development Logic

The post-DSE programme is structured into two phases leading to entry into commercial service in 2035. The first phase, industrial-level design, runs parallel tracks of BWB research, supplier coordination, detailed design, design tests, and prototype manufacture over approximately three and a half years, converging at a first test flight in 2030, ahead of

the 2031 first flight requirement. The second phase, certification and service introduction, covers approximately three years of ground and flight testing running concurrently with design finalisation, Low-Rate Initial Production, and type certification, followed by route proving flights and operator cooperation, with aircraft delivery and entry into service in 2035, satisfying the requirement that the aircraft shall be operable by 2035.

Conclusion

The Post-Oil Global Airliner is a technically feasible and commercially viable concept. The converged preliminary design demonstrates compliance with the key CS-25 take-off, structural, and stability requirements at preliminary design level. The all-business-class market niche, supported by escalating regulatory carbon costs and Corporate Sustainability Reporting Directive (CSRD) corporate sustainability obligations, provides a credible commercial rationale for the programme. No fundamental engineering or operational showstoppers have been identified, and the primary risks (pressurisation structural integrity, FBW certification, and OEI yaw authority) are well characterised and carry defined mitigation actions into the next design phase.

A top view of the POGA can be found below in Figure 2.

Figure 2: Model Top View

Contents

Nomenclature

Abbreviations

Abbr.	Definition
AC	Air Conditioning Unit
ACN	Aircraft Classification Number
ADG	Aircraft Design Group
AEO	All Engines Operating
AF	Airframe
AIAA	American Institute of Aeronautics and Astronautics
AL	Aircraft Level
AOA	Angle of Attack
API	Air Conditioning, Pressurisation, and Icing
APU	Auxiliary Power Unit
AR	Aspect Ratio
AS	Air Start Unit
ASK	Available Seat Kilometre
ASTM	American Society for Testing and Materials
ATC	Air Traffic Control
AVL	Athena Vortex Lattice
B2F	Back-to-Front
BFL	Balanced Field Length
Bio-ACN	Bio-acrylonitrile
Bio-SAF	Bio-based Sustainable Aviation Fuel
BLI	Boundary Layer Ingestion
BPR	Bypass Ratio
BWB	Blended Wing Body
CA	Clean Aviation
CAGR	Compound Annual Growth Rate
CAPEX	Capital Expenditures
CB	Conveyor Belt
CBS	Cost Breakdown Structure
CC	Cabin Crew
CFD	Computational Fluid Dynamics
CFRP	Carbon Fibre Reinforced Polymer
CG	Centre of Gravity
CNC	Computer Numerical Control
CO_2	Carbon Dioxide
CORSIA	Carbon Offsetting and Reduction Scheme for International Aviation
CPI	Consumer Price Index
CS FTL	Certification Specifications for Flight and Duty Time Limitations
CSRD	Corporate Sustainability Reporting Directive
DAPCA	Development and Procurement Costs of Aircraft
DOC	Direct Operating Cost
DOT	Design Option Tree
DSE	Design Synthesis Exercise
EASA	European Union Aviation Safety Agency
ECS	Environmental Control System
ECSS	European Cooperation for Space Standardization
EIS	Entry Into Service
EN	European Standard
EU ETS	European Union Emissions Trading System
FAA	Federal Aviation Administration
FAI	First Article Inspection
FBD	Functional Breakdown Diagram
FBW	Fly-By-Wire
FC	Fuel Cell
FDP	Flight Duty Period
FFD	Functional Flow Diagram
FHA	Functional Hazard Assessment
FT	Fischer–Tropsch
FUEL	Fuel Hydrant Dispenser or Tanker
GFRP	Glass Fibre Reinforced Polymer
GHG	Greenhouse Gas
GPU	Ground Power Unit
GSE	Ground Service Equipment
HBR	High Bypass Ratio
HEFA	Hydroprocessed Esters and Fatty Acids
IAP	Instrument Approach Procedure
IATA	International Air Transport Association
ICAO	International Civil Aviation Organisation
ILUC	Indirect Land Use Change
ILT	Inspectie Leefomgeving en Transport
IRL	Infrastructure Readiness Level
ISA	International Standard Atmosphere
KPI	Key Performance Indicator
L/D	Lift-to-Drag Ratio
LBR	Low Bypass Ratio
LCA	Life Cycle Assessment
LEMAC	Leading Edge of the Mean Aerodynamic Chord
LHV	Lower Heating Value
LHS	Latin Hypercube Sampling
LRIP	Low-Rate Initial Production
LV	Lavatory Vehicle
MAC	Mean Aerodynamic Chord
MAI	Manufacturing, Assembly & Integration
MDAO	Multidisciplinary Design Analysis and Optimisation
MDO	Multidisciplinary Design Optimisation
MEL	Minimum Equipment List
MLG	Main Landing Gear
MNS	Mission Need Statement
MOC	Method of Compliance
MRO	Maintenance, Repair and Operations
MS	Mission System
MTOM	Maximum Take-off Mass
MTOW	Maximum Take-off Weight
N^2	N-squared Diagram
NASA	National Aeronautics and Space Administration
NDV	Net Design Volume
NLG	Nose Landing Gear
NLBGS	Non-Linear Block Gauss-Seidel
NOx	Nitrogen Oxides
O&L	Operations and Logistics
OBS	Organisational Breakdown Structure
OEI	One Engine Inoperative
OEM	Original Equipment Manufacturer
OEW	Operating Empty Weight
OMGWS	Outer Main Gear Wheel Span
OPEX	Operating Expenses
ORA	Organisational Risk Assessment
ORO	Air Operations Regulation (EASA Part-ORO)
PAN	Polyacrylonitrile
PANS-OPS	Procedures for Air Navigation Services – Operations
PAX	Passengers
PBB	Passenger Boarding Bridge
PCN	Pavement Classification Number
PFS	Petroleum Fuel Share
PLD	Payload
PM	Project Management
POGA	Post-oil Global Airliner
POS	Project Objective Statement
PP	Power and Propulsion
PS	Passenger Stairs
PtL	Power-to-Liquid
RAMS	Reliability, Availability, Maintainability and Safety
RASK	Revenue Available Seat Kilometre
RAT	Ram Air Turbine
RDT	Requirements Discovery Tree
REQ	Requirement
RFF	Rescue and Firefighting
RoI	Return on Investment
RPK	Revenue Passenger Kilometre
SAF	Sustainable Aviation Fuel
SAM	Serviceable Addressable Market
SAS	Stability Augmentation System
SBW	Strut-Braced Wing
SDG	Sustainable Development Goal
SE	Systems Engineering
SFC	Specific Fuel Consumption
SH	Stakeholder
SLS	Sea Level Static
SMS	Sustainable Material Share
SOM	Serviceable Obtainable Market
STC	Supplemental Type Certificate
SWOT	Strengths, Weaknesses, Opportunities, Threats
TAM	Total Addressable Market
TAW	Tube-and-Wing
TC	Type Certification
TLAR	Top-Level Aircraft Requirement
TO	Trade-off
TOFL	Take-Off Field Length
TOW	Tow Tractor
TRL	Technology Readiness Level
UCO	Used Cooking Oil
UHARW	Ultra High Aspect Ratio Wing
ULD	Unit Load Device
VAT	Indicated Airspeed at Threshold
VFSG	Variable Frequency Starter Generator
V&V	Verification and Validation
WATS	World Air Transport Statistics
WBS	Work Breakdown Structure
WFD	Work Flow Diagram
WV	Potable Water Vehicle
XFLR5	Aerodynamic analysis software
ZFW	Zero Fuel Weight

Symbols

Symbol	Definition
a	Acceleration [m/s^2]
a_0	2D lift-curve slope of airfoil [1/°]
A	Cross-sectional area [m^2]
A_f	Airfoil technology factor [-]
AR	Aspect ratio [-]
b	Wing span [m]
b_{half}	Half-span [m]
$\bar{c}$	Mean aerodynamic chord [m]
c	Chord length [m]
c_j	Specific fuel consumption [kg/(N·s)]
c_l	Fraction of chord with laminar flow [-]
c_{kink}	Chord at kink station [m]
$c_{\text{root,w}}$	Root chord of outer wing [m]
c_{tip}	Tip chord [m]
C_D	Drag coefficient [-]
$C_{D,0}$	Zero-lift drag coefficient [-]
C_{D_i}	Induced drag coefficient [-]
C_f	Skin friction coefficient [-]
C_L	Lift coefficient [-]
$C_{L,0}$	Zero-incidence lift coefficient [-]
C_{L_α}	Lift-curve slope [1/°]
$C_{L_{\text{TO}}}$	Take-off lift coefficient [-]
C_{L_L}	Landing lift coefficient [-]
$C_{L_{\text{max},f}}$	Maximum fuselage lift coefficient [-]
$C_{L_{\text{max},w}}$	Maximum outer wing lift coefficient [-]
C_m	Pitching moment coefficient [-]
C_{m_α}	Pitching moment slope [1/rad]
C_{m_q}	Pitch damping derivative [-]
$C_{m_{ac}}$	Pitching moment about aerodynamic centre [-]
C_{w_L}	Lift-dependent wave drag coefficient [-]
C_{n_β}	Directional stability derivative [-]
C_{l_β}	Lateral stability derivative [-]
C_{Y_β}	Side force due to sideslip [-]
d_n	Nacelle diameter [m]
D_{fan}	Fan diameter [m]
e	Oswald efficiency factor [-]
e_i	Structural e-value of fuselage section [-]
e_o	Structural e-value of outer wing [-]
F_{OP}	Operational items factor [-]
FF	Form factor [-]
g	Gravitational acceleration [m/s^2]
g_i	Failure margin of structural member i [-]
h	Altitude [m]
h_{screen}	Screen height [m]
I	Second moment of area [m^4]
I_x	Roll moment of inertia [kg·m^2]
I_y	Pitch moment of inertia [kg·m^2]
I_z	Yaw moment of inertia [kg·m^2]
I_{xz}	Product of inertia [kg·m^2]
k	Scaling factor [-]
k_{int}	Nacelle interference factor [-]
K_n	Static margin [-]
l_n	Nacelle length [m]
L	Lift force [N]
L_{cabin}	Cabin length [m]
L_{fus}	Lift generated by fuselage [N]
L_w	Lift generated by outer wing [N]
m	Mass [kg]
m_{fuel}	Fuel mass [kg]
M	Bending moment [N·m]
M_{cr}	Design cruise Mach number [-]
M_{ff}	Overall mission fuel fraction [-]
n	Number of … / load factor [-]

Symbol	Definition
q	Dynamic pressure [Pa] or distributed load [N/m]
r	Yaw rate [rad/s]
R	Range [m]
Re	Reynolds number [-]
R_w	Wetted-to-reference area ratio [-]
s	Beam coordinate [m]
s_g	Ground roll distance [m]
s_{flare}	Flare distance [m]
S_f	Fuselage planform area [m^2]
S_{ref}	Reference wing area [m^2]
S_w	Outer wing area [m^2]
S_{wet}	Wetted area [m^2]
S_{rud}	Rudder planform area [m^2]
t	Wall thickness [m]
t/c	Thickness-to-chord ratio [-]
t_{req}	Required structural thickness [m]
t_{min}	Minimum gauge thickness [m]
T	Thrust [N]
T_{SLS}	Sea level static thrust [N]
U_0	Trim airspeed [m/s]
V	Volume [m^3] or velocity [m/s]
V_1	Decision speed [m/s]
V_2	Take-off safety speed [m/s]
V_{app}	Approach speed [m/s]
V_{cr}	Cruise true airspeed [m/s]
V_{LOF}	Lift-off speed [m/s]
V_{MC}	Minimum control speed [m/s]
V_{SR}	Reference stall speed [m/s]
w	Width [m]
W_{PL}	Payload weight [kg]
W_{OE}	Operating empty weight [kg]
W_{TO}	Take-off weight [kg]
x_{cg}	Centre of gravity position from nose [m]
x_{LEMAC}	LEMAC position from nose [m]
$\bar{x}_{\text{cg}}$	CG position as MAC fraction [-]
y	Spanwise coordinate [m]
z	Normal coordinate [m]
z_{max}	Maximum distance from neutral axis [m]
α	Angle of attack [°]
β	Sideslip angle [rad]
γ	Ratio of specific heats [-] or flight path angle [rad]
δ_a	Aileron deflection angle [°]
δ_e	Elevon deflection angle [°]
δ_r	Rudder deflection angle [°]
Δp	Cabin pressure differential [Pa]
Δs_i	Contour segment length [m]
ζ	Damping ratio [-]
η_θ	Overall propulsion efficiency [-]
η_{th}	Thermal efficiency [-]
η_p	Propulsive efficiency [-]
η_t	Transfer/transmission efficiency [-]
λ	Taper ratio [-]
Λ	Sweep angle [°]
$\Lambda_{0.25}$	Quarter-chord sweep angle [°]
Λ_{LE}	Leading-edge sweep angle [°]
μ	Ground friction coefficient [-]
π_c	Compressor pressure ratio [-]
ρ	Air density [kg/m^3]
σ	Real part of eigenvalue [1/s]
σ_b	Bending stress [MPa]
σ_{allow}	Allowable stress [MPa]
τ	Time constant [s]
ϕ	Bank angle [rad]
ω_n	Natural frequency [rad/s]
$\mathcal{O}(X)$	Order of magnitude (X)

1 Introduction

Current commercial aviation is still strongly dependent on petroleum. This is not only because most aircraft use Jet-A or Jet-A1 as fuel, but also because many aircraft materials, such as conventional composites and interior materials, are still highly petroleum-based. The sector currently accounts for roughly 2.5% of global anthropogenic CO_2 emissions [1], and meeting the United Nations net-zero target by 2050 requires a significant change beyond only incremental efficiency improvements[1]. At the same time, conventional aircraft architectures remain closely linked to petroleum [13], both through fuel and through petroleum-based structural and interior materials [14].

This project looks at one possible solution by designing a Post-oil Global Airliner (POGA). The aircraft operates with Bio-Sustainable Aviation Fuel (Bio-SAF), which is a non-petroleum-based fuel and minimises the use of petroleum-derived materials where possible. The aircraft is capable of carrying at least 120 passengers in all business-class, fly 5,530 km in one leg, and cover 16,000 km within a 24-hour operational cycle. The aircraft is also designed to be highly compatible with existing international route networks and major hub airports. The target is to make the aircraft operable by 2035, with a first flight target in 2031, within a development budget of 50 billion euros.

The POGA is developed by group 29, consisting of ten students from the Faculty of Aerospace Engineering at Delft University of Technology. The project is part of the AE3200 Design Synthesis Exercise. The project started from a broad design space, where different energy carriers, propulsion systems, aircraft configurations, engine positions, energy storage layouts, and material strategies were considered. During the midterm phase, this design option tree was explored, pruned, and assessed through a trade-off. For the final phase, the work focuses on the selected concept and its preliminary design.

The selected concept is a Blended Wing Body (BWB) aircraft powered by high-bypass turbofan engines using Bio-SAF. The engines are placed above the body and the fuel is stored in load-bearing tanks. Conventional carbon fibre and glass fibre with conventional epoxy are selected as the main material strategy, due to the fact that this gives a more realistic path towards entry into service by 2035. At the same time, the design still considers a future retrofit and forward-fitting strategy, where more sustainable materials can be introduced once they become mature enough.

This final report continues from the concept selection and develops the aircraft further. Chapter 2, Chapter 3, and Chapter 4 first define the aircraft systems, functions, and requirements. From this, the design remains traceable from the mission need to the subsystem level. Chapter 5 then summarises the trade-off process and the selected concept, while Chapter 6 discusses the main post trade-off risk mitigation.

The technical sizing part starts with Chapter 7, which is the introduction to the multidisciplinary design method and the OpenMDAO framework used to connect the design modules and parametrize the design variables. Chapter 8 gives the Class I weight estimation, while Chapter 9 defines the BWB geometry, cabin layout, airfoil selection and planform. Chapter 10 and Chapter 11 present the aerodynamic estimation and propulsion sizing methods. Chapter 12 continues with the Class II weight estimation, and Chapter 13 brings the main sizing results together into the preliminary aircraft design.

The following parts analyse the selected preliminary design in detail. Chapter 14 discusses stability, control, landing gear positioning, manoeuvres and control surface sizing. Chapter 15 then analyses the aerodynamic performance, while Chapter 16 analyses the structure of the BWB centrebody, pressure shell and internal cabin structure. Chapter 17 gives the main performance analysis. The design tools and results are checked in Chapter 18 through verification, validation, and sensitivity analysis. To summarise, the main system-level characteristics are summarised by Chapter 19.

The report also considers how the aircraft would be used outside the aircraft design calculation. Chapter 20 discusses mission and route operation, airport compatibility, turnaround, bio-SAF logistics, maintenance access, passenger and crew operation, diversion, and abnormal operation. Chapter 21 then discusses the market position, cost, sales potential, and SWOT analysis of the designed aircraft. Finally, Chapter 22 considers Bio-SAF, material sustainability, retrofit strategy, and life cycle assessment. Chapter 23 outlines the manufacturing, assembly, and integration plan. Chapter 24 identifies the main RAMS characteristics and technical risks that still need to be monitored in future design phases. Chapter 25 then describes the post-DSE development plan, while Chapter 26 and Chapter 27 give the final recommendations and conclusion.

Overall, this final report presents the preliminary design of the POGA. The aim is to show that the selected BWB bio-SAF concept can be developed into a technically and operationally realistic aircraft concept for a 2035 entry into service.

[1] URL `https://www.un.org/en/climatechange/net-zero-coalition` [Cited 21/05/2026]

Part I: Systems Engineering

2

Aircraft Systems

The aircraft is a combination of components interconnected with each other. Those components, connected by the same use, form subsystems, which aggregate to form systems. In order to go more in depth during the preliminary design, the aircraft's systems and subsystems have to be defined, as done in Section 2.1, after which their respective functions and requirements can be defined to showcase capabilities and constraints. The architecture in which this function and requirement analysis takes place is described in Section 2.2.

2.1. Systems definition

To establish the functions and requirements of the system, it is necessary to first define them. The systems' definitions come primarily from pre existing system architectures, specifically, the stratification is inspired by JASC [15]. For the defined project and trade-off result from Chapter 5, the chosen systems configuration is shown in Table 2.1.

Table 2.1: Aircraft Systems and Subsystems Breakdown.

Major System	Subsystems
Airframe	Structures, Doors, Lifting Surface, Windows, Landing gear, Furnishing
Power and Propulsion	Energy Storage, Energy Distribution, Engines, Auxiliary Power, Secondary Power, Emergency Power
Monitoring and Control	Ice & Rain Protection, Fire Protection, Thermal Management, Avionics, Environmental Control, Command & Data Handling, Cabin, External Lights
Flight Control & Stability	Flight Control, Stabilisers

For a Blended Wing Body (BWB) aircraft, there aren't separate fuselage and wing subsystems, instead they are merged into one lifting surface subsystem that encompasses both functionalities. Furthermore, due to the large surface area available, no high lift devices were selected as, through initial analysis, they were deemed unnecessary for performance, thus the Flight Control & Stability system is only made up of the stabilisers and the flight controls itself.

Airframe Subsystems

Structures Subsystem	Load-bearing elements of the aircraft, including fuselage, wings, and stabilisers, providing strength, stiffness, and attachment points for systems.
Doors Subsystem	Enables safe ingress, egress, and cargo handling, while maintaining pressurisation and structural integrity.
Lifting Surface	Houses passengers, cargo, subsystems, and equipment, maintaining pressurisation, structural integrity, and integration of other subsystems as well as generating lift and providing structural support for fuel, engines, and flight control surfaces.
Windows Subsystem	Provides visibility and environmental separation for passengers and crew, contributing to safety and comfort.
Landing Gears Subsystem	Supports aircraft during ground operations, enabling take-off, landing, and taxiing while absorbing impact and maintaining stability.
Furnishings Subsystem	Cabin interior components, including seating, storage, and amenities, ensuring passenger comfort and functional use of space.

Power & Propulsion Subsystems

Energy Storage Subsystem	Retains the main energy carrier for use during flight, peak-demand periods, or contingencies, ensuring energy availability when needed.
Energy Distribution Subsystem	Prepares, conditions and transports the primary energy carrier for propulsion while ensuring redundancy, interfaces with energy storage, engines and auxiliary power unit. Also allows for the discharging of fuel in case of emergency and venting the fuel tank in case of overpressure.
Engine Subsystem	The core thrust-producing component, converting energy into controlled propulsion to move the aircraft, as well as electricity to power the subsystems of the aircraft.
Auxiliary Power Subsystem	A secondary energy source providing power for ground operations, system startup, or emergency use, independent of the main engine.
Secondary Power Subsystem	Converts electricity from the Power Distribution Subsystem into required hydraulic, pneumatic or mechanical power for use across the aircraft's subsystems.
Emergency Power Subsystem	Provides electrical power for the startup of the Auxiliary Power Unit (APU) as well as back-up electrical and hydraulic power for the systems in case of engine and APU failure or energy distribution subsystem failure.

Monitoring & Control Subsystems	
Ice & Rain Protection Subsystem	Detects and prevents ice accumulation on critical surfaces to maintain aerodynamic performance and safety.
Fire Protection Subsystem	Detects, suppresses, and isolates fire hazards in engines, systems, and cabin areas.
Thermal Management Subsystem	Regulates temperatures for systems and energy carriers to ensure operational efficiency and safety.
Avionic Subsystem	Provides navigation, communication, and flight management capabilities for safe aircraft operation.
Environmental Control Subsystem	Maintains a safe and comfortable cabin environment by controlling temperature, airflow and pressure.
Command & Data Handling Subsystem	Collects, processes, and communicates data between systems and with ground support, enabling monitoring, control, and safe operations.
Cabin Subsystem	Provides communication for the crew and monitoring elements, in-flight entertainment for the passengers, provides and controls cabin lighting, galley equipment and water and waste of the lavatories.
External Lighting Subsystem	Makes sure that the aircraft is visible to other aircraft, the pilot has more visibility during critical phases of flight and ground operations, or serves another specific purpose.

Flight Controls & Stability Subsystems	
Flight Control Subsystem	Provides automatic computation and adjustment of control inputs to maintain aircraft stability and achieve desired flight performance. It ensures proper longitudinal, lateral, and directional control, compensating for inherent instability or external disturbances.
Stabilisers Subsystem	Provides longitudinal and lateral stability and control, including pitch and yaw regulation.

2.2. Systems Engineering Architecture

The systems engineering process starts from the very beginning of the project, as in order to become a successful project, a certain amount of funding, resources and facilities are required; as well as a market need for the product. For this reason, the entities that can influence and be influenced by the project need to be identified, and their expectations have to be identified and met. This is done through the stakeholder analysis, after which the stakeholder requirements can be derived in the language of the stakeholder. These requirements, however, still have to be translated into the requirements specific to the project in a more detailed and concise terminology. These requirements are called the Mission Requirements: they encompass all the necessities that the product has to fulfil throughout its lifecycle. However, these Mission Requirements don't just purely stem from the stakeholders; they are also derived from the functions the product has to fulfil at an aircraft level, which in return is also partly derived from the functional flow of the project itself, as well as the capabilities a general aircraft design needs to fulfil. In addition, CS-25 requirements have also been considered to maintain the certification viability of the product.

From the aircraft level functions and system definitions, the system functions themselves can be derived, from which the system requirements can also be derived. Note that there are certain requirements that stem from the Mission Level Requirements. Generally, most requirements at a specific level stem from the same level functions and may be a more detailed version of a higher level requirement, while functions are a hierarchical flow down from the level above. Thus, all the subsystem functions are derived from the system-level functions, from which the subsystem requirements can be defined. This systems engineering architecture can be seen in Figure 2.1

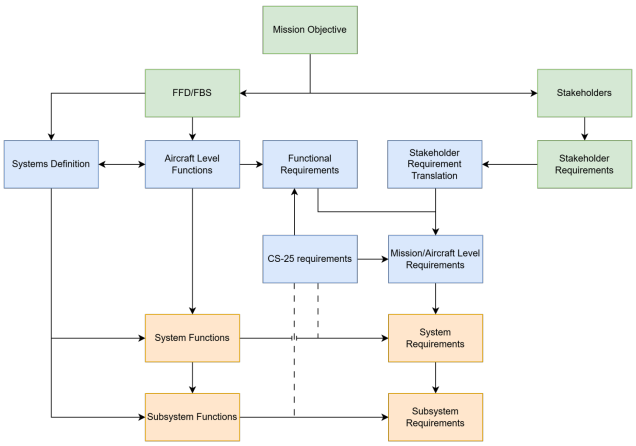

Figure 2.1: Systems Engineering Architecture

3
Functions

The functions are an essential part of the design. They dictate the flow of the requirements on each level and define the capabilities the aircraft must perform. Starting off the functions at mission level can be derived as discussed throught the Functional Flow Diagram and the Functional Breakdown Diagram in Section 3.1. After which the aircraft level functions can be derived, also based off on general aviation knowledge as shown in Section 3.2, from which then the system and subsystem functions are derived. Note that the functional flowdown

3.1. Functional Flow Diagram and Functional Breakdown Diagram

For the functions to be generated, the aircraft life cycle is divided into distinct phases: design, produce, test, operate, and dispose. These phases form the basis for both the Functional Flow Diagram (FFD), which can be seen in Figure 3.1 and the Functional Breakdown Diagram (FBD), which can be seen in Figure 3.2, and together reflect the full scope of the project.

3.1.1. Designing the Aircraft

During the design phase, the concept of the aircraft is developed and refined. This includes formulating the mission need statement, deriving mission, aircraft, and system requirements, performing trade-off studies, and establishing conceptual and preliminary designs. Mass estimations, detailed systems design, and final design validation conclude this phase.

3.1.2. Producing the Aircraft

The production phase covers the complete manufacturing chain of the aircraft, from raw material processing to final assembly and system integration. It includes the production of bulk materials, semi-finished products, and airframe parts, which are assembled into the main structure. After the primary structure is built, the landing gear, propulsion system, aircraft shipsets, and cabin interior are integrated.

3.1.3. Testing the Aircraft

The testing phase consists of three main functions: performing ground tests, performing flight tests, and certifying the aircraft. These activities verify that the aircraft meets the required performance and safety standards before entry into service. Only after successful completion of this phase can the aircraft proceed to operations.

3.1.4. Operating the Aircraft

The operating phase is the most extensive part of the FFD and contains the largest number of functions. It begins with pre-flight operations such as flight planning, crew briefing, cargo loading, dispatch release, passenger boarding, and aircraft walk-around. The sequence continues with push-back, engine start, taxi-out, take-off, climb, cruise, descent, approach, landing, taxi-in, turnaround operations, and post-flight inspection.

The FFD also includes decision paths for abort take-off, go-around, and operations under emergency, failure, and one-engine-inoperative conditions. These branches ensure that the functional model covers both nominal and off-nominal operation throughout the aircraft's service life.

3.1.5. Disposing the Aircraft

The disposal phase covers the end-of-life treatment of the aircraft. After collection and dismantling, reusable components are recovered, recyclable waste is separated and recycled, and non-recyclable waste is disposed of. This phase supports the sustainability strategy of the project by reducing waste and enabling reuse of materials and components.

3.1.6. Functional Flow Diagram

The Functional Flow Diagram (FFD) presents the aircraft life cycle in a logical and sequential form, showing what must happen and in what order for the system to fulfil its mission. It includes the design, production, testing, operating, and disposal phases, with explicit branching where alternative or exceptional paths exist.

3.1.7. Functional Breakdown Diagram

The Functional Breakdown Diagram (FBD) provides a hierarchical decomposition of the mission functions into smaller functional elements. It is structured as an AND-tree, starting at the system level and breaking down into lower-level functions and subsystems. The diagram clarifies how the aircraft functions are grouped per lifecycle phase and how production and operation are distributed across the system architecture.

Post oil airliner

1 Design aircraft → 2 Produce aircraft → 3 Test aircraft → 4 Operate aircraft → 5 Dispose aircraft

Legend

Level 0 | Level 1 | Level 2 (1.1 AS) | Level 3 (1.1.1 AS) | Level 4 (1.1.1.1 AS) | OR | AND

All - All systems

Ops - Operations

Design aircraft

Formulate mission need statement 1.1 All → Derive mission requirements 1.2 All → Define aircraft requirements 1.3 All → Define system requirements 1.4 All → Design option tree 1.5 All → Conduct trade-off 1.6 All → Establish conceptual design 1.7 All → Determine Cabin planform 1.8 All → Determine Fuselage planform 1.9 All → Perform detailed systems design 1.12 All → Establish preliminary design 1.13 All → Perform design analysis 1.14 All → Finalise design 1.15 All

Establish conceptual design 1.7 All → Perform I class mass estimation 1.10 All → Perform II class mass estimation 1.11 All → Perform detailed systems design 1.12 All

Produce aircraft

Produce Bulk material 2.1 All → Produce Semi-finished products 2.2 All → Produce Airframe Parts 2.3 All → Assemble BWB structures 2.4 All → Integrate further aircraft systems 2.5 All

2.1 Produce Bulk Materials: Process raw material 2.1.1 All → Produce bulk material 2.1.2 All → Verify Bulk Material Quality 2.1.3 All

2.2 Produce Semi-finished products: Produce sandwich materials 2.2.1 All → Integrate Sandwich panel 2.2.2 All → Produce Al - Li stuctural components 2.2.3 All

2.3 Produce Airframe Parts: Produce center body structural parts 2.3.1 All → Produce pressure module structural parts 2.3.2 All → Produce wing components 2.3.3 All; Produce movables 2.3.5 All → Produce wing components 2.3.4 All

2.4 Assemble BWB structures: Assemble pressure module 2.4.1 All → Assemble center-body structure 2.4.2 All → Assemble Wingbox and outer wings 2.4.3 All → Integrate BWB structure 2.4.4 All

2.5 Integrate further aircraft systems: Install landing gear 2.5.1 All → Install propulsion system 2.5.2 All → Install aircraft systems shipsets 2.5.3 All → Install cabin interiour 2.5.4 All

Test aircraft

Show means of compliance 3.1 All → AND → Perform ground test 3.2 All; Perform flight test 3.3 All → AND → Certificate the aircraft 3.4 All

Operate aircraft

Perform pre-flight operations 4.1 All → Taxi-out 4.2 All → Take-off 4.3 All → Climb 4.4 All → Cruise 4.5 All → Descend / Approach 4.6 All → Land aircraft 4.7 All → Taxi-in 4.8 All → Perform turnaround operations 4.9 All → Inspect / maintain aircraft 4.10 All → Operate under special or abnormal conditions 4.11 All

Prepare flight plan 4.1.1 All → AND

AND → Crew briefing 4.1.2 All; Load cargo 4.1.3 All; Dispatch release 4.1.4 All; Board passengers 4.1.5 All; Refuel / recharge / energy loading 4.1.6 All; Perform aircraft walk-around 4.1.7 All

4.1.5 Board Passengers: Dock PBB / Stairs 4.1.5.1 Ops; Remove PBB / Stairs 4.1.5.2 Ops

4.2.1 Perform push-back: Connect the push-back truck 4.2.1.1 All; Push-back the aircraft to designated location 4.2.1.2 All

Perform push-back 4.2.1 All → Start the engines 4.2.2 All → Taxi to runway 4.2.3 All → Extend HLDs to take-off settings 4.2.4 All → Line up the Runway 4.3.1 All → Accelerate for take-off 4.3.2 All → At decision speed V1 4.3.3 All → OR → Take-off 4.3.4 All → Rotate the aircraft 4.3.5 All- → Climb positive rate 4.3.6 All

4.2.3 Taxi to runway: Taxi checks 4.2.3.1 All; Stop at allocated positions 4.2.3.2 All

4.3.6 Climb positive rate: Retract landing gears 4.3.6.1 All; Retract HLDs 4.3.6.2 All

At decision speed V1 4.3.3 All → OR → Abort Take-off 4.3.7 All → Vacate the runway 4.3.8 All

Rotate the aircraft 4.3.5 All- → Deflect the elevator 4.3.5.1 All → Trim the aircraft 4.3.5.2 All

Climb positive rate 4.3.6 All → Reduce climb rate 4.4.1 All → Adjust heading as required 4.4.2 All → Maintain heading 4.4.2.2 All; Turn to designated heading 4.4.2.1 All → Adjust altitude as required 4.4.3 All → Level-off at Cruise Altitude 4.4.4 All → OR → Continue as flight plan 4.5.1 All; Follow ATC instructions 4.5.2 All

Continue as flight plan 4.5.1 All → Manage energy 4.6.1 All → Descend 4.6.1 All → OR → Continue descend 4.6.2 All → Hold at certain altitude 4.6.3 All

4.6.6 Set Landing Configuration: Extend HLDs for landing 4.2.3.1 All; Extend landing gears 4.2.3.2 All

Set Landing Configuration 4.6.6 All → Approach 4.6.5 All → Reduce speed 4.6.4 All

Decision Height 4.6.7 All → OR → Go around 4.6.8 All; Continue approach 4.6.9 All → Flare 4.7.1 All → OR → Touch down 4.7.2 All → Decelerate 4.7.3 All → Vacate the runway 4.8.1 All → Taxi to the gate 4.8.2 All → Shut down engine 4.9.1 All

Disembark passengers 4.9.2 All; Unload cargo 4.9.3 All; Dispose waste 4.9.4 All; Refuel / recharge / energy loading 4.9.5 All

Perform mission OEI 4.11.1 All; Perform mission under emergency situation 4.11.2 All; Perform mission with system failure 4.11.3 All

Post-flight inspection 4.10.1 All → Finish cycle 4.10.2 All

Dispose aircraft

Collect aircraft 5.1 All → Remove reusable AC components 5.2 All → Reuse components 5.2.1 All; Dismantle AC 5.3 All → AND → Collect recyclable wastes 5.4 All → Recycle recyclable wastes 5.5 All; Collect non - recyclable wastes 5.6 All → Dispose non - recyclable wastes 5.7 All

Figure 3.1: Functional Flow Diagram

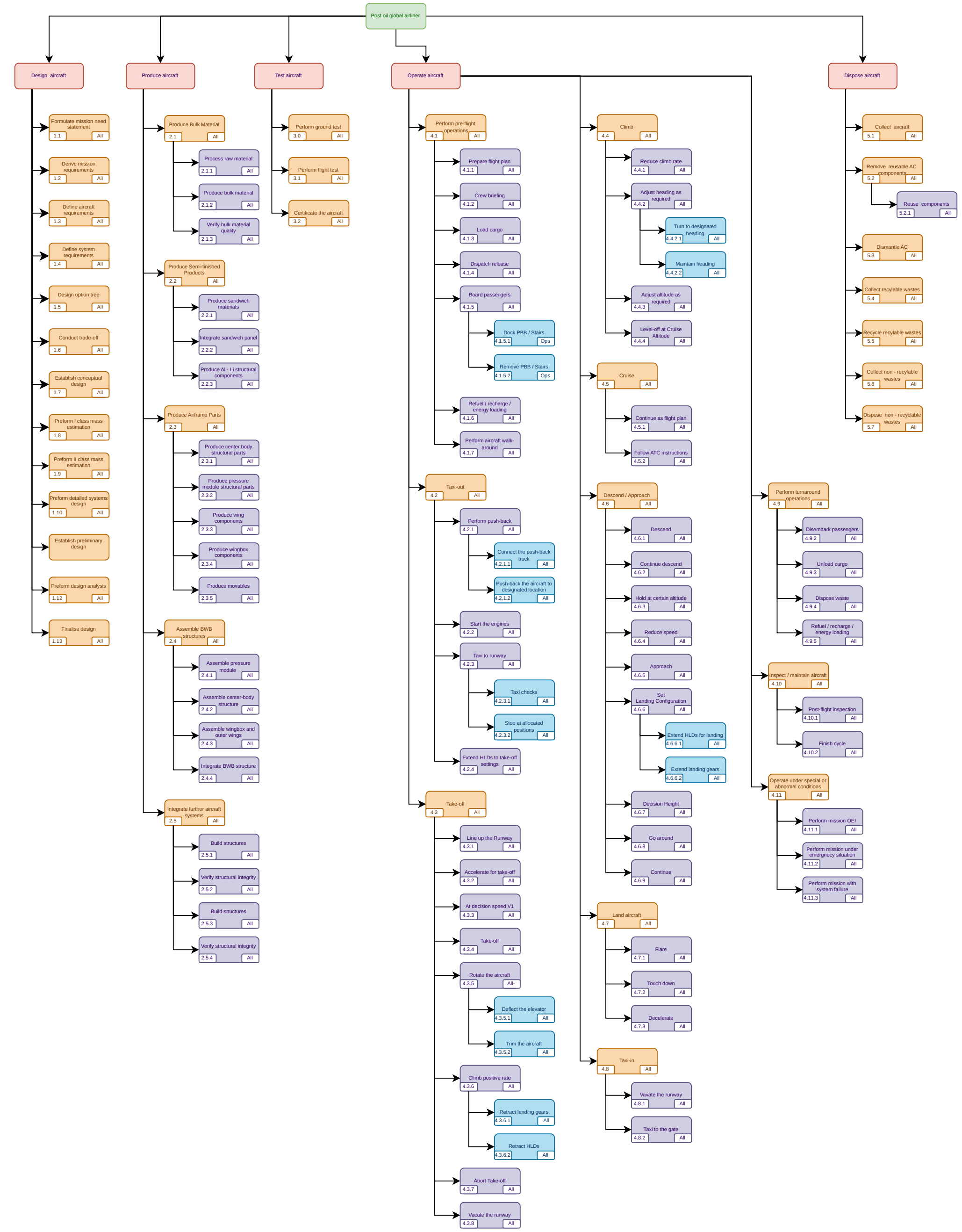

Figure 3.2: Functional Breakdown Diagram

3.2. Aircraft Level Functions

From Figure 3.2, from general aviation knowledge and from the system architecture shown in Figure 2.1, the aircraft-level functions can be derived. From that point, the system and, consequently, the subsystem functions can also be derived.

Table 3.1: Aircraft Level Functions

AL-FUN-	Aircraft Level Functions	Relation
1	**Provide structural integrity**	FFD-4.3 - 4.7
2	**Provide stability and control in flight**	
2.1	Control pitch in flight	FFD-4.3.5, FFD-4.4, FFD-4.6.1 - 4.6.2, FFD-4.7.1
2.2	Control roll in flight	FFD-4.4.2, FFD-4.5, FFD-4.6.1 - 4.6.2
2.3	Control yaw in flight	FFD-4.4.2, FFD-4.5, FFD-4.6.1 - 4.6.2
2.4	Maintain stability	FFD-4.4, FFD-4.5, FFD-4.6.1 - 4.6.2, FFD-4.11
2.5	Control flight path	FFD-4.4, FFD-4.5, FFD-4.6
3	**Provide Lift**	
3.1	Generate lift	FFD-4.3.5 - 4.3.6, FFD-4.4, FFD-4.5, FFD-4.6.1 - 4.6.2
3.2	Control lift	FFD-4.3.6, FFD-4.6.6, FFD-4.7.1
4	**Control aircraft on ground**	
4.1	Accelerate on ground	FFD-4.3.2
4.2	Decelerate on ground	FFD-4.7.3, FFD-4.8.1
4.3	Control direction on ground	FFD-4.2.3, FFD-4.3.1, FFD-4.8.2
5	**Control in flight velocity**	
5.1	Accelerate in flight	FFD-4.3.6, FFD-4.4
5.2	Decelerate in flight	FFD-4.6.4, FFD-4.6.6
5.3	Maintain cruise velocity	FFD-4.5
6	**Store energy**	
6.1	Provide storage	FFD-4.1.6, FFD-4.9.5
6.2	Maintain storage conditions	FFD-4.4, FFD-4.5, FFD-4.6.1 - 4.6.2
6.3	Monitor energy quantity	FFD-4.1.6, FFD-4.5, FFD-4.9.5
7	**Manage Energy**	
7.1	Control energy flow	FFD-4.3.2 - 4.3.6, FFD-4.4, FFD-4.5, FFD-4.6.1 - 4.6.2
7.2	Distribute energy to systems	FFD-4.3.2 - 4.3.6, FFD-4.4, FFD-4.5, FFD-4.6.1 - 4.6.2, FFD-4.11
7.3	Replenish energy	FFD-4.1.6, FFD-4.9.5
8	**Provide power**	
8.1	Provide mechanical power	FFD-4.3.2 - 4.3.6, FFD-4.4, FFD-4.5, FFD-4.6.1 - 4.6.2
8.2	Provide propulsive power	FFD-4.3.2 - 4.3.6, FFD-4.4, FFD-4.5, FFD-4.6.1 - 4.6.2, FFD-4.11.1
8.3	Provide electric power	FFD-4.3.2 - 4.3.6, FFD-4.4, FFD-4.5, FFD-4.6.1 - 4.6.2, FFD-4.11
8.4	Provide hydraulic power	FFD-4.3.6, FFD-4.6.6, FFD-4.7.3, FFD-4.11.2 - 4.11.3
8.5	Provide pneumatic/pressurisation power	FFD-4.4, FFD-4.5, FFD-4.6.1 - 4.6.2
8.6	Provide thermal power	FFD-4.4, FFD-4.5, FFD-4.6.1 - 4.6.2
8.7	Monitor power levels	FFD-4.3.2 - 4.3.6, FFD-4.4, FFD-4.5, FFD-4.6.1 - 4.6.2, FFD-4.11
9	**Provide flight information**	
9.1	Provide aircraft and flight information to crew	FFD-4.1.2, FFD-4.3.2 - 4.3.6, FFD-4.4, FFD-4.5, FFD-4.6
9.2	Provide aircraft and flight information to ATC	FFD-4.5.2, FFD-4.6.5, FFD-4.6.7
9.3	Communicate ground-to-ground	FFD-4.1.1, FFD-4.9.2 - 4.9.5
9.4	Communicate air-to-ground	FFD-4.5.2, FFD-4.6.5, FFD-4.11.2
9.5	Communicate air-to-air	FFD-4.5.2
9.6	Communicate intra-vehicle	FFD-4.1.2, FFD-4.3.2 - 4.3.6, FFD-4.4, FFD-4.5, FFD-4.6
10	**Accommodate payload**	
10.1	Control environment	FFD-4.4, FFD-4.5, FFD-4.6.1 - 4.6.2
10.2	Accommodate crew	FFD-4.1.2, FFD-4.3, FFD-4.4, FFD-4.5, FFD-4.6
10.3	Accommodate cargo	FFD-4.1.3, FFD-4.9.3
10.4	Accommodate passengers	FFD-4.1.5, FFD-4.9.2
10.5	Accommodate ground operations	FFD-4.1.4, FFD-4.1.7, FFD-4.2.1, FFD-4.8, FFD-4.10
11	**Provide Safety**	
11.1	Ensure safe operation under all operational conditions	FFD-4.3.3, FFD-4.3.7 - 4.3.8, FFD-4.11.2 - 4.11.3
11.2	Monitor and detect system faults	FFD-4.11.2 - 4.11.3
11.3	Mitigate faults and failures	FFD-4.11.2 - 4.11.3
11.4	Provide system redundancy	FFD-4.11
11.5	Withstand external environment	FFD-4.4, FFD-4.5, FFD-4.6.1 - 4.6.2
11.6	Comply with regulations	FFD-4.11
11.7	Provide the passengers with emergency exits	FFD-4.11.2
11.8	Provide electromagnetic isolation for EMI-sensitive components.	—

3.3. Power & Propulsion System and Subsystem Functions

Table 3.2: Propulsion Power Functions

PP-FUN-	Propulsion Power Functions	Related AL-FUN
1	Isolate energy carrier from the airframe	AL-FUN-6.1
2	Control internal storage environment	AL-FUN-6.2
3	Transduce energy carrier quantity into system data	AL-FUN-6.3
4	Provide interface for energy carrier replenishment	AL-FUN-7.3
5	Control energy carrier transfer conditions	AL-FUN-7.1
6	Monitor replenishment progress	AL-FUN-7.3
7	Condition energy carrier for conversion	AL-FUN-7
8	Interpret power demand	AL-FUN-7.1
9	Modulate energy carrier transfer rate	AL-FUN-7.1
10	Generate shaft torque for secondary loads	AL-FUN-8.1
11	Generate controlled thrust	AL-FUN-8.2
12	Generate electrical power	AL-FUN-8.3
14	Integrate power sources	AL-FUN-7.1
15	Distribute energy across system boundaries	AL-FUN-7.2
16	Pressurise fluid media for actuation	AL-FUN-8.4
17	Condition compressed gaseous media	AL-FUN-8.5
18	Expose thermal loads to interfaces	AL-FUN-8.6
19	Measure system power levels	AL-FUN-8.7
20	Energy carrier safety release	AL-FUN-7.1 AL-FUN-11.1
21	Provide interfaces for hazard suppression	AL-FUN-11.1 - 11.3
22	Provide manual lockout	AL-FUN-11.3
23	Provide multiple energy paths	AL-FUN-11.4
24	Segregate critical functions	AL-FUN-11.4
25	Provide backup power	AL-FUN-11.4
26	Shield components from external loads	AL-FUN-11.5
27	Shield components from external temperature	AL-FUN-11.5

Table 3.2: Power & Propulsion Subsystem Functions

ID	Function	Relation
ES-FUN-	**Energy Storage**	
1	Contain energy carrier	PP-FUN-1
2	Isolate fuel from airframe	PP-FUN-1
3	Regulate ullage pressure	PP-FUN-2
4	Maintain fuel temperature	PP-FUN-2
5	Inert ullage volume	PP-FUN-2
6	Measure fuel quantity	PP-FUN-3
7	Balance fuel between tanks	PP-FUN-3 PP-FUN-9
8	Provide refuel interface	PP-FUN-4
ED-FUN-	**Energy Distribution**	
1	Transfer fuel to engines	PP-FUN-9
2	Pressurise fuel lines	PP-FUN-5 PP-FUN-9
3	Filter fuel	PP-FUN-7
4	Enable crossfeed	PP-FUN-23
5	Dump fuel overboard	PP-FUN-20
6	Segregate fuel lines	PP-FUN-24
7	Monitor transfer conditions	PP-FUN-3
EN-FUN-	**Engines**	
1	Generate thrust	PP-FUN-11
2	Drive accessory gearbox	PP-FUN-10
3	Generate electrical power	PP-FUN-12
4	Accept fuel input	PP-FUN-7 PP-FUN-9
5	Modulate thrust	PP-FUN-8 PP-FUN-11
6	Provide structural mount	PP-FUN-26
AP-FUN-	**Auxiliary Power**	
1	Generate electrical power on ground	PP-FUN-12
2	Start main engines	PP-FUN-12
3	Accept fuel input	PP-FUN-7
4	Provide structural mount	PP-FUN-26
SP-FUN-	**Secondary Power**	
1	Pressurise hydraulic circuits	PP-FUN-16
2	Maintain two independent hydraulic circuits	PP-FUN-23 PP-FUN-24
3	Supply mechanical shaft power	PP-FUN-10
4	Supply pneumatic power	PP-FUN-17
EP-FUN-	**Emergency Power**	
1	Deploy RAT	PP-FUN-25
2	Generate emergency hydraulic power	PP-FUN-16 PP-FUN-25
3	Generate emergency electrical power	PP-FUN-12 PP-FUN-25
4	Store battery energy	PP-FUN-25
5	Supply battery power	PP-FUN-25
6	Store hydraulic accumulator energy	PP-FUN-25
PD-FUN-	**Power Distribution**	
1	Integrate power sources	PP-FUN-14
2	Distribute power to consumers	PP-FUN-15
3	Execute load shedding	PP-FUN-24 PP-FUN-25
4	Monitor bus power levels	PP-FUN-19
5	Regulate power quality	PP-FUN-15

3.4. Airframe System & Subsystems

Table 3.3: Airframe Functions

AF-FUN-	Airframe Functions	Relation
1	**Accommodate pitch moment**	
1.1	Withstand loads connected to pitch moment	AL-FUN-2.1
1.3	Integrate control surfaces to generate pitch moment	AL-FUN-2.3
2	**Accommodate roll moment**	
2.1	Withstand loads connected to roll moment	AL-FUN-2.2
2.2	Integrate control surfaces to generate roll moment	AL-FUN-2.2
2.3	Generate restoring roll moment	AL-FUN-2.2 AL-FUN-2.4
3	**Accommodate yaw moment**	
3.1	Withstand loads connected to yaw moment	AL-FUN-2.3
3.2	Integrate control surfaces to generate yaw moment	AL-FUN-2.3
3.3	Generate restoring yaw moment	AL-FUN-2.3 - 2.4
5	**Maintain airframe shape under aerodynamic loading**	
5.1	Provide load path for aerodynamic forces	AL-FUN-1
5.2	Limit structural deflection	AL-FUN-1
5.3	Provide torsional stiffness	AL-FUN-1
5.4	Withstand thermal expansion and contraction	AL-FUN-11.5
6	**Provide lift regulation possibility**	
6.1	Generate lift	AL-FUN-3.1
6.4	Minimise drag	AL-FUN-5.3
7	**Withstand loads**	
7.1	Withstand aerodynamic loads within defined flight envelope	AL-FUN-1
7.2	Withstand propulsive loads during acceleration	AL-FUN-1 AL-FUN-4.1
7.4	Withstand braking loads during ground deceleration	AL-FUN-1 AL-FUN-4.2
7.5	Withstand landing impact vertical load	AL-FUN-1
7.6	Withstand inertial forces	AL-FUN-1 AL-FUN-4.1 - 4.2 AL-FUN-5.1
8	**Provide ground operations possibility**	
8.1	Provide ground clearance	AL-FUN-4
8.2	Provide turn fall over stability	AL-FUN-4
8.3	Provide possibility for steering	AL-FUN-4.3
11	**Provide isolation**	
11.1	Withstand pressurisation	AL-FUN-10.1
11.3	Provide noise isolation	AL-FUN-10.2 AL-FUN-10.4
11.5	Provide physical barrier from corrosion	AL-FUN-6.2 AL-FUN-10.3
11.7	Provide static electric discharge	AL-FUN-11.5
12	**Support non-structural internal mass**	
12.1	Support loads created by crew mass	AL-FUN-1 AL-FUN-10.2

Table 3.3: Airframe Subsystem Functions

ID	Function	Relation
DO-FUN-	**Doors**	
1	Provide structural access capability for operational use	AF-FUN-13.1 AF-FUN-13.2
2	Provide certified emergency exit system integration	AF-FUN-13.3
3	Maintain fuselage enclosure integrity under pressurisation	AF-FUN-11.1
WI-FUN-	**Windows**	
1	Maintain pressure boundary integrity of transparent and sealed structures	AF-FUN-13.4
2	Provide environmental protection for structural interfaces	AF-FUN-11.5
3	Provide acoustic isolation	AF-FUN-11.3
4	Maintain structural resistance to external impact loads	AF-FUN-14.4
LG-FUN-	**Landing Gear**	
1	Transfer ground operational loads into primary structure	AF-FUN-7.4 AF-FUN-7.5
2	Absorb and dissipate landing impact energy	AF-FUN-7.5 AF-FUN-14.1
3	Maintain ground operational stability and clearance	AF-FUN-8.1 AF-FUN-8.2
4	Enable ground manoeuvring and handling interface	AF-FUN-8.3
FR-FUN-	**Furnishings**	
1	Provide internal payload volume and spatial accommodation	AF-FUN-15
2	Support and distribute internal payload loads into the airframe	AF-FUN-12.2
3	Maintain cabin evacuation and movement pathways	AF-FUN-13.1
4	Provide cabin system integration support	AF-FUN-12.6
5	Ensure fire resistant cabin structural behaviour	AF-FUN-14.1
LS-FUN-	**Lifting Surfaces**	
1	Generate and regulate aerodynamic lift across flight phases	AF-FUN-6.1 AF-FUN-7.1
2	Provide aerodynamic efficiency through drag reduction	AF-FUN-6.4
3	Integrate aerodynamic control and stability surfaces	AF-FUN-1.3 AF-FUN-2.2 AF-FUN-3.2
4	Integrate ingress an egress location such that evacuation of 120 passengers + crew can be done within regulatory time requirement	AF-FUN-13.1 AF-FUN-13.3
5	Provide structural volume for payload and baggage storage	AF-FUN-15.2 AF-FUN-15.5
SM-FUN-	**Structural Mechanics**	
1	Provide continuous structural load paths between the lifting surfaces and the fuselage/centrebody.	AF-FUN-5
2	Carry longitudinal bending loads through the outer aerodynamic contour.	AF-FUN-5 AF-FUN-6

12.2	Support loads generated by payload mass	AL-FUN-1 AL-FUN-10.3 - 10.4
12.4	Support loads created by propulsion system	AL-FUN-1 AL-FUN-8.2
12.5	Support loads created by energy carrier mass	AL-FUN-1 AL-FUN-6.1
12.6	Support internal components	AL-FUN-10.2 - 10.4
13	**Provide access and enclosure**	
13.1	Enable normal ingress and egress	AL-FUN-10.2 AL-FUN-10.4
13.2	Provide possibilities of accessing inner structure for service	AL-FUN-11.2
13.3	Provide emergency exit access	AL-FUN-11.7
13.4	Provide sealing of openings	AL-FUN-10.1
14	**Provide structural safety**	
14.1	Provide fail-safe load structures	AL-FUN-11.4
14.4	Withstand bird strike	AL-FUN-11.5
14.5	Provide alternative load paths	AL-FUN-11.4
14.6	Provide lightning strike protection	AL-FUN-11.5
15	**Provide payload space**	
15.1	Provide space for crew	AL-FUN-10.2
15.2	Provide space for cargo	AL-FUN-10.3
15.3	Provide space for passengers	AL-FUN-10.4
15.4	Provide space for propulsion system	AL-FUN-8.2
15.5	Provide space for energy carrier	AL-FUN-6.1

3	Transfer outer-wing bending loads into the centrebody structure.	AF-FUN-5 AF-FUN-6
4	Transfer outer-wing shear loads into the centrebody structure.	AF-FUN-5 AF-FUN-6
5	Withstand the selected cabin differential pressure.	AF-FUN-11
6	Transfer pressure-shell reactions into the internal walls, floor, ceiling and columns.	AF-FUN-11
7	Support the selected passenger, crew, cargo, floor, systems and equipment loads.	AF-FUN-12
8	Provide structural containment for the required fuel storage.	AF-FUN-15

3.5. Monitoring and Control System Functions

Note that the Monitoring and Control System has only been explored at a system level as seen in Table 3.4.

Table 3.4: Mission Control Subsystem Functions

MC-FUN-	Function	Relation
1	**Provide Ice and Rain Protection**	
1.1	Prevent ice formation on aircraft surfaces and systems	AL-FUN-11.1, AL-FUN-11.5
1.2	Detect ice formation on the aircraft	AL-FUN-11.2
1.3	Remove ice formation from aircraft surfaces and systems	AL-FUN-11.3
1.4	Distribute de-icing agents across the aircraft	AL-FUN-11.3
2	**Provide Aircraft Lighting**	
2.1	Provide external lighting for aircraft visibility and navigation	AL-FUN-9.2, AL-FUN-11.1
2.2	Illuminate the landing and ground taxiing environment	AL-FUN-4.3, AL-FUN-11.1
3	**Provide Fire Protection**	
3.1	Detect the possibility of fire or overheating	AL-FUN-11.2
3.2	Detect active fire events across aircraft zones	AL-FUN-11.2
3.3	Mitigate and suppress fire events	AL-FUN-11.3
3.4	Contain fire and prevent spread between aircraft zones	AL-FUN-11.1, AL-FUN-11.3
4	**Manage Aircraft Thermal State**	
4.1	Acquire and manage waste heat from aircraft heat-generating systems	AL-FUN-7.1, AL-FUN-8.6
4.2	Redistribute waste heat to beneficial aircraft systems	AL-FUN-7.2
4.3	Expel excess heat out of the aircraft system	AL-FUN-8.6, AL-FUN-11.1
5	**Provide Communication and Monitoring Capability**	
5.1	Provide external communications with ATC and other aircraft	AL-FUN-9.4, AL-FUN-9.5
5.2	Provide intra-vehicle crew and passenger communications	AL-FUN-9.6
5.3	Provide in-flight passenger entertainment	AL-FUN-10.4
6	**Provide Navigation and Situational Awareness**	

MC-FUN-	Function	Relation
6.1	Collect and process flight environment data	AL-FUN-9.1
6.2	Indicate aircraft attitude and flight parameters to crew	AL-FUN-2, AL-FUN-9.1
6.3	Aid approach, landing, and ground taxiing operations	AL-FUN-4.3
6.4	Provide global positioning capability	AL-FUN-9.1
6.5	Provide situational awareness and hazard avoidance	AL-FUN-11.1, AL-FUN-11.2
7	**Provide Surveillance and Flight Data Management**	
7.1	Provide ATC surveillance and aircraft identification	AL-FUN-9.2
7.2	Provide digital data link communications	AL-FUN-9.4
7.3	Display integrated flight and systems information to crew	AL-FUN-9.1, AL-FUN-11.2
8	**Control the Aircraft Cabin Environment**	
8.1	Supply and maintain pressurised air within the cabin	AL-FUN-8.5, AL-FUN-10.1
8.2	Control and maintain cabin temperature	AL-FUN-10.1
8.3	Control and maintain cabin humidity	AL-FUN-10.1
8.4	Monitor cabin air quality and alert crew	AL-FUN-11.1, AL-FUN-11.2
9	**Provide Centralised Data Management and System Integration**	
9.1	Operate and manage the aircraft data bus network	AL-FUN-9.1
9.2	Interface with and acquire data from all aircraft systems	AL-FUN-9.1, AL-FUN-11.2
9.3	Continuously monitor system health across all subsystems	AL-FUN-11.2
9.4	Detect, isolate, and manage system faults	AL-FUN-11.2, AL-FUN-11.3, AL-FUN-11.4
9.5	Record mandatory flight data	AL-FUN-9.1, AL-FUN-11.6
10	**Accommodate Passengers and Provide Cabin Safety**	
10.1	Provide seating, galley, lavatory, and passenger facilities	AL-FUN-10.4
10.2	Provide cabin illumination and emergency lighting	AL-FUN-11.1, AL-FUN-11.7
10.3	Provide emergency exit access and passenger safety systems	AL-FUN-11.7
10.4	Provide passenger address and cabin noise management	AL-FUN-10.4, AL-FUN-11.1

3.6. Flight Controls & Stability System Functions

Note that the Flight Controls & Stability System has only been explored at a system level as seen in Table 3.5.

Table 3.5: Flight Control Functions

FC-FUN-	Flight Control Functions	Related AL-FUN
Longitudinal Stability & Control		
1	Generate restoring pitching moment	AL-FUN-2.4
2	Trim aircraft in pitch	AL-FUN-2.1
3	Maintain CG within envelope	AL-FUN-2.1, AL-FUN-2.4
Lateral-directional stability		
4	Generate restoring yawing moment	AL-FUN-2.2, AL-FUN-2.3, AL-FUN-2.4
5	Generate dihedral effect	AL-FUN-2.2, AL-FUN-2.3, AL-FUN-2.4
6	Damp spiral mode	AL-FUN-2.2, AL-FUN-2.3, AL-FUN-2.4
Dynamic Stability		
7	Damp Dutch roll	AL-FUN-2.4
8	Damp phugoid	AL-FUN-2.4
9	Damp roll	AL-FUN-2.4
Control Authority		
10	Control roll	AL-FUN-2.2
11	Control yaw	AL-FUN-2.3
12	Provide stall warning	AL-FUN-2.4, AL-FUN-11.1
Manoeuvres		
13	Sustain structural load limits	AL-FUN-1, AL-FUN-2.5
14	Complete ICAO holding turn	AL-FUN-2.5
15	Achieve loiter	AL-FUN-2.5

4
Requirements

This chapter establishes the requirements baseline for the aircraft, starting from a stakeholder analysis in Section 4.1 from which stakeholder requirements are derived in Table 4.2. These are then translated into mission level requirements in Section 4.3, from which the aircraft-level requirements are derived in Section 4.4, and consequently the system and subsystem level requirements are derived for the Power & Propulsion, Airframe and Flight Control & Stability Systems in Chapter 11, Section 4.6 and Section 4.7, respectively.

It is also important to note that due to the fact that this project is a preliminary design of an aircraft, there are a lot of requirements to consider for general completeness, in fact over 400 requirements were written throughout the project. While that is very useful for future development, for the scope of the project, only about 170 requirements were set as verifiable and verified. Thus to stay within the appropriate scope, only the requirements set as verifiable within project scope are included in this report at system and subsystem level. Due to this reason the requirements for Monitoring & Control System were not included in this report. On the other hand, for completeness and demonstration of thought, all the stakeholder and mission level requirement are included, furthermore the functions of each system and subsystem are kept as detailed in Chapter 3.

Each requirement is assigned a verifiability flag and a means of compliance, forming the basis of the project's compliance matrix. The definitions of this requirement classification can be found in Chapter 4. The column for 'V' identifies if the requirement is verifiable within the scope of the project, while the 'MoC' column represents the Means of Compliance for how the requirement verification is to take place as seen in Table 4.1. It is to be noted that only the requirements that are deemed verifiable within the scope of this project are included in the compliance matrix.

Killer	Requirements that are critical to the mission and shape the available design space, which, if not met, must enter negotiation with the key stakeholder.
Driving	Requirements that drive the overall design of the aircraft, its systems and subsystems. Driving requirements set critical constraints or boundaries that strongly influence performance, cost, risk and schedule, but do not automatically dictate trade-offs.
Key	Requirements that are of primary importance for the customer, or requirements known or expected to be a risk item.
Supporting	All remaining requirements that enable the system to function but do not drive the design or constitute critical risks.

Table 4.1: Means of compliance codes and descriptions

Number	Description
0	Definition / Direct Answer
1	Description
2	Calculation / Analysis
3	Safety / Risk Assessment
4	Laboratory Tests
5	Ground Test
6	Flight Test
7	Inspection By Airworthiness Authorities
8	Simulation
9	Equipment Qualification
10	Visual inspection

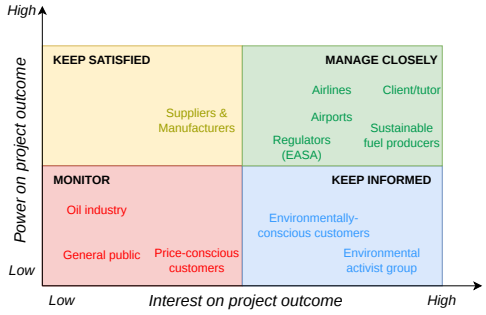

Figure 4.1: Interest-influence map of the project outcome

4.1. Stakeholder Analysis

A stakeholder is any party that is affected by or has the ability to affect the mission. Identifying them before setting requirements is essential, since different stakeholders place different demands on the design and its development. The

stakeholders for the Post-Oil Global Airliner (POGA) are placed on the interest–influence map in Table 4.1.

Client and Investors
The client serves as the primary stakeholder for project delivery, while investors and subsidies provide the necessary capital for research, facilities, and employees. The client defines the core mission requirements and performance benchmarks. To maintain the trust of these stakeholders, the project must strictly adhere to the predefined scope and high-level requirements.

Airlines
The airlines are the main customers of this mission, more specifically the flag carriers and global groups that operate intercontinental routes in the more than 3,000 km range and have committed to net-zero by 2050. The main concerns of these stakeholders are as follows:

- **Capital Expenditures (CAPEX):** Airlines are highly sensitive to the non-recurring costs associated with the acquisition or leasing of a new fleet. The price of a novel non-petroleum airliner must be competitive to ensure an achievable transition from traditional aircraft.
- **Operating Expenses (OPEX):** The most critical factor is the recurring cost of fuel, followed by airport fees and environmental taxes. For a new propulsion concept to be successful, its energy-related costs must remain within a sustainable margin of traditional jet fuel.
- **Operational Efficiency:** Maximising revenue requires high aircraft utilisation. Minimising turnaround time is significant, as faster ground handling and flight durations allow for more frequent rotations and increased fleet productivity. A typical turnaround includes passenger (dis)embarkation, baggage (un)loading, cleaning, technical checks, etc. Current heavy aircraft in Europe often require around two hours of turnaround time, while medium aircraft are closer to one hour, depending on the airport and operator procedures [16].
- **Sustainability and Brand Equity:** Beyond meeting regulatory net-zero targets, airlines prioritise sustainable solutions to enhance corporate image and meet the rising demand from passengers for non-carbon travel options.

Suppliers and Manufacturers
Once the design is complete, the aircraft must be assembled by a manufacturing company using a combination of internally produced components and specialised parts sourced from a network of suppliers. For the scope of this project, companies minimising the use of petroleum while developing aerospace materials play an important role. Additionally, manufacturing companies need detailed specifications from the design team to manufacture the aircraft as intended. Certain standards and requirements must be followed when creating the manufacturing plans.

The suppliers play a significant role as well, since they often develop highly specialised sub-systems, such as fuel system and propulsion unit, that define the aircraft's performance. Consequently, the design team must provide these suppliers with detailed requirements and specification in order to ensure that all components function as one coherent unit. If the standards and requirements are not properly followed by the suppliers and manufacturers, there may be inconsistencies of components and incoherence of systems during assembly, leading to significant delays of the aircraft, as experienced by Airbus during the two-year delay in the production of the A380 due to a wiring mismatch[1].

Sustainable fuel producers
Sustainable fuel producers are important stakeholders whose commercial interests are tied to the creation of a viable market for bio-SAF at the scale required for global airline operations. Unlike novel energy carriers requiring dedicated propulsion architecture, bio-SAF is a drop-in fuel chemically compatible with conventional turbofan engines, removing any technical interdependency between fuel chemistry and propulsion design. The stakeholder relationship is therefore primarily commercial rather than technical: the aircraft's operating economics are directly governed by feedstock availability and bio-SAF production volume, since insufficient scale-up of Fischer-Tropsch and HEFA pathways would keep prices elevated and erode the cost advantage over conventional kerosene. A strategic partnership with fuel producers is necessary to secure long-term supply agreements and to ensure feedstock production scales in line with the aircraft's entry into service in 2035.

Authorities
Before the aircraft can actually enter service, it must have the appropriate certifications and approvals from the relevant regulatory bodies such as EASA. The airliner is expected to be certified by the Dutch Human Environment and Transport Inspectorate (ILT). Hard requirements are set for certain categories of aircraft by these regulatory bodies; if it does not pass a requirement, it cannot go into service. However, such regulations and requirements on novel designs may not yet exist; only certain relevant requirements and regulations must be complied with, while others will have to be created during the project, and are subject to approval by the relevant regulatory bodies [17, 18].

[1] "Wiring Fixed for First A380 Only – Airbus," Reuters, Aug. 9, 2007, URL `https://www.reuters.com/article/business/autos-transportation/wiring-fixed-for-first-a380-only-airbus-idUSL26784850/` [cited 01/05/2026]

Airports
Once the aircraft is approved and certified, it still needs to comply with the rules and regulations for each relevant airport and be compatible with their ground handling operations, such as passenger stairs, cargo loaders and maintenance platforms. The aircraft's 64.9 m wingspan places it within Aerodrome Reference Code 4E, consistent with existing wide-body infrastructure, meaning no new runway, taxiway, or gate category is required at major international airports. Because bio-SAF is a drop-in fuel compatible with existing Jet-A storage and refuelling infrastructure, airports require no new fuel storage, transfer equipment, or specialised trained staff, in contrast to the infrastructure overhaul that a cryogenic or electric energy carrier would demand. The principal airport-side consideration instead concerns the blended wing body's unconventional fuselage geometry, which may require adapted boarding bridges, ground equipment positioning, and cargo door access compared to a tube-and-wing aircraft of similar size. Therefore, airports are considered as stakeholders with high power as well as high interest in the project outcome.

Maintenance, Repair and Overhaul
To maintain safety and the lifetime of the aircraft, Maintenance, Repair and Overhaul (MRO) companies are necessary. These companies must have the right facilities, equipment, and approved personnel to handle the novel aircraft and ensure a safe return to service. Thus, they also need incentives to create the right infrastructure to maintain the novel aircraft, as without MROs to maintain or repair the aircraft, no airline is likely to purchase the aircraft.

Notably, the distinction between manufacturers and service providers is increasingly blurred, as Original Equipment Manufacturers (OEMs) frequently act as the MROs themselves. This vertical integration allows for tighter control over the technical life cycle of the aircraft and thus ensuring reliability throughout its operational life.

Customers
The aircraft's all-business-class, 120-seat cabin defines a customer base distinct from the broader passenger market: corporate travel managers at companies with mandatory Scope 3 emissions reporting obligations, boutique premium operators, and flag carriers on high-yield long-haul corridors. These customers do not have influence on the aircraft design, but their interest in the project outcome differs by purchasing motivation. Corporate Sustainability Reporting Directive (CSRD)-bound corporate travel buyers are primarily interested in the sustainability credentials of the aircraft, since premium-cabin travel is disproportionately weighted in Scope 3 carbon accounting and a certified zero-petroleum-fuel option directly reduces a reportable compliance liability. Premium leisure and boutique-operator customers instead prioritise the value proposition relative to ticket price, given that business-class fares already command a substantial premium over economy. Balancing these interests is critical, as the project must deliver a credible sustainability case without pricing the aircraft outside what either segment is willing to pay.

Environmental activist group
While environmental activist groups are highly interested to see innovative fuel concepts that contribute positively to a more sustainable environment, this group has little to no power on the project outcome; however, this group should still be informed. By maintaining transparent communication, the project can leverage these groups as allies to build market demand and mitigate the risk of negative PR or lobbying that could arise from perceived "greenwashing".

The stakeholder analysis forms the foundation for the requirements derivation process. By systematically identifying all parties affected by, or capable of influencing the mission, and assessing their respective interests and levels of influence, a set of stakeholder requirements were retrieved in the Baseline Report [19]. With the stakeholder landscape established, the mission's commercial position can be assessed against its broader market environment.

4.2. Stakeholder Requirements

After having identified the stakeholders, the stakeholder requirements can be derived, as seen in Table 4.2.

Table 4.2: Stakeholder Requirements

SH-REQ-	Requirement	V	TO
	User Requirements		
1 Airlines			
1.01	The aircraft shall operate using non-petroleum derived energy carriers during normal flight operations.	Y	Yes
1.02	The aircraft shall be compatible with airport refuelling or recharging infrastructure at entry into service in 2035.	Y	Yes
1.03	The aircraft shall be capable of operating at major international airports using standard runways, taxiways, gates, and ground handling facilities.	Y	Yes
1.04	The aircraft shall transport at least 120 passenger and associated cargo on intercontinental routes.	Y	Yes
1.05	The aircraft shall achieve a standard turnaround time of no more than 120 minutes at major hub airports.	Y	Yes
1.09	The aircraft shall achieve an unscheduled maintenance event rate not exceeding 1 events per 1,000 flight hours. (assuming average flight time of 8 hours)	N	No
1.10	The aircraft shall comply with all applicable CS-25 / FAR Part 25 / ICAO certification requirements at entry into service.	N	No
1.11	The aircraft shall satisfy applicable operational safety requirements for commercial passenger transport.	N	No

SH-REQ-	Requirement	V	TO
1.12	The aircraft shall have competitive direct operating costs associated with aircraft of similar type and capability.	Y	Yes
1.13	The aircraft shall demonstrate compliance with the applicable operational, environmental, and noise requirements.	N	No
1.16	The aircraft shall achieve low energy consumption and CO_2 emissions per passenger-kilometre during normal operations.	N	No
1.17	The aircraft shall fly intercontinentally with a diversion time up to 180 minutes at one-engine-inoperative cruise speed (within ETOPS regulations).	Y	Yes
2 Passengers			
2.02	The aircraft shall provide passenger seating with atleast 100 cm leg room, support, and comfort for the intended flight duration.	Y	Yes
2.03	The aircraft shall provide 45 cm cabin aisle space and unobstructed access for normal passenger movement during flight.	Y	Yes
2.04	The aircraft shall provide accessible, functional and enough passenger facilities, including restrooms and food service areas, that meet current commercial standards of comfort and usability.	N	No
2.05	The aircraft shall maintain cabin noise levels within 80 dB during cruise flight.	N	No
2.06	The aircraft shall provide sufficient baggage storage and handling capacity for the intended passenger load and route type.	Y	Yes
2.07	The aircraft shall maintain acceptable cabin temperature, ventilation, and air quality during all normal operations.	N	No
2.08	The aircraft shall provide sufficient lighting and visibility for passengers during day and night flights.	N	No
2.09	The aircraft shall maintain a cabin altitude not exceeding 8,000 ft during normal cruise operations.	N	No
2.10	The aircraft shall achieve Revenue Available Seat Kilometre (RASK) of $TBD for operation on target routes.	Y	Yes
2.11	The aircraft shall provide individual passenger entertainment systems with current commercial aircraft standards.	N	No
Enablers Requirements			
3 Airports			
3.01	The aircraft shall be compatible with the critical taxiways leading to the ramp without posing a risk of collision with objects near the taxiways.	Y	Yes
3.02	The aircraft shall be compatible with at least 5 gates at major airports, based on typical gate size and configuration.	Y	Yes
3.04	The aircraft shall enable the loading and unloading of passengers at a rate of 4 passengers per minute through airbridges and movable stairs.	Y	Yes
3.05	The aircraft shall enable cargo and catering service loading/unloading at a rate of 9 tons per hour.	N	No
3.09	The aircraft shall be certified to fly into the country of the airport and meet any national aviation authority requirements for entry.	N	No
3.11	The aircraft shall be compatible with standard airport pushback vehicles, and provide clear guidelines for ground handling teams.	Y	Yes
3.13	The aircraft shall be compatible with airport waste management systems, ensuring compliance with environmental and safety protocols.	N	No
3.14	The aircraft shall be compatible with runways of at least 2800 meters in length and meet all applicable takeoff and landing angle specifications.	Y	Yes
4 Regulatory Bodies			
4.02	The aircraft shall meet the applicable requirements outlined in CS-25 amendment 28, as relevant to the novel design, through the applicable Acceptable Means of Compliance (AMCs) provided by EASA.	N	No
4.04	Any new or modified requirements created due to the novel design shall be approved by IL&T and EASA before proceeding with design, development, or production.	N	No
4.06	A compliance matrix shall be maintained, tracking the applicable regulatory requirements and documenting how each is met.	Y	Yes
4.08	All novel design solutions, modifications, and safety cases shall be documented, demonstrating how they meet the equivalent safety level.	N	No
5 MRO			
5.05	The aircraft manufacturer shall provide initial type training, certification, and ongoing support to MRO and its personnel to ensure they are qualified to maintain the new aircraft type.	N	No
5.07	The aircraft shall feature a manual lockout system to ensures all propulsion and energy systems are physically de-energised during maintenance.	N	No
5.08	The aircraft shall provide external visual indicators to signal the safety status of energy storage systems to ground personnel before they approach the aircraft.	N	No
5.09	The aircraft shall include pressure-relief and venting systems that discharge energy storage safely during maintenance, preventing hazardous conditions.	N	No
5.10	The aircraft shall be designed to prevent the accumulation of hazardous gases in maintenance-accessible compartments.	N	No
6 Manufacturer			
6.03	The design team shall provide documentation that specifies all critical dimensions, tolerances, and material properties required for assembly.	N	No
6.05	The design shall maximise the use of standardised aerospace hardware to ensure a stable supply chain and simplify the procurement process.	N	No
6.06	The aircraft shall be designed to meet certifiable manufacturing standards, ensuring that all processes are controlled for consistency and can be verified through quality inspections.	N	No

SH-REQ-	Requirement	V	TO
6.08	The manufacturer shall have the right to propose process-driven design changes to improve the yield and repeatability of the fabrication process.	N	No
7 Energy Carrier Provider			
7.01	A proprietary or new-standard intake interface shall be defined that allows the provider to develop matching delivery hardware.	N	No
7.02	The aircraft shall provide dedicated internal venting or cooling paths to manage heat or pressure build-up generated during the high-speed transfer of the new energy carrier.	N	No
7.03	The aircraft shall incorporate failsafe isolation systems to ensure that the energy carrier is contained within the storage system even if the external delivery line is compromised.	N	No
7.04	The aircraft shall be designed with specific intake locations that account for the unique geometry of the airframe such that the provider's equipment does not clash with the wing's leading edges or control surfaces.	N	No
8 Investors			
8.01	The aircraft shall have a minimum flight range of 3000 km.	Y	Yes
8.02	The aircraft shall be capable of covering 6000 km within 24 hours.	Y	Yes
8.03	The aircraft shall accommodate a minimum of 120 passengers in business configuration.	Y	Yes
8.04	Conditions at aircraft level that can lead to a catastrophic event shall be identified.	Y	Yes
8.05	The fuel shall not be petroleum-derived.	Y	Yes
8.06	The aircraft should minimise the use of petroleum derived materials.	Y	Yes
8.07	The first flight shall take place by 2031.	Y	Yes
8.08	The aircraft shall be operable by 2035.	Y	Yes
8.09	The maximum development cost shall be no more than 50 billion euros.	Y	Yes
External Requirements			
9 Environment & Society			
9.01	The aircraft shall achieve a net zero CO_2 lifecycle footprint by utilising an energy carrier that provides a minimum of 80% reduction in total carbon intensity compared to fossil-based kerosene.	Y	Yes
9.03	The aircraft shall be designed with End-of-Life (EoL) recyclability in mind, ensuring that at least 60% of the airframe and energy storage components can be recovered or repurposed.	Y	Yes
9.04	The aircraft shall utilise sustainable and ethically sourced materials in its construction to minimise the environmental impact of the manufacturing supply chain.	Y	Yes

4.3. Mission Requirements

The mission requirements in Table 4.3 translate the stakeholder requirements into design-actionable statements, grouped by the functional areas they constrain. Each requirement links back to its originating stakeholder requirement and specifies its verifiability and means of compliance.

Table 4.3: Mission Requirements

MS-REQ-	Requirement	Relation	V	MoC
1 Achieve Aircraft Certification Approval				
1.1 Satisfy Applicable Regulations				
1.1.1	The aircraft shall comply with all applicable regulations and ICAO certification requirements for both EASA and contracting state at entry into service.	SH-REQ-1.10	N	1, 3
1.1.2	The aircraft shall meet the applicable requirements outlined in CS-25 Amendment 28 through the applicable AMCs provided by EASA.	SH-REQ-4.02	N	1, 3
1.1.5	The aircraft shall be certified to fly into the country of the airport and meet national aviation authority requirements.	SH-REQ-3.09	N	1, 7
1.1.7	The aircraft shall meet compliance with the ICAO Annex 16 chapter 14.4 "Maximum noise levels".	SH-REQ-1.13	N	2, 6
1.1.8	The aircraft shall be designed to meet certifiable manufacturing standards, ensuring all processes are controlled for consistency and verifiable through quality inspections.	SH-REQ-6.06	N	1, 10
1.2 Get Novel Design Approved				
1.2.2	Any new or modified requirements due to the novel design shall be approved by ILT and EASA before proceeding.	SH-REQ-4.04	N	1, 7
1.2.4	All novel design solutions, modifications, and safety cases shall be documented, demonstrating how they meet the equivalent safety level.	SH-REQ-4.08	N	1, 3
1.3 Manage Compliance				
1.3.1	A compliance matrix shall be maintained, tracking applicable regulatory requirements and documenting how each is met.	SH-REQ-4.06	Y	1
2 Perform Mission Within Cost Limit				
2.2	The aircraft shall have competitive direct operating costs for aircraft of similar type and capability.	SH-REQ-1.12	Y	2
2.3	The aircraft shall achieve Revenue Available Seat Kilometre (RASK) of 100 for operation on target routes.	SH-REQ-2.10	Y	2
2.5	The design shall prioritise the use of standardised aerospace hardware to ensure a stable supply chain and simplify procurement.	SH-REQ-6.05	N	1
2.6	The maximum development cost shall be no more than 50 billion euros.	SH-REQ-8.08	Y	1
3 Perform Mission Within Schedule				
3.1	The first flight shall take place by 2031.	SH-REQ-8.07	Y	1

MS-REQ-	Requirement	Relation	V	MoC
3.2	The aircraft shall be operable by 2035.	SH-REQ-1.02, SH-REQ-8.08	Y	1
3.4	The aircraft shall achieve a standard turnaround time of no more than 120 minutes at major hub airports.	SH-REQ-1.05	Y	1
4 Perform Mission With Minimal and Only Acceptable Risks				
4.01	The aircraft design process shall include a risk management phase for all novel requirements, where risks with a product of likelihood and consequence exceeding 12/36 are considered unacceptable and require corrective action.	SH-REQ-8.07, SH-REQ-8.09	Y	3
4.02	The aircraft shall be compatible with airport refuelling or recharging infrastructure at entry into service in 2035.	SH-REQ-1.02, TR-06	Y	1
4.05	Conditions at aircraft level that can lead to a catastrophic event shall be identified.	SH-REQ-8.04	Y	1
Requirements From Risk Analysis				
4.08	The design process shall include an iterative weight-tracking system during the mass estimation phase.	TR-03	Y	1
4.09	Structural materials shall be limited to those with a proven availability to meet the 2035 entry-into-service target.	TR-02	Y	1
4.11	Critical aircraft components and spare parts shall be standardised across the fleet.	TR-07	N	1, 10
4.12	Ground operations systems shall be designed in collaboration with airport authorities to maintain compatibility with existing gate limits.	TR-06	N	1
4.13	The project management shall establish and maintain active communication channels with EASA/FAA working groups.	TR-05	N	1
4.14	The propulsion-airframe integration shall ensure that structural natural frequencies are separated by at least 10% from the primary structural excitation frequencies.	TR-04	N	2, 5
4.15	The aircraft program must ensure novel composite structures can be inspected without increasing operational downtime.	TR-08	N	1, 10
4.16	The aircraft shall follow a "Design for Disassembly" protocol.	TR-09	N	1, 10
5 Performance				
5.1	The aircraft shall accommodate a minimum of 120 passengers in a business configuration.	SH-REQ-1.04, SH-REQ-8.03	Y	1
5.2	The aircraft shall have a minimum flight range of 3000 km.	SH-REQ-8.01	Y	2
5.3	The aircraft shall be capable of covering 6000 km within 24 hours.	SH-REQ-8.02	Y	1, 2
5.4	The aircraft shall have a maximum fuel consumption of no more than 0.04 kg per passenger kilometer during cruise.	SH-REQ-1.16	Y	2
5.5	The aircraft shall comply with runways of at least 2000 meters in length and meet all applicable takeoff and landing angle specifications.	SH-REQ-3.14	Y	2
6 Operations				
6.1	The aircraft shall be compatible with standard airport turnaround operations, including compatibility with airbridges, ground handling equipment, and gate configurations.	SH-REQ-3.02, SH-REQ-3.04, SH-REQ-3.05, SH-REQ-3.11	Y	1
6.2	The aircraft shall be capable of operating at major international airports using standard runways, taxiways, gates, and ground handling facilities.	SH-REQ-1.03, SH-REQ-3.01	Y	2
7 Safety				
See Functional Requirements AL-REQ-11				
7.09	The aircraft shall fly intercontinentally with a diversion time up to 180 minutes at OEI cruise speed within ETOPS regulations.	SH-REQ-1.17	Y	2
7.11	The aircraft shall satisfy applicable operational safety requirements for commercial passenger transport.	SH-REQ-1.11	N	1, 3
7.12	The aircraft shall maintain a safe cabin environment during operational conditions.	SH-REQ-2.09	N	2, 8
7.13	The aircraft shall include pressure-relief and venting systems that discharge hazardous vapour or gases safely before maintenance, preventing hazardous conditions.	SH-REQ-5.09	N	1
7.14	The aircraft shall allow for fuel discharge in order to meet the maximum allowed landing weight in case of an emergency.	SH-REQ-4.02	N	1
8 Maintenance				
8.5	The design shall include defined access points and internal clearances to allow installation and inspection of systems within the airframe structure.	SH-REQ-6.02	N	1, 10
8.7	The aircraft manufacturer shall provide initial type training, certification, and ongoing support to MRO personnel.	SH-REQ-5.05	N	1
9 Sustainability				
9.1	The aircraft shall operate using non-petroleum-derived energy carriers.	SH-REQ-1.01, SH-REQ-8.05	Y	0
9.2	The aircraft shall minimise the use of petroleum-derived materials for manufacturing.	SH-REQ-8.06	Y	1
9.3	The aircraft shall achieve a net-zero CO2 lifecycle footprint by utilising an energy carrier that provides a minimum 80% reduction in total carbon intensity compared to fossil-based kerosene.	SH-REQ-9.01	Y	0, 2
9.4	The aircraft shall not exceed 125 grams of CO2 per passenger-kilometer during standard operational cruise conditions.	SH-REQ-1.16	Y	2
9.6	The aircraft shall utilise sustainable and ethically sourced materials in its construction to minimise environmental impact of the manufacturing supply chain.	SH-REQ-9.04	Y	1

MS-REQ-	Requirement	Relation	V	MoC
9.7	The aircraft shall be designed with end-of-life recyclability in mind, ensuring that at least 60% of the airframe and energy-storage components can be recovered or repurposed.	SH-REQ-9.03, Lifecycle Analysis	Y	1
10 Reliability				
10.2	The aircraft shall achieve an unscheduled maintenance event rate not exceeding 1 events per 1000 flight hours. (assuming average flight time of 8 hours)	SH-REQ-1.09	N	2, 8
11 Functionality				
See Functional Requirements AL-REQ-1 until AL-REQ-10				
12 Manufacturability				
12.2	The design team shall provide documentation specifying all critical dimensions, tolerances, and material properties required for assembly.	SH-REQ-6.03	N	1, 10
12.5	The manufacturer shall have the right to propose process-driven design changes.	SH-REQ-6.08	N	1
12.6	The manufacturing process of the prototype shall take place within 12 months, and the large-scale production of a unit within 6 months.	SH-REQ-8.08	Y	1
13 Comfort				
13.1	The cabin and furnishing subsystems shall be tailored to provide sufficient passenger comfort, meeting airline-specific needs and standards for seating, space, and amenities.	SH-REQ-2.02, SH-REQ-2.03, SH-REQ-2.04	Y	2

4.4. Aircraft Level Requirements

The aircraft-level requirements in Section 4.4 decompose the mission requirements into functional capabilities the aircraft must provide, such as structural integrity, stability and control, lift, and power. Each requirement is traced to its parent mission or stakeholder requirement and assigned a verifiability flag and means of compliance.

AL-REQ-	Functional Requirements	Relation	V	MoC
1 Provide structural integrity				
1.1	The aircraft shall withstand all flight, ground, pressurisation, and emergency loads for MTOW = 131,553 kg.	AL-FUN-1, 25.3010	Y	2
1.2	The aircraft shall withstand all flight, ground, pressurisation, and emergency loads with ultimate −1G to 2.5 G.	AL-FUN-1, 25.3030	Y	2
2 Provide stability and control in flight				
2.1	The aircraft shall provide sufficient pitch authority to trim and manoeuvre across the flight envelope.	AL-FUN-2.1, 25.1450	Y	1
2.2	The aircraft shall achieve roll rates ≥ 15 deg/s in cruise and landing configurations.	AL-FUN-2.2, 25.1470	Y	2
2.3	The aircraft shall maintain directional control in OEI conditions with rudder deflection ≤ 30 deg.	AL-FUN-2.3, 25.1490	Y	2
2.4	The aircraft shall maintain acceptable stability, and flying qualities in all axes across the flight envelope, with active-control equivalent criteria.	AL-FUN-2.4, 25.1710	Y	2, 6
2.5	The airframe shall have centre of gravity within the most forward and most aft limit under any certified loading.	AL-FUN-2.4, SH-REQ-3.02	Y	2
3 Provide Lift				
3.1	The aircraft shall be capable of maintaining steady, level flight at MTOW at 10,669 m altitude under ISA+0°C conditions.	AL-FUN-3.1, 25.1050	Y	2
3.2	The aircraft shall achieve $C_L \geq 1.0$ to meet take-off and landing field length ≤ 2,500 m.	AL-FUN-3.2, 25.1250	Y	2
4 Control aircraft on ground				
4.1	The aircraft shall achieve take-off within TODA ≤ 2,500 m at MTOW, consistent with ICAO runway performance and declared distances.	AL-FUN-4.1, 25.1130	Y	2
4.2	The aircraft shall meet landing distance ≤ 2,500 m and rejected take-off stopping distance ≤ 2,500 m.	AL-FUN-4.2, 25.1090	Y	2
4.3	The aircraft shall maintain directional control in crosswinds up to 20 kt during taxi, take-off, and landing.	AL-FUN-4.3, 25.2330	Y	2
4.4	The aircraft shall remain compatible with ICAO Code 4E airport limits (including wingspan, gear span, pavement loading, and gate operations).	AL-FUN-4.3	Y	0
5 Control in flight velocity				
5.1	The aircraft shall reach cruise Mach 0.79 within 40 min.	AL-FUN-5.1, 25.1110	Y	2
5.3	The aircraft shall maintain cruise at Mach 0.79 and altitude 10,668 m with range and reserve requirements satisfied.	AL-FUN-5.3	Y	2
6 Store energy				
6.1	The aircraft shall store 35,000 kg usable bio-SAF to fulfil including ICAO reserve requirements.	AL-FUN-6.1	Y	2

ID	Functional Requirements	Relation	V	MoC
7 Manage energy				
7.3	The energy system shall allow refuelling or recharging within turnaround time ≤ 95 min under airport operating conditions.	AL-FUN-7.3	Y	2
8 Provide power				
8.2	The propulsion system shall provide thrust sufficient for take-off, climb, cruise, and OEI performance requirements.	AL-FUN-8.2	Y	2, 5, 6
8.3	The aircraft shall supply electrical power sufficient for all onboard electric systems and mission needs.	AL-FUN-8.3	Y	2
8.5	The aircraft shall have sufficient power for pressurisation capability to maintain cabin altitude ≤ 8000 ft during cruise.	AL-FUN-8.5, 25.8410	Y	2
8.6	The aircraft shall have sufficient power to maintain system temperatures within operative range for all components, and the energy system.	AL-FUN-8.6	Y	4, 5, 8
8.8	The propulsion and power system shall support safe continued flight and landing after loss or degradation of one power source.	AL-FUN-8.7	Y	3, 5, 6
10 Accommodate payload				
10.5	The aircraft shall carry cargo mass ≥ 9,000 kg with standard loading systems.	AL-FUN-10.3, 25.8550	Y	2
10.7	The aircraft shall provide a certified cabin environment equipped with integrated seating, life support, and utility systems necessary to sustain passenger safety and comfort for the duration of the mission.	AL-FUN-10.4	Y	1
10.9	The aircraft shall be compatible with ICAO aerodrome code 4E.	AL-FUN-10.5	Y	2
12 Maintainability				
12	The aircraft shall enable routine turnaround inspections within TBD minutes with no need for disassembly of multiple parts.	SH-REQ-3.12	N	5, 10
13 Airport compatibility				
13	The aircraft shall be compatible with airport waste management systems.	SH-REQ-3.13	N	5, 9

4.5. Power & Propulsion System Requirements

The power and propulsion requirements in Table 4.5 specify the energy storage, conversion, distribution, and fault-management capabilities the system must provide to satisfy the aircraft-level requirements. They are grouped by function and traced back to their originating requirements.

Table 4.5: Power & Propulsion Requirements

PP-REQ-	Requirement	Relation	V	MoC
1 Energy Storage and Conditioning				
1.1	The power and propulsion system shall isolate the primary energy source from the aircraft and external environment.	PP-FUN-1	Y	1
1.4	The power and propulsion system shall integrate monitoring of the internal storage environment to ensure all critical parameters are within safe operating thresholds.	PP-FUN-3	Y	1
1.6	The power and propulsion system shall condition the energy source to meet the required state for power conversion, as required by the conversion units.	PP-FUN-5, PP-FUN-7	Y	1
1.7	The power and propulsion system shall regulate the rate of energy transfer from storage to conversion units.	PP-FUN-9	Y	1
1.8	The power and propulsion system shall ensure compatibility with designated ground infrastructure to facilitate replenishment of the required energy content.	PP-FUN-4, SH-REQ-1.02, SH-REQ-7.01	Y	1
1.10	The power and propulsion system shall monitor the replenishment progress.	PP-FUN-6	Y	1
1.11	The power and propulsion system shall have segregated primary and backup energy sources if applicable.	PP-FUN-24	Y	1
2 Power Conversion and Distribution				
2.1	The power and propulsion system shall generate enough controlled thrust from the available energy sources, to pass the CS-25 OEI climb requirements and have a TOFL no longer than 2800 meters.	PP-FUN-11, SH-REQ-3.14	Y	2
2.2	The power and propulsion system shall generate enough electrical power from the energy conversion unit(s) such that all the functionalities of the aircraft can be achieved at all stages of the mission profile.	PP-FUN-12	Y	0,2
2.6	The power and propulsion system shall be sized to provide an additional 10% power reserve above the total maximum operational demand.	PP-FUN-10	Y	1,2
2.8	The aircraft's propulsion system shall achieve an overall efficiency of at least 35% during cruise.	SH-REQ-1.16	Y	2
3 Control and Fault Management				
3.2	The power and propulsion system shall allocate power demand among available energy sources in accordance with pre-defined allocations.	PP-FUN-15	Y	1

PP-REQ-	Requirement	Relation	V	MoC
3.3	The power and propulsion system shall provide a back-up energy source in events of loss of a primary energy source.	PP-FUN-15, PP-FUN-23, PP-FUN-25	Y	1
3.4	The power and propulsion system shall contain independent alternative paths in case of failure or malfunction.	PP-FUN-15, PP-FUN-23	Y	1
3.5	The power and propulsion system shall physically and functionally segregate primary and backup control paths to ensure that a localized failure cannot result in the total loss of a critical function.	PP-FUN-24	Y	1
4 Thermal Management				
5 Monitoring and Data Handling				
6 Structural and Integration				
6.2	The power and propulsion system shall stay within its designated weight allocation of 73 tons.	Budget Analysis	Y	2

4.5.1. Subsystem Requirements

The subsystem requirements in Table 4.6 further decompose the power and propulsion requirements into specific demands on the energy storage, distribution, engine, and power-distribution subsystems.

Table 4.6: Energy & Propulsion Subsystem Requirements

ID	Requirement	Relation	V	MoC
1 Energy Storage				
ES-REQ-2	The tanks shall be capable of storing 35 tons of bio-SAF.	ES-FUN-1	Y	2
2 Energy Distribution				
ED-REQ-8	The energy distribution subsystem shall provide crossfeed capability, allowing any engine to be fed from any tank combination.	ED-FUN-4	Y	1
3 Engines				
EN-REQ-1	The engines shall generate at least 288.5 kN of static thrust at sea level.	EN-FUN-1	Y	9
EN-REQ-2	The engine-driven generators shall be capable of supplying a continuous electrical output of at least 884 kW during all flight phases.	EN-FUN-3	Y	9
EN-REQ-3	The engines shall have went through testing on neat SAF.	EN-FUN-1	Y	9
EN-REQ-6	The engines shall achieve a thrust-specific fuel consumption of no greater than 15 mg/Ns at cruise conditions.	EN-FUN-1	Y	2
4 Auxiliary Power				
5 Secondary Power				
6 Emergency Power				
7 Power Distribution				
PD-REQ-12	The power generation system shall provide a total installed electrical generation capacity of at least 884 kW during all flight phases, with sufficient redundancy such that the loss of any single generator does not result in total loss of essential load supply.	PD-FUN-1	Y	1,2

4.6. Airframe System Requirements

The airframe requirements in Table 4.7 specify the structural, geometric, and operational demands placed on the airframe to support flight control, ground operations, and payload accommodation, derived from the aircraft-level requirements.

Table 4.7: Airframe Requirements Verification Matrix

AF-REQ-	Requirement	Relation	V	MoC
2.3	The airframe shall provide a positive restoring roll moment in response to a sideslip angle.	AF-FUN-2.3	Y	2
3.2	In the case of one engine inoperative, the drag-split rudders shall generate sufficient yaw control to counteract the yaw moment generated by the remaining engine of 2451kN.	AF-FUN-3.2	Y	2
5.1	The airframe shall provide load path for aerodynamic forces to the main structure.	AF-FUN-5.1	Y	1,2
6.1	The airframe shall provide sufficient aerodynamic lift to balance aircraft weight across the operational flight envelope.	AF-FUN-6.1	Y	
7.6	The airframe shall withstand the vertical inertail forces during take-off, positive manouvre, negative maouvre and approach.	AF-FUN-7.6	Y	2
8.2	The airframe shall incorporate landing gears placement such that the tip over angle is 15 prevent from tipping over.	AF-FUN-8.2		
11.1	The airframe shall maintain the cabin pressure altitude of no more then 8000 feet.	AF-FUN-11.1	Y	
12.4	The airframe primary structure shall withstand the longitudinal bending moment resulting from the selected structural load cases, including the 5623 kg engine mass contribution, without exceeding the allowable stress of the selected structural material.	AF-FUN-12.4	Y	

AF-REQ-	Requirement	Relation	V	MoC
12.5	The airframe primary structure shall withstand the bending moment contributions induced by the 7304 kg outer-wing fuel mass and the 10879 kg transition-volume fuel mass per wing without exceeding the allowable stress of the selected primary structure material.	AF-FUN-12.5	Y	2
12.6	The airframe primary structure shall withstand the spanwise shear force contributions induced by the 7304 kg outer-wing fuel mass and the 10879 kg transition-volume fuel mass per wing without exceeding the allowable stress of the selected primary structure material.	AF-FUN-12.5	Y	2
13.11	The airframe doors shall use specified standard dimenions allowing passengers to board or unboard at a rate of 3 passengers per minute.	AF-FUN-13.1, SH-REQ-3.04	Y	1
13.3	The airframe shall provide a cabin exit configuration such that all required emergency exits remain unobstructed, operable, and accessible for use within 90 seconds with up to 50% of exits inoperative in case of emergency evacuation.	AF-FUN-13.3	Y	1
15.2	The airframe shall accomodate a separate non pressurised cargo hold sufficient to hold 120 passengers luggage, with assumed baggage weight per passenger of 75 kilograms.	AF-FUN-15.2, SH-REQ-2.06	Y	1
15.3	The airframe shall provide 800 meter cubic of space for passengers, including seating andemergency paths.	AF-FUN-15.3	Y	2
15.5	The airframe shall provide TBD meters cubic space for energy carrier, including structures	AF-FUN-15.5		
16.1	The aircraft shall have a maximum wingspan of 64.9 meters.	SH-REQ-3.02, SH-REQ-3.05	Y	2
16.2	The aircraft shall have a maximum height of 24.5 meters from the ground.	AF-OPS-0.00	Y	2
16.3	The aircraft shall have a maximum length of 90 meters.	AF-OPS-0.00, SH-REQ-3.02	Y	2
16.4	The airframe shall provide a maximum sill height of 5 meters	AF-OPS-0.00	Y	2
16.5	The airframe shall provide a maximum outer main gear wheel span of less then 15 meters	AF-OPS-0.00	Y	2

4.6.1. Subsystem Requirements

The subsystem requirements in Table 4.8 further decompose the airframe requirements into specific demands on the doors, landing gear, furnishings, lifting surfaces, and primary structures.

Table 4.8: Aircraft Structural and Operational Requirements

ID	Requirement	Relation	V	MoC
DO-REQ-	**Doors and Access**			
1	The passenger and cargo doors shall have dimensions and locations allowing passenger boarding, cargo loading, and service operations.	DO-FUN-1	Y	1, 5, 7
2	The passenger doors shall include type A exits.	DO-FUN-2	Y	1, 5, 7
3	The passenger door sill height shall not exceed 5.5 m from the ground to ensure compatibility with passenger boarding equipments.	DO-FUN-1	Y	2, 10
LG-REQ-	**Landing Gear**			
5	The landing gear placement shall prevent aircraft tipping during ground turning at 60 knots, while keeping the outer main gear wheel span below 15 m.	LG-FUN-3	Y	2, 10
7	The aircraft shall be compatible with standard airport pushback vehicles and provide clear guidelines for ground handling teams.	LG-FUN-4	Y	9
FR-REQ-	**Furnishings**			
3	The furnishing subsystem shall provide safe and usable space for crew, passengers, and cargo within the available airframe volume.	FR-FUN-1	Y	1
4	The furnishing subsystem shall provide passenger seating and cabin arrangement for at least 120 passengers in the selected cabin configuration.	FR-FUN-1	Y	2
5	The furnishing layout shall preserve emergency paths and allow all passengers to access emergency exits during evacuation.	FR-FUN-3	Y	1
6	The aircraft shall provide passenger seating with 100 cm leg room, support, and comfort for the intended flight duration.	FR-FUN-1	Y	2
7	The aircraft shall provide 45 cm cabin aisle space and unobstructed access for normal passenger movement during flight.	FR-FUN-3	Y	2
8	The aircraft shall provide accessible, functional, and sufficient passenger facilities, including restrooms and food service areas, meeting current commercial standards.	FR-FUN-1	Y	1
9	The aircraft shall provide individual passenger entertainment systems consistent with current commercial aircraft standards.	FR-FUN-4	Y	1
LS-REQ-	**Lifting Surfaces**			
1	The lifting surface shall incorporate 6.3 m^2 of the rudder.	LS-FUN-3	Y	2
2	The lifting surface shall incorporate 7.84 m^2 for the outer elevon.	LS-FUN-3	Y	2
3	The lifting surface shall incorporate 50.14 m^2 for the inner elevon.	LS-FUN-3	Y	2
4	The lifting surface shall incorporate 45.12 m^2 for the centre elevon.	LS-FUN-3	Y	2
5	The lifting surface shall incorporate the winglets with root width of 3.5 meters.	LS-FUN-3	Y	2

ID	Requirement	Relation	V	MoC
6	The lifting surface shall generate a lift coefficient of 1 at 64.76 m/s velocity during the take-off.	LS-FUN-1	Y	2
7	The lifting surface shall generate a lift coefficient of 0.23 at cruise velocity and altitude.	LS-FUN-1	Y	2
8	The lifting surface shall generate a lift coefficient of 0.44 of lifting force at 82.58 m/s velocity during landing.	LS-FUN-1	Y	2
9	The lifting surface shall achieve a higher L/D than an A320.	LS-FUN-2	Y	2
11	The airframe shall provide a total of 27 cubic meters of designated space for cargo.	LS-FUN-5	Y	1, 2
STR-REQ-	**Structural**			
1.1	The primary structure shall provide a continuous load path between the lifting surfaces and the centrebody.	SM-FUN-1	Y	1, 10
1.2	The outer aerodynamic contour shall be sized for the critical longitudinal bending moment identified in the fuselage bending analysis.	SM-FUN-2	Y	2
1.3	The pressurised shell structure shall withstand the selected maximum cabin differential pressure without exceeding the allowable stress of the selected shell material.	SM-FUN-5	Y	2
1.4	The internal sandwich-panel structure shall transfer pressure-shell reactions into the walls, floor and ceiling with non-negative margins for face yielding, Euler buckling, face dimpling, face wrinkling and crimping.	SM-FUN-6	Y	2
1.5	The internal column structure shall transfer pressure-shell reactions with non-negative margins for compressive yielding and Euler buckling.	SM-FUN-6	Y	2
1.6	The cabin-floor support structure shall carry the selected passenger, crew and seat inertial loads with non-negative preliminary sizing margins.	SM-FUN-7	Y	2
1.9	The fuel-tank structural cavity shall provide usable fuel volume not lower than the required mission fuel volume.	SM-FUN-8	Y	2
1.10	The fuel-tank structural cavity shall provide clearance to the surrounding primary structure according to the tank layout assumptions.	SM-FUN-8	Y	1, 10
1.11	The primary structure shall be sized and assessed for the four selected preliminary structural load cases: take-off at ($n = 1.15$), positive manoeuvre at ($n = 2.5$), negative manoeuvre at ($n = -1.0$) and landing at ($n = 1.0$), using the corresponding aircraft mass, speed and aerodynamic load distributions.	SM-FUN-4, SM-FUN-3, SM-FUN-2	Y	2

4.7. Flight Controls and Stability Requirements

The flight control requirements in Table 4.9 specify the longitudinal and lateral-directional stability, handling-quality, and control-authority criteria the aircraft must satisfy, derived from the aircraft-level stability and control requirements.

Table 4.9: Flight Control Requirements

FC-REQ-	Requirement	Relation	V	MoC
1 Maintain Longitudinal Stability and Control				
1.1	The aircraft shall exhibit positive effective static margin SM $\geq$ 5.0 % MAC (augmented, aft CG limit) at all certified flight conditions, OR employ FBW/SAS to provide equivalent effective stability.	FC-FUN-1.1	Y	2
1.2	The aircraft shall maintain pitch trim with ganged elevon deflection $\lvert\delta_e\rvert \leq 30^\circ$ throughout the certified CG envelope at all certified speeds (V_S to V_D).	FC-FUN-1.2	Y	2
1.3	The aircraft CG shall remain within the certified envelope (13.85 m to 14.87 m, nose datum) for all loading/unloading sequences from OEW to MTOW.	FC-FUN-1.3	Y	2
2 Maintain Lateral-Directional Stability				
2.1	The aircraft shall exhibit positive weathercock stability $C_{n\beta} > 0$ at all certified flight conditions including approach and crosswind.	FC-FUN-2.1	Y	2
2.2	The aircraft shall exhibit a stabilising dihedral effect $C_{l\beta} < 0$ at all certified flight conditions.	FC-FUN-2.2	Y	2
2.3	If the spiral mode is unstable, its doubling time shall be $T_{double} \geq 20$ s.	FC-FUN-2.3	Y	2
3 Provide Adequate Handling Qualities				
3.1	The Dutch roll mode shall satisfy $\zeta_{DR} \geq 0.08$, $\omega_{n,DR} \geq 0.4$ rad/s, and $\zeta\omega_n \geq 0.15$ rad/s at all certified flight conditions.	FC-FUN-3.1	Y	2
3.2	The phugoid mode shall satisfy $\zeta_{ph} \geq 0.04$ at all certified flight conditions.	FC-FUN-3.2	Y	2
3.3	The roll mode time constant shall be $\tau_{roll} \leq 1.4$ s at approach and cruise conditions.	FC-FUN-3.3	Y	2
4 Provide Control Authority				
4.1	The aircraft shall achieve a roll rate of $\geq 30\,^\circ$/s at approach speed ($V_{REF} = 85$ kt) with maximum elevon deflection.	FC-FUN-4.1	Y	2
4.2	The aircraft shall maintain directional control after failure of the critical engine at V_1 without exceeding V_{MC}, per CS-25.149 ($V_{MC} \leq 1.13\,V_S$).	FC-FUN-4.2	Y	2, 8
5 Perform Safe Manoeuvres				
5.1	The aircraft shall sustain limit manoeuvring load factors of +2.5 g and -1.0 g at all speeds up to V_D within the certified weight range.	FC-FUN-5.1	Y	2
5.2	The aircraft shall complete a standard ICAO holding turn at TBD ft with bank $\leq 25^\circ$ and rate $\leq 3^\circ$/s, at $\leq$ 230 kt IAS (below 14,000 ft).	FC-FUN-5.2	Y	2

5
Trade-off Summary

Based on the design specifications provided by the stakeholders, the full design space was identified through an in-depth literature review of current and novel technologies capable of producing a petroleum-free intercontinental airliner. In order to guide the exploration of the design space, the design was structured into selection of a propulsion system, aircraft configuration, and material selection strategy, as shown in Figure 5.1.

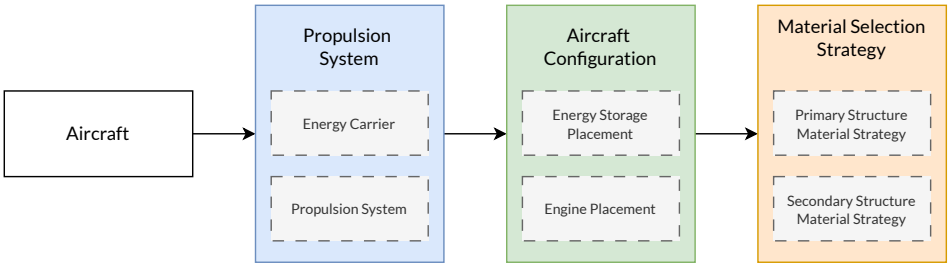

Figure 5.1: Structure of design space

Figure 5.1 additionally shows the elements of each top-level design choice. Choosing the propulsion system consists of choosing an energy carrier and the propulsion system (engine) itself, the aircraft configuration chooses the positioning of energy storage and engine, and finally the material selection strategy chooses a material strategy for both primary and secondary structures. These elements were identified as the key design parameters with the greatest potential of minimising the overall petroleum use of the aircraft. Within the material selection strategy, composite systems using conventional carbon and glass fibres, bio-based acrylonitrile (Bio-ACN) carbon fibre, and bio-based epoxies were included to vary both structural performance and petroleum content.

This chapter outlines the design space explored in Section 5.1, culminating in the full design option tree. Section 5.2 analyses the feasibility of the concepts generated by the design option tree through a systematic feasibility framework, while Section 5.3 then discusses the methodology of how feasible concepts are evaluated and compared, including how low-Technology Readiness Level (TRL) bio-based materials are traded against certification and supply-chain risk, in order to arrive at a final design concept in Section 5.4.

5.1. Design Option Tree

Based on a literature review and novel concepts, the design option tree was populated by solutions that are thought to be able to avoid the use of petroleum in aviation and achieve the top-level aircraft requirements as shown in Table 5.1. Notably, the energy carriers, with the exception of synthetic kerosene, are all non-hydrocarbon based fuels. SAF and liquid hydrogen (LH_2) were identified in particular as the most promising energy carriers for the given top-level aircraft requirements, largely due to their ability to achieve the minimum flight range of 3000 km. On the materials side, strategies span from extensive use of high-performance Carbon Fibre Reinforced Polymer (CFRP) and Glass Fibre Reinforced Polymer (GFRP) to concepts that deliberately minimise composite use, combined with either conventional or bio-based fibre–matrix systems.

Table 5.1: Top-level Aircraft Requirements

Requirement ID	Description
MS-REQ-2.6	The maximum development cost shall be no more than 50 billion euros.
MS-REQ-3.1	The first flight shall take place by 2031.
MS-REQ-3.2	The aircraft shall be operable by 2035.
MS-REQ-5.2	The aircraft shall have a minimum flight range of 3000 km.
MS-REQ-5.3	The aircraft shall be capable of covering 6000 km in 24 hours.

5.2. Design Space Pruning

A comprehensive analysis was performed on all of the 421,120 resultant design options shown in Section 5.2. The pruning was performed through an analysis of each concept's technology readiness level and achievable range in the design. Based on the top-level aircraft requirements shown in Table 5.1, any concept that did not pass all of these requirements was entirely eliminated as a considered design option.

A TRL prediction model was used to gain a quantitative understanding of each technology's feasibility of application.

Any design with a first flight or certification probability below 70% was eliminated. For the range-based requirements, the Breguet equations were used and any concept unable to reach 3,000 km was pruned.

For material strategies, TRLs were assigned to the full composite system (fibre, matrix and manufacturing route) using a weakest-link principle. Conventional CFRP and GFRP with petroleum-based epoxy are already certified on current aircraft and therefore received high TRL and material-availability scores, while bio-epoxies and Bio-ACN carbon fibres are still scaling up towards aerospace use and thus scored lower on both TRL and availability, especially when combined. As a result, aggressive bio-composite strategies remained technically attractive but were treated as higher risk for the 2031/2035 schedule.

The result of this pruning process was an elimination of 99.97% of all design options, leaving only 124 feasible design options able to be flown by 2031 and certified by 2035, matching the wishes of the stakeholders.

5.3. Trade Off Methodology

These 124 design concepts were then also comprehensively analysed through a Python program that assigned weights to many different qualities of each design, ranging from aerodynamic performance to market niche.This broad spectrum of considerations meant that the stakeholders were able to choose a trade-off strategy that aligned with their personal interests. The proposed trade-off strategies with their respective weights are shown in Table 5.2.

Table 5.2: Top-level criteria weights per strategy.

Criterion	Strategy		
	Market Niche	**Sustainability**	**Performance**
Mission Performance	25%	20%	35%
Technical Feasibility & Performance	15%	20%	20%
Operations	30%	20%	15%
Material Sustainability	15%	30%	10%
Safety	5%	5%	5%
Risk	10%	5%	15%

It is noted that the criteria shown in Table 5.2 are only the top-level criteria and also include many sub-criteria which have been omitted from this report to keep it concise. For material strategies, the trade-off explicitly balances structural performance and non-petroleum content against TRL and material-availability risk. Bio-ACN and bio-epoxy systems increase Sustainable Material Share but currently have lower maturity and less proven supply chains, whereas conventional CFRP and GFRP with conventional epoxy provide high TRL and availability at the cost of higher petroleum content.

5.4. Trade Off Result

The result of this extensive pruning and trade-off process was a presentation of six strawman concepts to the stakeholder, where the selected design was a bio-SAF blended wing body aircraft using mostly conventional materials. This design is described in Table 5.3.

Table 5.3: Selected Design Concept from Trade Off

Design Option	Selected Option
Energy Carrier	Bio-SAF
Propulsion System	High Bypass Turbofan
Aircraft Configuration	Blended Wing Body
Engine Location	Above Body Engine(s)
Storage Location	Load-Bearing Tank(s)
Primary Material Strategy	Minimise CFRP use + Conventional Carbon Fibre + Conventional Epoxy
Secondary Material Strategy	Minimise CFRP use + Conventional Carbon Fibre + Conventional Epoxy Minimise GFRP use + Glass Fibre + Conventional Epoxy

From a material-strategy perspective, the selected concept represents a risk-based compromise. Concepts with Bio-ACN carbon fibre and bio-epoxy offered higher non-petroleum content and future market differentiation, but their lower TRL and uncertain large-scale availability by 2031, when combined with other novel features such as the BWB and load-bearing tanks, would have significantly increased development and certification risk. Selecting conventional carbon and glass fibre composites with conventional epoxy maintains TRL 9 maturity and robust supply chains, while the 'minimise CFRP/GFRP use' strategy still reduces overall petroleum-derived material mass compared to an unconstrained composite-maximisation approach.

In the longer term, a retrofitting strategy, outlined in Section 22.5, foresees retrofitting interior and secondary structures with bio-based or recycled alternatives as these reach sufficient TRL, so that the Sustainable Material Share can increase over the aircraft lifetime without jeopardising the entry-into-service schedule.

Fuel Option
Hydrogen
Gaseous Hydrogen
Liquid Hydrogen
SAF - Synthetic/e-kerosene
Blended Synthetic Kerosene
Neat Synthetic Kerosene
Gases
Ammonia
Methane
Battery
Aircraft
Propulsion System
Energy Carrier
Propulsion System
Aircraft Configuration
Energy Storage Placement
Engine Placement
Material Selection Strategy
Primary Structure Material Strategy
Secondary Structure Material Strategy
LH2 Propulsion Systems
Combustion
Hydrogen Turbofan
Hydrogen Turboprop
Hydrogen Open Rotor/Propfan
Fuel Cell Electric Propulsion
FC Electric Propellor
FC Distributed Electric Propulsion
Hybrid Hydrogen Propulsion
FC + Battery Hybrid-Electric
Turboelectric
Hydrogen/Kerosene Hybrid
SAF Propulsion Systems
Conventional kerosene gas turbines
Turbojet
Low-bypass turbofan
High-bypass turbofan (incl. geared turbofan)
Turboprop
Advanced kerosene gas turbines
Open rotor
Boundary layer ingesting gas turbine fans
Piston engines
Compression-ignition piston engines
Hybrid-electric
Kerosene gas turbine + electric motor
Kerosene gas turbine + distributed electric fans
Kerosene piston generator + electric propulsors
Non Tube and Wing
Blended Wing Body
Flying Wing
Lifting Fuselage
Below Body Engine
Above Body Engine
Integrated Engine
Tube and Wing
Conventional Tube and Wing
Fuselage + Wing + Canards
Strut Braced Wing
Oblique Wing
Joined Wing
C-Wing
Above Wing Engine(s)
Below Wing Engine(s)
Fuselage Mounted Engine(s)
Tail Mounted Engine(s)
Wing Integrated Engine(s)
Rear Fuselage Plug Tanks
Extra Lobe Tank (Double Bubble)
Forward Fuselage Tanks
Spine Tank
Underfloor Tanks
Annular Tank
Wing-box Integrated Tanks
Pod-mounted External Tanks
Load-bearing Tanks
Distributed Micro Tanks
Primary Structures
Primary Structures' CFRP Strategy
Use CFRP where design allowables can be established
Minimise CFRP use
Carbon Fibre Strategy
Conventional Carbon Fibre
Bio-AN Carbon Fibre
Primary Structures' CFRP Matrix
Bio-epoxy
Conventional Epoxy
Secondary Structures
Secondary Structures' CFRP Strategy
Use CFRP where design allowables can be established
Minimise CFRP use
Carbon Fibre Strategy
Conventional Carbon Fibre
Bio-AN Carbon Fibre
.Secondary Structures' CFRP Matrix
Bio-epoxy
Conventional Epoxy
GFRP Strategy
Use GFRP where design allowables can be established
Minimise CFRP use
Secondary Structures' GFRP Matrix
Bio-epoxy
Conventional Epoxy
Natural Fibre Composite Strategy
Maximise natural fibre composite use
Use when convenient
Legend:
Pruned Concept
Feasible only for 2035 first flight
Feasible Concept

Figure 5.2: Design option tree

6
Post Trade-Off Risk Mitigation

This chapter presents the main technical risks identified after the concept selection. It focuses on the risks for which mitigation actions were implemented during the preliminary design phase. First, the risk assessment method used to compare the identified risks is defined in Section 6.1, while the mitigated risks are summarised in a technical risk register in Section 6.2. Finally, the pre- and post-mitigation risk maps are compared in Section 6.3 to show how the risk level changed and which risks still require further monitoring.

6.1. Risk Assessment Method

To evaluate the risks consistently, the likelihood, consequence and detectability scales are defined as follows.

Likelihood

1 **Remote:** the risk is very unlikely and would only occur if the design assumptions or protection measures prove incorrect.
2 **Improbable:** the risk is unlikely but could still occur if one key assumption or estimate proves incorrect.
3 **Probable:** the risk is likely to occur if not actively controlled.
4 **Frequent:** the risk is almost certain to occur if not mitigated.

Consequence

1 **Negligible:** local impact, minor schedule and cost consequences. No reduction in technical performance.
2 **Marginal:** partial impact on schedule and cost. Limited reduction in technical performance.
3 **Critical:** substantial cost impact and/or major schedule impact. Technical performance is noticeably affected; mission success may be questionable.
4 **Catastrophic:** one or more top-level requirements cannot be achieved.

Detectability

1 **Easily detectable:** the risk can be detected with early design checks or simple calculations.
2 **Detectable:** the risk can be detected during detailed analysis, simulations, design reviews, compliance checks or operational checks.
3 **Validation dependent:** the risk is detectable through prototype or integrated subsystem testing, certification feedback or detailed operational checks.
4 **Difficult to detect:** the risk is difficult to detect before flight testing or operation.

6.2. Mitigated Risk Register

The mitigated technical risks are summarised in Table 6.1. Each risk is evaluated using the previously defined likelihood (L), consequence (C) and detectability (D) scales. The corresponding mitigation actions and residual status are also reported.

Table 6.1: Technical risk register: mitigated risks

ID	Area	Risk statement	Final L/C/D	Mitigation implemented	Residual status
TR-01	Mission sizing	The selected concept may not meet the required 6000 km within 24 h mission after refined sizing, due to insufficient fuel volume, lower aerodynamic efficiency or an increase in aircraft mass.	1/4/1	Mission performance was evaluated using the updated mass, aerodynamic and fuel-consumption models. The final design achieves a direct one leg range of 5530 km and a 24-hour route coverage of 16000 km with a planned intermediate technical stop.	Mitigated at preliminary design level.
TR-02	Stability and control	The BWB configuration may have insufficient stability and controllability due to its tailless layout and limited control moment arms.	3/4/2	The CG range, loading diagram and static stability were assessed. The results showed that the aircraft needs fly-by-wire stability augmentation for aft-CG conditions. Candidate control surfaces were also considered, but the control-authority results still need higher-fidelity verification.	Partly mitigated; the risk remains high and requires higher-fidelity stability and control verification.
TR-06	Ground operations	Turnaround time may increase excessively due to the BWB cabin layout, above-body engine access and load-bearing tank inspection requirements.	2/3/2	A representative turnaround and GSE layout was defined, assuming parallel servicing where possible. The study considered stand clearance, service-vehicle positioning and access needs caused by the BWB cabin, above-body engines and load-bearing fuel tanks.	Reduced; detailed GSE layout and maintenance-access validation are still required.

ID	Area	Risk statement	Final L/C/D	Mitigation implemented	Residual status
TR-07	Fuel-tank maintenance	Load-bearing fuel tanks may be difficult to inspect and maintain, creating leakage/fatigue monitoring issues.	2/3/2	The maintenance concept includes routine inspection of the integrated load-bearing fuel tanks. Leak checks, sensor checks and pressure/strain monitoring are proposed to detect leakage or fatigue damage during line maintenance, A-checks and deeper internal inspections.	Reduced; detailed access, sealing and sensor integration still need to be designed.
TR-11	Evacuation	The BWB cabin layout may not allow passenger evacuation within the required certification limits.	2/4/3	The cabin layout was defined with multiple aisles and distributed emergency exits sized using CS-25 guidance. This provides several evacuation routes and reduces the dependence on a single exit path.	Partly mitigated; a detailed evacuation simulation is still required to verify compliance with the 90 s evacuation requirement.
TR-12	Pressurisation	The non-cylindrical BWB pressure vessel may not demonstrate sufficient structural integrity under cabin pressurisation loads.	2/4/2	A multi-bubble pressure shell concept was selected and sized for the cabin pressure loads. The pressure shell thickness and the internal trapezoidal support structure were sized at preliminary level.	Partly mitigated; carried forward to future risks.
TR-16	Diversion operations	Suitable diversion airports may be insufficient for some routes because the BWB configuration requires adequate runway length, stand clearance, taxiway compatibility, passenger handling and maintenance access after abnormal operations.	2/3/2	Airport compatibility checks were included for runway length, stand clearance, taxiway compatibility, outer main gear wheel span and ground-support access. These checks reduce the risk that the selected BWB concept is incompatible with major airport infrastructure.	Reduced; route-specific checks remain required.

6.3. Pre- and Post- Mitigation Risk Maps

Based on the evaluation of the risks described in Section 6.2, the following risk maps are produced.

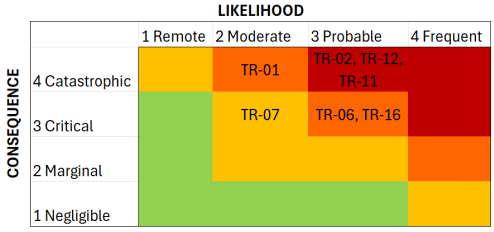

Figure 6.1: Pre-mitigation technical risk map

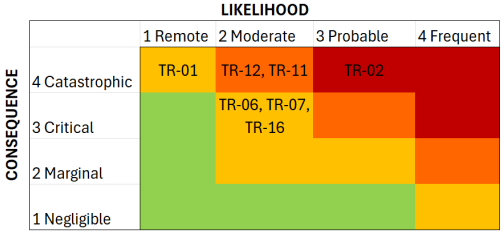

Figure 6.2: Post-mitigation technical risk map

The post-mitigation risk map shows that most risks moved to a lower likelihood level after the mitigation actions were applied. TR-01 shows the largest reduction while TR-02 remains in the high-risk region. Although stability and control analyses were performed and fly-by-wire (FBW) stability augmentation system (SAS) was included in the concept, the preliminary results needs to be confirmed with higher-fidelity methods. Therefore, the risks that are only partly mitigated, namely TR-02, TR-11 and TR-12, are carried forward to the future risk analysis, presented in Chapter 24.

Part II: Technical Sizing

7

Multidisciplinary Design Analysis and Optimisation

Multidisciplinary Design Optimisation (MDO) provides a systematic framework for aircraft design by treating key disciplines, such as aerodynamics, structures, propulsion, and stability and control, as a coupled system. For a BWB configuration, many of the trade-offs are strongly interconnected, so a purely sequential design strategy risks converging to an inconsistent or sub-optimal solution. By contrast, an MDO framework enables the definition of system-level design variables, constraints, and objectives, and ensures that changes are propagated across all disciplines.

To implement this framework, OpenMDAO was selected as the primary tool. OpenMDAO is an open-source Python package that facilitates multidisciplinary design analysis and optimisation, which allows modular model construction, explicit definition of interfaces between disciplines, and, in principle, the application of automated optimisation [3]. In this project, OpenMDAO is used primarily as an analysis tool, taking geometry, aerodynamics, mass estimation, propulsion, and stability all into account. This is particularly valuable for the BWB concept, since the non-conventional geometry make manual tracking of variables both difficult and error-prone.

Industrial-grade MDO frameworks are typically the result of extensive development and refinement, for example, the AGILE project - a collaboration between 19 industry partners - took 15 months to deploy their MDO system [20]. Given this project's team's limited prior experience with OpenMDAO or MDO frameworks in general, and the limited timespan of 3 weeks to develop and execute, this tool is developed with an emphasis on learning rather than an expectation of a fully mature tool. And as such, a lower level of robustness and completeness is acknowledged and accepted.

This chapter therefore has two main objectives. First, section 7.1 presents the overall model architecture, including the problem formulation, disciplinary decomposition, and data flow between modules. The rationale behind these choices is discussed in the context of BWB design. Secondly, section 7.2 describes the practical implementation in OpenMDAO, with particular attention to subsystem interfaces, encountered challenges, and limitations. Where the initial goal of full optimisation could not be realised, the model instead functions as a consistent coupled analysis tool, and the implications of this are critically assessed.

7.1. Model Architecture

The multidisciplinary design analysis model is structured according to the architecture shown in figure 7.1. The eXtended Design Structure Matrix (xDSM) illustrates the primary analysis blocks, design variables, coupling variables, and the flow of information required to reach a consistent aircraft design [21].

A notable feature of this architecture is the placement of the Class I and Class II weight estimation modules around the remainder of the system. This reflects the fact that a valid design solution is obtained when the maximum take-off weight (MTOW) converges to a consistent value. The associated feedback loop is solved using a Nonlinear Block Gauss–Seidel (NLBGS) method, which applies fixed-point iteration across the coupled subsystems.

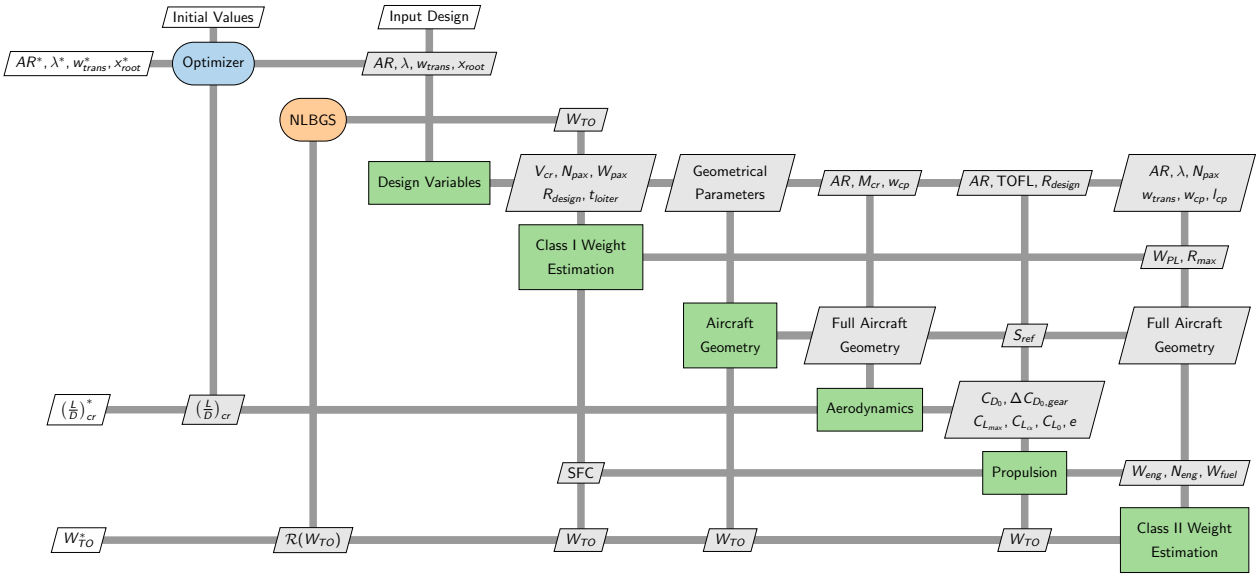

Figure 7.1: xDSM of the BWB design tool

The execution order of the modules, shown in Figure 7.1, proceeds from left to right. This ordering is chosen to minimise backward coupling and reduce the number of required iterations. It broadly follows the conventional aircraft design sequence, which similarly limits iteration when performed manually.

Although the xDSM is presented here as a documentation tool, it would have been beneficial to construct a similar design structure earlier in the project. Instead, the model architecture was developed using OpenMDAO's N2 diagram in combination with whiteboard sketches. The N2 diagram proved particularly valuable due to its interactive nature, and was instrumental in debugging and refining the model structure.

7.2. MDAO Implementation

Each module shown in Figure 7.1 has a defined interface, although maintaining consistency across these interfaces remains a key challenge. OpenMDAO mitigates part of this complexity by enforcing unit consistency between connected variables, reducing the risk of propagation of conversion errors through the model.

7.2.1. Framework Overview

OpenMDAO represents the design problem as a hierarchical system of `Group` and `ExplicitComponent` objects, each defining its own inputs, outputs, and partial derivatives. This structure allows the framework to assemble a global Jacobian and manage data flow across the coupled system [3].

Each disciplinary group is developed based on a high-level feasibility analysis aligned with its respective requirements. Subsection 7.2.2 outlines the structure of the codebase and the role of each module within the overall system.

7.2.2. Discipline Groups

Geometry Group

The `GeometryGroup` incrementally builds up the full three-dimensional aircraft geometry, as shown in Figure 7.2. This process is further detailed in Chapter 9.

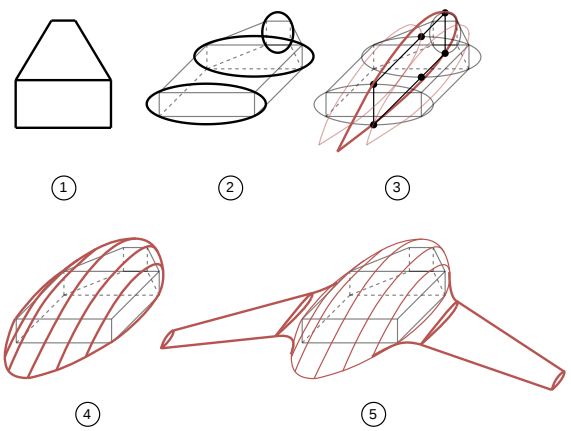

Figure 7.2: BWB Geometry Build-up

Aerodynamics Group

The `AerodynamicsGroup` interfaces with the Athena Vortex Lattice (AVL) solver to evaluate aerodynamic performance at key operating conditions, primarily cruise at $M_{cr} = 0.79$ and $h = 10{,}668$ m [22].

The geometry from `GeometryGroup` must be in an AVL-friendly format, and this requirement guided the development of the aircraft geometry build-up.

Propulsion Group

The `PropulsionGroup` sizes the propulsion system using the `PropulsionSizingComponent`, based on three primary considerations: balanced field length, take-off climb gradient, and cruise fuel consumption.

7.2.3. Solver Strategy

The top-level MTOW feedback loop, is solved using a `NonlinearBlockGaussSeidel` solver with Aitken relaxation. The initial relaxation factor is set to $\omega_0 = 0.4$, increasing adaptively up to 1.0. Convergence is defined by an absolute residual of 1 kg on MTOW, with a maximum of 150 iterations.

Aitken relaxation is required to stabilise the iteration, which otherwise oscillates due to strong coupling between aerodynamic efficiency, fuel mass, and structural weight. A feasible initial guess of $W_{MTO,0} = 100{,}000$ kg ensures convergence within the desired solution space.

7.2.4. Model Verification

Model verification follows a structured approach:

1. **Connection verification:** The N2 diagram and `prob.list_problem_vars()` are used to confirm correct variable connections and identify unconnected inputs or outputs.
2. **Unit consistency:** OpenMDAO enforces unit definitions for all variables and flags inconsistencies during connections, reducing the likelihood of unit-related errors.

8
Class I Weight Estimation

This chapter presents a Class I estimation of the maximum take-off weight (MTOW). The payload weight, fuel fraction (via fixed mission fractions and the Breguet equations), and a statistical OEW relation are combined iteratively to converge on the MTOW estimate.

In order to obtain an initial estimate of the MTOW, a Class I weight estimation is performed. Following the methodology of Roskam [23] as applied to a BWB by van Dommelen and Vos [5], the payload weight is first computed using Equation 8.1

$$W_{\text{PL}} = N_{\text{pax}} \left(W_{\text{pax}} + W_{\text{lug}} \right), \tag{8.1}$$

where N_{pax} is the number of passengers, W_{pax} the assumed person weight, and W_{lug} the luggage weight per person, and the last two combined is assumed to be 150 kg, thus yielding a total payload weight of 18,000 kg.

The overall fuel fraction M_{ff} is obtained through Equation 8.2 [5, 23]:

$$M_{\text{ff}} = \prod_{n=1}^{m} \frac{W_{n+1}}{W_n}, \tag{8.2}$$

where W_n represents the fixed fuel fractions for each stage. These span engine start-up, taxi, take-off, climb, descent, and landing, and their values are taken from Roskam [23] as listed in Figure 8.1.

Table 8.1: Fixed mission fuel fractions [5, 23].

	Phase	Fuel fraction
$M_{1,0}$	Start-up	0.990
$M_{2,1}$	Taxi	0.995
$M_{3,2}$	Take-off	0.980
$M_{4,3}$	Climb	0.980
$M_{6,5}$	Descent	0.990
$M_{8,7}$	Landing, taxi, shut-down	0.995

Regarding the three primary fuel-consuming phases (cruise, alternate-destination cruise, and loiter), the fuel fractions are computed using Breguet's range and endurance equations [5] outlined by Equation 8.3:

$$R_{\text{cruise}} = \frac{V}{c_j\, g} \frac{L}{D} \ln\left(\frac{W_4}{W_5}\right), \qquad E_{\text{loiter}} = \frac{1}{c_j\, g} \frac{L}{D} \ln\left(\frac{W_6}{W_7}\right), \qquad R_{\text{cruise,alt}} = \frac{V}{c_j\, g} \frac{L}{D} \ln\left(\frac{W_8}{W_9}\right), \tag{8.3}$$

where V is the true airspeed, c_j the specific fuel consumption (SFC) in kg fuel/(N thrust s), g the gravitational acceleration, and L/D the lift-to-drag ratio. Rearranging each of these expressions for the corresponding weight fraction yields Equation 8.4:

$$\frac{W_{n+1}}{W_n} = \exp\left(-\frac{R\, c_j\, g}{V\,(L/D)}\right) \quad \text{(cruise segments)}, \qquad \frac{W_{n+1}}{W_n} = \exp\left(-\frac{E\, c_j\, g}{L/D}\right) \quad \text{(loiter)}. \tag{8.4}$$

The SFC value is $5.80 \cdot 10^{-6}$ kg/(N · s). For BWB aircraft, the maximum lift-to-drag ratio $(L/D)_{\text{max}}$ is taken from Liebeck [24], and the cruise value is estimated following Raymer as $0.866\,(L/D)_{\text{max}}$ [25].

The MTOW is determined from balancing payload weight, operational empty weight (OEW), and fuel weight (FW) using Equation 8.6 [5, 23]:

$$W_{TO} = W_{PL} + W_{OE} + (1 - M_{ff})\, W_{TO} \tag{8.5}$$

which can be rearranged to solve for W_{TO} using Equation 8.6.

$$W_{TO} = \frac{\left(W_{PL} + \frac{W_{OE}}{W_{TO}} \cdot W_{TO}\right)}{M_{ff}}, \tag{8.6}$$

where, since no detailed component breakdown is available at this stage, the OEW is related to MTOW through the statistical relation viewed on Figure 8.1:

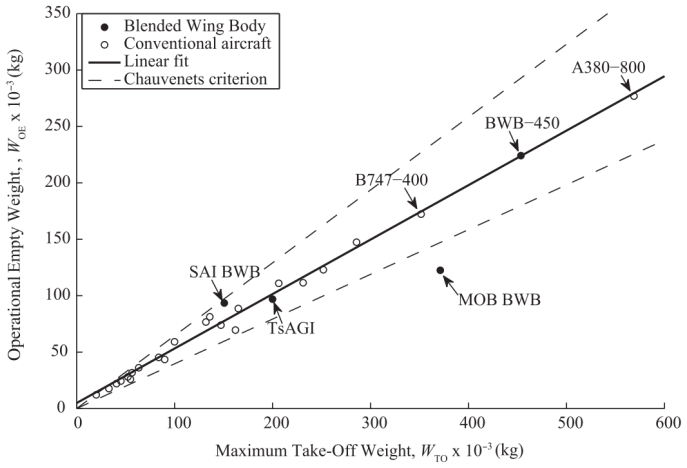

Figure 8.1: Take-off weight versus operational empty weight. Conventional aircraft from Roskam, and BWB-450 data from Liebeck [8, 24].

An initial guess for W_{TO} is taken as an input and it iterates until convergence.

9
Geometry & Layout

The geometry and layout is the backbone for the whole analysis. Starting with the cabin geometry and airfoil selection, base dimensions for fuselage and wing sizing are defined, which are after fed to the next analysis modules. The cabin geometry is discussed in Section 9.1, while the cabin fitting with the airfoil and cabin layout, and airfoil selection are explained in Section 9.2 and Section 9.3. Finally, the determination of the wing planform can be found in Section 9.4.

9.1. Cabin Geometry

The aircraft geometry sizing starts with the cabin geometry, following the BWB method of Brown and Vos [26]. This is suitable for the present aircraft because the centrebody size is main driven by the passenger cabin size. The cabin is first defined as a two-dimensional planform in the x-y plane. The vertical section is considered afterwards by fitting the cabin inside the selected centrebody airfoil and forming the oval shaped multi-section pressure shell around it.

The cabin planform consists of a forward tapered section and a constant-width rectangular centre section. In the general method, an aft tapered section can also be included [26]. The length of the forward section is denoted as l_0. Specifically, the centre and aft lengths are then written in Equation 9.1.

$$w_1 = v_1 l_0, \qquad w_2 = v_2 l_0, \tag{9.1}$$

where v_1 and v_2 are width-to-length ratios. This way, the cabin length is not chosen directly. It is an output from the required cabin floor area and the selected shape ratios.

The required floor area is calculated from the passenger number and the assumed passenger density. For the POGA, the cabin is sized for 120 business-class passengers. A design value of 2.5 m^2 per passenger is used, including seats, aisles, lavatories, galleys and local service space. This gives:

$$S_{\text{floor}} = 120 \times 2.5 = 300 \text{ m}^2.$$

The floor area of the parametrised cabin can be written as Equation 9.2:

$$S_{\text{floor}} = [0.5 v_1 + u_1 v_1 + 0.5 u_2 (v_1 + v_2)] l_0^2 + 0.5 w_{\text{cp}} l_0, \tag{9.2}$$

where w_{cp} is the most forward cockpit/cabin width [26]. For the aircraft with low passenger numbers, the aft cabin taper is not used in the seated cabin sizing, so $u_2 = 0$ and $v_2 = 0$. With $w_{\text{cp}} = 4.50$ m, $u_1 = 1.05$ and $v_1 = 1.95$, solving Equation 9.2 gives $l_0 = 9.60$ m. As a result, the main cabin length and maximum width are therefore:

$$l_{\text{cabin}} = (1 + u_1) l_0 = 19.68 \text{ m}, \qquad w_{\text{max}} = v_1 l_0 = 18.72 \text{ m}.$$

With the parameters defined, the cabin planform is defined and shown in Figure 9.1.

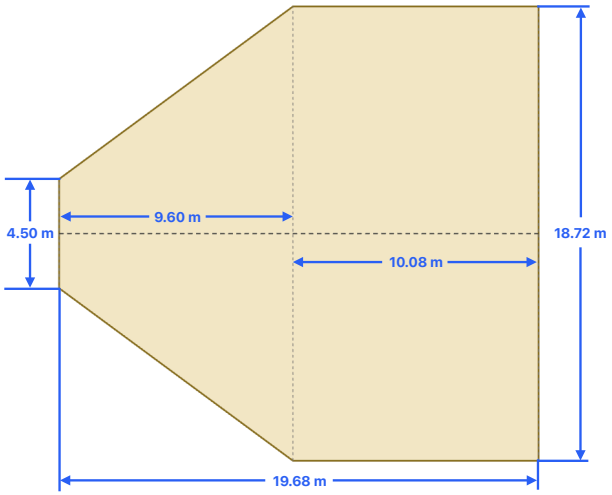

Figure 9.1: Cabin planform dimensions used for the present BWB layout

Furthermore, an alternate economy-class configuration would allow 250 passengers at 1.2 m^2 per passenger with the same cabin geometry. The wide planform is one of the main reasons why the BWB cabin can be much shorter than a tube-and-wing (TAW) cabin with the same passenger number, which reduces the profile drag.

After the planform is sized, the cabin is fitted inside the selected centrebody airfoil with airfoil selection details depicted in Section 9.3. The geometry and layout checks whether the required cabin length and structural height can be contained within the available airfoil length and thickness. This should be done without having an over-sized length for the fuselage. The cabin floor is used as the reference, while the cabin height together with the upper and lower shell clearances define the required structural height, as shown in Equation 9.3.

$$h_{\text{struc}} = h_1 + h_{\text{cab}} + h_3, \tag{9.3}$$

where h_{cab} is the clear cabin height, and h_1 and h_3 are the upper and lower shell heights as illustrated in Figure 9.2. These two shell heights are kept non-zero, because a flat pressure shell would be structurally inefficient under cabin pressurisation. The resulting cross-section is is treated as an oval pressure shell instead of a rectangular box. Since the shells are also pressurized, h_1 is designed for the crew rest area and h_3 for the lower luggage deck.

9.2. Cabin Layout

The cabin layout is made according to the cabin planform. The layout examines how the aircraft can include 120 passenger under business class layout. Seats are distributed within the cabin area while the remaining space is used for aisles, lavatories, galleys and service areas. The layout remains conceptual. The aim is to check if the cabin geometry gives enough usable floor area and feasible passenger arrangement for the BWB planform dimension.

As illustrated, the cabin width changes along the tapered section. Therefore, the number of seats in each row depends on the local cabin width. The rectangular section carries more than half of the passengers. Cabin doors are distributed along the cabin sides. The position should be checked together with the evacuation analysis and detailed structural analysis. The layout design can be found in Chapter 13.
The vertical cabin fit is selected and checked with MH82 centre-body airfoil, as shown in Figure 9.2. The figure illustrates that the cabin planform can be places inside the available airfoil section. The thickness above and below the cabin is used for pressure shell and local structural integrity.

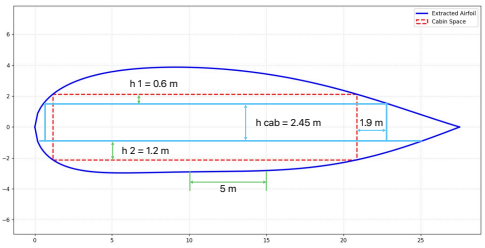

Figure 9.2: Cabin section fitting with MH82 airfoil

A 1.9 m service section is added at the rear of the cabin. It is also pressurised and continuous with the main cabin but not used for passenger and crew seats. It is reserved for lavatories, galleys and service equipments. Therefore, it increases the useful cabin volume, but is not counted as an additional to the fore mentioned 300 m^2 seated floor area. This gives an extension as a negative taper in the rear fuselage in the two-dimensional geometry planform, illustrated in Figure 13.1. In Figure 9.3 the geometry build up logic can be inspected.

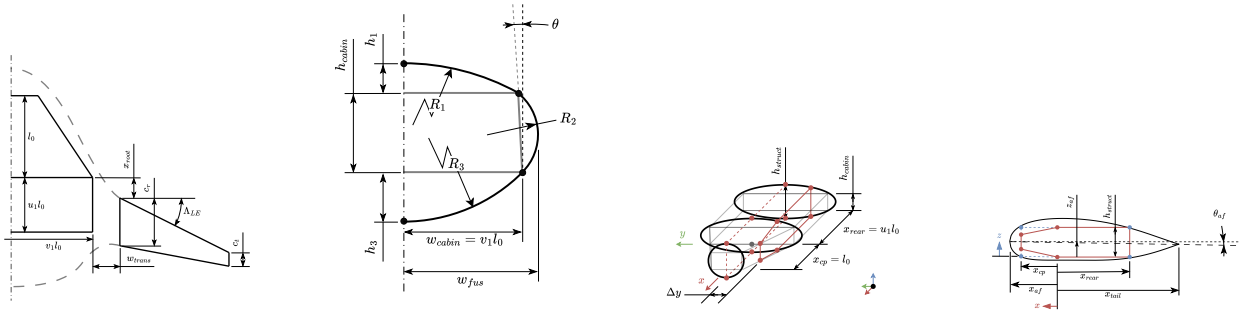

(a) Aircraft planform definition **(b)** Fitted oval geometry **(c)** Fuselage box slices **(d)** Airfoil fitting geometry

Figure 9.3: Aircraft geometry definitions

9.3. Airfoil Selection

To begin with fuselage planform, the airfoil has to be selected. For BWB aircraft, the fuselage itself and the outer wing have different selected airfoils.

9.3.1. Fuselage Airfoil

One of the most challenging aspects of the BWB is the stability, which is why the reflexed airfoils were chosen for the centrebody of the aircraft. In total, five of the airfoils were chosen, and are shown in Table 9.1 along with their basic characteristics.

Table 9.1: Parameters of Candidate BWB Airfoil Profiles

Airfoil	Max Thickness	Thickness Position	Max Camber	Camber Position
BW 05 02 09[1]	9.3%	31.92% c	1.9%	28.24% c
Fauvel-il[2]	14.0%	25.20% c	1.9%	28.24% c
MH78[3]	14.4%	22.10% c	1.9%	17.90% c
MH82[4]	13.3%	24.60% c	3.9%	24.60% c
TL54[5]	10.0%	26.46% c	2.4%	33.83% c

For the selection, it is essential to choose criteria based on which the trade-off is to be conducted. Those criteria are: C_l/C_d at 2° angle of attack, cabin fitting, C_l at 2° angle of attack, stability, and transonic regime adaptation. All of those parameters are highly important, so it is chosen to give them the same weight of 20%. To assess the trade-off, each airfoil received the grade 1-5 for each criteria and consequently the best airfoil was chosen.

The airfoil lift to drag (L/D) is the parameter that compares performance. This parameter is evaluated based on the XFLR5 analysis. Because this program is not made for the transonic regime it is decided to use Mach = 0.00, but adjust the Reynolds number to 5,000,000 to compensate for the cruise Mach. While the values might be non-representative for cruise speed, it is expected to see the overall ranking to be correct. The angle of attack is decided based on the fact that the cruise is usually around 2°.

The lift coefficient at 2° of angle of attack is parameter comparing the lift potential of the airfoil at the cruise conditions. Similarly the lift to drag parameter is estimated based on the XFLR5 analysis, along with the stability of the airfoil. It is preferable that C_m/α is positive for the stability of the airfoil. The results of the XFLR5 analysis can be seen in the Figure 9.4.

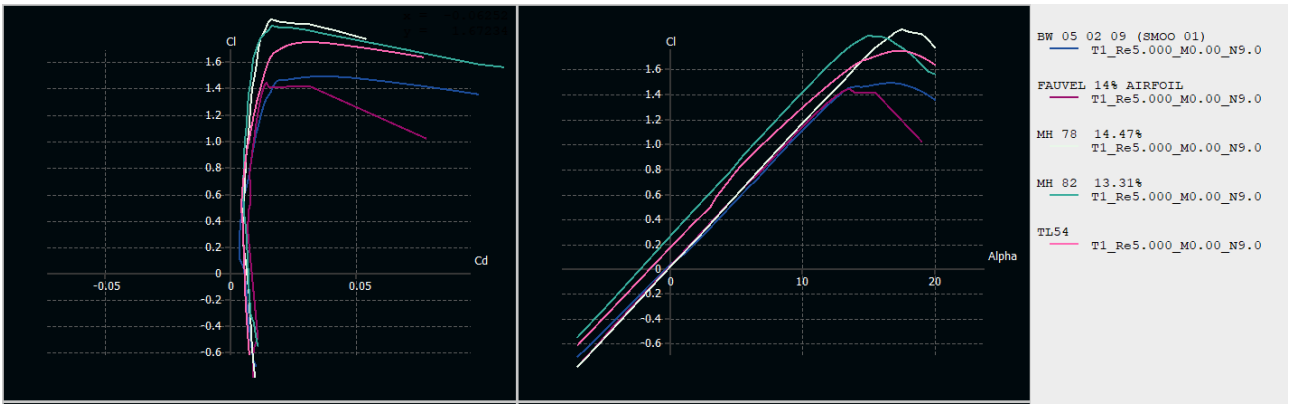

Figure 9.4: Aerodynamic pressure distribution across the BWB centrebody.

The cabin fitting is the parameter that compares on how easy it is to fit the rectangular cabin in the airfoil. This parameter is estimated based on how much effective space is occupied by the rectangular cabin with respect to area of the airfoil. Lastly, the transonic regime adaptation. Since the shock wave creation on the surface on the airfoil cannot be estimated, it is to be done qualitatively. The main characteristics that point towards better airfoil for transonic regime are flatter top, lower thickness to chord ratio, higher radius leading edge and thinner trailing edge [27], which are to be qualitatively assessed. The grading as well as final ranking is shown in Table 9.2.

Table 9.2: Airfoil Selection Trade-off Matrix (Equal Weights)

Airfoil	C_l/C_d	Cabin Fit	C_l	Stability	Transonic	Total	Rank
BW 05 02 09	3	5	2	2	5	3.4	3
Fauvel-il	2	3	2	2	2	2.2	5
MH78	2	5	2	2	2	2.6	4
MH82	5	4	5	5	3	4.4	1
TL54	3	3	4	4	5	3.8	2

Based on the trade-off, the MH82 is chosen as a body airfoil for the BWB.

9.3.2. Change of Body Airfoil

After running the analysis with the chosen airfoil, it is clear that there is no feasible designs. After fitting the cabin inside the airfoil the body length came out to be 44.98 meters, and the corresponding reference area of the whole lifting surface was calculated to be 1098.65 m^2. Such a high area crashed aerodynamic aspect of the design, as the drag increases drastically, which resulted to the maximum L/D being 7.12. This increase in drag also directly affected the fuel consumption to be multiple times higher than conventional airliners. Thus, radical changes had to be made to make the design feasible. The airfoil was optimised to fit the the cabin with the smallest possible chord, such that the

[1] URL `https://www.bigfoil.com/e82a78a0-2e3b-4dde-bd60-7643d3a49ebf_info.php` [Cited 2nd of June 2026]
[2] URL `http://airfoiltools.com/airfoil/details?airfoil=fauvel-il` [Cited 2/06/2026]
[3] URL `http://airfoiltools.com/airfoil/details?airfoil=mh78-il` [Cited 2/06/2026]
[4] URL `http://airfoiltools.com/airfoil/details?airfoil=mh82-il` [Cited 2/06/2026]
[5] URL `https://www.bigfoil.com/300f6d16-4a85-4f35-bcc7-57113a80fae4_info.php` [Cited 2/06/2026]

reference area decreases.

The Class Shape Transformation was chosen, which is based on the MH82 airfoil. It was done through the AeroSandbox Python package, which had the cabin size as the only constraint. Final results can be observed in Figure 9.2. The parameters of the new airfoil, called MH82-AR, are compiled in Table 9.3.

Table 9.3: Comparison between MH82 and Optimized MH82 Airfoils

Airfoil / Configuration	Thickness [%]	at [%]	Camber [%]	at [%]
MH82	13.30	22.92	4.01	23.03
MH82-AR	24.69	30.83	1.75	34.93

As can be observed, the t/c of the MH82-AR is almost twice higher then the MH82, which does give high disadvantage at higher Mach number. While camber is lower, which potentially leads to lower lift generation. To make a full comparison, the XFLR5 analysis is established with results in Figure 9.5.

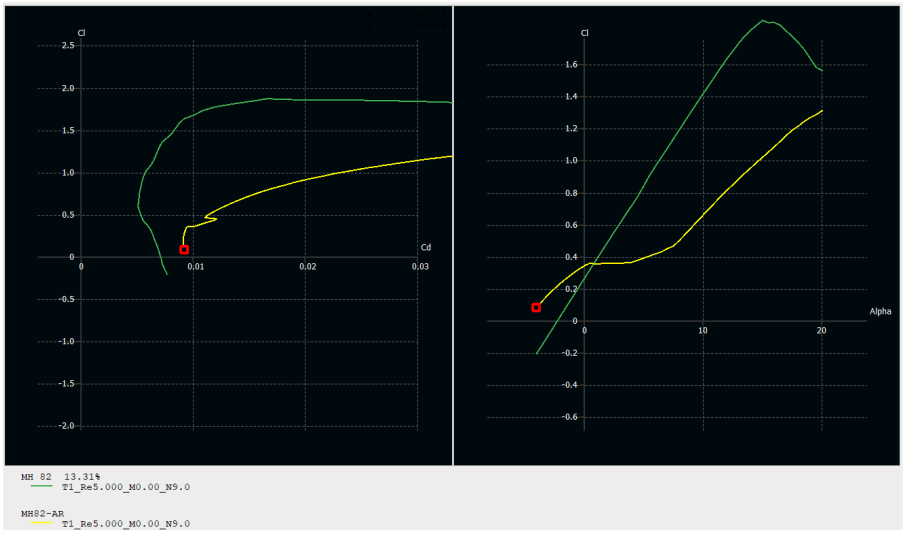

Figure 9.5: MH82 and MH82-AR comparison

While it clearly can be seen that the MH82-AR preforms worse in every aspect, when it comes to airfoil analysis, it gives an advantage of reduction of surface area, which is demonstrated in Chapter 13.

9.3.3. Outer Wing Airfoil

For the outer wing, supercritical airfoils are required to achieve acceptable performance at the cruise Mach number of $M = 0.79$. Additionally, since the BWB is a tailless configuration, the pitching moment coefficient C_m of the outer wing sections must remain moderate, as there is no horizontal tail to provide trim compensation. Five candidate sections were selected and are shown in Table 9.4 with their basic characteristics.

Table 9.4: Geometric Parameters of Candidate BWB Airfoil Profiles for the outer wing.

Airfoil	Max Thickness	Thickness Position	Max Camber	Camber Position
NASA SC(2)-0714[6]	14.0%	37.0% c	2.50%	81.0% c
Whitcomb supercritical[7]	11.0%	35.0% c	2.4%	82.50% c
NASA S(2)-0710[8]	10.0%	37.0% c	2.1%	81.0% c
NASA SC(2)-0414[9]	14.0%	36.0% c	1.5%	83.0% c
FX 63-137[10]	13.7%	30.9% c	6%	53.3% c

For the selection it is essential to choose criteria based on which the trade-off will be conducted. Those criteria are: C_l/C_d at 2° angle of attack, C_m at 2° angle of attack, $C_{l,\max}$ and Transonic regime adaptation

As all of these parameters are highly important, they are given the same weight of 25 %. To assess the trade-off, each airfoil received a grade from 1 to 5 for each criteria and then the best airfoil was chosen. The airfoil lift to drag is the parameter that compares performance. This parameter is evaluated based on the XFLR5 analysis. Since this program is not made for the transonic regime, it is decided to use Mach = 0.0, but adjust the Reynolds number to 5 million, to compensate for the cruise Mach. while the values might be non-representative for cruise speed, it is expected to see the overall ranking to be correct. The angle of attack is decided based on the fact that the cruise is usually around 2°.

The pitching moment coefficient C_m at 2° angle of attack is the critical parameter distinguishing the outer wing

[6] URL `http://airfoiltools.com/airfoil/details?airfoil=sc20714-il` [Cited 2/06/2026]
[7] URL `http://airfoiltools.com/airfoil/details?airfoil=whitcomb-il` [Cited 2/06/2026]
[8] URL `http://airfoiltools.com/airfoil/details?airfoil=sc20710-il` [Cited 2/06/2026]
[9] URL `http://airfoiltools.com/airfoil/details?airfoil=sc20414-il` [Cited 2/06/2026]
[10] URL `http://airfoiltools.com/airfoil/details?airfoil=fx63137-il` [Cited 2/06/2026]

selection from the fuselage airfoil selection. Since the BWB is a tailless configuration, there is no horizontal tail surface to generate a compensating moment. A strongly nose-down C_m therefore cannot be trimmed without deflecting control surfaces on the wing itself, directly incurring trim drag. It is therefore preferable to select an airfoil with C_m as close to zero as possible. This parameter is likewise evaluated from the XFLR5 analysis.

The maximum lift coefficient $C_{l,\max}$ compares the lift potential of each airfoil at low-speed conditions, which is relevant for approach and take-off performance. Similarly to the lift-to-drag parameter it is estimated based on the XFLR5 analysis.

Lastly, the transonic regime adaptation. Because the shock wave creation on the surface of the airfoil cannot be estimated with XFLR5, it will have to be done qualitatively. The main characteristics that point towards a better airfoil for the transonic regime are a flatter top surface, lower thickness to chord ratio, higher leading edge radius and thinner trailing edge [27]. Furthermore, the aft position of maximum camber, visible in Table 9.4 for all supercritical candidates, is indicative of aft-loaded pressure distributions which delay shock formation. The FX 63-137, with its maximum camber at only 53.3% chord, does not exhibit this characteristic and is therefore expected to perform poorly in the transonic regime. Those characteristics will be qualitatively assessed.

The results of the XFLR5 analysis can be seen in Figure 9.6a.

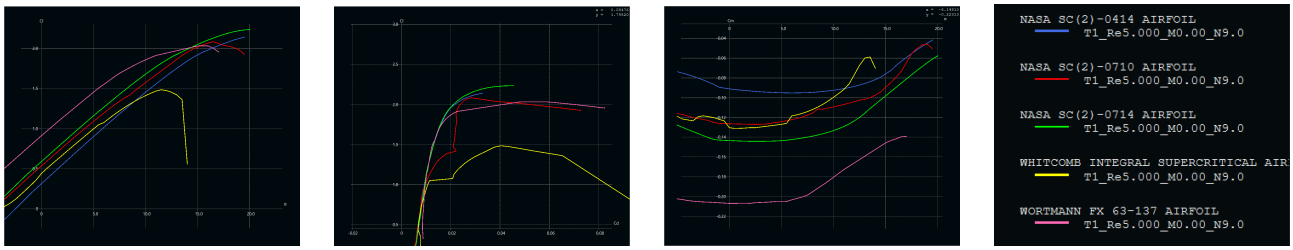

(a) Cl-alpha curves **(b)** Drag polar curves **(c)** Cm-alpha curves **(d)** Outer wing airfoils legend

Figure 9.6: XFLR 5 analysis of the airfoil selection.

The grading as well as final ranking is shown in Table 9.5.

Table 9.5: Trade-off of candidate outer wing airfoil sections (1 = worst, 5 = best).

Airfoil	C_l/C_d at 2°	C_m at 2°	$C_{l,\max}$	Transonic	**Total**
NASA SC(2)-0414	4	5	4	5	18
NASA SC(2)-0710	4	4	4	5	17
NASA SC(2)-0714	5	3	5	5	18
Whitcomb	3	3	2	4	12
Wortmann FX 63-137	2	1	4	1	8

The NASA SC(2)-0714 and NASA SC(2)-0414 share the highest total score of 18. As a tiebreaker, the design lift coefficient is considered: the SC(2)-0714 was designed for $C_l = 0.70$, which is more representative of the outer wing loading at cruise for a BWB transport, compared to $C_l = 0.40$ for the SC(2)-0414. Therefore, the **NASA SC(2)-0714** is selected as the outer wing airfoil section.

9.4. Wing Planform

The wing planform is build upon the MTOW and the fuselage reference area. The highest possible wing loading is achieved on the conditions of highest lift coefficient at the MTOW loading. The fuselage reference area is known, so it is possible to calculate the lift fuselage generates under this loading at the approach speed with Equation 9.4.

$$L_{\text{fus}} = 0.5 \cdot \rho_0 \cdot V_{\text{app}}^2 \cdot S_f \cdot C_{L_{\max_f}}, \tag{9.4}$$

where L_{fus} is the Lift that the fuselage generates, $\rho_0 = 1.225$ is the density during approach, V_{app} the approach velocity, which is defined to be maximum 166 knots [28], S_f is the fuselage reference surface area, known to be $463 m^2$, and $C_{L_{\max_f}}$ is the assumed maximum lift coefficient of the fuselage. This coefficient is estimated based on assumed maximal lift coefficient during take-off/landing, which without leading edge flaps is 0.85 [29], and the lift coefficient difference between the fuselage and the wing, which is assumed to be $C_{L_{\max_w}} = n \cdot C_{L_{\max_f}}$, where n is between 2 and 3, with the latter being chosen the sizing [24]. The $C_{L_{\max_w}}$ is estimated to be 1.275, while the $C_{L_{\max_f}}$ is 0.425.

To approximate the wing area, the lift generated by the fuselage is subtracted from the MTOW and divided by 2, such that the lift that needs to be produced per wing is estimated.

Next step is the estimation of the reference area of the wing based on the lift required. The area comes from the rearranged formula Equation 9.4.

$$S_{\text{w}} = \frac{L_{\text{w}}}{0.5 \cdot \rho_0 \cdot V_{\text{app}}^2 \cdot C_{L_{\max_w}}}$$

With this equation, the reference area to generate lift is calculated, the lift parameters such as aspect ratio, root chord, taper ratio and similar parameters need to be established. It is decided to start with the aspect ratio (AR) of the wing being the only design variables, which is to be optimised. With the wing aspect ratio and wing reference area, the wing semi-span and wingspan can be calculated with Equation 9.5.

$$b_{\text{half}} = \frac{\sqrt{AR \cdot S_{\text{w}}}}{2}, \qquad b = 2y_{\text{w}} + 2b_{\text{half}}, \tag{9.5}$$

where b_{half} is the half width of the fuselage at the connection to the wing. Next, the root chord is estimated. To achieve that, another design variable is established, specifically the taper ratio λ. The formula for root chord is geometrically estimated based on the assumption of trapezoidal geometry in Equation 9.6:

$$c_{\text{root}} = \frac{2.0 \cdot S_{\text{w}}}{b_{\text{half}} \cdot (1.0 + \lambda)}, \qquad c_{\text{tip}} = \lambda \cdot c_{\text{root}}. \tag{9.6}$$

The leading edge sweep angle is decided to be left as a design variable for the iterations. The sweep angle at quarter chord, middle chord and trailing edge are calculated based on Equation 9.7.

$$\tan(\Lambda_x) = \tan(\Lambda_{\text{LE}}) - \frac{4}{\text{AR}_{\text{w}}} \cdot x \cdot \left(\frac{1-\lambda}{1+\lambda}\right), \tag{9.7}$$

With everything listed above, Table 9.6 lists all the parameters that are needed/assumed for the wing planform and the calculated parameters.

Table 9.6: Wing Planform Design Module: Input and Output Parameters

INPUTS		**OUTPUTS**	
Maximum Takeoff Weight	Cabin Structural Width	Reference Wing Area	Leading-Edge Sweep Angle
Outer Wing Aspect Ratio	Transition Segment Width	Total Calculated Wingspan	Quarter-Chord Sweep Angle
Centrebody Surface Area	Design Cruise Mach Number	Tip Chord	Mid-Chord Sweep Angle
Outer Wing Taper Ratio	Target Cruise Altitude	Outer Wing Surface Area	Trailing-Edge Sweep Angle
Maximum Landing Lift Coeff.	Reference Approach Speed	Outer Wing Root Chord	Total Geometric Surf. Area
Maximum Wing Lift Coeff.	Aero-Structural Sizing Factor	Cruise Lift Coefficient	

This was verified through unit tests as well as by comparing hand calculated results to the outputs of the wing planform module, along with visual inspection of the geometry.

10
Aerodynamics

The aerodynamics are one of the most essential parts of the preliminary design establishment and future aircraft performance. Based on trade-off and stakeholders decision, the Blended Wing Body was chosen as the conceptual design. The BWB is a novel concept, thus it poses challenges in approximating essential aerodynamic parameters. Therefore, it is decided to use Athena Vortex Lattice (AVL) software as the main source of the aerodynamic analysis. This software was chosen based on the Okonkwo's choice in his study [4]. In Section 10.1, the usage and limitation of the AVL is discussed. Section 10.2 analyses the aerodynamic characteristics for the preliminary design.

10.1. AVL

The AVL developed by Mark Drela from MIT is the software for 3 dimensional aerodynamic analysis. This tool uses Vortex Lattice method which models the wing as horseshoe vortexes distributed along the chord and span [30]. This method is considered accurate in approximating the lift curve, induced drag and lift distribution, but poses few limitations, which has to be take into account.

10.1.1. Limitations of Vortex Lattice method

For the case of BWB flying at cruise Mach number of 0.79, there are few limitations that directly affect the results. First, compressibility of the flow is accounted by the Prandtl-Glauert correction, which can be considered accurate until the Mach number of 0.6, which is lower then the design cruise Mach [22]. The viscous drag and thickness is neglected during the AVL analysis [30]. Those limitations pose high inaccuracy considering the choice of BWB, as body airfoils thickness and viscous effect thickness would be problematic to neglect for aerodynamic analysis. Overall drag is not properly accounted for, that is why it is chosen to use the correction proposed by Okonkwo for the wave drag and profile drag [4]. With those corrections, the AVL analysis can be concluded with an adequate level of accuracy.

10.1.2. AVL Software Setup

To integrate AVL from Python, the open-source Chrysopelea github repository is used[1]. AVL itself is a command-line program with no Python API, it reads a geometry input file, accepts text commands through standard input, and writes results to standard output. Chrysopelea bridges this gap by providing a set of Python classes that represent the AVL geometry in memory, and a runner that handles all the file I/O and subprocess communication automatically. The four main classes are `Avl`, `Surface`, `Section`, and `Control`, which map directly onto the hierarchical structure of an AVL input file. An `Avl` object holds the top-level configuration: the reference quantities (reference area, mean aerodynamic chord, moment reference point) and the Mach number. It contains one or more `Surface` objects, each of which represents a lifting surface and holds a list of `Section` objects. Each `Section` defines a spanwise station with its leading-edge position, local chord, twist angle, and the path to an airfoil coordinate file in Selig format. Where a control surface is needed, a `Control` object is attached to the relevant sections, specifying the hinge position and deflection sign convention.

When an analysis is triggered, Chrysopelea processes this object tree into a valid AVL input file, writes it to a temporary directory, and launches the AVL executable as a subprocess. It then pipes a sequence of commands to AVL's standard input, setting the operating conditions, running the vortex lattice solve for each angle of attack, and requesting the force and moment output, and reads the results back from standard output. The parsed results are returned as Python dictionaries, from which the relevant aerodynamic coefficients can be extracted directly.

The BWB geometry is assembled from the outputs of the OpenMDAO sizing components. There are two main geometries that AVL will take into account, the centrebody and the outer wings. The centrebody is modelled with multiple spanwise stations derived from the fuselage planform geometry, capturing the variation in chord and leading-edge position across the wide inner section. The outer wing is defined as a separate spanwise region that attaches to the centrebody at the junction point. Together these form a single continuous lifting surface in AVL, with the port side generated automatically by mirror symmetry using the YDUPLICATE option so that only the starboard half needs to be specified. The spanwise and chordwise panel counts are set to give a reasonable resolution across both regions.

Two airfoils sections are assigned across the span. The centrebody uses the MH82 profile, and the outer wing uses the NASA SC(2)-0714 supercritical aerofoil, consistent with the design cruise Mach number of 0.79. Both profiles are provided as Selig-format .dat files. The reference area used for coefficient normalisation is the full BWB planform area S_{ref} from the wing sizing component, which includes both the centrebody and outer-wing panels.

The analysis itself is run as an angle-of-attack sweep over the linear part of the lift curve. From this sweep, a linear fit gives the lift curve slope CL_α and the zero-incidence lift coefficient CL0. The induced drag coefficient and Oswald efficiency factor are extracted at the cruise lift coefficient and these outputs are returned to OpenMDAO. Profile drag is not predicted by AVL since it is an inviscid method. It is instead estimated separately using a skin friction model and added to the induced drag to form the total drag polar used in performance analysis.

[1] URL `https://github.com/micaiah-sp/Chrysopelea`[Cited 17/06/2026]

10.2. First Aerodynamic Estimation

To begin, the basis for the aerodynamic analysis is the AVL. From the AVL, the lift coefficient and the induced drag coefficient are taken for each angle of attack. While angle of attack is representative, as mentioned in Subsection 10.1.1, the drag coefficient is incomplete taking into account only induced drag. The method of drag build up is chosen. The profile drag, wave drag and drag from engine shall be considered to form a full picture.

The wave and profile drag coefficients are calculated based on the method proposed by Okonkwo, in Equation 10.1 and Equation 10.2 [4].

$$C_{D,0} = 0.005\left(1 - \frac{2c_l}{R_w}\right)\bar{\tau}\left[1 - 0.2M_N + 0.12\left(\frac{M_N\sqrt{\cos\Lambda_{0.25}}}{A_f - (t/c)}\right)^{20}\right]R_w T_f S^{-0.1}, \tag{10.1}$$

$$\bar{\tau} = \frac{(R_w - 2)}{R_w} + \frac{1.9}{R_w}\left(1 + 0.526\left(\frac{t/c}{0.25}\right)^3\right), \tag{10.2}$$

where A_f is the airfoil factor, which is 0.93 for advanced airfoil [4], M_N is a Mach number, which is 0.79, c_l is the fraction of chord over which flow is laminar, at 0.79 Mach the 0.3 is taken as a conservative assumption, S is the reference value of the wing, which is taken from wing planform during iteration, $\Lambda_{0.25}$ is the sweep of the quarter chord, which is established by iteration, t/c is the thickness to chord ratio, which is 0.2469 for the optimized variant of the MH82 airfoil, and 0.14 for the NASA SC2 0714, the R_w is the ratio weighted area, which is estimated to be 5.5 for airliners [4] and T_f is the factor that accounts for non-ideal shape, which is chosen to be 1.15 [4].

The wave drag is calculated with Equation 10.3.

$$C_{w_L} = 0.12 \cdot M^6 \cdot C_{d_i}, \tag{10.3}$$

where C_{d_i} is taken from the AVL as an input.

Next station of drag is from the engine. It is calculated based on the standard drag build up method, described by Raymers [25], with the additional equations provided by Prof. Dr Dieter Scholz from university of Hamburg [31].

$$C_f = \frac{0.074}{Re^{0.2}}, \qquad FF = 1.0 + \frac{0.35}{l_n/d_n}$$

$$C_{D,\text{nacelle}} = C_f \cdot FF \cdot \left(\frac{S_{\text{wet,nacelle}}}{S_{\text{ref}}}\right), \qquad \Delta C_{D,0,\text{engine}} = n_{\text{engines}} \cdot k_{\text{int}} \cdot C_{D,\text{nacelle}},$$

where Re is the Reynolds number, which is assumed to be 6.5 million, l_n is the nacelle length, assumed to be 3.95 meters, d_n is the nacelle diameter, assumed to be 2.12, n_{engines} is the number of engines, depending on the iterations the number scales from 2 to 4, k_{int} is the interference factor, which is assumed to be 1.12 [31] and S_{wet} is the wetted area. The parameters for l_n, d_n and S_{wet} are inspired based on existing engines used by Airbus.

All of those drag coefficients are directly combined with the induced drag coefficient obtained from the AVL to establish the main aerodynamic parameters, such as L/D and lift coefficient graphs with respect to angle of attack.

Lastly, the cruise L/D is established. During the cruise stage of the lift shall be equal to weight. But it should be accounted for that the fuselage generates 3 times lower lift per surface area. The formula for cruise C_L is shown in Equation 10.4.

$$C_{L_{cr}} = \frac{MTOW \cdot g}{0.5 \cdot S_{L_{\text{ref}}} \cdot \rho_{cr} \cdot V_{cr}^2}, \qquad \text{with} \qquad S_{L_{\text{ref}}} = S_w + S_f/3. \tag{10.4}$$

Overall with the AVL and drag addition, all the input and output parameters from the aerodynamic module are listed in the Table 10.1.

Table 10.1: Wing Planform Design Module: Input and Output Parameters

INPUT PARAMETERS	**OUTPUT PARAMETERS**
Wingspan (b)	Max Lift-to-Drag Ratio ($(L/D)_{\max}$)
Reference Wing Area (S_{ref})	Optimum Alpha (α_{opt})
Spanwise Center of Gravity (y_{ow})	Cruise Lift Coefficient ($C_{L_{\text{cr}}}$)
Outer Wing Root Chord ($c_{\text{root\_ow}}$)	Cruise Induced Drag ($C_{D_{i_{\text{cr}}}}$)
Wing Tip Chord (c_{tip})	Cruise Total Drag ($C_{D_{\text{total\_cr}}}$)
Leading-Edge Sweep Angle (Λ_{LE})	Cruise Lift-to-Drag Ratio ($(L/D)_{\text{cr}}$)
Quarter-Chord Sweep Angle (Λ_{025})	Pitching Moment Derivative (C_{m_α})
Thickness-to-Chord Ratio (t/c)	Aerodynamic Center (AC)
Aspect Ratio (AR)	Zero-Lift Profile Drag (C_{D_z})
Design Cruise Mach Number (M_{cr})	Lift-Dependent Wave Drag (C_{wL})
Cabin Length (L_{cabin})	Engine Drag Increment ($\Delta C_{D_{0,\text{engine}}}$)
Fuselage Length (L_{fuse})	Total Zero-Lift Drag (C_{D_0})
Cockpit Length (L_{cp})	Lift-Curve Slope (C_{L_α})
Cockpit Width (W_{cp})	Zero-Angle Lift Coefficient (C_{L_0})
	Pitching Moment Pitch-Rate Derivative (C_{m_q})
	Lift Coefficient Pitch-Rate Derivative (C_{L_q})
	Neutral Point Position (x_{np})

10.2.1. Verification and Validation

To verify the code, the response to change of geometry test was performed. Such that if the geometry is drastically changed, the AVL outputs the expected values.

Specifically, if the wingspan is increased, the L/D graph should increase.

First, in the code, the wingspan for the outer wing was increased from 45 to 65, there has been an increase in L/D by 45%.

The test confirmed the expectations, when wingspan was changed to the higher value, the L/D is increased.

For validation the visual inspection of the results was used. The program prints all the aerodynamic parameters for each angle of attack. The values are then saved.

11
Power and Propulsion

Power and propulsion is an important aspect in the design, as it determines the range and efficiency of the aircraft. The design of the power and propulsion starts with the engine sizing in Section 11.1, followed by fuel mass calculation and model validation in Section 11.2 and Section 11.3, respectively. Finally, the chapter summarizes the system layout in Section 11.4.

The power and propulsion consist of the seven subsystems as defined in Table 2.1. However, the first and foremost step consists of finding the overall system mass for the Class II estimation, for which the two main contributors are the engine weight and the fuel mass, as the fuel tanks are integrated into the wing and hence do not add to the system mass. Furthermore, the weight for other equipment, sensors, piping, etc., is accounted for by applying a safety factor of 1.2 on the fuel mass. Accordingly, the first step is to size the engines, after which the fuel consumption can be calculated based on engine data, the mission profile and aircraft performance. Following, the electrical power required for systems can be evaluated, and the electrical generators for the engines can be sized and selected, along with the Auxiliary Power Unit (APU), the emergency back-up battery and the Ram Air Turbine (RAT). The fuel tank sizing is detailed in Section 16.3.1.

11.1. Engine Sizing

Engines are sized according to performance and CS-25 requirements as per AL-REQ-8.2. The most critical phases to be evaluated are the phases of the Take-Off Path as stated in CS-25.111, including reaching a screen height of 35 feet by the end of the runway, and the One Engine Inoperative initial climb conditions specified under CS-25.121, out of which the most constraining thrust requirement will be used to size the engine. The requirements employed can be seen in Table 11.1. Note that after initial evaluations, CS-25 115,119 and 121(d) are not constraining and hence are excluded from this report; furthermore, only dry conditions were subject to evaluation, as wet conditions would be particularly difficult and time-consuming to simulate, thus instead a safety factor of 1.2 will be applied for the calculation of the finalised Take-Off Field Length (TOFL).

Table 11.1: Take-Off Path Requirements.

Reference ID	Requirement Description
MS-REQ-5.5	The aircraft shall be compatible with runways of at least 2800 meters in length and meet all applicable takeoff and landing angle specifications.
CS-25.113(a)	Take-off distance on a dry runway shall be the greater of: the horizontal distance along the take-off path from the start of the take-off to the point at which the aeroplane is 11 m (35 ft) above the take-off surface or 115% of the horizontal distance along the take-off path, with all engines operating, from the start of the take-off to the point at which the aeroplane is 11 m (35 ft) above the take-off surface, as determined by a procedure consistent with CS 25.111.
CS-25.121(a)	The aircraft shall achieve a positive climb gradient for two-engined aeroplanes, ≥ 0.3% for three-engined aeroplanes, and ≥ 0.5% for four-engined aeroplanes, in the critical take-off configuration with landing gear extended, from V_{LOF} until the landing gear is fully retracted, with the critical engine inoperative and remaining engines at available thrust, without ground effect.
CS-25.121(b)	The aircraft shall achieve a climb gradient of ≥ 2.4% for two-engined aeroplanes, ≥ 2.7% for three-engined aeroplanes, and ≥ 3.0% for four-engined aeroplanes, in the take-off configuration with landing gear fully retracted, from gear retraction up to 122 m (400 ft) above the take-off surface, at V_2 with the critical engine inoperative and remaining engines at take-off thrust, without ground effect.
CS-25.111(c)	The aircraft shall accelerate at a constant altitude of 122 m (400 ft) above the take-off surface from V_2 to V_{FTO} in the take-off configuration, with the critical engine inoperative and remaining engines transitioning from take-off to maximum continuous thrust.
CS-25.121(c)	The aircraft shall achieve a climb gradient of ≥ 1.2% for two-engined aeroplanes, ≥ 1.5% for three-engined aeroplanes, and ≥ 1.7% for four-engined aeroplanes, climbing from 122 m (400 ft) to 450 m (1500 ft) above the take-off surface in the en-route configuration at V_{FTO}, with the critical engine inoperative and remaining engines at maximum continuous thrust.

While the take-off path is likely to be the most constraining, it must also be evaluated that no other flight segment, as per the mission profile shown in Figure 17.4, exceeds this thrust requirement, or in the case it does, adjust the engine sizing accordingly.

The thrust required for each climb gradient can easily be obtained from the general equations of motion for an aircraft as shown in Equation (11.1):

$$\begin{aligned} \sum F_x : T\cos(\alpha) - W\sin(\gamma) - D &= m\frac{dV}{dt} \\ \sum F_y : T\sin(\alpha) - W\cos(\gamma) + L &= mV\frac{d\gamma}{dt}, \end{aligned} \tag{11.1}$$

where the x axis is tangential to the free stream velocity (positive upstream), and the y axis is perpendicular to the free stream velocity (positive upward).

The following assumptions stand: The aircraft will perform a climb at a constant flight path angle in all segments that require climb (or descent), thus the term $\frac{d\gamma}{dt}$ is equal to zero while $\frac{dV}{dt}$ is not necessarily zero, therefore the aircraft will need constant trimming managed by the flight control subsystem. The aircraft is also assumed to be in a symmetric flight for this calculation; in reality, a yaw damper will be employed to minimise uncommanded side slip at all possible times. Furthermore, during initial evaluations, the angle of attack was iterated for; however was found to have a negligible impact compared to the small angle approximation, therefore the angle of attack is assumed to be small.

During the initial climb segments as provided in Table 11.1, the aircraft is in a steady climb, meaning that $\frac{dV}{dt}$ is zero as well, thus the equations of motion can simply be evaluated for Thrust based on the climb requirement, where the climb requirement translates to the flight path angle as shown in Equation (11.2).

$$\gamma = \arcsin\left(\frac{\text{Climb Gradient(\%)}}{100}\right). \tag{11.2}$$

For the acceleration segment $\frac{dV}{dt}$ can be evaluated as shown in Equation (11.3).

$$\frac{dV}{dt} = \frac{V_{\text{FTO}}^2 - V_2^2}{2 \cdot s_{\text{acc}}}, \tag{11.3}$$

where s_{acc} is the distance across the acceleration, this value was set to be 2000 meters since the one engine inoperative condition will require a significant distance for the acceleration of the aircraft without having to oversize the engines, resulting in unnecessary system mass and fuel consumption. Furthermore V_{FTO} is the final take off speed (also known as lift off speed) set to be $1.1V_S$ where V_S is the stall speed. V_2 is the speed which the aircraft has to reach by the end of the runway or in other words when the screen height is reached, V_2 is defined to be $1.13VS$ by CS-25.107(b) [9].

For the case of evaluating climb and descent conditions through the mission profile, the acceleration is non-zero as the aircraft moves through different velocities, altitudes and distances; therefore Equation (11.1) has to be evaluated in terms of change in velocity, altitude and distance. This can be done by using Equation (11.3), where the term x_acc is repurposed instead of level displacement to slanted displacement as shown in Equation (11.4), while $sin(\gamma)$ is replaced as shown in Equation (11.5)

$$x_{\text{acc, climb}} = \sqrt{(h_2 - h_1)^2 + s_i^2}, \tag{11.4}$$

$$\sin(\gamma) = \frac{h_2 - h_1}{(h_2 - h_1)^2 + s_i^2}, \tag{11.5}$$

where s is the horizontal displacement of segment i along the ground, and h represents the initial and final altitudes

Furthermore, since drag is dependent on both altitude and velocity, a midpoint value is taken between the variables as shown in Equation (11.6). Hence, the finalised thrust requirement expression can be seen in Equation (11.6).

$$\overline{D} = \frac{D(h_1, V_{\text{init}}) + D(h_2, V_{\text{fin}})}{2}, \qquad T = \overline{D} + W\left(\frac{(h_2 - h_1) + \frac{1}{2g}(V_{\text{fin}}^2 - V_{\text{init}}^2)}{\sqrt{(h_2 - h_1)^2 + s_i^2}}\right). \tag{11.6}$$

Finally, the take-off requirement CS-25.113(a) can also be evaluated. This requirement has two possible conditions: one in which, at some point along the runway, an engine fails, then the pilot has to decide whether to take off or abort; both possible conditions need to be possible and are evaluated at different engine failure speeds. The distance needed to accelerate out after OEI (accelerate go) is plotted as a function of the square of its respective failure velocity, forming a curve. The same is repeated for the decelerating condition after OEI (accelerate stop), the intersection point of these two curves will provide the Balanced Field Length (BFL) and the decision speed (V_1). The second requirement condition is 115% of the distance the aircraft needs to start from rest and reach a screen height of 35 feet by the end of the runway with all engines operating (AEO); the highest value of the BFL or AEO take off run will become the required TOFL, with an additional safety factor of 1.2 accounting for adverse weather. Note that high altitude and warm temperature take-off conditions would have to be evaluated separately and would be done so through the flight management computer; this is not involved in the scope of this project, where standard ISA MSL conditions are used.

The standard take-off consists of two segments, the ground roll and the initial climb to the screen height where V_2 is reached. To find the ground roll, the equations of motion have to be reevaluated for ground conditions as shown in

equation (11.7).

$$\sum F_x : T - \mu(W - L) - D = m\frac{dV}{dt}, \tag{11.7}$$

where the coordinate system remains the same as for Equation (11.1) and μ is the friction coefficient assumed to be 0.02 for paved surfaces [32].

Re-arranging the equation and expressing the drag in terms of drag and lift coefficients yields Equation 11.8.

$$\begin{aligned} C_F = \frac{T}{W} - \mu\,,\ C_A = -\frac{1}{2}\frac{\rho S}{W}(C_D - \mu C_L) \\ \Rightarrow \frac{dV}{dt} = a = g\left(C_F + C_A V^2\right). \end{aligned} \tag{11.8}$$

Starting from the general relation $ads = VdV$, we get the resultant ground displacement as shown in equation (11.9):

$$\begin{aligned} \int ds = \int_{V_{\text{init}}}^{V_{\text{fin}}} \frac{V}{a}\,dV = \int_{V_{\text{init}}}^{V_{\text{fin}}} \frac{V}{g(C_F + C_A V^2)}\,dV \\ s_g = \frac{1}{2gC_A} ln\left(\frac{C_F + C_A V_{\text{fin}}}{C_F + C_A V_{\text{init}}}\right). \end{aligned} \tag{11.9}$$

Note that initially, this equation is used in reverse to find the thrust required for a TOFL of 2500 meters, as per MS-REQ-1.5, from which an initial ground roll estimate is made. The distance in the air to reach the screen height is then evaluated by Equation (11.10) and iterated along with the ground distance such that the thrust requirement from the take-off roll is minimised while the screen height is reached [4].

$$s_{\text{flare}} = \frac{h_{\text{screen}}}{\gamma_{\text{flare}}} + \frac{V_{\text{transition}}^2}{g(n_{\text{flare}} - 1)}\frac{\gamma_{\text{flare}}}{2}, \tag{11.10}$$

where n is the load factor of the flare, set to 1.15 [32], $V_{\text{transition}}$ is the average speed between V_{LOF} and V_2 and γ_{flare} is calculated by substituting the thrust found through Equation (11.9) with $V_{\text{fin}} = V_{\text{LOF}}$ and $V_{\text{init}} = 0$ into Equation (11.1) with the assumption of a steady climb.

For the calculation of the BFL, the accelerate go and accelerate stop distances have to be found as a function of the critical velocity V_{crit}, the velocity at which the engine failed. The initial acceleration component s_acc up until the point of V_{crit} can be simply found from Equation (11.9); furthermore, a two-second pilot decision time displacement $2V_{\text{crit}}$ has to be added to the distance for both cases. For the accelerate go condition, the following acceleration to V_{LOF} from the critical engine failure speed has to be added by also using Equation (11.9) and using Equation (11.10) to find the displacement during the transition period, with the available thrust scaled accordingly to the number of engines of the aircraft.

On the other hand, for the accelerated stop distance, after the pilot reaction time displacement, the stopping distance has to be calculated. This can also be done via Equation (11.9) with the following modifications as shown in Equation (11.11) [32].

$$\begin{aligned} C_F = -\mu, \\ C_A = -\frac{1}{2}\frac{\rho S}{W}(C_D + \Delta C_{D,\text{windmill}} + \Delta C_{D,\text{trim}} + \Delta C_{D,\text{spoilers}} - \mu C_L), \\ \Delta C_{D,\text{windmill}} = 0.3 \cdot \frac{\left(\frac{\pi \cdot D_{\text{fan}}^2}{4}\right)}{S_{\text{ref}}},\ \Delta C_{D,\text{trim}} = 0.05 \cdot C_{D,0},\ \Delta C_{D,\text{spoilers}} = 0.08. \end{aligned} \tag{11.11}$$

According to CS-25.109, no reverse thrust may be used for the calculation; thus, the thrust component is removed. Furthermore, drag increments are added from the windmilling of the failed engine, the drag from the stabiliser trimming required to keep the aircraft from veering off its path, as well as the drag from the spoilers deployed. Note that due to the large lifting surface area of the BWB aircraft, no flaps were employed; thus, there is no flap-related drag component.

Finally, these calculations are iterated over different speeds ranging from 0.7 V_S to 1.1 V_S (as if the failure happens above V_{LOF} the aircraft is likely already airborne). Then the distances are plotted against the square of these velocities as shown in Figure 11.1.

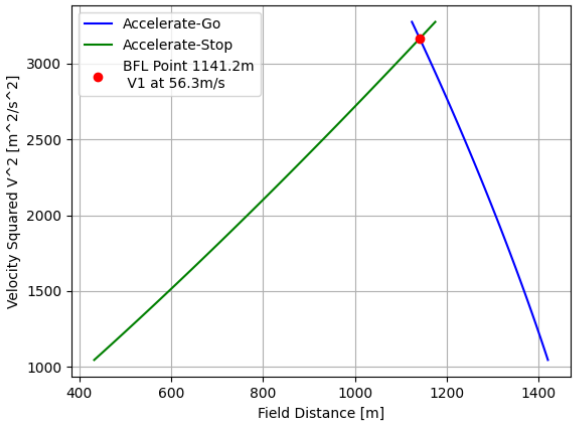

Figure 11.1: Balanced Field Length Plot

As can be seen, for a BWB with a large surface area and a high thrust-to-weight ratio, the BFL will be considerably shorter than comparably weighted aircraft. The reason for the high thrust also stems from the large surface area, as the thrust required increases to fight against the increased drag.

Once all the thrust requirements have been calculated as described above, the largest value can be selected, and the engines can be sourced. Like most other aircraft manufacturers, the engines will be outsourced from an external company, as developing an engine in-house would be far too expensive and complicated, rather than outsourcing it to a trusted party. A list of available High Bypass Turbofan Engines has been compiled that have been tested on neat SAF from large engine manufacturers such as General Electric, Rolls-Royce, Pratt & Whitney, etc. The engine selection is based on the minimum required thrust with an additional safety margin of 1.2, as well as an efficiency factor stemming from the product of the engine weight and thrust-specific fuel consumption in cruise.

However, note that the engine manufacturer provides a value for Sea Level Static (SLS) Thrust, which is different from the flight conditions at which we are evaluating our thrust; therefore, for each segment, this conversion has to be made to find the actual required SLS Thrust. This can be done as shown in Equation (11.12) and Equation (11.13) [4].

$$T_{\text{SLS}} = \frac{T_{\text{req}}}{T_{\text{fac}}}, \tag{11.12}$$

$$T_{\text{fac}} = F_\tau \left[k_{1\tau} + k_{2\tau} \times \text{BPR} + (k_{3\tau} + k_{4\tau} \times \text{BPR}) M\right] \sigma^{\text{alt}_{\text{factor}}} \tag{11.13}$$

Table 11.2: Thrust lapse piece-wise model constants (BPR = 8, dry conditions) [4].

Mach Range	$k_1\tau$	$k_2\tau$	$k_3\tau$	$k_4\tau$	$\text{alt}_{\text{factor}}$	F_τ
$M \leq 0.4$	1.00	0.000	−0.595	−0.030	0.7	1.0
$0.4 < M < 0.9$	0.89	−0.014	−0.300	0.005	0.7	1.0

Once the engines are selected, the take-off distance AEO and the BFL can be recalculated for the adapted engine and its characteristics, as the input thrust will be higher for safety reasons, which will result in a decreased take-off distance AEO and BFL simultaneously compared to the initial estimate. The final TOFL shall be selected as the highest from the take-off distance AEO and BFL, after which multiplied by a safety factor of 1.2 to account for adverse weather conditions and increase general safety.

11.2. Fuel Mass Calculation

Once the engine is selected as described in Section 11.1, the fuel mass can be calculated from Equation (11.14).

$$m_{\text{fuel}} = \sum_{i=0}^{n} SFC_i \cdot T_{\text{req},i} \cdot t_i, \tag{11.14}$$

where SFC_i is the Thrust Specific Fuel Consumption in segment i, $T_{\text{req},i}$ is the thrust required for segment i as can be and t_i is the time spent in segment i.

The SFC is dependent on the altitude and velocity of the aircraft, as the engine efficiency is highly dependent on that. Thus, the SFC can be calculated for each segment as shown in Equation (11.15) and Equation (11.16) [32].

$$SFC = \frac{V}{\eta_\theta \cdot LHV_{\text{SAF}}} \quad \text{,where} \quad \eta_\theta = \eta_{th} \cdot \eta_p \cdot \eta_t, \tag{11.15}$$

$$\eta_{\text{th}} = 1 - \left(\frac{1}{\pi_c}\right)^{\frac{\gamma-1}{\gamma}}, \quad \eta_p = \frac{2V}{\left(\frac{T_{\text{thrust}}}{\dot{m}_{\text{airflow}}}\right) + 2V}, \quad \eta_t = \frac{1+\text{BPR}}{1+\frac{\text{BPR}}{\eta_f \cdot \eta_t}}$$
$$\dot{m}_{\text{airflow}} = M \cdot \frac{\pi \cdot D_{\text{fan}}^2}{4} \cdot \frac{P(h)}{\sqrt{T(h)}} \cdot \sqrt{\frac{\gamma}{R}}, \tag{11.16}$$

where LHV_{SAF} is the Lower Heating Value of Sustainable Aviation Fuel (44 MJ/kg), η_θ is the overall propulsion efficiency, η_{th} is the thermal efficiency of the engine, η_p is the propulsive efficiency, η_t is the transfer/transmission efficiency accounting for the fan and bypass duct losses, η_f and η_t is the fan and turbine efficiency respectively, both assumed to be 0.95 as an initial estimate [32]. Furthermore, $\dot{m}_{\text{airflow}}$ represents the total engine mass flow rate, M is the flight Mach number, D_{fan} is the fan diameter, $P(h)$ and $T(h)$ are the ambient pressure and temperature as a function of altitude, γ is the ratio of specific heats (1.4 for air), R is the specific gas constant (287.05 J/(kg·K)), π_c is the compressor pressure ratio, V is the free stream velocity, T_{thrust} is the engine net thrust, and BPR is the engine bypass ratio.

Note that for phases including climbing or descent, or in other words, changing altitudes and velocities, the parameters that depend on these variables were averaged between the two endpoint values.

Finally, the segment time can be calculated as seen in Equation (11.17):

$$t_i = \sqrt{\frac{(h_2 - h_1)^2 + s_i^2}{\frac{1}{2}\left(V_2^2 + V_1^2\right)}}. \tag{11.17}$$

11.3. Model Validation

The model described in Section 11.1 and Section 11.2 can be subject to validation based on reference aircraft with existing engine combinations, as well as the A220, which was taken as a reference aircraft. The goal was to choose a cluster with a wide range of MTOWs to ensure the model functions in each weight category; the MTOWs range from 71 to 283 tons from the A220 to the A350-900, respectively. The main outputs that are validated for is the engine type, TOFL and the fuel mass, to see if the model's physics work well enough to choose the right engine model or one that is very close in characteristics, as well as to correctly estimate the TOFL and fuel weight of the aircraft, which then translates to a correct propulsion system mass prediction. Since this is a second-order estimation, at least an average error below 10% is expected, and as can be seen from Table 11.3, this is not just achieved on average with a score of 4% but also for each individual score itself.

Table 11.3: Class II Sizing Model Validation Against Certified Aircraft Specifications

Aircraft	Pred. Eng.	Actual Eng.	Pred. TOFL [m]	Actual TOFL [m]	Prediction Error	Pred. Fuel Mass [kg]	Actual Fuel Mass [kg]	Prediction Error
787-9	GEnx	GEnx	2897	2900	0.10%	110 120	101 456	8.54%
A350-900	GE90	XWB-84	2520	2600	3.08%	129 166	133 190	3.02%
737 MAX 8	LEAP1B	LEAP1B	2184	2090	4.50%	21 510	20 895	2.94%
A321 NEO	LEAP1A	LEAP1A	2347	2200	6.68%	18 961	18 440	2.83%
A220-300	1100G	1500G	1780	1890	5.82%	16 573	17 213	3.72%
Average					4.04%			4.21%

Finally, to note some discrepancies with the engine selection, for the A220, the PW1500G itself is not listed on the engine selection sheet; the closest existing engine to the PW1500G used by the A220 is the PW1100G, with almost identical power settings, which is exactly what was chosen by the model. On the other hand, for the A350-900, the GE90 is slightly weaker than the XWB-84; however, the calculated specific fuel consumption for cruise was lower for the GE90, resulting in the decision. Note that however, in real life, this is not the case; the XWB-84 is newer and more efficient than the GE90. This leads to the conclusion that while the SFC is rather accurate over the entire mission profile, as shown by the validation, it might not accurately resemble the engine itself in specific segments. Unfortunately, to increase this accuracy, proprietary information about the engine would have to be known, which is not released to the public. Another alternative would be to size the engines and develop them in-house within the project itself, but that is too time-consuming and complicated for the scope of this project; thus, the best effort was made to get an appropriate estimate.

11.4. System Layout

The Power and Propulsion system consists of the bio-SAF fuel, the fuel storage where the fuel tanks are integrated into the wings and fuselage, energy distribution which includes the transfer of fuel from the tanks to the power sources using piping, valves, pumps, etc., the main power source itself: two engines, located at the aft section of the top of the fuselage, the Auxiliary Power Unit: providing power on the ground and the compressed air needed to start the engines. Both the engines and the APU have two electrical generators attached, called Variable Frequency Starter Generator (VFSG), normally used for the Boeing 787 in order to generate electricity to start the engine or to provide the power needed for the operation of the aircraft.

Furthermore, there is secondary power generation, which consists of generating the necessary hydraulic power for flight control and landing gear actuation, the pneumatic power generation for pressurisation, air conditioning, anti-ice systems, etc., as well as mechanical power generation for the trim system, recirculation fans, pumps, windshield wipers, and so on. Likewise, emergency and start-up power has to be provided; this can be done through the use of batteries to start the APU when the aircraft is cold-started, as well as to provide backup power until the Ram Air Turbine (RAT) is deployed in case the engines and the APU are not available. The RAT is also included in this emergency power provision, as generating multiple kilowatts of power is necessary for such an aircraft to have the absolute minimum functionality required. It is a mechanical propeller that drops down below the fuselage of the aircraft automatically in case the engines and APU are shut off. The RAT uses an electrical generator to provide the aircraft with power and a mechanical hydraulic pump to accommodate key flight controls. Two RATs will be employed to accommodate the power needs of the Flight Control Subsystem due to the aircraft's inherent instability; a higher drag penalty is an acceptable trade-off for the controllability of the aircraft.

Finally, the energy distribution subsystem itself, which provides the necessary power to all the other systems and subsystems for the aircraft to maintain its full functionality. The interactions between the systems and subsystems via the energy distribution subsystem can be seen in Figure 19.1, while the layout and interactions of the energy storage, energy distribution, engine and auxiliary power unit subsystems can be seen in Figure 11.2

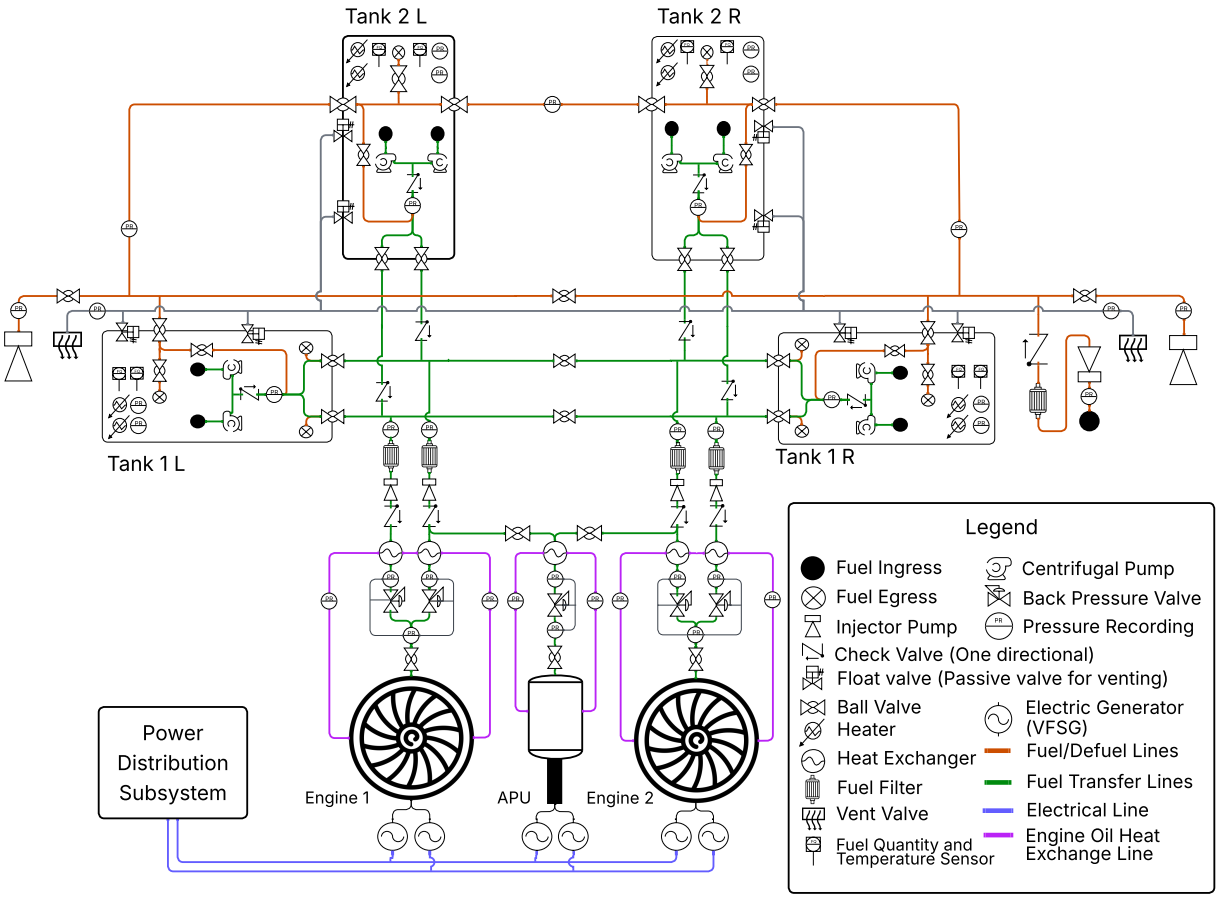

Figure 11.2: Energy Storage, Energy Distribution, Engines and Auxiliary Power Subsystems Detailed Interaction Graph

12
Class II Weight Estimation

This chapter will lay out the general method that was used to perform the Class II weight estimation. two methods were chosen for this estimation, namely the Howe method [6, 7] and the General Dynamics (GD) method found in Roskam [8]. Even though, it is ill advised to mix and match Class II methods, it was seen as the best course of action. The GD method, simply allowed for a more detailed breakdown of the furniture and instruments. The methods found in Howe are explained in Section 12.1, whereas Section 12.2 will explain the Roskam methods. After explaining the methods, the model will be verified in Section 12.3. Please note that the results of this chapter will not be shown here, this is done in Section 13.2

12.1. Howe Method

The methods described in this section have been mainly mainly sourced from Denis Howe [6, 7]. They provide an empirically weighted theoretical approach. The Howe method can be divided over the two sources as follows, the airframe equations are derived from his paper on BWBs [6], whereas all the other parts come from his book titled: "Aircraft Conceptual Design Synthesis" [7].

Airframe

The airframe structures are specified for BWB designs, allowing the methods to be implemented directly, next to none modifications. Howe divides the airframe into two distinct sections, the inner wing (fuselage) and the outer wing. This division can be seen in figure 12.1.

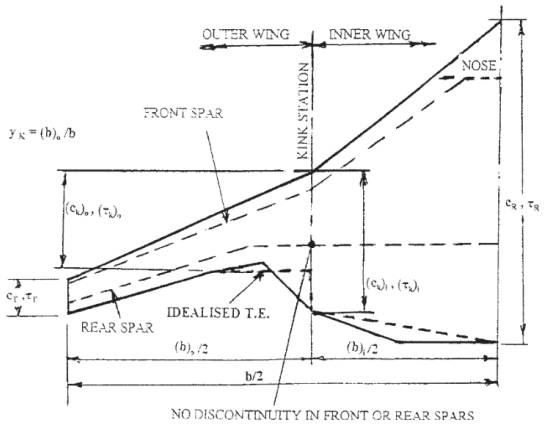

Figure 12.1: Howe definition of a BWB [6]

As a BWB can be seen as one big wing, most of the equations will seem similar for both parts, however the main differentiator lies within the relief factors and e-values (the ratio of the width of the structural box in the line of flight to the wing aerodynamic chord) of both the structures. That is due to the fact that, these values are highly dependent on the specific configurations and/or attachments made to either the inner or outer structure.

As the method was already highlighted in Howe's paper [6], the equations will not be explicitly stated here. However, the e-values for both the inner and outer wing will be stated here, as they are not shown in the paper. Equation (12.1) shows the formulation of the factor for specifically the outer wing.

$$e_o = \frac{(w_{\text{wingbox}})_o}{MAC_o}, \tag{12.1}$$

where $(w_{\text{wingbox}})_o$ can be defined as follows:

$$(w_{\text{wingbox}})_o = MAC_o \cdot (c_{os2} - c_{os1}) \cdot \cos(\Lambda_{0.25,o}).$$

For the outer wing it is stated that the values should be taken at the average value of the wing, so that is why the MAC of the outer wing has been selected [6]. c_{os1} is the assumed location of the front spar, whereas c_{os2} is the assumed location of the rear spar, both as a fraction of the chord. $\Lambda_{0.25}$ is the sweep of the wing at the quarter chord, and MAC_o is the MAC of the outer wing in metres.

The formulation for the fuselage is nearly identical to the wing, the main difference is in the reference point. For this e-value, the reference should be at the kink station [6]. The definition of this station is shown in Figure 12.1. Equation (12.2) shows the full equation.

$$e_i = \frac{(w_{\text{wingbox}})_i}{c_{\text{kink}}}, \tag{12.2}$$

where $(w_{\text{wingbox}})_i$ can be defined as:

$$(w_{\text{wingbox}})_i = c_{\text{kink}} \cdot (c_{is2} - c_{is1}) \cdot \cos(\Lambda_{0.25,i}).$$

In these equations, c_{kink} is the chord at the kink station in metres, c_{is1} and c_{is2} are the locations of the front an rear of the cabin as a fraction of the full fuselage length, and $\Lambda_{0.25,i}$ is the sweep of the fuselage at the quarter chord.

Operational

For the operational items, Equation 12.3 was selected from Howe [7, p. 156].

$$m_{\text{ops}} = 85 \cdot \left(n_{\text{pilots}} + n_{cc}\right) + F_{OP} \cdot n_{\text{pax}}. \tag{12.3}$$

In this equation, n_{pilots}, n_{cc}, and n_{pax} are the number of pilots, cabin crew (CC), and passengers. F_{OP} is the operating items factor, for this a value of 16 has been selected as that is stated for long range/executive aircraft.

Miscellaneous Systems

Other systems also needed to be sized for stability and control considerations as shown in Chapter 14. Therefore these systems were also sized using the Howe method [7], where they were only functions of the MTOW. Table 12.1 shows these components as a percentage of MTOW, as well as the sourced page.

Table 12.1: Class 2 estimates used by Howe [7]

Component	MTOW [%]	Page Number
Main Landing Gear	4.0	354
Nose Landing Gear	0.5	354
Auxiliary Power Unit	0.3	358
Hydraulics	1.0	358
Air Conditioning, Pressurisation, and Icing	2.1	357
Electrical Systems	2.0	357
Flight Controls like the control surfaces	1.0	357

12.2. Roskam Method

Next to the Howe method, other components were sized using the Roskam/GD method. These components are the instruments, and the furnishing. Please note however, these equations are stated in imperial units, they first need to be converted to work with the metric system.

Instruments

The instruments can be subdivided into 3 parts, the flight instruments, the engine instruments, and a miscellaneous group. The equations for these subdivisions can be found in the Roskam book [8, p. 103]. As these are just functions of the MTOW, they have been omitted for the sake of brevity.

Furnishings

The furnishings, just like the instruments, can once again be subdivided into three parts, the seats, the lavatory and food provision, and other miscellaneous items again. Unlike the instruments, two of these components will be explored more in dept, as they are more specific to this specific aircraft. Equation (12.4) is the mass of the seats, and equation (12.5) is the mass of lavatory and food provision. These equations can be found in the Roskam [8, p. 108].

$$m_{\text{seats}} = 55 \cdot n_{\text{pilots}} + 220 \cdot n_{\text{pax}} + 15 \cdot n_{cc} \tag{12.4}$$

In this equation, n_{pilots}, n_{cc}, and n_{pax} are the number of pilots, cabin crew, and passengers. However, note the red 220. This is different from the formulated 32 in the book because of the requirement for business class passengers, and these weigh 220 pounds[1] instead of the 32 in Roskam.

$$m_{\text{lav\&buf}} = k_{\text{lav}} \cdot (n_{\text{pax}})^{1.33} + k_{\text{buf}} \cdot (n_{\text{pax}})^{1.12} \tag{12.5}$$

In this equation, n_{pax} is the number of passengers, and k_{lav} and k_{buf} are the scaling factors for the lavatories and food provisions respectively. k_{lav} was selected as 3.90, and k_{buf} as 5.68, as these were both mentioned for long range/executive aircraft.

12.3. Verification and Validation

To make sure that the class 2 module works, verification and validation has to occur. The used mass estimation method has also been used before by Brown and Vos, who have also verified and validated the method [26]. That is why only code verification will be performed on our own model, as the method is seen as correct.

Verification

In order to verify the model, the translation from the established methods to the code was checked with the help of unit tests [6–8]. Each equation was checked manually, with realistic inputs, to see if the computational model returned the correct values. As for verification for the full model, a similar method has been applied as in the paper [26]. The results of this method can be seen in Table 12.2.

[1] URL `https://simpleflying.com/why-next-generation-business-class-seats-heavier-lighter/` [Cited 12/06/2026]

Table 12.2: Ratio of airframe component mass to MTOW from Howe and the Initiator [26]

Component	Suggested	POGA	BWB150	BWB250	BWB400
Wing Function					
Covers	–	0.052	0.066	0.077	0.088
Ribs	–	0.033	0.041	0.038	0.039
Secondary	–	0.032	0.031	0.031	0.031
Sub total	–	0.117	0.138	0.146	0.158
Fuselage Function					
Nose	0.010	0.014	0.021	0.012	0.009
Press. Membrane	0.010	0.052	0.044	0.034	0.061
Bulkheads	0.007	0.01	0.012	0.004	0.004
Pax floor	0.017	0.0246	0.017	0.013	0.015
Cargo floor	–	–	0.003	0.004	0.005
Doors	0.010	0.009	0.003	0.002	0.002
Windows	0.003	0.003	0.003	0.003	0.003
Sub total	–	0.113	0.104	0.071	0.099
Total airframe	–	**0.230**	**0.242**	**0.217**	**0.257**

From this table it becomes clear that the total airframe mass lies within a realistic range. However, the wing function is underestimated, whereas the fuselage function is overestimated. Specific outliers include the doors, passenger and cargo floors, and the covers. The difference in door mass can be explained by simply having more doors installed in the design. The difference in flooring can be explained by having extra floor area per passenger.

This means the aircraft has a relatively low payload mass, and therefore MTOW. This leads to the floor relatively being larger. The covers can be explained by unoptimised idealisation, but it still falls within an acceptable margin. This combined with the unit tests means that the class II weight estimation is verified.

13
Preliminary Design

The preliminary design of the POGA is discussed in this chapter. Design outputs with parameters are given using the methodology discussed in earlier chapters. The cabin layout is outlined in Section 13.1, followed by the mass estimation and budgets in Section 13.2 and Section 13.3, respectively. Finally, the volume budget is explained in Section 13.4.

Table 13.1: Comprehensive aircraft parameters compiled from design specifications

Variable	Value	Variable	Value
Design Inputs & Mission Constraints		**Geometry Details**	
Cruise Mach	0.79	Cabin Width	18.7
Cruise speed	268.4	Cabin Length	19.7
Taper ratio	0.40	Planform Area	475.0
Number of passengers	120	Cabin Area	368.21
Surface area per passenger	2.5	Floor Area	300.0
Transition width	5.0	x_{cp}	9.6
Cruise altitude	10 668	x_{nose}	11.6
Approach speed	85.4	l_{fuselage}	27.55
$C_{L_{\max,L}}$	0.425	Length to the Tail	3.71
$C_{L_{\max,W}}$	1.275	Cockpit Length	1.2
k_A	0.95	Fuselage Planform Area	442.72
t_c (reference airfoil)	0.14	Reference Planform Area	600.60
dM_dd	0.05	Wingspan	64.9
Maximum wingspan	65.0	Mean Aerodynamic Chord	23.19
Cockpit width	4.5	Outer Wing Root Chord	5.54
x_root (LE at root)	–2.5	Tip Chord	2.22
ρ_{cruise}	0.380	Outer Wing Area	78.94
Passenger mass	150.0	Leading Edge Sweep	22.9
TOFL requirement	2500	Quarter Chord Sweep	20.9
Loiter time	45.0	Trailing Edge Sweep	14.5
		Half Chord Sweep	18.8
		y_{MAC}	20.51
		Distance to the outer wing	14.36
		Outer Wing Thickness-to-Chord	0.14
Aerodynamic Characteristics		**Propulsion Performance**	
L/D_{max}	17.65	Engine Mass	5623
$\alpha_{L/D_{max}}$	3	Single Engine Thrust	296 000
$C_{L_{cruise}}$	0.4107	Number of Engines	2
L/D_{cruise}	17.31	Total Fuel Mass	36 367
$C_{L_{app}}$	0.6	BFL	884
$C_{L_{TO}}$	1.00	V1	48.2
		$\text{SFC}_{\text{cruise}}$	$5.80{\cdot}10^{-06}$
		TOFL	920
		Engine Length	4.69
		Mass Installed Engine	11 246
Mass Estimation Breakdown		**Stability, Control & Center of Gravity**	
Payload Mass	18 000	Wetted Area	1700
Mass Fuel Fraction	0.814	S_i	302
Class I MTOW	100 097	$\text{LEMAC}_{\text{nose}}$	3.49
Max Range	7209	Position of quarter MAC from nose	9.29
Class I Fuel Mass	18 613	CG position of wing	0.12
Final MTOW	131 554	Position of CG from nose	–0.37
OEW	77 188	Position of CG of MTOW from nose	14.86
ZFW	95 188	Position of CG of ZFW from nose	14.17
Wing Mass	5098	Position of CG of OEW from nose	14.12
Fuselage Mass	23 691	Position of CG of MTOW	–4.07
Landing Gear Mass	4500	Position of CG of ZFW	–3.37
Propulsion System Mass	17 544	Position of CG of EOM	–3.33

Continued on next page

Table 13.1 – continued from previous page

Variable	Value	Variable	Value
Instrument Mass	1241	α_{trim}	0.27
Hydraulics mass	1000	$\delta_{e_{trim}}$	–26.48
Furnishing Mass	14 076	Cm_{ac}	0.28
API Mass	2100	CG forward margin from MAC	28.18
Operational Item Mass	4640	CG aft margin from MAC	32.64
Electronics Mass	2000	CG most forward from MAC	28.23
Flight Control Mass	1000	CG most aft from MAC	32.59
APU Mass	300	CG forward margin from nose	12.48
		CG aft margin from nose	16.24
		CG most forward from nose	13.85
		CG most aft from nose	14.86

13.1. Cabin Layout

The cabin layout is shown in Figure 13.1. The cabin is arranged for 120 passengers in a business-class configuration. The layout is divided by the main structural columns for the multi-bubble design. These columns are kept inside the cabin layout and the seats are arranged accordingly. The central structural region together with the 2 by 2 seat arrangement separate the cabin into several passenger zones. This helps to keep the walking distance to exits limited.

Four type A cabin doors are include. These doors are used for normal boarding, catering servicing, and emergency evacuation. In addition, two ventral exits are placed at the rear of the aircraft. This gives a total of six emergency exits. The aft ventral exits are added because the BWB cabin side at the rear is blended into the transition area to the wing. External sidewalls are not available at the rear.

The galleys and working areas are placed uniformly across the cabin, close to the exits. Lavatories are also distributed in the cabin so it remains accessible from the whole passenger areas. The entrance to the crew rest area is placed at the start of the forward upper bubble, matching the available volume above the passenger cabin described in Section 9.1. There are also entrance from the rear of the cabin for the crew rest area. Overall, the layout uses the large BWB cabin width for passenger comfort, while still respecting the structural columns, service areas and emergency exit arrangement.

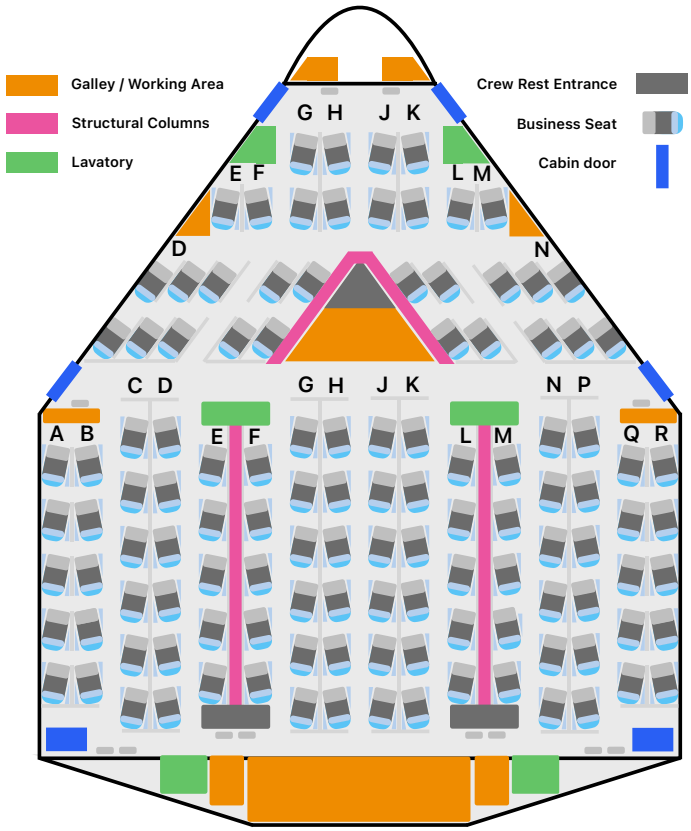

Figure 13.1: Cabin Layout

As described in Section 9.1, the cabin height is divided into three main parts: the upper shell, the passenger cabin, and the lower shell. The passenger cabin is placed on the main floor, while the space above the cabin is reserved for the crew rest area. This area is located in the middle upper bubble and between the main structural columns. The available height of 0.6 m may require usage of the space in the overhead compartment without interfering the cabin layout.
The lower bubble is used for the luggage hold with available heigh of 1.2 m. Since the aircraft is designed for 120 passengers in an all-business layout, no large cargo deck is required for unit loading device (ULD). Therefore, the lower volume is allocated to passenger baggage with an available volume of 27 m^3. This volume is already enclosed by the pressurised lower shell. As a result, both the upper and lower shell heights in the middle bubble are used functionally.

13.2. Mass Estimation

From Table 13.1 the results from the Chapter 8 and Chapter 12 weight estimations can be seen. This resulted in the final MTOM of 131544 kg, which can be divided further amongst smaller categories. The result of this division is shown in figure 13.2a, after which the EOW is further subdivided in figure 13.2b.

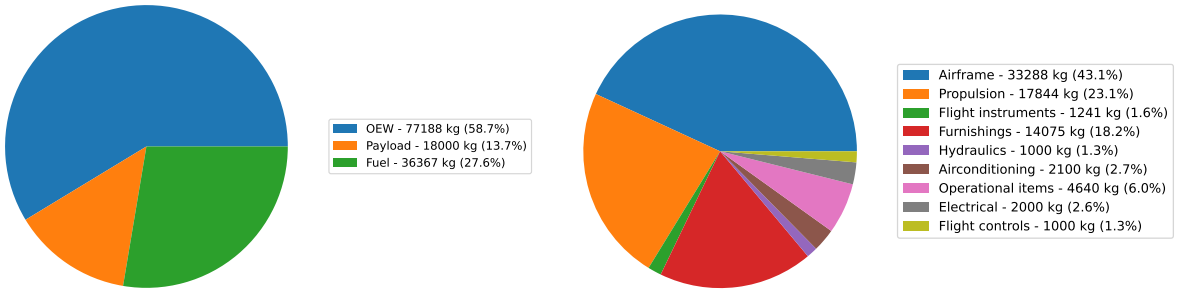

(a) MTOM breakdown **(b)** EOW breakdown

Figure 13.2: Mass breakdowns

The MTOM consists of the payload mass, fuel mass, the OEW. Of these three th OEW takes up the highest percentage, being 58.7%. This 58.7% can then be further broken down into subgroups. Consisting of the airframe, propulsion system, and other smaller subsystems. However, the furnishings also take up a large percentage because as mentioned in Section 12.2 the weight of business class seats is simply much larger than those of economy class.

13.3. Mass Budgets

Table 13.2: Preliminary mass budget breakdown including margins.

Subsystem	Original Baseline Mass [kg]	New Computed Mass [kg]	Margin [%]	Final Budgeted Mass [kg]
Airframe incl. landing gear	23,556	33,288	35	44,939
Power and Propulsion	47,845	54,210	35	73,184
Payload	13,068	18,000	6	19,080
Aircraft systems and fixed equipment	12,760	26,056	35	35,176
Total	**97,229**	**131,554**	–	**172,379**

It can be seen that there are large discrepancies between the original values found in the baseline report, and the values found of the preliminary design [19]. The main reason for this discrepancy is the addition of requirement `MS-REQ-5.1`. Initially at the baseline stage it was assumed that the passengers could be in a regular economy class configuration, however, after discussions with the stakeholders, this was changed to business class. This started a snowball effect by first increasing the weight and volume of the required cabin. Causing all the surrounding systems to also grow.

In addition to the higher initial values, the margins have also been revised to be more accurate with comparable projects. According to Chai and Whilhite, the average mass growth from the start of the project up until the end is around 35% [33]. Even though this paper was written for space programs, the data used included aviation projects as well. That is why for the airframe, power and propulsion, and the aircraft systems this has been taken as a design margin.

For the new payload mass, a 6% safety margin was taken. This margin was taken based on average passenger masses published by EASA[1]. Based on the normal distribution and standard deviation, the 6% margin ensures that the aircraft is equipped to handle 97.4% of business class passengers without exceeding the designated payload mass.

13.4. Volume Budget

In addition to mass, volume is also an important design characteristic. Net Design Volume (NDV) is a great metric to see, if the aircraft has enough space left, for the structure, avionics, systems, equipment, landing gear, routing, and access provisions [11]. It is therefore critical this is also considered in the design of this aircraft. As this blended wing body will have above the body mounted engines, only the fuel and payload volume were seen as critical to determine NDV. Raymer gave Equation 13.1 as a definition of NDV.

$$NDV = (V_{\text{fus}} + V_{\text{wing}}) - V_{\text{payload}} - V_{\text{fuel}}, \tag{13.1}$$

where V denotes the volume of each subsystem mentioned [11]. Table 13.3 will show the total volumes of these subsystems as well as the NDV.

[1] URL `https://www.easa.europa.eu/en/document-library/research-reports/easa2021c24` [Cited 16/06/2026]

Table 13.3: Preliminary volume budget breakdown including margins.

Subsystem	Baseline Budgeted Volume [m^3]	Computed volume [m^3]	Margin [%]	Budgeted volume [m^3]
Fuel tanks	0.432	45.5	35	61.4
Payload	0.396	1154.3	66	1915.1
NDV	0.828	924.7	–	148
Total Volume	**1.000**	**2124.5**	**–**	**2124.5**

The fuel tank size has been computed by dividing the fuel mass in Table 13.1 by the density of bio-SAF. The total volume of the payload was a bit harder to compute. This was done by computing the cabin volume based on the area and height in Table 13.1. This volume was then multiplied by the ratio of a cabin section and the total pressurised shell area. A section can be seen in Figure 16.1. The total volume was calculated, by using the model Aerosandbox[2]. NDV was then determined with the use of Equation 13.1.

Currently the design aims for a 5200 ft^3 of NDV. In line with in line with the same paper by Raymer [11]. This is done through limiting the size of the payload and fuel tanks with margins. For the fuel system an additional 35% is taken to comply with CS 25.969, this accounts for the additional expansion of the fuel within the fuel tanks [9]. This also makes sure that the fuel tanks can be feasible with the overall mass growth determined in Section 13.3. The 66% margin for the payload is put in place to make sure that the aforementioned volume for NDV can be realised.

[2]URL `https://aerosandbox.readthedocs.io/en/master/` [Cited 22/06/2026]

Part III: Design Analysis

14 Stability and Control

Due to the unconventional nature of BWBs, the methods to quantify and check for stability and control differ from conventional aircraft. Firstly, assumptions used in this chapter are introduced in Section 14.1. Subsequently, a calculator tool had to be developed to enable the calculation of certain parameters in Section 14.2. After this, the centre of gravity (CG) range could be calculated in Section 14.3. Moreover, longitudinal stability, turbulence handling and trim are documented in Section 14.4, Section 14.5 and Section 14.6, respectively, followed by the lateral and directional static stability characteristics in Section 14.7. The eigenmotions were analysed in Section 14.8 in order to initialise the longitudinal and lateral dynamic stability in Section 14.9 and Section 14.10, respectively. Ground stability and manoeuvres are outlined in Section 14.11 and Section 14.12, respectively. Finally, the control surfaces sizing is detailed in Section 14.13.

14.1. Assumptions

This section outlines the key assumptions underpinning the stability and control analysis in this chapter, defining the scope and limitations of the methods applied. These assumptions are made to simplify the modelling at this preliminary design stage and apply throughout unless stated otherwise.

1. **Decoupled longitudinal and lateral-directional dynamics.** The equations of motion are separated into two independent fourth-order systems. The product-of-inertia term I_{xz} is assumed small enough to neglect, consistent with the aircraft's bilateral symmetry.
2. **International Standard Atmosphere.** All aerodynamic and performance calculations use the ISA troposphere model (lapse rate $\lambda = 6.5$ K/km, $T_0 = 288.15$ K). Hot-day (ISA) deviations relevant to take-off performance are noted but not propagated into the stability derivative set.
3. **AVL vortex-lattice fidelity.** Stability derivatives are obtained from the AVL code, which provides inviscid, attached-flow solutions. Derivatives are considered reliable for $M \lesssim 0.6$ and moderate α. Compressibility corrections (Prandtl–Glauert) are applied where noted; viscous corrections to C_{m_α} are not applied at this stage.
4. **Constant mass properties during a manoeuvre.** Fuel burn during any single manoeuvre or analysis window is negligible relative to total fuel mass. Mass m and moments of inertia I_y, I_x, I_z are treated as fixed at the analysis mass point.
5. **Thrust acts along the body x-axis.** Engine thrust eccentricity and its pitching or yawing moment contributions are neglected. In practice, engine placement on a BWB may produce significant pitching moments; this is deferred to detailed design [25].
6. **Linear control surface effectiveness.** Elevon and split drag-rudder effectiveness ($C_{L_{\delta_e}}$, $C_{m_{\delta_e}}$, $C_{n_{\delta_r}}$) are assumed linear in deflection angle up to the physical limit of $\pm 30^\circ$. Saturation, aerodynamic non-linearity, and hinge-moment limits at large deflections are not modelled at this stage [25].
7. **Fly-by-wire augmentation assumed.** The BWB configuration is expected to be statically unstable in pitch ($C_{m_\alpha} > 0$) at some or all CG positions. A fly-by-wire (FBW) flight control system is assumed to provide artificial stability augmentation (SAS/CAS) to achieve the equivalent of CS-25.173 compliance; handling-quality targets are stated for the augmented aircraft [9].
8. **Mass properties from MDAO outputs.** CG positions (OEW, ZFW, MTOW) and rotational inertias are taken directly from the multi-disciplinary analysis (OpenMDAO) outputs. Uncertainties in mass distribution are not propagated into the stability analysis.
9. **Standard day, still-air holding.** The ICAO holding turn analysis uses ISA conditions with no wind component. Wind effects on holding airspeed and bank angle limits are acknowledged but not modelled.
10. **Single operating point for handling qualities.** Dynamic mode eigenvalue analysis is performed at one representative condition (holding altitude, loiter speed). Variation of mode characteristics across the full flight envelope is not mapped at this design stage.
11. **Speed–pitch coupling neglected.** The speed-dependent force and moment derivatives C_{D_u}, C_{D_α}, C_{L_u}, and C_{m_u} are small relative to their reference aerodynamic coefficients C_D, C_L, and C_m respectively, and are omitted from the longitudinal equations of motion. This simplification is consistent with a clean, subsonic configuration operating well below the drag-divergence Mach number, where thrust–speed coupling and aeroelastic effects remain negligible [34].

14.2. MAC, LEMAC Calculator

The mean aerodynamic chord (MAC) and its leading-edge location (LEMAC) are the reference from which the different CG locations depend on. For a conventional aircraft, these are a single value, but the BWB centrebody introduces multiple chordwise kinks which require a panel-by-panel integration, as explained in Subsection 10.1.2.

The centrebody planform is discretised into a series of spanwise stations containing the spanwise position (y_i), the leading-edge x-coordinate ($x_{LE,i}$), and the local chord (c_i). To these stations, two additional ones are appended, representing the outer wing root and tip. The y-position of the root is determined by the outermost station, while the x-position was chosen by trading off the L/D and static stability margin to reach a compromise. In order to determined the coordinates of the wing tip, Equation 14.1 was used:

$$y_{\text{tip}} = y_{\text{root}} + \frac{S_{\text{ref}} - S_b}{c_r(1+\lambda)}, \qquad x_{\text{tip,nose}} = x_{\text{root,nose}} + \tan(\Lambda_{\text{LE}}) \cdot \frac{b}{2}, \tag{14.1}$$

where S_{ref} is the reference surface area of the aircraft and S_b of the centrebody, c_r is the outer-wing root chord, λ the taper ratio, Λ_{LE} the leading-edge sweep angle, b the full span, and nose refers to the x-position from the nose, as the x-axis of the reference frame does not coincide with the nose, while the y-axis does with the centreline of the aircraft. All leading edge positions are converted from the aircraft reference frame (x positive forward, nose at $x_{\text{nose,aircraft}}$) to the nose-datum frame (distance aft of the nose) using Equation 14.2:

$$x_{0,i} = x_{\text{nose,aircraft}} - x_{\text{LE},i}. \tag{14.2}$$

For each panel i, the taper ratio λ_i, fractional width ζ_i, and panel area S_i are computed using Equation 14.3, using P. Okonkwo's method for BWB design [4].

$$\lambda_i = c_{i+1}/c_i, \qquad \zeta_i = \Delta y_i/(b/2), \qquad S_i = \zeta_i \cdot (b/2) \cdot \frac{c_i(1+\lambda_i)}{2}. \tag{14.3}$$

The MAC is then computed using Equation 14.4:

$$\bar{c} = \frac{2}{3} \frac{\sum_{i=1}^{m+1} c_{i-1}^2 \left(1 + \lambda_i + \lambda_i^2\right) \zeta_i}{\sum_{i=1}^{m+1} c_{i-1} (1+\lambda_i) \zeta_i}. \tag{14.4}$$

The quarter-chord x-position of each panel's MAC $\bar{x}_{c/4,i}$ (in the nose-datum frame) is defined by Equation 14.5:

$$\bar{x}_{c/4,i} = x_{0_{i-1}} + (x_{0_i} - x_{0_{i-1}}) \cdot \frac{1+2\lambda_i}{3(1+\lambda_i)} + \frac{c_i}{4}, \tag{14.5}$$

with the overall quarter-chord x-position and LEMAC calculated using Equation 14.6, as area-weighted averages:

$$\bar{x}_{c/4} = \frac{\sum_{i=1}^{m+1} \bar{x}_{c/4,i} \cdot S_i}{\sum_{i=1}^{m+1} S_i} \qquad x_{\text{LEMAC}} = \bar{x}_{c/4} - \frac{\bar{c}}{4}. \tag{14.6}$$

All of these values are provided in both the nose-datum frame and the aircraft reference frame for downstream connectivity.

14.3. Centre of Gravity (CG) Range

Given the component masses obtained as detailed in Chapter 12, the overall CG for three loading states (MTOW, ZFW, and OEW) can be calculated by a mass-weighted moment sum over all airframe components.

Moment arms follow the Okonkwo formulation [4], where each arm is measured from the nose, with the CG of the wing-and-fuselage structural group derived from the panel-based wing-CG non-dimensional fraction using Equation 14.7 [4]:

$$x_{cg_p} = \frac{1}{56}\left[13 - \frac{(27\lambda^2 + 1.75AR(1-\lambda^2)(1+4\lambda+\lambda^2) \cdot \tan(\Lambda_{0.25}))}{(1+\lambda+\lambda^2)^2}\right], \tag{14.7}$$

where λ is the taper ratio, AR the aspect ratio, and $\Lambda_{0.25}$ the quarter-chord sweep.

An area-weighted average x_{cg_w} over all panels is then used to find the CG for the structural group in the nose-datum frame, which then can be easily converted to the aircraft-frame. This and the MAC position of the wing-group CG are

determined by Equation 14.8:

$$x_{cg_w} = \frac{\sum_{i=1}^{m+1} S_i \cdot x_{cg_{p_i}}}{\sum_{i=1}^{m+1} S_i}, \qquad x_{cg_{mac}} = \frac{(x_{cg_w} \cdot c_r) - \bar{x}_{1/4}}{\bar{c}}, \tag{14.8}$$

where S_i is the area of each of the panels, and $x_{cg_{p_i}}$ their respective CGs; c_r is the root chord, $\bar{x}_{1/4}$ the quarter-chord position of the MAC, and $\bar{c}$ the MAC length.

Then, building upon the Okonkwo method [4], the known or computed weights and moment arms were substituted in, leading to Equation 14.9, Equation 14.10 and Equation 14.11.

$$\begin{aligned} \mathrm{MOM_{mtow}} = {} & (m_{\mathrm{eng}} \times x_{cg_{\mathrm{eng}}}) + ((m_{\mathrm{fuse}} + m_{\mathrm{wing}})[\bar{x}_{1/4} + (x_{cg_{\mathrm{mac}}} \times \bar{c})]) + ((m_{LG} + m_{\mathrm{hydr}})(x_{cg_{LG}})) \\ & + (m_{\mathrm{payload}} \times x_{cg_{PL}}) + ([m_{\mathrm{IAE}} + m_{\mathrm{API}} + m_{\mathrm{APU}} + m_{\mathrm{fltcon}}] \times [0.5 \times 0.25c_0]) \\ & + ((m_{\mathrm{ops}} + m_{\mathrm{furn}}) \times [0.25c_0 + 0.5l_{\mathrm{cabin}}]) + (m_{\mathrm{elec}} \times [0.25 \times c_0]) + (m_{\mathrm{fuel}} \times x_{cg_{\mathrm{fuel}}}), \end{aligned} \tag{14.9}$$

$$\begin{aligned} \mathrm{MOM_{oem}} = {} & (m_{\mathrm{eng}} \times x_{cg_{\mathrm{eng}}}) + ((m_{\mathrm{fuse}} + m_{\mathrm{wing}})[\bar{x}_{1/4} + (x_{cg_{\mathrm{mac}}} \times \bar{c})]) + ((m_{LG} + m_{\mathrm{hydr}})(x_{cg_{LG}})) \\ & + ([m_{\mathrm{IAE}} + m_{\mathrm{API}} + m_{\mathrm{APU}} + m_{\mathrm{fltcon}}] \times [0.5 \times 0.25c_0]) + ((m_{\mathrm{ops}} + m_{\mathrm{furn}}) \times [0.25c_0 + 0.5l_{\mathrm{cabin}}]) \\ & + (m_{\mathrm{elec}} \times [0.25 \times c_0]), \end{aligned} \tag{14.10}$$

$$\begin{aligned} \mathrm{MOM_{zfw}} = {} & (m_{\mathrm{eng}} \times x_{cg_{\mathrm{eng}}}) + ((m_{\mathrm{fuse}} + m_{\mathrm{wing}})[\bar{x}_{1/4} + (x_{cg_{\mathrm{mac}}} \times \bar{c})]) + ((m_{LG} + m_{\mathrm{hydr}})(x_{cg_{LG}})) \\ & + (m_{\mathrm{payload}} \times x_{cg_{PL}}) + ([m_{\mathrm{IAE}} + m_{\mathrm{API}} + m_{\mathrm{APU}} + m_{\mathrm{fltcon}}] \times [0.5 \times 0.25c_0]) \\ & + ((m_{\mathrm{ops}} + m_{\mathrm{furn}}) \times [0.25c_0 + 0.5l_{\mathrm{cabin}}]) + (m_{\mathrm{elec}} \times [0.25 \times c_0]). \end{aligned} \tag{14.11}$$

The moment arm for the fuel was calculated as explained in Subsection 16.3.1, while the determination of the location of the landing gears required certain iterative loops due to its interdependence with longitudinal stability detailed in Section 14.11. The CG is then calculated as the ratio of the total first moment to the state mass as described by Equation 14.12:

$$x_{cg_{\mathrm{mtow}}} = \frac{\mathrm{MOM_{mtow}}}{\mathrm{MTOW}}, \qquad x_{cg_{\mathrm{oew}}} = \frac{\mathrm{MOM_{oew}}}{\mathrm{OEW}}, \qquad x_{cg_{\mathrm{zfw}}} = \frac{\mathrm{MOM_{zfw}}}{\mathrm{ZFW}}, \tag{14.12}$$

yielding $x_{cg_{\mathrm{mtow}}} = 14.86\mathrm{m}$, $x_{cg_{\mathrm{oew}}} = 14.12\mathrm{m}$, $x_{cg_{\mathrm{zfw}}} = 14.17\mathrm{m}$, measured as distances from the nose. From this, the loading diagram can be built. This diagram traces the movement of the CG as passengers board and as fuel is added, starting from the OEW CG, with two boarding sequences simulated:

1. **Front-to-back (F2B):** outer/window seats filled front-to-rear, followed by centre/aisle seats in the same order and finally fuel is added.
2. **Back-to-front (B2F)**: centre/aisle seats filled front-to-rear, followed by outer/window seats in the same order and finally fuel is added.

At each instance, the CG is updated as shown in Equation 14.13:

$$x_{cg,new} = \frac{W_{cur} \cdot x_{cg,cur} + \Delta W \cdot x_i}{W_{cur} + \Delta W}, \tag{14.13}$$

where W_{cur} and $x_{cg,cur}$ are the current weight and position of the CG, ΔW the increment in weight, and x_i the position of the added item.

The CG positions are expressed as MAC fractions from LEMAC following Equation 14.14

$$x_{cg} = \frac{x_{cg} - x_{LEMAC}}{\bar{c}}. \tag{14.14}$$

From this, forward and aft CG limits are set with a ±5% MAC margin on the extreme values found across all sequences with Equation 14.15:

$$\bar{x}_{fwd} = \min(\bar{x}_{cg}) - 0.05, \qquad \bar{x}_{aft} = \max(\bar{x}_{cg}) + 0.05, \tag{14.15}$$

which yields a forward CG extreme of $\bar{x}_{cg,\mathrm{fwd}} = 28.23\%$ MAC and an aft CG extreme of $\bar{x}_{cg,\mathrm{aft}} = 32.59\%$ MAC. Applying the ±5% MAC margin from Equation 14.15 gives a forward CG limit of $\bar{x}_{\mathrm{fwd}} = 28.18\%$ MAC and an aft CG limit of $\bar{x}_{\mathrm{aft}} = 32.64\%$ MAC, corresponding to absolute positions of $x_{\mathrm{fwd}} = 12.48\,\mathrm{m}$ and $x_{\mathrm{aft}} = 16.24\,\mathrm{m}$ from the nose. These values can be visualised in the loading diagram in Figure 17.5, in Chapter 17.

14.4. Longitudinal Static Stability

The longitudinal static stability of the bare airframe is characterised by the change in pitching moment C_{m_α}, whose negative value determines static stability, while a positive one indicates instability.

The stability metric in the design is the static margin calculated using Equation 14.16 [4, 35]:

$$K_n = \frac{x_{np} - x_{cg}}{\bar{c}} = -\frac{C_{m_\alpha}}{C_{L_\alpha}}, \tag{14.16}$$

where x_{np} is the neutral point location obtained from AVL. A positive K_n indicates static stability, while a negative value indicates relaxed stability, acceptable with a fly-by-wire Stability Augmentation System (SAS) [36]. Poor longitudinal static stability is a well-known characteristic of the BWB configuration, as the absence of a horizontal tail and the typically forward position of the aerodynamic centre relative to the centre of gravity produce an destabilising pitching tendency [4, 37]. The results from AVL yields a neutral point position $x_{np} = 13.60$ m from the nose. Comparing this to the CG envelope established in Equation 14.15, the static margin evaluates to $K_n = +4.83\%$ MAC at the forward CG limit and $K_n = -11.39\%$ MAC at the aft CG limit. The aircraft is therefore statically stable at forward CG positions, but becomes increasingly unstable as the CG moves aft beyond the neutral point at $x_{np} = 13.60$ m. This result is consistent with the inherent stability characteristics of BWBs, and the relaxed static stability in the aft CG regime is managed by the fly-by-wire SAS.

The AVL-computed stability derivatives, could not be verified due to numerical issues in the AVL model explained in Section 14.14. Consequently, the static margin could not be confirmed via the derivative ratio in Equation 14.16, and the neutral point position x_{np} serves as the sole stability indicator available from the current aerodynamic analysis.

14.5. Turbulence-Handling Criterion

In order to verify that the pitching-moment response to a vertical gust is self-correcting, Equation 14.17 can be used [4]:

$$a = \frac{C_{m_\alpha}}{C_{m_q}} - \frac{(C_{L_\alpha} + C_D)\rho S_{ref}\bar{c}}{2 \cdot W} < 0, \tag{14.17}$$

where ρ is the cruise air density, and W the aircraft mass at different states. This criterion is evaluated at each CG position to ensure the CG envelope is within the turbulence-safe range. As mentioned above and in Section 14.14, AVL did not yield reliable outputs, thus numerical results are not discussed in this section.

14.6. Longitudinal Trim

At trim, all aerodynamic and mechanical forces are perfectly balanced, with the pitching moment being zero. With a linear aerodynamic model, the trim equations form a 2×2 system as see in Equation 14.18 [35, 38]:

$$\begin{pmatrix} C_{L_\alpha} & C_{L_{\delta_e}} \\ C_{m_\alpha} & C_{m_{\delta_e}} \end{pmatrix} \begin{pmatrix} \alpha_{\text{trim}} \\ \delta_{e,\text{trim}} \end{pmatrix} = \begin{pmatrix} C_{L,\text{trim}} - C_{L_0} - C_{L_\beta}\beta \\ -C_{m_0} - C_{m_\beta}\beta \end{pmatrix} \tag{14.18}$$

This can be solved using Cramer's rule; for effective elevon trim, the determinant must be non-zero:

$$\Delta = C_{L_{\delta_e}} C_{m_\alpha} - C_{L_\alpha} C_{m_{\delta_e}} \neq 0$$

The pitching moment coefficient about the aerodynamic centre is defined by Equation 14.19

$$C_{m,ac} = C_L \cdot \frac{x_{np} - x_{cg}}{\bar{c}}, \tag{14.19}$$

confirming that relaxed stability reduces the elevon trim deflection and its associated trim drag. As the control derivatives $C_{L_{\delta_e}}$ and $C_{m_{\delta_e}}$ are extracted from AVL, numerical results are subject to the same modelling issue discussed in Section 14.14 and are not reported here. Trim is additionally evaluated in the manoeuvre analysis in Section 14.12.

14.7. Lateral-Directional Static Stability

For a BWB, lateral and directional static stability presents a unique challenge due to the absence of a conventional vertical empennage [39]. Directional control must instead rely entirely on winglet-mounted drag-split rudders, while lateral control is managed by elevons [40]. This section evaluates the effectiveness and sizing of this control architecture by verifying its aerodynamic stability and control authority against two critical EASA CS-25 certification constraints: maintaining a steady sideslip during a crosswind approach, and recovering from asymmetric thrust during a One Engine Inoperative (OEI) event.

14.7.1. Crosswind CS-25.237 Requirement

Certification (CS-25.237) requires a demonstrated crosswind capability of 20 kt [9]. Flying an approach in a crosswinds means flying maintaining constant sideslip. This is computed by Equation 14.20.

$$\beta = \arctan\left(\frac{V_c}{V_{app}}\right), \tag{14.20}$$

where $V_c = 20$ kt and $V_{app} = 1.23\,V_{stall}$. This requires simultaneous balance of side force, rolling and yawing moment. From EOM for steady asymmetric horizontal flight and applying the straight-flight condition $rb/(2V) = 0$ [41], the non-dimensional equilibrium system is given by Equation 14.21:

$$\begin{bmatrix} C_L & C_{Y_\beta} & C_{Y_{\delta_a}} & C_{Y_{\delta_r}} \\ 0 & C_{\ell_\beta} & C_{\ell_{\delta_a}} & C_{\ell_{\delta_r}} \\ 0 & C_{n_\beta} & C_{n_{\delta_a}} & C_{n_{\delta_r}} \end{bmatrix} \begin{pmatrix} \phi \\ \beta \\ \delta_a \\ \delta_r \end{pmatrix} = \mathbf{0} \tag{14.21}$$

For a conventional aircraft, several terms in this system are small and can thus be considered negligible, yielding decoupled expressions for ϕ, δ_a, and δ_r [41]. However, for a BWB these simplifications are not applicable as, firstly, the lack of a vertical tail means C_{n_β} may be small, making the neglected cross-coupling terms relatively more significant. Additionally, the rudder deflections required to maintain directional equilibrium may be large, meaning the side force generated by the rudder $C_{Y_{\delta_r}}\delta_r$ can no longer be neglected in the lateral force balance.

By determining β using Equation 14.20, the system can be solved numerically using the stability and control derivatives obtained from AVL. The crosswind requirement is satisfied if the resulting deflections remain within the bounds of the maximum control surfaces deflection, as represented by Equation 14.22:

$$|\delta_r| \leq \delta_{r,\max} \quad \text{and} \quad |\delta_a| \leq \delta_{a,\max} \tag{14.22}$$

The numerical results obtained from carrying out this analysis are not reported here as they depend critically on the lateral-directional stability derivatives (C_{n_β}, C_{l_β}, C_{Y_β}) and control derivatives ($C_{n_{\delta_r}}$, $C_{l_{\delta_a}}$) extracted from AVL. The current AVL model has a divergence error that renders all stability and control derivatives unreliable as explained in detail in Section 14.14.

14.7.2. One Engine Inoperative (OEI) Yaw Requirement

Without a vertical stabiliser, yaw control fully relies on drag-split rudders, which are located on the winglets. The drag generated by one fully-opened panel provides the restoring yaw moment in case of one engine being inoperative.The certification requirement which oversees this is CS-25.149 [9], which states that the minimum control speed V_{MC} must satisfy Equation 14.23:

$$V_{MC} \leq 1.13 \cdot V_{SR} b1 \tag{14.23}$$

where V_{SR} is the reference stall speed defined in CS-25.103 which may not be less than a 1-g stall speed [9], the value taken for standard sea-level ISA evaluation condition ($V_{SR} = V_{S1g}$). Furthermore, CS-25.149(b) specifies that V_{MC} is the calibrated airspeed at which it is possible to maintain control of the aircraft with that engine still inoperative, and maintain straight flight with a bank angle not greater than 5° [9].

In order to ensure lateral stability in case of OEI, first the yaw demand is established, followed by the quantification of rudder authority, the analytical determination of V_{MC}, and the verification of the bank angle constraint.

$V_2 = 1.20\,V_{SR}$ is the take-off safety speed defined in CS-25.113 [9], which represents the minimum airspeed at which the aircraft can safely climb after an engine failure.

1. Asymmetric thrust yaw moment

After the failure of one engine, the remaining engine produces an asymmetric yawing moment about the CG of the aircraft, as visualised in Equation 14.24:

$$N_{thrust} = T_{one} \cdot y_{eng}, \qquad T_{one} = \frac{T_{total}}{N_{eng}} \tag{14.24}$$

where y_{eng} is the lateral distance from the aircraft CG to the engine, and T_{total} and T_{one} are the total thrust and thrust produced by one engine, respectively.

2. Windmiling drag yaw moment

The failed engine generates an additional drag force on its fan area, which increases the yaw demand as it acts in the same direction as the thrust. This is detailed in Equation 14.25 below:

$$A_{fan} = \pi \left(\frac{D_i}{2}\right)^2, \qquad D_{wm} = C_{D,wm}\, q, \qquad N_{wm} = D_{wm} \cdot y_{eng} \tag{14.25}$$

where A_{fan} is the area of the fan, D_i the engine inlet diameter, q the dynamic pressure, N_{wm} the resulting moment caused by windmilling drag, y_{eng} the distance of the engines from the centreline, and $C_{D,wm}$ the windmilling area drag for a high-bypass turbofan calculated using Equation 14.26 [42, p. 564]:

$$C_{D_{wm}} = 0.0785 \cdot D_{fan}^2 + \frac{2}{1 + 0.16 \cdot M^2} \cdot A_N \cdot \frac{V_N}{V} \cdot \left(1 - \frac{V_N}{V}\right) \tag{14.26}$$

where $\frac{V_N}{V}$ is 0.92 for a high bypass engine, M the Mach number, and A_N the area of the nozzle. As it scales with dynamic pressure q, it is therefore speed-dependent. The total OEI yawing moment is therefore defined by Equation 14.27:

$$N_{\text{OEI}} = N_{\text{thrust}} + N_{\text{wm}} \tag{14.27}$$

3. Available yaw moment from split-drag rudder
The drag-split rudder on each winglet is made up of a trailing-edge panel of chord fraction r_f, which gives a one-sided rudder area defined by Equation 14.28:

$$S_{\text{rud}} = r_f \cdot c_w \cdot h_w \tag{14.28}$$

where c_w and h_w are the winglet chord and height respectively. During OEI only one of the rudder panels is opened, with the other one not producing any additional drag.

The drag coefficient $C_{D,\delta}$ of the deflected panel depends on deflection angle, panel aspect ratio, and local flow conditions at the winglet. At this stage of the design, it cannot be determined analytically to sufficient accuracy, and would require CFD analysis or wind tunnel testing. For the purposes of preliminary sizing, a constant value of $C_{D,\delta} = 1.17$ is assumed, representative of a bluff body at high deflection angles[1]. The drag force and resulting yawing moment produced by the open rudder panel is then defined by Equation 14.29:

$$D_{rud} = C_{D,\delta}\, q\, S_{rud}, \qquad N_{rud} = D_{rud} \cdot y_{rud}, \tag{14.29}$$

where y_{rud} is the lateral distance from the aircraft CG to the winglet drag-split rudder.

4. Minimum control speed V_{MC}
Following the yaw moment equilibrium condition, V_{MC} can be determined, as the available rudder moment must be greater than or equal to the total OEI demand. Substituting the previously stated relations, this is shown by Equation 14.30:

$$C_{D,\delta}\, \tfrac{1}{2}\rho V^2\, S_{\text{rud}}\, y_{\text{rud}} \;=\; \left(T_{\text{one}} + C_{D,wm}\, \tfrac{1}{2}\rho V^2\right) y_{\text{eng}}, \qquad V_{\text{MC}} = \sqrt{\frac{2\, T_{\text{one}}\, y_{\text{eng}}}{\rho\left(C_{D,\delta}\, S_{\text{rud}}\, y_{\text{rud}} - C_{D,wm}\, y_{\text{eng}}\right)}}. \tag{14.30}$$

5. Verification at key speeds
Beyond V_{MC}, the drag-split rudder must also provide sufficient yaw authority at takeoff and at approach, with speeds V_2 and V_{app}, respectively. At each of these conditions, the yaw authority margin is defined by Equation 14.31 as:

$$\eta_{yaw} = \frac{N_{rud}}{N_{OEI}} \geq 1, \tag{14.31}$$

where N_{OEI} is evaluated at the respective speed and thrust setting.

At V_2 maximum takeoff thrust is used, while at V_{app} the analysis is conducted ≈15% of the maximum thrust, as the failure is assumed to have occurred earlier in flight.

6. Bank angle constraint
As mentioned above, there is a 5° bank angle constraint, which, while for a conventional rudder this is driven by the need to balance the rudder side force with a weight component $W \sin\phi$, the drag-split rudder produces only a streamwise drag force and has essentially no aerodynamic side-force component ($C_{Y,\delta_r} \approx 0$). With zero sideslip (the standard V_{MC} evaluation condition), the lateral force equilibrium therefore requires negligible bank angle from the aerodynamic balance alone.

However, a conservative upper bound can be computed by treating the full rudder drag as if it were a lateral side force using Equation 14.32, giving:

$$\phi \leq \arctan\left(\frac{D_{\text{rud}}}{W}\right). \tag{14.32}$$

If this overestimate satisfies $\phi \leq 5°$, the CS-25.149(b) constraint is verified without requiring a detailed rolling-moment analysis. The actual true bank angle for a drag-split device is lower because the side-force balance contributes nothing; a non-zero ϕ could only arise from the rolling moment induced by the asymmetric drag force at the winglet tip, which is small and is deferred to the control-law design phase.

Results
This analysis is performed at sea-level ISA with $y_{eng} = 8$ m, $T_{one} = 296$ kN, and a drag-split rudder area $S_{rud} = 6.3$ m^2 ($r_f = 0.40$, $c_w = 3.5$ m, $h_w = 4.5$ m), yielding an asymmetric thrust moment of 2368 kN· m. At approach speed V_{app} = 278 kt, the windmilling drag sums an additional $N_{wm} = 83$ kN· m, totalling an OEI yaw demand of $N_{OEI} = 2451$ kN· m. The available rudder moment at V_{app} is $N_{rud} = 3007$ kN· m, yielding a margin of $\eta_{yaw} = 1.23$, thus directional control is maintained, while at $V_2 = 271$ kt the margin is 1.17.

[1] URL `https://www.grc.nasa.gov/www/k-12/VirtualAero/BottleRocket/airplane/shaped.html` [Cited 14/06/2026]

Solving the yaw equilibrium for V_{MC} gives $V_{MC} = 251$ kt, against the CS-25.149 limit of $1.13 \times V_{SR} = 256$ kt, satisfying the requirement with $V_{MC}/V_{SR} = 1.107$. The bank angle upper bound at V_{MC} is $\phi \leq \arctan(D_{rud}/W) = 4.10°$, within the 5° limit of CS-25.149.

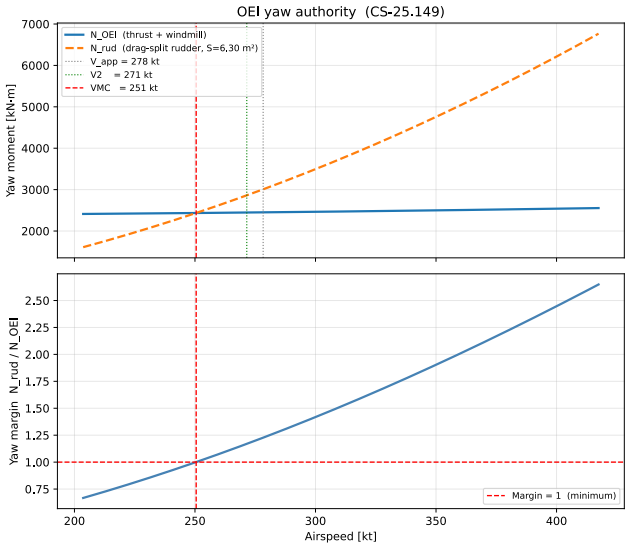

Figure 14.1: One Engine Inoperative yaw authority

Figure 14.1 shows the yaw moment balance and margin as a function of airspeed. In the upper subplot, N_{OEI} is nearly flat with speed as N_{thrust} dominates and is speed-independent, while N_{rud} grows with V^2 since it is driven by dynamic pressure. The two curves intersect at $V_{MC} = 251$ kt, below which the rudder is insufficient. The lower subplot shows the yaw margin $\eta_{yaw} = N_{rud}/N_{OEI}$ directly, crossing unity at V_{MC} and reaching 1.23 at V_{app}, thus confirming adequate authority across the take-off and approach envelope.

14.8. Eigenmotion Analysis

To determine the physical flight eigenmodes of a BWB from stability derivatives, a structured mathematical approach is followed involving the construction of state-space models and the analysis of their eigenvalues and eigenvectors. First of all, the state equation represents the motion of an aircraft in natural form and it is defined as Equation 14.33 for a trimmed aircraft [43].

$$\dot{x} = A\vec{x} + B\vec{u} \tag{14.33}$$

where A and B are the state and control coefficient matrices, respectively with state vector $\vec{x}$ and control vector $\vec{u}$. The state equation is used to describe the control and stability of an aircraft for known inputs. Subsequently, the eigenvalues (λ) of each state matrix are found by solving the characteristic equation $\det(\lambda I - A) = 0$. These eigenvalues represent the "poles" of the system. Their location on the complex plane determines the stability and type of the mode [44]. The real axis indicates stability: negative value is damping or stable, while positive values indicate divergence or instability. Furthermore, a non-zero imaginary part indicates oscillations mode and provide the frequency.

Each eigenvalue is identified as a specific physical mode based on its frequency, damping, and which state variables it primarily influences.

Longitudinal Modes

Short Period Mode: Identified as a high-frequency, heavily damped oscillatory mode. It primarily acts on the angle of attack (α) and pitch rate (q). In unstable BWBs, this may split into two real poles, one of which is positive, indicating strong longitudinal instability.

Phugoid Mode: Identified as a low-frequency, lightly damped oscillation. It characterises a slow exchange between kinetic and potential energy, primarily affecting airspeed (V) and pitch attitude (θ) while the angle of attack remains nearly constant.

Lateral-Directional Modes

Dutch Roll Mode: A coupled yaw-roll oscillation identified as a complex conjugate pair of eigenvalues [45]. It typically features a relatively low frequency and can be poorly damped or unstable in BWB configurations without vertical surfaces.

Roll Subsidence Mode: A non-oscillatory, pure roll decay mode. It is identified by a single large negative real eigenvalue and primarily dictates how fast the roll rate (p) converges following a disturbance.

Spiral Mode: A slow, real-root mode corresponding to bank angle (ϕ) and heading divergence or convergence. It is identified by a real eigenvalue very close to the origin; if positive, it signifies spiral divergence, where a small bank angle increases over time.

14.9. Longitudinal Dynamic Stability

The dynamic stability of the aircraft is assessed by constructing a linearised state-space model about the trimmed cruise flight condition. The equations of motion are decoupled into two independent fourth-order systems: one governing the longitudinal motion and one governing the lateral-directional motion. For each system, the eigenvalues of the state matrix determine the stability and character of the natural flight modes, while the corresponding eigenvectors identify which state variables are primarily involved in each mode [43].

The state vector defines the appearance of the coefficient matrix A; it is therefore defined first in Equation 14.34 for the longitudinal motion [35]:

$$\mathbf{x} = \langle u,\ w,\ q,\ \theta \rangle, \tag{14.34}$$

where u and w are the velocities in the x- and z-directions, respectively, q is the pitch rate, and θ is the pitch angle.

The state matrix A is defined in Equation 14.35, where g is the gravitational acceleration, U_0 is the trim airspeed, and the entries X_u, X_w, Z_u, Z_w, M_u, M_w, and M_q are the aerodynamic stability derivatives describing the sensitivity of the axial force, normal force, and pitching moment to perturbations in forward speed, heave velocity, and pitch rate, respectively. From the eigenvalues and eigenvectors of this matrix, the modal properties of the longitudinal motion can be computed.

$$A \triangleq \begin{bmatrix} X_u & X_w & 0 & -g \\ Z_u & Z_w & U_0 & 0 \\ M_u & M_w & M_q & 0 \\ 0 & 0 & 1 & 0 \end{bmatrix} \tag{14.35}$$

The speed-dependent force derivatives X_u and Z_u capture the change in aerodynamic drag and lift with forward-speed perturbation, and are given by Equation 14.36:

$$X_u = \frac{\rho \cdot S \cdot u}{m} \cdot \left(-C_D - C_{D_u}\right), \qquad Z_u = \frac{\rho \cdot S \cdot u}{m} \cdot \left(-C_L - C_{L_u}\right), \tag{14.36}$$

where ρ is the air density, S is the reference wing area, m is the aircraft mass, C_D and C_L are the trim drag and lift coefficients, and C_{D_u} and C_{L_u} are the compressibility correction terms, which can be neglected as they are significantly smaller than C_D and C_L.

The angle-of-attack force derivatives X_w and Z_w describe the change in axial and normal forces arising from a perturbation in velocity w, which is equivalent to a perturbation in angle of attack $\alpha = w/U_0$. They are given by Equation 14.37:

$$X_w = \frac{-\rho \cdot S \cdot U_0}{2m} \cdot \left(C_{D_\alpha} - C_L\right), \qquad Z_w = \frac{-\rho \cdot S \cdot U_0}{2m} \cdot \left(C_{L_\alpha} + C_D\right), \tag{14.37}$$

where C_{D_α} and C_{L_α} are the drag and lift curve slopes with respect to angle of attack, which can be neglected as they are significantly smaller than C_D and C_L.

The moment derivatives in the state matrix must account for the coupling between pitch-rate acceleration and the heave velocity through the downwash lag term $M_{\dot{w}}$. The corrected (tilde) moment derivatives are therefore introduced and defined in Equation 14.38:

$$\tilde{M}_u = M_u + M_{\dot{w}} \cdot Z_u, \qquad \tilde{M}_w = M_w + M_{\dot{w}} \cdot Z_w, \qquad \tilde{M}_q = M_q + U_0 \cdot M_{\dot{w}}, \tag{14.38}$$

where $M_{\dot{w}}$ is the pitch-rate acceleration derivative arising from the lag in the downwash field. In each corrected derivative the second term represents this lag contribution; without it, the pitching moment response to heave and pitch-rate perturbations would be overestimated. The base moment derivatives M_u, M_w, and M_q are defined below.

The base pitching moment derivative with respect to forward speed, M_u, is given by Equation 14.39:

$$M_u = \frac{\rho \cdot S \cdot U_0 \cdot \bar{c}}{I_y} \cdot \left(C_{m_u} + C_m\right), \tag{14.39}$$

where $\bar{c}$ is the mean aerodynamic chord, I_y is the moment of inertia about the pitch axis, C_m is the trim pitching moment coefficient, and C_{m_u} is the Mach-number-dependent pitching moment derivative. Since C_{m_u} is very small compared with C_m at the cruise condition, it is neglected in the calculation.

The angle-of-attack pitching moment derivative M_w and the static stability coefficient C_{m_α} are directly related to the longitudinal static stability of the aircraft, and are defined in Equation 14.40:

$$M_w = \frac{\rho \cdot S \cdot U_0 \cdot \bar{c}}{2I_y} \cdot C_{m_\alpha}, \qquad C_{m_\alpha} = \frac{\partial C_m}{\partial \alpha}. \tag{14.40}$$

A negative value of C_{m_α} indicates static longitudinal stability, as a positive angle-of-attack perturbation produces a nose-down restoring moment. The pitch-rate damping derivative M_q quantifies the aerodynamic moment generated

in opposition to a pitch rate, and is the primary source of short-period damping. It is defined in Equation 14.41:

$$M_q = \frac{\rho \cdot S \cdot U_0 \cdot \bar{c}^2}{4 I_y} \cdot C_{m_q} \tag{14.41}$$

where C_{m_q} is the non-dimensional pitch damping coefficient obtained from AVL.

14.9.1. Eigenvalues and Modal Characteristics

The eigenvalues of the longitudinal state matrix A (Equation 14.35) were extracted at the reference cruise condition ($M = 0.79$, $h = 35\,000$ ft, $\alpha = 0.44°$, $m = 130$ t) to identify the phugoid and short-period modes. Figure 14.1 reports $\lambda = \sigma + j\omega$, the time constant $\tau = 1/|\sigma|$, and the time to half/double amplitude $t = \ln 2/|\sigma|$.

Table 14.1: Longitudinal eigenvalues at the reference cruise condition.

Mode	σ	ω	τ [s]	$t_{1/2}\,/\,t_2$ [s]
Phugoid	−20.854	0	0.05	0.03 ($t_{1/2}$)
Short Period	+10.242	0	0.10	0.07 (t_2)

Phugoid: stable. Short period: unstable. All σ, ω in rad/s.

Both eigenvalues are purely real ($\omega = 0$), indicating aperiodic motion for both modes. The positive short-period root confirms the divergent character from the unstable pitch stiffness ($C_{m_\alpha} > 0$). The strongly damped phugoid ($\tau = 0.05$ s) conflicts with the multi-second periods in Subsection 14.9.2

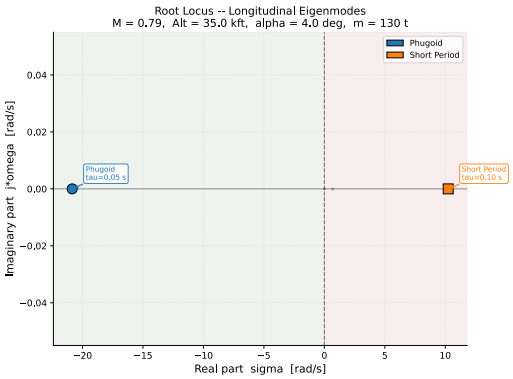

Figure 14.2: Root locus at the reference cruise condition. All four roots lie on the real axis; the Dutch roll pair of Subsection 14.10.2 is absent from this dataset.

14.9.2. Phugoid

According to ICAO criteria, satisfactory phugoid characteristics require positive damping ($2\zeta\omega_n > 0.01$ to 0.05), while acceptable emergency limits tolerate mild instability down to $2\zeta\omega_n \geq -0.023$ (provided the period $T \geq 15$ s) [46]. As shown in Figure 14.3, the aircraft fails to meet the satisfactory baseline at any flight condition. Increasing altitude continuously degrades dynamic stability: the phugoid period T decreases from approximately 76 seconds at sea level ($H = 0$ km) to 62 seconds at $H = 12$ km, while the damping metric $2\zeta\omega_n$ becomes progressively more negative. Consequently, while flight points up to 9 km remain within the acceptable emergency buffer, the pronounced instability at the maximum evaluated altitude of 12 km pushes a segment of the flight envelope into the unacceptable zone ($2\zeta\omega_n < -0.023$).

14.9.3. Short Period

According to ICAO criteria, standard short-period longitudinal dynamics are bounded by natural frequency (ω_n) and total damping ($2\zeta\omega_n$) thresholds [46]. However, as illustrated in Figure 14.4, the evaluated BWB aircraft exhibits unstable pitch stiffness ($C_{m_\alpha} > 0$), resulting in a non-oscillatory, overdamped mode that must be evaluated using the dominant time constant ($\tau = 1/|\sigma|$). At lower altitudes (up to 9 km), the aircraft maintains a fast response that falls comfortably within the satisfactory region ($\tau \leq 2$ s). At the maximum evaluated altitude of 12 km, the response slows considerably, causing a portion of the flight envelope to degrade into the acceptable buffer region. Despite this high-altitude performance drop, the short-period divergence remains manageable, and no evaluated flight points cross the 5-second threshold into the unacceptable zone.

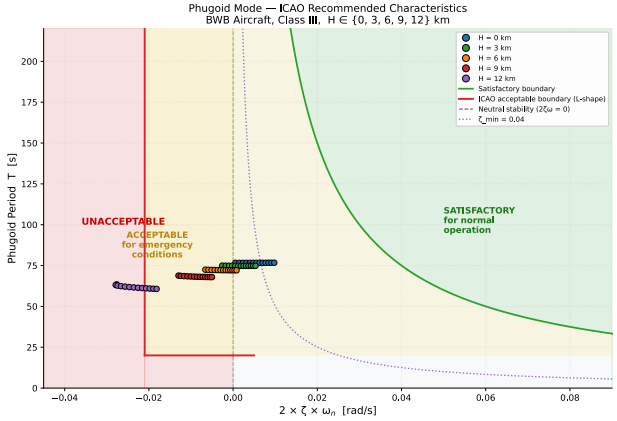

Figure 14.3: ICAO recommended characteristics map for the phugoid mode of a Class III BWB aircraft. Data points illustrate the inverse relationship between altitude ($H = 0$ to 12 km) and dynamic stability, mapping the shift from acceptable emergency conditions toward the unacceptable boundary.

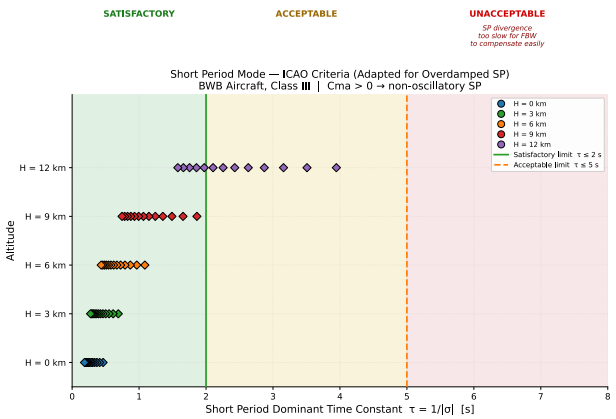

Figure 14.4: Short Period mode characteristics adapted for an overdamped response ($\tau = 1/|\sigma|$). The data maps the dominant time constants for a Class III BWB aircraft across varying altitudes against modified ICAO boundaries.

14.10. Lateral Dynamic Stability

The state vector for the lateral-directional motion is $\mathbf{x} = \langle v,\ p,\ r,\ \phi \rangle$, where v is the lateral velocity perturbation, p the roll rate, r the yaw rate, and ϕ the bank angle. The corresponding state matrix is defined in Equation 14.42, where Y_v is the lateral force derivative with respect to sideslip velocity, and the primed derivatives L'_i and N'_i incorporate the inertial cross-coupling correction due to the product of inertia I_{xz}.

$$A \triangleq \begin{bmatrix} Y_v & 0 & -1 & g/U_0 \\ L'_\beta & L'_p & L'_r & 0 \\ N'_\beta & N'_p & N'_r & 0 \\ 0 & 1 & 0 & 0 \end{bmatrix} \tag{14.42}$$

The lateral force derivative Y_v and its non-dimensional coefficient C_{y_β} are defined in Equation 14.43:

$$Y_v = \frac{\rho \cdot U_0 \cdot S}{2m} \cdot C_{y_\beta}, \qquad C_{y_\beta} = \frac{\partial C_y}{\partial \beta} \tag{14.43}$$

Since the aircraft has a non-zero product of inertia I_{xz}, the roll and yaw equations of motion are inertially coupled. The primed derivatives decouple this coupling and are defined in Equation 14.44:

$$L'_i = L_i + \frac{I_{xz}}{I_z} \cdot N_i, \qquad N'_i = N_i + \frac{I_{xz}}{I_z} \cdot L_i \tag{14.44}$$

where I_z is the yaw inertia and i denotes the lateral-directional perturbation variables (β, p, r). The sideslip derivatives L_β and N_β indicate lateral and directional static stability, respectively, and are defined via their non-dimensional coefficients in Equation 14.45:

$$L_\beta = \frac{\rho \cdot U_0^2 \cdot S \cdot b}{2I_x} \cdot C_{l_\beta}, \qquad C_{l_\beta} = \frac{\partial C_l}{\partial \beta}, \qquad N_\beta = \frac{\rho \cdot U_0^2 \cdot S \cdot b}{2I_z} \cdot C_{n_\beta}, \qquad C_{n_\beta} = \frac{\partial C_n}{\partial \beta} \tag{14.45}$$

where b is the wing span and I_x is the roll inertia. Lateral and directional stability require $C_{l_\beta} < 0$ and $C_{n_\beta} > 0$ to provide restoring moments. The roll-rate derivatives L_p and N_p (Equation 14.46) represent the primary roll damping and roll-yaw coupling, respectively.

$$L_p = \frac{\rho \cdot U_0 \cdot S \cdot b^2}{4I_x} \cdot C_{l_p}, \qquad C_{l_p} = \frac{\partial C_l}{\partial\left(\dfrac{pb}{2U_0}\right)}, \qquad N_p = \frac{\rho \cdot U_0 \cdot S \cdot b^2}{4I_z} \cdot C_{n_p}, \qquad C_{n_p} = \frac{\partial C_n}{\partial\left(\dfrac{pb}{2U_0}\right)} \tag{14.46}$$

The yaw-rate derivatives L_r and N_r in Equation 14.47 describe the rolling and yawing moments generated by a yaw rate perturbation. N_r is the dominant yaw damping term and the primary source of Dutch roll damping, while L_r couples the yaw and roll dynamics and influences the spiral mode.

$$L_r = \frac{\rho \cdot U_0 \cdot S \cdot b^2}{4I_x} \cdot C_{l_r}, \qquad C_{l_r} = \frac{\partial C_l}{\partial\left(\dfrac{rb}{2U_0}\right)}, \qquad N_r = \frac{\rho \cdot U_0 \cdot S \cdot b^2}{4I_z} \cdot C_{n_r}, \qquad C_{n_r} = \frac{\partial C_n}{\partial\left(\dfrac{rb}{2U_0}\right)} \tag{14.47}$$

All non-dimensional stability derivatives above are obtained from the Athena Vortex Lattice (AVL) code.

14.10.1. Eigenvalues and Modal Characteristics

The eigenvalues of the lateral-directional state matrix A defined in Equation 14.42 were extracted at the same reference condition. Figure 14.2 reports the full eigenvalue set; the corresponding root locus is shown in Figure 14.5.

Table 14.2: Lateral-directional eigenvalues at the reference cruise condition.

Root	σ	ω	τ [s]	$t_{1/2}$ / t_2 [s]
1 (fastest decay)	−2.773	0	0.36	0.25 ($t_{1/2}$)
2	−1.126	0	0.89	0.62 ($t_{1/2}$)
3	−0.026	0	39.2	27.2 ($t_{1/2}$)
4 (fastest growth)	+0.938	0	1.07	0.74 (t_2)

Roots 1–3 stable; Root 4 unstable. All σ, ω in rad/s.

As in the longitudinal case, all lateral roots are real: no complex-conjugate pair exists, so no oscillatory Dutch roll mode is present in this linearisation, in direct conflict with the ζ/ω_n-based treatment. The previous extraction retained only the two extreme roots (Roll and Spiral) and discarded the two intermediate ones; Root 3 ($\tau \approx 39$ s) is far more consistent with a slow lateral mode.

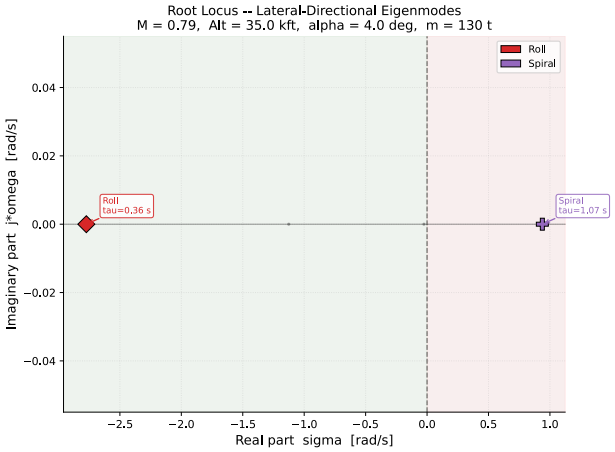

Figure 14.5: Root locus of the lateral-directional eigenmodes at the reference cruise condition. All four roots lie on the real axis.

The spiral time-to-double of 0.74 s (Root 4) is also implausibly fast as typical transport-aircraft spiral divergence doubles over tens of seconds. Unlike the longitudinal case, no single grossly non-physical derivative is evident among C_{Y_β}, C_{l_β}, C_{n_β}; the absence of a Dutch roll pair should thus be verified directly against the AVL stability-derivative output.

14.10.2. Dutch Roll

Based on ICAO criteria, satisfactory Dutch roll handling requires a damping ratio $\zeta \geq 0.08$ and natural frequency $\omega_n \geq 0.4$ rad/s, while acceptable emergency limits are relaxed to $\zeta \geq 0.02$ and $\omega_n \geq 0.15$ rad/s [46]. However, as shown in Figure 14.6, the evaluated BWB aircraft exhibits significant lateral-directional deficiencies. Although inherently stable, damping degrades at higher altitudes and airspeeds, causing 25.5% of the flight points to fall below the $\zeta = 0.08$ threshold. Furthermore, all 1000 evaluated points fail the minimum $\zeta\omega_n \geq 0.15$ rad/s requirement. This complete non-compliance stems from the aircraft's lack of a vertical tail, which results in remarkably weak weathercock stability ($C_{n\beta} \approx 0.00067$ rad^{-1}) and an unusually low natural frequency, dictating the need for stability augmentation [45].

14.10.3. Roll

According to MIL-SPEC criteria , the lateral-directional roll mode is evaluated based on the roll mode time constant (τ_R), which dictates the required responsiveness of the aircraft [46]. As illustrated in Figure 14.7, the evaluated BWB aircraft exhibits exemplary, highly stable roll dynamics across varying true airspeeds and altitudes. As τ_R remains well below 1.0 second. This performance comfortably satisfies the stringent Level 1 flying qualities requirement ($\tau_R \leq 1.4$ s), demonstrating an responsive roll mode that requires no additional physical augmentation.

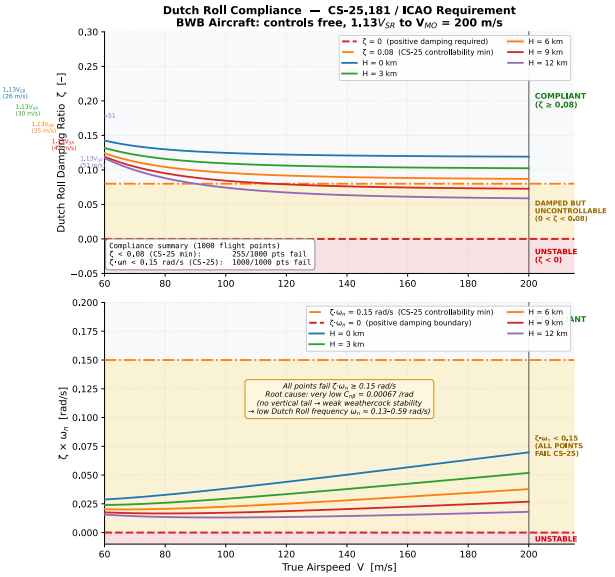

Figure 14.6: Dutch Roll compliance across true airspeed and altitude. The lack of a vertical tail results in weak weathercock stability, causing universal failure of the $\zeta\omega_n \geq 0.15$ rad/s criteria.

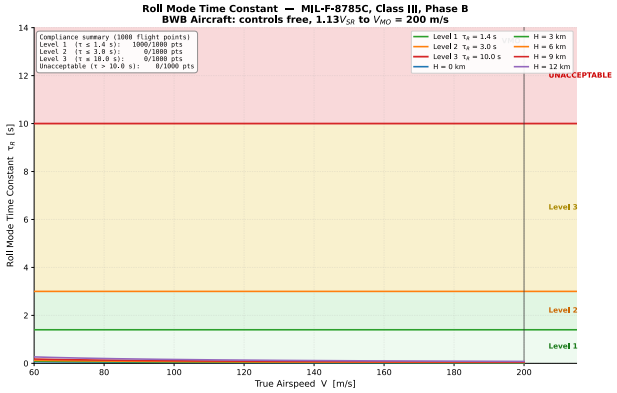

Figure 14.7: Roll Mode time constant τ_R evaluated against MIL-F-8785C limits. The configuration demonstrates highly responsive, Level 1 compliant roll characteristics across all evaluated altitudes and airspeeds.

14.10.4. Spiral

For the spiral mode, positive damping of the spiral motion is assessed using Equation 14.48, which is derived from the Routh–Hurwitz stability criterion for the asymmetric equations of motion [47]:

$$C_{\ell_\beta} C_{n_r} - C_{n_\beta} C_{\ell_r} > 0 \tag{14.48}$$

The criterion states that a stable spiral mode requires the product of the dihedral effect and the yaw damping to exceed the product of the directional stability and the roll-due-to-yaw-rate derivative. Physically, a large dihedral effect C_{ℓ_β} and strong yaw damping C_{n_r} promote spiral stability, while a strong directional restoring moment C_{n_β} combined with a large C_{ℓ_r} tends to destabilise the spiral. The control derivatives in Equation 14.48 are computed by AVL. The resulted values for $C_{\ell_\beta} C_{n_r} - C_{n_\beta} C_{\ell_r} = 0.598$ indicates that the BWB is spirally stable.

14.11. Landing Gear Positioning

The landing gear arrangement must satisfy longitudinal and lateral ground-stability criteria during all possible loading configurations [48]. In accordance with the design principles, the undercarriage configuration must comply with three primary constraints:

1. **Nose-Gear Load Fraction:** To ensure compliance with CS 25.233 (Directional stability and control), which mandates adequate steering capability without uncontrollable ground-looping tendencies (e.g., in 90° crosswinds), the static load on the nose landing gear (NLG) must remain within bounds to preserve traction without risking structural damage [9]:

$$0.08 \leq \frac{F_N}{W} \leq 0.15 \tag{14.49}$$

2. **Turnover Angle:** To prevent lateral tip-over during ground manoeuvring and to satisfy the $0.5g$ lateral turning load requirement dictated by CS 25.495 (Turning), the turnover angle (ψ) must not exceed a critical threshold [9]:

$$\psi < 55^\circ \tag{14.50}$$

3. **Pitch Angle (Tip-Back) Limit:** To prevent the aircraft from rotating aft onto its tail, either under extreme aft-biased ground loading or during the take-off rotation manoeuvre, the angle (β) subtended at the MLG ground-contact point between the vertical and the line to the most-aft CG must exceed the maximum nose-up attitude attainable with the gear struts fully extended before tail contact ($\theta_{\text{tipback}} \approx 15^\circ$) [48]:

$$\beta > \theta_{\text{tipback}} \tag{14.51}$$

4. **CG Envelope:** Driven by the requirements of CS 25.471 (General ground loads) and CS 25.489 (Ground handling conditions), the aircraft's CG must strictly remain inside the triangle formed by the nose gear and the main landing gear (MLG) units for all critical loading configurations to prevent tail-tipping during operations like towing, braking, or uphill pivoting [9].

14.11.1. Nose Landing Gear (NLG) Longitudinal Position

The NLG position from the nose (x_{NLG}) is calculated using static moment equilibrium about the ground contact point of the main gear. The balance of vertical forces and pitching moments gives:

$$W = 2F_M + F_N \qquad 2F_M b_M - F_N b_N = 0, \tag{14.52}$$

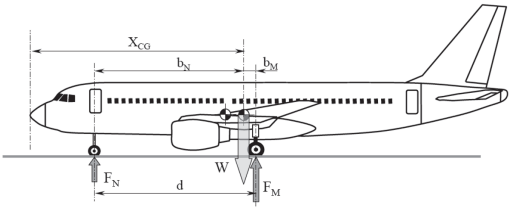

Figure 14.8: Side-view free-body diagram illustrating the longitudinal static loads (F_N, F_M) and geometric moment arms used to calculate landing gear weight distribution [48].

where $b_M = x_{\text{MLG}} - x_{\text{cg}}$ is the MLG lever arm from the CG, $b_N = x_{\text{cg}} - x_{\text{NLG}}$ is the NLG lever arm from the CG, and $d = x_{\text{MLG}} - x_{\text{NLG}}$ is the total wheel base. Equation 14.52 simplifies to the standard load fraction formula:

$$\frac{F_N}{W} = \frac{b_M}{d} \tag{14.53}$$

To respect the upper and lower bounds of the load fraction (defined in Equation 14.53) across the entire loading envelope, two distinct minimum wheel base parameters are checked:

1. **Forward CG Case ($x_{\text{cg,fwd}}$):** Dictates that the maximum nose load must not exceed the maximum allowable fraction ($(F_N/W)_{\max} = 0.15$):

$$d_{\text{fwd}} = \frac{x_{\text{MLG}} - x_{\text{cg,fwd}}}{(F_N/W)_{\max}} \tag{14.54}$$

2. **Aft CG Case ($x_{\text{cg,aft}}$):** Dictates that the minimum nose load must not fall below the minimum operational fraction ($(F_N/W)_{\min} = 0.08$):

$$d_{\text{aft}} = \frac{x_{\text{MLG}} - x_{\text{cg,aft}}}{(F_N/W)_{\min}} \tag{14.55}$$

To satisfy both constraints simultaneously, the larger required wheel base is chosen, setting the final nose gear coordinate to:

$$d = \max(d_{fwd}, d_{aft}) \quad \Longrightarrow \quad x_{NLG} = x_{MLG} - d \tag{14.56}$$

14.11.2. Pitch Angle (Tip-Back) Limit

In addition to the load-fraction check, the longitudinal placement of the MLG must guarantee that the aircraft cannot rotate aft onto its tail, whether under extreme aft ground loading or during the take-off rotation manoeuvre.

As illustrated in Figure 14.9, the pitch angle β is defined in Equation 14.57 as the angle, measured at the MLG ground-contact point, between the vertical line and the line connecting that point to the CG. The most-aft CG position is the critical loading case, since it minimises the horizontal arm $\left(x_{\text{MLG}} - x_{\text{cg}}\right)$ and therefore minimises β.

$$x_{\text{MLG}} = x_{\text{cg,aft}} + Z_{\text{CG}} \cdot \tan(\beta), \qquad \beta = \arctan\left(\frac{x_{\text{MLG}} - x_{\text{cg,aft}}}{Z_{\text{CG}}}\right). \tag{14.57}$$

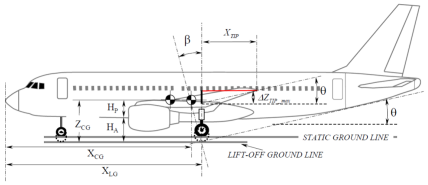

Figure 14.9: Geometric definition of pitch (β) and tip-back (θ_{tipback}) angles at the MLG contact point, relative to the CG with struts fully extended [48].

Stability against tip-back requires β to exceed the tip-back angle θ_{tipback} (Equation 14.58), defined as the maximum nose-up attitude the aircraft can reach before the tail contacts the ground.

$$\beta > \theta_{\text{tipback}}, \qquad \theta_{\text{tipback}} \approx 15^\circ. \tag{14.58}$$

If this margin is not met, the most-aft CG lies far enough aft relative to the MLG position and the CG height Z_{CG} that the aircraft would rotate backward onto its tail before reaching the tail-strike attitude — for example during aft-biased cargo or passenger loading, or while parked nose-up on a sloped ramp.

14.11.3. Main Landing Gear Track Width and Lateral Stability

The half-track width (Y_{LG}, the lateral distance from the aircraft centerline to a single MLG strut) is selected to meet the maximum turnover angle ($\psi_{\max}$) constraint in Figure 14.10. The turnover angle corresponds to the orientation of the resultant force vector when the aircraft is on the verge of rolling over its outer wheel track during ground turning. From the geometric projection, the plan-view angle of the landing gear rollover line (α) is formulated as:

$$\alpha = \arctan\left(\frac{Y_{\text{LG}}}{d}\right) \tag{14.59}$$

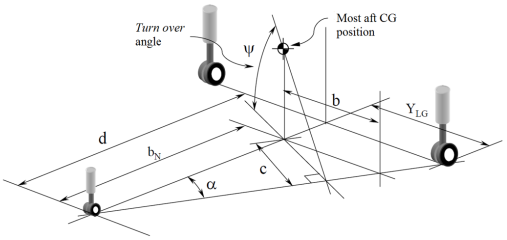

Figure 14.10: Geometric layout for aircraft lateral ground stability and turnover angle (ψ) derivation. The diagram illustrates the relationship between the wheel base (d), main landing gear half-track (Y_{LG}), and the clearance distance (c_t) from the NLG to the CG projection [48].

The minimum lateral clearance distance from the NLG to the CG projection (c_t) is calculated in Equation 14.60 based on the NLG lever arm in the critical most-aft CG state ($b_{\text{N,aft}} = x_{\text{cg,aft}} - x_{\text{NLG}}$)

$$c_t = b_{\text{N,aft}} \cdot \sin(\alpha) = b_{\text{N,aft}} \cdot \frac{Y_{\text{LG}}}{\sqrt{Y_{\text{LG}}^2 + d^2}} \tag{14.60}$$

The maximum turnover angle requirement dictates that $\tan(\psi_{\max}) = \frac{Z_{\text{CG}}}{c_{\text{t,min}}}$, which yields the minimum baseline clearance (Equation 14.61).

$$c_{\text{t,min}} = \frac{Z_{\text{CG}}}{\tan(\psi_{\max})} \tag{14.61}$$

Defining a geometric ratio constant $K = \frac{c_{\text{t,min}}}{b_{\text{N,aft}}}$, the analytical solution for the minimum required half-track width is isolated by solving the quadratic relationship in Equation 14.62.

$$K = \frac{Y_{\text{LG}}}{\sqrt{Y_{\text{LG}}^2 + d^2}} \quad \Longrightarrow \quad Y_{\text{LG,min}} = \frac{d \cdot K}{\sqrt{1 - K^2}} \tag{14.62}$$

To ensure ground safety against dynamic lateral rolling variations, a 10% safety margin is added over the minimum track width, establishing the final result in Equation 14.63.

$$Y_{\text{LG}} = 1.10 \cdot Y_{\text{LG,min}} \quad \Longrightarrow \quad Y_{FT} = 2 \cdot Y_{\text{LG}} \tag{14.63}$$

14.11.4. Resulting Geometry and Discussion

Since CG position depends on the gear's own mass and moment contribution, the CG range and gear geometry are coupled and were solved iteratively: an assumed gear position gives a CG range, which is fed back into the x_{NLG}, x_{MLG}, and Y_{LG} equations until both converge. Using the converged CG range $x_{\text{cg,fwd}} = 13.855$ m, $x_{\text{cg,aft}} = 14.865$ m, and CG height $Z_{\text{CG}} = 4.00$ m, this yields the gear layout in Table 14.3.

Table 14.3: Converged landing gear geometry.

Parameter	Value
NLG position, x_{NLG}	1.530 m
MLG position, x_{MLG}	16.024 m
Wheel base, d	14.495 m
MLG half-track, Y_{LG}	3.425 m
Full track width, $2Y_{\text{LG}}$	6.850 m
CG height, Z_{CG}	4.00 m

Ground-stability is verified at both CG extremes by checking the nose-wheel load fraction F_N/W, tip-back angle ψ, and overturn angle β, summarised in Table 14.4. Both cases pass, with load fractions sitting at $F_N/W = 0.1497$ (forward) and exactly 0.0800 (aft) against bounds of 0.15 and 0.08 — a tight but feasible design. The 55° turnover limit is also met in both cases, though not by the case used to size Y_{LG}: sized on the aft-CG case, the half-track gives $\psi = 52.59°$ there, but the forward-CG case is actually governing at $\psi = 54.75°$, only 0.25° below the limit, since a shorter NLG-to-CG arm b_N raises ψ for the same track width. This shows the importance of checking the turnover angle for every loading case, not just the sizing case.

Table 14.4: Verification of ground-stability constraints for all loading cases.

Parameter	Most forward	Most aft
x_{cg} [m]	13.855	14.865
F_N/W	0.1497	0.0800
ψ [°]	54.36	52.52
β [°]	23.46	16.17
Status	Pass	Pass

14.12. Manoeuvres

In order to evaluate the different manoeuvres the aircraft is to carry out, different modes have to be taken into account, which are detailed below.

14.12.1. Loiter Condition

Maximum endurance (loiter) occurs at the speed that maximises the lift-to-drag ratio L/D. By differentiating the drag polar equation with respect to C_L and setting $d(C_D/C_L)/dC_L = 0$, as seen in Equation 14.64, the optimum lift coefficient can be obtained [49]:

$$C_L^* = \sqrt{\frac{C_{D_0}}{K}}. \tag{14.64}$$

At this condition $C_{D_0} = KC_L^{*2}$, so the induced and profile drag contributions are equal, and thus $(L/D)_{\max} = 1/(2\sqrt{KC_{D_0}})$.

For level, unaccelerated flight ($n = 1$) the corresponding true airspeed is represented by Equation 14.65

$$V^* = \sqrt{\frac{2W}{\rho(h)\, S_{\text{ref}}\, C_L^*}}. \tag{14.65}$$

14.12.2. Trim Analysis

The BWB configuration has three sets of elevon surfaces (inner, mid, and outer), each contributing independently to lift and pitching moment. For a preliminary trim analysis, all three sets are assumed to deflect by the same angle δ_e, which is the conservative assumption that maximises the trim authority required from a single input channel. Under this assumption, the effective control derivatives are the sum of individual surface contributions [25]:

$$C_{L_{\delta_e}}^{\text{eff}} = \sum_{i=1}^{3} C_{L_{\delta_{e,i}}}, \qquad C_{m_{\delta_e}}^{\text{eff}} = \sum_{i=1}^{3} C_{m_{\delta_{e,i}}}, \tag{14.66}$$

where $i \in \{\text{inner, mid, outer}\}$. These are obtained directly from AVL by running individual surface deflections.

At load factor n and airspeed V, longitudinal trim must satisfy Equation 14.67 [25]:

$$C_L = \frac{2nW}{\rho V^2 S_{\text{ref}}}, \qquad C_L = C_{L_{\text{ref}}} + C_{L_\alpha}\,\Delta\alpha + C_{L_{\delta_e}}^{\text{eff}}\,\delta_e, \qquad C_m = C_{m_{\text{ref}}} + C_{m_\alpha}\,\Delta\alpha + C_{m_{\delta_e}}^{\text{eff}}\,\delta_e = 0, \tag{14.67}$$

where $C_{L_{\text{ref}}}$ and $C_{m_{\text{ref}}}$ are the AVL reference values at angle of attack α_{ref}. This leads to solving Equation 14.68 simultaneously:

$$\delta_e = \frac{C_{m_\alpha}(C_L - C_{L_{\text{ref}}}) - C_{L_\alpha}\, C_{m_{\text{ref}}}}{C_{L_\alpha} C_{m_{\delta_e}}^{\text{eff}} - C_{m_\alpha} C_{L_{\delta_e}}^{\text{eff}}}, \qquad \Delta\alpha = \frac{C_L - C_{L_{\text{ref}}} - C_{L_{\delta_e}}^{\text{eff}}\,\delta_e}{C_{L_\alpha}}. \tag{14.68}$$

Trim is considered achievable when the ganged deflection satisfies $|\delta_e| \le \delta_{e,\max} = 30^\circ$ [25]. Since all three surfaces are assumed to deflect equally, this represents the minimum authority case; in practice, independent scheduling of the three surfaces (e.g. inner surfaces carry pitch trim, while outer surfaces remain undeflected to preserve roll authority) would reduce the required deflection on any individual surface and improve drag performance.

14.12.3. ICAO Holding Turn

ICAO Doc 8168 Vol. I specifies holding airspeed limits and bank-angle constraints [50], where the governing bank angle is the lesser of:

1. the bank angle that produces a standard rate turn of $\dot{\psi} = 3^\circ/\text{s}$:

$$\phi_{rate} = \arctan\left(\frac{\dot{\psi}\, V}{g_0}\right), \tag{14.69}$$

2. a fixed bank angle of 25°.

The resulting load factor, turn rate, and turn radius are as represented by Equation 14.70 [49]:

$$n = \frac{1}{\cos\phi}, \qquad \dot{\psi} = \frac{g_0 \tan\phi}{V}, \qquad R = \frac{V^2}{g_0 \tan\phi} \tag{14.70}$$

The ICAO speed limit in the altitude band below 4267m (14000ft) is 230kt indicated airspeed [50].

14.12.4. V-n Manoeuvre Envelope

The V-n diagram bounds the flight envelope by three independent constraints.

Stall boundary: The maximum aerodynamic load factor at a given airspeed is limited by $C_{L_{\max}}$ [9, 49], as seen in Equation 14.71:

$$n_{\text{stall}}(V) = \frac{\rho\, V^2\, S_{\text{ref}}\, C_{L_{\max}}}{2W}. \tag{14.71}$$

Structural limit: The limit manoeuvring load factor for transport category airplanes is prescribed by CS-25.337 [9]:

$$n_{\max,\text{struct}} = +2.5\, g, \qquad n_{\min,\text{struct}} = -1.0\, g. \tag{14.72}$$

Sustained turn boundary: A banked turn can be sustained only if available thrust equals drag, where the available thrust at altitude is modelled with a power-law lapse in Equation 14.73 [25]:

$$T_{\text{avail}}(h) = T_{\text{SL}}\left(\frac{\rho}{\rho_0}\right)^{\beta}, \tag{14.73}$$

where T_{SL} is sea-level static thrust and β is the lapse exponent (where $\beta \approx 0.8$, a typical value for high-bypass turbofans [25]). The sustained load factor, which satisfies $T_{\text{avail}} = D$, is solved for in Equation 14.74:

$$T_{\text{avail}} = \frac{1}{2}\rho V^2 S_{\text{ref}}\left[C_{D_0} + K\left(\frac{2nW}{\rho V^2 S_{\text{ref}}}\right)^2\right], \qquad n_{\text{sust}}(V) = \frac{\rho V^2 S_{\text{ref}}}{2W}\sqrt{\frac{T_{\text{avail}}/(\frac{1}{2}\rho V^2 S_{\text{ref}}) - C_{D_0}}{K}}. \tag{14.74}$$

Attainable load factor: The binding limit at any speed is represented by Equation 14.75:

$$n_{\text{lim}}(V) = \min\Big(n_{\text{stall}}(V),\, n_{\text{sust}}(V),\, n_{\text{max,struct}}\Big). \tag{14.75}$$

Best sustained turn: The peak of $n_{\text{lim}}(V)$ over the speed range $[V_{\text{lo}}, V_{\text{hi}}]$ defines the best sustained turn condition:

$$V_{\text{BST}} = \arg\max_{V}\, n_{\text{lim}}(V). \tag{14.76}$$

The corresponding turn rate and radius follow from Equation 14.70 with $\phi = \arccos(1/n_{\text{BST}})$.

Results
As explained in Section 14.14, trim deflection results are pending corrected AVL control derivatives. The required lift coefficients at the two trim conditions are identical ($C_{L,\text{trim}} = 0.458$) since both cases are evaluated at the maximum L/D speed where $C_{L,md} = \sqrt{C_{D_0}/K}$ is independent of altitude and load factor; the only difference being that $V_{md} = 306$ kt at cruise and $V_{md} = 269$ kt at sea level. For the ICAO holding turn, the bank angle is limited to 25° by CS-25.149, giving a load factor of $n = 1.10$ g, a turn rate of $\dot{\psi} = 1.67°/\text{s}$, and a turn radius of $R = 5.40$ km.

At 35,000,ft, stall speed is $V_S = 181$,kt and manoeuvre speed is $V_A = 287$,kt. Thrust limits the loiter sustained load factor to $n = 2.43$,g (just below the 2.5,g structural cap). The optimum sustained turn at 317,kt yields $n = 2.50$,g, $\dot{\psi} = 7.90$,deg/s, and $R = 1.18$,km. Because C_{D_0}, K, and thrust lapse models carry design uncertainty, these figures remain indicative. Visualisations are provided in Figure 17.6 (Chapter 17) and Figure 17.7.

14.13. Control Surfaces Sizing

The control surfaces of the BWB are sized to provide sufficient authority in pitch, roll, and yaw across all critical flight conditions. CS 25.233 explicitly mandates that aeroplanes must be satisfactorily controllable, without exceptional piloting skill or alertness [9]. As the BWB lacks a conventional tail, all three axes must be controlled by control surfaces, making the sizing process tightly coupled [46]. The configuration, the aerodynamic model, and the three authority checks are described below, followed by the comparison of six candidate configurations.

14.13.1. Aerodynamic Derivative Sources

For each configuration, an AVL vortex-lattice analysis is performed to extract the stability-axis control derivatives [22], which are listed in Table 14.5. AVL is run at cruise speed and hinge moments are not output by AVL and remain analytical throughout.

Table 14.5: AVL stability-axis derivatives used in the sizing model.

Symbol	Description	Units
C_{L_α}	Whole-aircraft lift-curve slope	rad^{-1}
C_{m_α}	Pitch stiffness derivative	rad^{-1}
C_{l_p}	Roll damping derivative	rad^{-1}
C_{m_q}	Pitch damping derivative	rad^{-1}
C_{n_β}	Yaw stiffness (weathercock)	rad^{-1}
$C_{L_{\delta_k}}, C_{m_{\delta_k}}, C_{l_{\delta_k}}, C_{n_{\delta_k}}$	Control derivatives per surface k	rad^{-1}

14.13.2. Pitch Authority

Pitch authority is checked at the approach condition, which is the most demanding because dynamic pressure is low while a relatively large pitching moment must be available for rotation [51]. The total pitching-moment control derivative is the sum of contributions from all three elevon groups acting symmetrically (Equation 14.77).

$$C_{m_{\delta,\text{tot}}} = 2\left(\left|C_{m_{\delta,o}}\right| + \left|C_{m_{\delta,i}}\right| + \left|C_{m_{\delta,cb}}\right|\right), \tag{14.77}$$

where subscripts o, i, and cb denote the outer, inner, and centrebody elevon pairs respectively, and the factors of two account for the two symmetric halves of the outer and inner pairs. For configurations assessed using AVL, the one-sided AVL derivatives $C_{m_{\delta_k}}$ are multiplied by two to give the symmetric contribution. The available pitch moment at maximum deflection $\delta_{\max}$ is therefore defined in Equation 14.78 as:

$$M_{\text{pitch,avail}} = C_{m_{\delta,\text{tot}}}\, \bar{q}_{\text{app}}\, S_{\text{ref}}\, \bar{c}\, \delta_{\max}, \tag{14.78}$$

where $\bar{q}_{\text{app}}$ is the approach dynamic pressure and $\bar{c}$ the MAC. Subsequently, the rotation moment requirement is expressed and assumed as a constant minimum whole-aircraft pitching-moment coefficient giving a required moment

in Equation 14.79:

$$C_{m,\text{req}} = 0.15, \qquad M_{\text{pitch,req}} = C_{m,\text{req}}\, \bar{q}_{\text{app}}\, S_{\text{ref}}\, \bar{c}. \tag{14.79}$$

The pitch authority margin is then defined in Equation 14.80 as:

$$\xi_{\text{pitch}} = \frac{M_{\text{pitch,avail}}}{M_{\text{pitch,req}}} = \frac{C_{m_{\delta,\text{tot}}}\, \delta_{\max}}{C_{m,\text{req}}}, \qquad \delta_{\text{pitch,req}} = \frac{C_{m,\text{req}}}{C_{m_{\delta,\text{tot}}}}, \tag{14.80}$$

which simplifies to a ratio independent of flight condition. A value $\xi_{\text{pitch}} \geq 1$ is required for feasibility. Furthermore, the deflection angle is required to remain below $\delta_{\max} = 30°$ according to reference values [40].

14.13.3. Roll Authority

Roll authority is assessed through the steady-state roll rate p_{ss} achievable with maximum antisymmetric elevon deflection at approach [35]. In steady rolling flight, the applied roll moment equals the aerodynamic roll damping (Equation 14.81):

$$C_{l_{\delta},\text{tot}}\, \delta_{\max} + C_{l_p}\, \frac{p_{ss}\, b}{2V} = 0, \tag{14.81}$$

where C_{l_p} is the roll damping derivative (negative by convention) and b the wing span. Solving for the non-dimensional roll rate and converting to a dimensional steady-state roll rate (Equation 14.82):

$$p_{ss} = \frac{-2\, C_{l_{\delta},\text{tot}}\, \delta_{\max}}{C_{l_p}} \cdot \frac{2V}{b}, \tag{14.82}$$

where $C_{l_{\delta},\text{tot}} = C_{l_{\delta,o}} + C_{l_{\delta,i}}$ is the total one-sided rolling-moment derivative for the outer and inner elevons. The centrebody elevon is excluded due to its negligible rolling moment. Roll damping C_{l_p} is taken directly from AVL. The roll authority margin is defined in Equation 14.83 as:

$$\xi_{\text{roll}} = \frac{p_{ss}}{p_{\text{target}}}, \tag{14.83}$$

where $p_{\text{target}} = 15$ deg/s is adopted from reference values [52]. A value $\xi_{\text{roll}} \geq 1$ is required for feasibility.

14.13.4. Yaw Authority

Directional control is provided by split-drag rudders on the winglets, with yaw authority checked using the same method described in Subsection 14.7.2. It is important to note that $\delta_{r,\max} = 60°$ according to reference values [52].

14.13.5. Configuration Comparison

To explore the control-surface sizing trade space, six candidate configurations are defined, each perturbing the spanwise extent and chord ratio of the outer, inner, and centrebody elevons, and/or the winglet and rudder geometry, relative to a common wing planform (S_{ref}, b, c_{root} held fixed). Table 14.6 summarises the geometry of each configuration.

Table 14.6: Control surface geometry for the six candidate configurations. Area is the total for both symmetric halves; location η is the spanwise fraction of the half-span ($\eta = 0$ at the centreline, $\eta = 1$ at the tip).

Surface	Quantity	Cfg 1	Cfg 2	Cfg 3	Cfg 4	Cfg 5	Cfg 6
Outer elevon (pair)	Area (m^2)	15.67	17.90	18.13	25.18	18.71	15.76
	Span (m)	8.12	6.50	8.12	8.12	7.15	6.50
	Location (η)	0.70–0.95	0.65–0.85	0.65–0.90	0.65–0.90	0.70–0.92	0.68–0.88
Inner elevon (pair)	Area (m^2)	100.27	137.87	72.38	98.70	137.51	68.33
	Span (m)	13.00	13.00	11.38	11.38	13.00	9.75
	Location (η)	0.30–0.70	0.25–0.65	0.30–0.65	0.30–0.65	0.20–0.60	0.32–0.62
Centrebody elevon (pair)	Area (m^2)	90.24	137.87	70.90	90.24	107.43	50.13
	Span (m)	11.70	14.30	11.70	11.70	13.00	9.10
	Location (η)	0.00–0.18	0.00–0.22	0.00–0.18	0.00–0.18	0.00–0.20	0.00–0.14
Winglet (fin, pair)	Area (m^2)	31.50	31.50	31.50	48.00	31.50	24.00
	Height (m)	4.5	4.5	4.5	6.0	4.5	4.0
Rudder panel (pair)	Area (m^2)	12.60	12.60	12.60	24.00	12.60	8.40
	Height (m)	4.5	4.5	4.5	6.0	4.5	4.0
Location (winglet & rudder)		Wingtip, fixed across all configurations					

The six proposed configurations systematically trade control authority across different axes to evaluate aerodynamic limits using AVL. Configuration 1 maximises roll authority by extending outer elevons, whereas Configurations 2 and 5 prioritise pitch by enlarging or shifting inner elevons inboard. Conversely, Configuration 4 focuses on directional stability by increasing winglet and rudder sizes. Finally, Configurations 3 and 6 test the minimum feasible bounds of the design by uniformly shrinking surface chords and overall spans to reduce actuator loads and wetted area, ultimately aiming to identify which control axis binds first during the margin evaluation.

It should be noted that the winglet chord exceeds the root tip chord. This is due to the large ruder surface required to obtain lateral controllability. This is solved by extending the winglet chord behind the root tip chord, including a smooth transition between the two components.

14.13.6. Hinge Moments and Actuator Power

Although hinge moments do not determine feasibility directly, they set actuator sizing and are evaluated analytically at cruise and approach. The hinge moment H and peak actuator power P_{act} for a maximum deflection rate $\dot{\delta}_{\max}$ are defined in Equation 14.84 as:

$$H = \left|C_{h_\delta}\right| \bar{q}\, S_{\text{surf}}\, \bar{c}_{\text{surf}}\, \delta, \qquad P_{\text{act}} = H \cdot \dot{\delta}_{\max} \tag{14.84}$$

where $C_{h_\delta} = -0.23\ \text{rad}^{-1}$ and $\bar{c}_{\text{surf}}$ is the control surface MAC [53] . Due to their short longitudinal lever arms, BWB elevons demand much higher deflection rates (60–100 deg/s) than conventional tail-aft aircraft (30 deg/s) to achieve equivalent pitching moments [40, 46, 54]. All six configurations were evaluated in AVL for pitch, roll, and yaw authority margins ($\xi \geq 1$ required), aiming to minimise total peak actuator power. However, due to computational errors, the numerical derivatives are unreliable and excluded from quantitative comparison. Consequently, Configuration 1 is selected as the provisional baseline for its geometric advantages: it maximises roll authority; typically the most critical axis for BWBs [44] by utilising the furthest outboard elevon while maintaining moderately sized inboard surfaces.

14.14. Verification and Validation

Code verification was performed by unit-testing the translation of each analytical method into the computational model, and then checking outputs against hand-calculated reference values for realistic inputs. The MAC and LEMAC calculator was verified by hand-calculating the panel-by-panel integration of Equation 14.4 and Equation 14.6 for a simplified three-panel planform and confirming that the code returned identical values. The CG equations for all three loading states were likewise checked by substituting representative component masses and moment arms manually and comparing against the model output. The eigenmodes state matrices (Equation 14.35 and Equation 14.42) and their associated dimensional derivatives were unit-tested against the formulations given by Nelson and Mulder [35, 47], confirming correct sign conventions and scaling factors throughout. Landing gear geometry was verified by running the sizing procedure with several perturbed input sets and checking that the nose-gear load fraction, turnover angle, and tip-back angle responded in the expected direction to changes in CG position, CG height, and wheel base.

Two significant model fidelity issues were identified during the analysis and are acknowledged here rather than corrected at this design stage. First, the lateral-directional stability derivatives extracted from AVL contain a divergence error that renders the full set of derivatives unreliable. Consequently, the crosswind equilibrium and turbulence handling analysis could not be completed quantitatively, and the lateral-directional eigenvalues reported in Subsection 14.10.1 should be treated with caution. In particular, the absence of a complex-conjugate Dutch roll pair and the implausibly fast spiral time-to-double of 0.74 s are inconsistent with the physically expected behaviour of a BWB configuration and are most likely artefacts of the erroneous derivatives rather than genuine features of the aircraft dynamics [4].

Secondly, the control surface sizing analysis was also affected, thus the values for the computed control derivatives are unreliable and are therefore not used for quantitative comparison. For several configurations, AVL either failed to converge or returned unrealistically values, particularly where local control deflection angles or sectional angles of attack were largest, which is consistent with the breakdown of AVL's linear, attached-flow vortex-lattice formulation outside the small-perturbation regime [22]. The authority margins could thus not be used to numerically compare and rank the configurations. This is an impactful limitation; re-running AVL with reduced deflection amplitudes, and cross-checking with a higher-fidelity method is recommended before finalising the sizing.

15
Aerodynamic Analysis

With the preliminary design known, the advanced aerodynamic analysis can be established. Before the aerodynamic characteristics are determined, assumptions are listed in Section 15.1. The preliminary aerodyanmic analysis is performed in Section 15.2, followed by an analysis of lift-off and landing in Section 15.3. The chapter concludes with a sanity check on the AVL results outlined in Section 15.4.

15.1. Assumptions

First, before analysis can even begin, the assumptions shall be listed.

1. **Limitations of AVL** It is assumed that flow is fully attached throughout the whole range of angles of attack due to the AVL limitations. Thus the $C_{L_{max}}$ and stall charactiristics cannot be approimated by this method.
2. **Simplified geometry for solver** It is assumed that the simplified geometry given into the AVL is representative.
3. **Simplification of drag calculations** It is assumed that other drag contributions then induced drag, profile drag, wave drag, engine drag and the landing gear drag are negligible.
4. **Constant** C_{D_0} It is assumed that the C_{D_0} is constant throughout the all AOA.
5. **Simplified engine and landing gear drag** It is assumed that simplified model of engine and landing gear drag is representative. Both are assumed to be constant throughout the whole range of AOA.

15.2. Aerodynamic Analysis of Preliminary Design

For the advanced aerodynamic analysis, the AVL is used, with the drag corrections as mentioned with the chosen engine characteristics, which are nacelle length of 4.572 m, nacelle diameter of 2.84 m and wetted area 32.3 m^2 [55] [56]. With this knowledge, essential aerodynamic parameters of the preliminary design can be estimated

15.2.1. Lift Coefficient

The lift coefficient over the angle of attack gives an idea at which angle of attack the airliner will be cruising. The Figure 15.1 provides insights into the C_L/α graph.

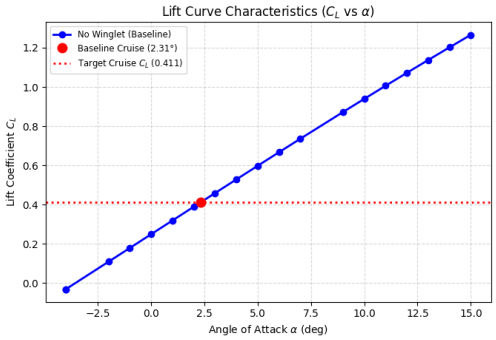

Figure 15.1: C_L/α of the clean geometry

By the linear interpolation, the angle of attack for cruise is found to be 2.31°. The result seems realistic for the cruise conditions. The 2.31° result is a desirable result for the passenger comfort, as it means that the plane is flying at almost levelled condition.

From the given graph, the C_{L_α} can be estimated. The method for it is chosen to be the standard Least-Square Regression. The formula for is provided in Equation 15.1.

$$C_{L_\alpha} = \frac{n\sum(\alpha \cdot C_L) - \sum\alpha\sum C_L}{n\sum(\alpha^2) - (\sum\alpha)^2} \tag{15.1}$$

For the accuracy of the results, the angles of attack are chosen corresponding to the closest to linear mode, which happens approximately between -2° and 4°, which gives a result of $C_{L_\alpha} = 0.07°$. In comparison, the Thin Airfoil Theory estimates $C_{L_\alpha} = 0.11°$ for flat infinite span plate. But it does not account for nuances of real 3D wing aerodynamics, such as downwash. The better estimation is provided by the John D. Anderson in the book Fundamentals of Aerodynamics, where C_{L_α} formula is proposed for finite swept wing.

$$C_{L_\alpha} = \frac{a_0 \cos\Lambda}{\sqrt{1 + \left(\frac{a_0 \cos\Lambda}{\pi \cdot AR}\right)^2} + \frac{a_0 \cos\Lambda}{\pi \cdot AR}} \tag{15.2}$$

The result of Equation 15.2 is calculated to be $C_{L_\alpha} = 0.0796°$, which is closer to the values given by AVL, but still higher. The lower value of C_{L_α} then expected is given by the non-elliptical lift distribution and transition period between 2 chosen airfoils.

Note that because of the linear potential flow theory, which is used by AVL, the software cannot predict the maximal lift coefficient, or any stall conditions.

15.2.2. Lift-to-Drag Ratio

For the goal of the project the most essential characteristic is the L/D ratio. It is estimated with the clean lifting surface geometry without winglets. The result can be observed in Figure 15.2.

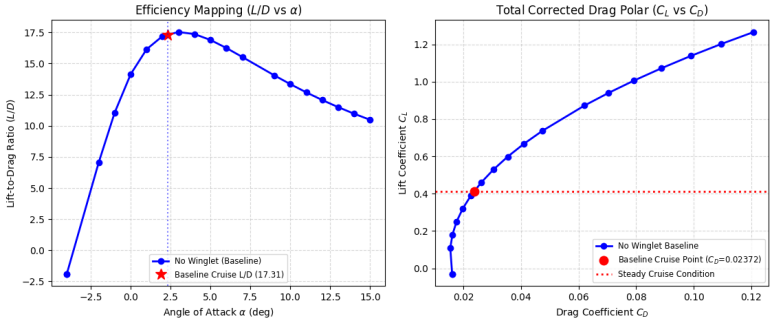

Figure 15.2: L/D of the clean geometry

The results show that clean wing configuration has a maximal L/D of 17.65, and cruise L/D of 17.31. For the reference, the Table 15.1 provides the L/D of commercial airliners.

Table 15.1: Historical Benchmark Data: Jetliner Cruise Lift-to-Drag (L/D) Ratios [57]

Jetliner	**Cruise** L/D	**Jetliner**	**Cruise** L/D	**Jetliner**	**Cruise** L/D
Lockheed L1011-100	14.5	Airbus A310-300	15.3	Airbus A320-200	16.3
McDonnell Douglas DC-10-40	13.8	Boeing 747-200	15.3	Airbus A310-300	18.1
Airbus A300-600	15.2	Boeing 747-400	15.5	Airbus A340-200	19.2
McDonnell Douglas MD-11	16.1	Boeing 757-200	15.0	Airbus A340-300	19.1
Boeing 767-200ER	16.1			Boeing 777-200	19.3

As can be seen, the cruise L/D is higher than Airbus A320 by 6.4%, but it is significantly losing to bigger airliners, such as Boeing 777, or Airbus A340-300. With the L/D known, the drag polar can be build and the oswalds efficiency estimated, as well as compared with the result from AVL. The Drag-polar is rearranged to Equation 15.3.

$$e = \frac{C_L^2}{\pi \cdot \mathrm{AR} \cdot (C_{D,\mathrm{total}} - C_{D0})} \tag{15.3}$$

Based on calculations, at cruise, the Oswald efficiency is 0.691. The AVL gives a result of 0.7947. In the book mentioned before, John D. Anderson gives a statistical data that for different airplanes Oswald's efficiency factor is usually 0.7 - 0.85. Knowing the nature of Blended Wing Body and previously mentioned in Chapter 10 fact that fuselage generates 2-3 times lower lift, it is safe to assume that the Oswald's efficiency of BWB shall lay below the conventional ariplane, so the result from AVL seems unrealistically high. Lift distribution will are discussed more into details at the Subsection 15.2.5.

Based on calculations, at cruise, the Oswald efficiency is 0.691. The AVL gives a result of 0.7947. John D. Anderson gives a statistical data that for different airplanes Oswald's efficiency factor is usually 0.7 - 0.85. Knowing the nature of BWB and previously mentioned in Chapter 10 fact that fuselage generates 2-3 times lower lift, it is safe to assume that the Oswald's efficiency of BWB shall lay below the conventional ariplane, so the result from AVL seems unrealistically high. Lift distribution will are discussed more into details at the Subsection 15.2.5.

15.2.3. Drag Coefficient Decomposition

To get a sense of the drag, the decomposition of drag over the angle of attack is formed. From the analysis in Figure 15.3, it is clear that wave drag and engine drag are significantly lower than profile drag and the induced drag. At the angle of attack around 2.5, the induced drag becomes dominant, while at the cruise, the profile drag is dominant.

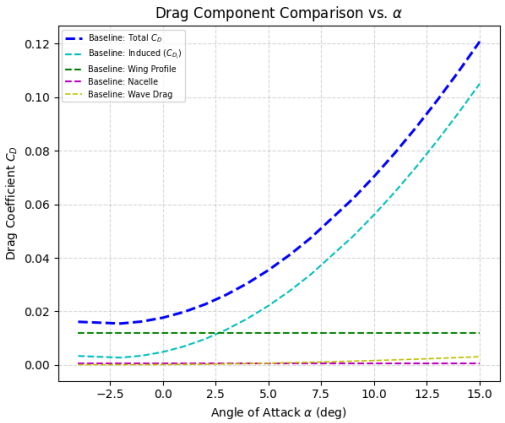

Figure 15.3: Drag decomposition of the clean geometry

15.2.4. Winglets Addition

As established in the section before, induced drag is one of the biggest components of drag. To decrease it, winglets are added. Winglets work on the basis of the reduction of tip vortices[1]. The winglets with the tip chord of 0.5 meters and length of 4 meters were added to the geometry to AVL. The Figure 15.4 shows the change in the graphs after addition of the vertices.

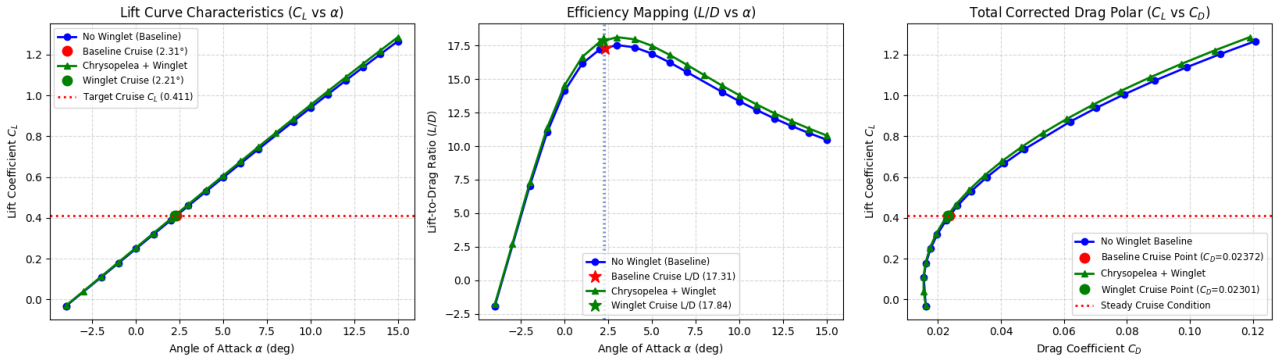

Figure 15.4: Aerodynamic analysis for configuration with winglets

The results show that the winglets increase the L/D at cruise conditions by 0.53, which gives 9.4% increase with respect to the Airbus A320, but still loses the competition to the bigger airliners, such as Boeing 777.

15.2.5. Lift Distribution Over Span

To fully understand the lift and drag generation, the lift distribution over the surface area is crucial.

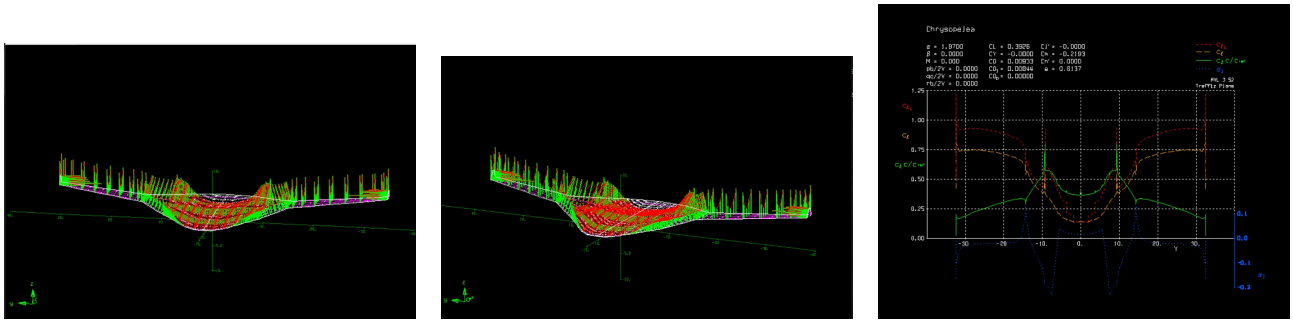

Figure 15.5: Lift distribution over the surface at cruise conditions

As can be seen on the Figure 15.5, the lift is indeed generated mostly by the outer wings. While body airfoil still generates lift, it is completely overthrown by the amount of drag it generates. The initial assumption that outer wings generate around 3 times higher drag is an underestimation, the right part of the Figure 15.5 shows that it is closer to 8-9.

The distribution shows clearly what makes L/D not as high as expected. The body airfoil was purely optimised for the cabin fitting, which led to smaller surface area, but performance is unfeasibly bad.

Going back to the evaluation of Oswald's efficiency, the Lift distribution showed that to e proposed by AVL is indeed inflated.

15.3. Lift-off and Landing

To proof that the designed BWB is functional at the take-off conditions and landing, it is essential to check aerodynamic conditions at those points.

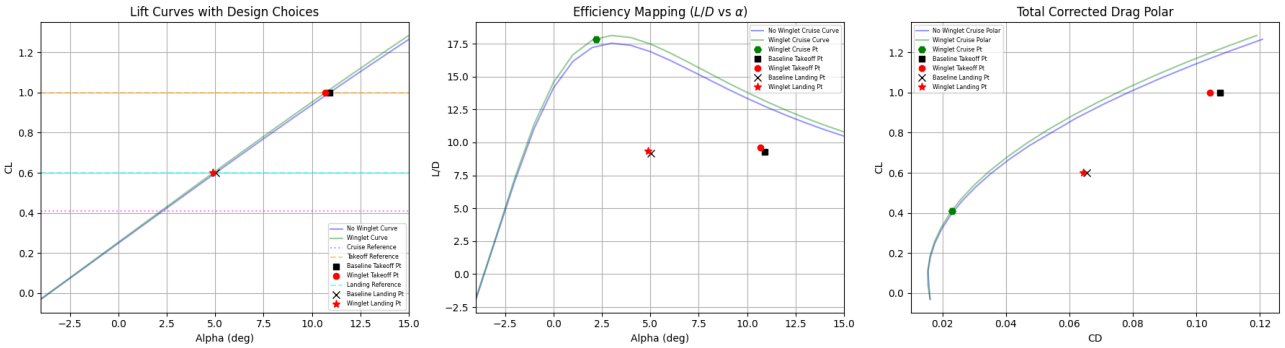

Figure 15.6: Aerodynamic parameters during take-off and landing

[1] URL `https://www1.grc.nasa.gov/beginners-guide-to-aeronautics/winglets/` [Cited 16/06/2026]

The Figure 15.6 shows that the $C_{L_{TO}}$ and C_{L_L} are achieved at the angles of attack of 10.69° and 4.9°, which are realistic and shows feasibility of the design for take-off and landing. Note that during lift-off and landing, the new drag component is added, which is the drag of the landing gear. Based on the study provided by Christoph Deiler and Nicolas Fezans, for the Airbus A320, the drag increase for fully extended main landing gear and nose gear is around 0.03, which will be used as a drag increase for the drag build up method [58].

15.4. AeroSandbox VLM3 analysis

To perform a sanity check on the results of the AVL, another aerodynamic solver is involved, which is AeroSandbox by Dr.Peter Sharpe from MIT. The Aerosandbox works on a similar basis as the AVL, which is the linear vortex lattice method, meaning that it shall give similar results. Note that the geometry used for the Aerosandbox is the geometry without the winglets.

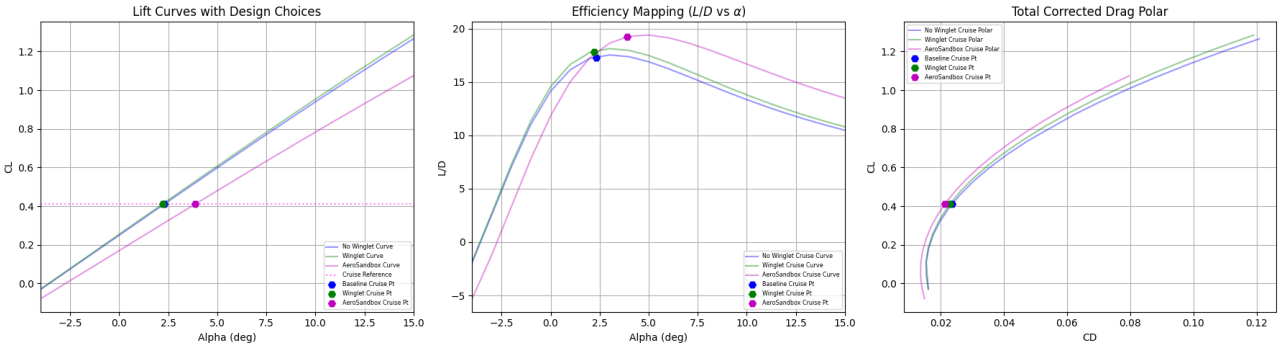

Figure 15.7: Aerosandbox and AVL results comparison

The Figure 15.7 demonstrates that the Aerosandbox gives higher performance to the chosen configuration, the specific aspects of the performance are compiled at the Table 15.2.

Table 15.2: Aerodynamic Performance Comparison for AVL and AeroSandbox

Flight Mode	Solver / Configuration	C_L	AoA [deg]	Oswald (e)	Eff. (L/D)
Cruise	AVL Baseline (No Winglet)	0.4109	2.31	0.691	17.31
	AVL Winglet	0.4109	2.21	0.738	17.84
	AeroSandbox	0.4109	3.88	0.875	19.21
Take-off	AVL Baseline (No Winglet)	1.0000	10.91	0.685	9.31
	AVL Winglet	1.0000	10.69	0.721	9.60
	AeroSandbox	1.0000	13.70	0.783	10.06
Landing	AVL Baseline (No Winglet)	0.6000	5.03	0.709	9.15
	AVL Winglet	0.6000	4.90	0.753	9.33
	AeroSandbox	0.6000	6.97	0.834	9.65

While graphs above corresponds to similar shape, the differences are visible. The lift curve is steeper for the AeroSandbox, which results into higher angle of attack needed for cruise, landing and take-off. The L/D at the cruise is higher by 11% with respect to no-winglets configuration, as well as take off and landing L/D is higher for the AeroSandbox.

The Oswald's efficiency for the Aerosandbox estimation shows even higher number, which gives even more unrealistic results. During cruise, the $e = 0.875$ would mean that the proposed geometry has closer to ideal lift distribution then the conventional airliners. The discrepancies between the results of the AVL and the AeroSandbox aerodynamic analysis shall be further studied to perform a more accurate overall performance analysis.

16
Structural Analysis

This chapter presents the preliminary structural layout for the selected BWB configuration. This analysis focuses mainly on the centrebody structural architecture, since the pressurisation of a non cylindrical cabin, combined with global bending and wing loads, represents one of the main design challenges for this configuration. The chapter first outlines the fuselage structural architecture in Section 16.1, followed by Section 16.2. Subsequently, the structural loads are modelled and verified in Section 16.3 and Section 16.4, respectively.

16.1. Fuselage Structural Architecture

As illustrated in Figure 16.1, the fuselage primary structure is divided into three main load-carrying components: the outer aerodynamic contour shown in blue, the pressurised cabin shell shown in light blue and the internal trapezoidal cabin structure shown in green. This split is motivated by the challenges of pressurising a non-cylindrical fuselage. Flattened BWB fuselages can in fact, due to the interaction of pressurisation and global bending loads, be subjected to high non-linear stresses [4].

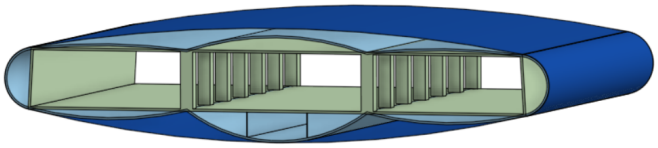

Figure 16.1: Simplified fuselage structural architecture used for preliminary sizing.

Several BWB cabin concepts have been investigated in literature, including integrated skin and shell, segregated multibubble and oval pressure cabin concepts [39]. An oval pressure shell was initially considered, offering a large uninterrupted cabin volume. However, to fit the required passenger capacity within the centrebody airfoil, the cabin had to be made relatively wide rather than excessively long. This resulted in a large radii of curvature and inefficient pressure sizing. Therefore, a simplified multibubble inspired pressure shell concept was selected.

16.2. Load Path Definition

The structural analysis is performed as a post-processing step using the converged MDAO geometry, mass breakdown, fuel mass, CG locations and AVL aerodynamic loads. For a preliminary structural analysis, the model is divided into three simplified load paths. The outer aerodynamic contour is assumed to carry the longitudinal bending loads of the fuselage. The multibubble pressure shell is sized for cabin pressurisation only. The reactions generated by pressurisation at the bubble intersection nodes are transferred to the internal trapezoidal structure. The trapezoid also carries the resultant wing shear and bending moment at the wing/cabin intersection, together with cabin floor loads.

16.2.1. Structural Load Cases

The preliminary structural sizing is performed for the load cases listed in Table 16.1. The cases differ in fuel fraction and load factor.

Table 16.1: Structural load cases considered for preliminary sizing

Case	Description	Fuel Fraction	Load Factor
LC01	Take-off / full fuel	1.00	1.15
LC02	Positive manoeuvre / turbulence	0.80	2.50
LC03	Negative manoeuvre	0.80	-1.00
LC04	Landing approach / low fuel	0.10	1.00

The same load cases are considered for both longitudinal fuselage load analysis and the wing root transfer estimation. For each analysis, the critical case is selected based on the largest relevant internal load.

16.3. Structural Load Modelling

The internal shear force and bending moment are obtained by integrating the applied load distribution along the structural beam models. For both the longitudinal fuselage model and the spanwise wing model, the internal loads are obtained from

$$\frac{\mathrm{d}V}{\mathrm{d}s} = -q(s), \qquad \frac{\mathrm{d}M}{\mathrm{d}s} = V(s),$$

where s is the beam coordinate. For the longitudinal fuselage analysis, $s = x$, while for the spanwise wing/carry-through analysis, $s = y$. The distributed load $q(s)$ follows the adopted sign convention. Concentrated forces produce jumps in the shear force diagram, while concentrated moments produce jumps in the bending moment diagram

16.3.1. Fuel Tank Placement

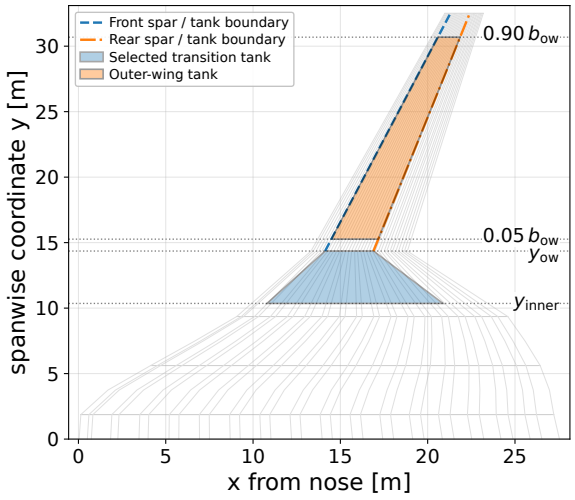

Figure 16.2: Fuel tank layout assumed. The outer wing tank and the transition wing tank are shown in orange and blue respectively.

The fuel tank layout is shown in Figure 16.2. The outer wing tank is placed inside the wingbox, between the front and rear spar boundaries, located respectively at 0.15 and 0.65 of the local chord. In the spanwise direction, the outer-wing tank extends from 0.05 to 0.90 of the outer wing semi-span, measured from the outer wing root. Since the outer wing tank capacity is not sufficient to store the total amount of fuel required for the mission, the remaining fuel is assigned to an additional tank in the transition region between the fuselage and the outer wing. This transition tank is modelled as a trapezoidal region, between the cabin side wall, with 1 meter clearance from the cabin side wall.

The resulting fuel distribution is used to compute the fuel centre of gravity and the fuel loads applied in the longitudinal fuselage and spanwise wing shear and bending analyses.

16.3.2. Longitudinal Fuselage Shear and Bending Loads

For the longitudinal load analysis, the fuselage is modelled as a one dimensional beam along the aircraft longitudinal axis, with origin (x=0) located at the nose. Using the beam-equilibrium relations introduced in Section 16.3 with $s = x$, the shear force and bending moment distributions are computed by numerical integration of the net vertical load. The aerodynamic and inertial loads considered in the longitudinal model are summarised in Table 16.2.

Table 16.2: Longitudinal load modelling assumptions for the fuselage NVM

Load source	Application region / station [m]	Representation	Note
AVL aerodynamic load	–	Distributed panel load	Scaled to required lift (L=nW)
Payload	1.20 - 20.87	Smooth distributed load	Distributed over the cabin region.
Fuselage and systems	0.00 - 27.55	Smooth distributed load	Remaining OEW mass after separate items are removed
Transition fuel	10.80 - 20.87	Smooth distributed load	Centred at transition tank CG
Outer-wing fuel	15.63 - 20.58	Smooth distributed load	Centred at outer-wing tank CG
Wing structural mass	15.59 / 19.78	Front/rear spar loads	Spar locations taken from the wingbox geometry
Engines	20.00	Point mass	Preliminary position
Landing gear	15.70	Point mass	Equivalent landing gear CG from MDAO input
Trim correction	14.79	Point moment	Used to close longitudinal moment equilibrium

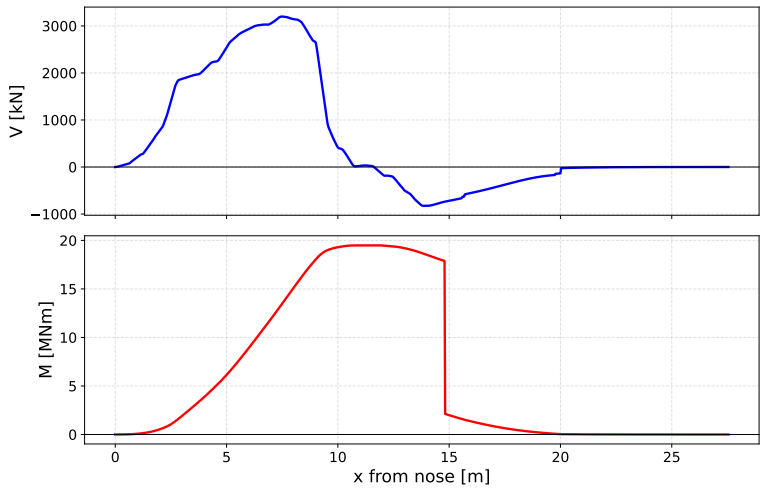

Figure 16.3: Longitudinal fuselage shear force and bending moment diagram for the critical load case LC03.

The resulting shear and bending moment distributions for the critical load case are shown in Figure 16.3. The critical case is LC03, which corresponds to negative manoeuvre with 80% fuel. The resultant maximum absolute bending moment is 19501.85 kN m occurring at x=11.62 m from the nose.

The shear force diagrams presents smooth variations where the aerodynamic load is dominant. Discontinuities are visible at the concentrated loads, namely landing gear, engines and equivalent spar reactions. The trim correction is currently applied as a point moment at the aircraft centre of gravity to balance the longitudinal beam model. The jump in the bending moment diagram is therefore a modelling correction introduced by a point moment. In a future design phase, this point moment should be replaced by distributed control surface loads obtained from a trimmed aerodynamic analysis.

16.3.3. Wing Spanwise Shear and Bending Loads

The spanwise load analysis is used to estimate the shear force and bending moment transferred from the wing and transition region into the central body structure. The spanwise coordinate y is measured from the aircraft centreline. The loads are integrated from the wing tip inwards, since the wing tip is treated as a free end where the internal shear force and bending moment are zero. A downward-positive sign convention is used.

Before the spanwise loads are computed, the fuel and structural mass distributions are idealised. For the transition tank, the effective height h_{eff} represents the local tank height used for volume estimation. The transition fuel mass is therefore distributed according to the local tank volume per unit span,

$$\frac{\mathrm{d}V_{\text{tank}}}{\mathrm{d}y} = \left[x_{\text{rear}}(y) - x_{\text{front}}(y)\right] h_{\text{eff}}(y).$$

The transition wingbox structural mass is distributed according to the local planform length $x_{\text{rear}}(y) - x_{\text{front}}(y)$. This is a first order approximation and does not include the variation of structural depth in the vertical direction. The load sources included in the spanwise shear and bending model are summarised in Table 16.3.

Table 16.3: Load sources included in the wing spanwise shear and bending models

Load source	Spanwise region	Representation
Aerodynamic lift	Cabin-side cut to wing tip	AVL panel vertical forces are selected for the outboard side, rescaled to the target lift of the load case, and converted to a distributed load
Outer-wing fuel mass	Outer-wing tank region	One-side MDAO tank weight distribution, scaled by fuel fraction and load factor
Transition fuel mass	Cabin-side cut to outer-wing root	Distributed according to the transition tank planform length and effective height
Outer-wing structural mass	Outer-wing region	Distributed proportional to the local outer-wing chord
Transition wingbox structural mass	Transition/carry-through region	Distributed proportional to the local transition planform length

The total distributed load is obtained by summing the aerodynamic, fuel and structural contributions:

$$q_{\text{total}}(y) = q_{\text{aero}}(y) + q_{\text{fuel}}(y) + q_{\text{struct}}(y).$$

Using the beam equilibrium relations introduced above with $s = y$, the shear force and bending moment are calculated by integrating the loads from the wing tip towards the centrebody:

$$V(y) = \int_{y}^{b/2} q_{\text{total}}(\eta)\,\mathrm{d}\eta,$$

$$M(y) = \int_{y}^{b/2} q_{\text{total}}(\eta)(\eta - y)\,\mathrm{d}\eta.$$

The resulting spanwise shear force and bending moment distributions for the critical load case LC02, are shown in Figure 16.4. The maximum one side shear force at the cabin cut is V_{cut} = 479.08 kNm and the corresponding one side bending moment is M_{cut} = 6233.35 kNm.

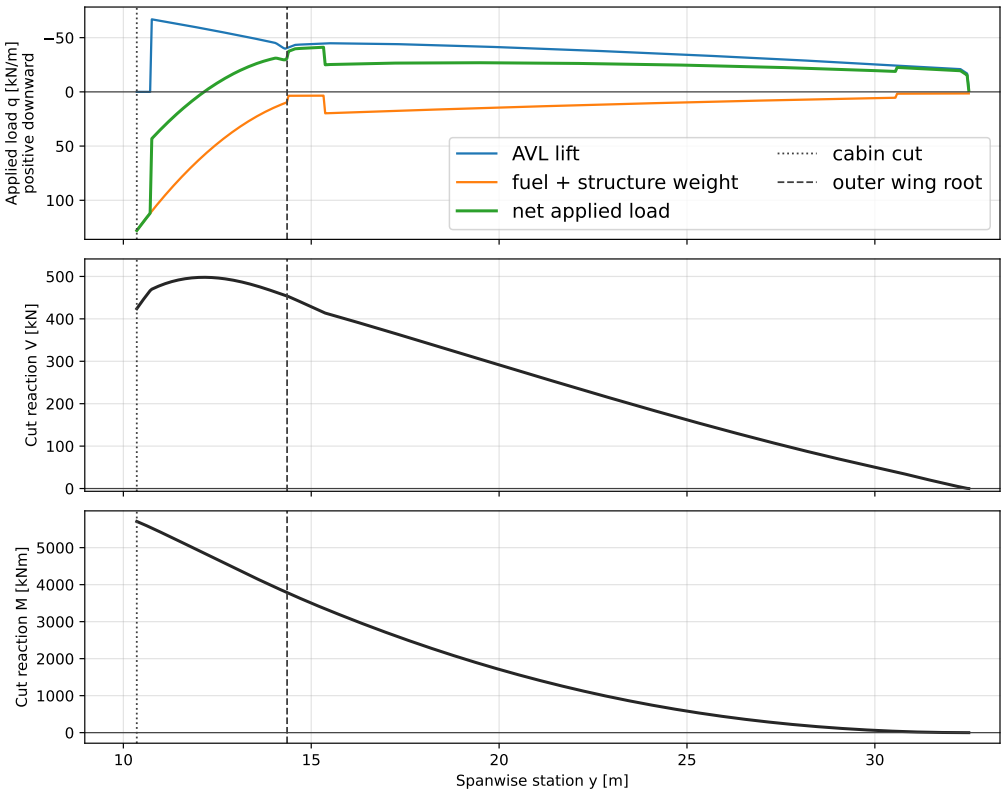

Figure 16.4: Spanwise wing shear force and bending moment diagram for the critical load case LC02.

16.3.4. Material Selection

In line with the material strategy defined in Section 5.4, the preliminary structural sizing uses only conventional metallic and composite materials with high Technology Readiness Levels, while minimising the use of petroleum-based composites. For the primary pressurised shell and main load path, this leads to a metallic baseline rather than a CFRP-dominated structure, with composites reserved for movables and interior applications in later design stages.

Two material selections are therefore used in the preliminary structural sizing. The outer aerodynamic contour, pressure shell and columns are made from aluminium-lithium alloy, selected for its low density, high specific strength and full industrial maturity by the 2031 first flight target. The internal ceiling, floor and side-wall members of the internal trapezoid are modelled as sandwich panels, using aluminium-lithium face sheets and Nomex aramid paper + phenolic resin composite honeycomb core. This combination is consistent with the chosen "minimise CFRP/GFRP use and conventional epoxy" strategy in Chapter 5, as it avoids large CFRP primary structures while still supporting the project aim of reducing petroleum-derived material use compared to a traditional aluminium–epoxy composite mix, even tough it utilizes a honeycomb core with traditional epoxy. The material properties used in the sizing are summarised in Table 16.4.

Table 16.4: Properties of the selected materials

Component	Material	Density kg/m^3	Elastic modulus GPa	Allowable stress MPa
Outer contour / pressure shell	Al-Li 2198-T8	2700	76.5	271
Sandwich face sheets	Al-Li 2198-T8	2700	76.5	271
Sandwich core	CORMASTER C1 (Nomex/phenolic)	80	–	–
Column posts	Al-Li 2198-T8	2700	76.5	271

The aluminium-lithium material properties are based on the Airware 2198-T8 datasheet[1], which gives a density of 2.7 g/cm^3, elastic modulus of 76.5 GPa and minimum yield strength of approximately 407 MPa for the considered sheet range. The allowable stress is obtained by applying a preliminary safety factor of 1.5, giving $\sigma_{\text{allow}} = 271$ MPa. A conservative value of 80 kg/m^3 is selected from the typical Nomex aramid paper with phenolic resin composite honeycomb density range for the preliminary sizing, which lies within the 20–80 kg/m^3 range reported for aerospace honeycomb cores[2].

[1] URL `https://www.smithshp.com/assets/pdf/aluminium/aluminium-lithium/airware-2198-aluminium-lithium-english.pdf` [Cited 16/05/2026]

[2] URL `https://www.schuetz-composites.net/downloads/datenblaetter/datenblatt-schuetz-cormaster-c1/datasheet-schuetz-cormaster-c1-en.pdf?cid=g4ae` [Cited 16/05/2026]

16.3.5. Outer Contour Sizing

The outer aeordynamic contour is modelled as a thin-walled member and sized from the resulting longitudinal bending moment obtained from fuselage shear and moment analysis. Since the external shape varies along the fuselage, the contour is extracted form the MDAO geometry at each fuselage station.

Figure 16.5: Aeordynamic contour model.

The centroid and second moment of inertia is then calculated at each station and the bending stress at each point of the contour is computed as

$$\sigma_b = \frac{Mz}{I},$$

where (M) is the local longitudinal bending moment, (z) is the vertical distance from the neutral axis to the considered point on the contour and (I) is the second moment of area of the section about the bending axis. Assuming a uniform thickness, the second moment of area is proportional to the shell thickness. The geometry is in fact fixed and an increase in thickness results in an increased amount of material along the same contour line. The contour is discretised into small straight segments, the second moment of area per unit thickness can thus be written as

$$\frac{I}{t} = \sum_{i=1}^{N_s} (z_i - \bar{z})^2 \, \Delta s_i,$$

where (N_s) is the number of contour segments, (z_i) is the vertical coordinate of the midpoint of segment (i), ($\bar{z}$) is the vertical coordinate of the section centroid and (Δs_i) is the segment length. The segment length is computed from the contour coordinates as

$$\Delta s_i = \sqrt{(y_{i+1} - y_i)^2 + (z_{i+1} - z_i)^2}.$$

The maximum distance from the neutral axis is then defined as

$$z_{\max} = \max_i |z_i - \bar{z}|.$$

Substituting (I=t(I/t)) into the bending stress equation gives the required equivalent thickness as

$$t_{\text{req}} = \frac{|M| z_{\max}}{\sigma_{\text{allow}} (I/t)}.$$

The required bending thickness was calculated at each fuselage station for all structural load cases. The critical case was LC03, corresponding to the positive manoeuvre/turbulence load case. The maximum absolute bending moment was $|M|_{\max} = 19245.95$ kNm at $x = 10.69$ m from the nose. This resulted in a required outer contour thickness of 4.70 mm.

16.3.6. Pressure Shell Sizing

For the pressure shell sizing, one representative cabin cross-section is used. This is a preliminary simplification that allows a first order sizing of the shell thickness without modelling the full three dimensional cabin geometry. The pressure end caps are not sized in this preliminary model since their geometry would require a separate detailed analysis.

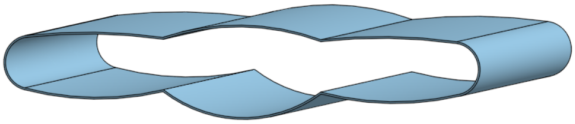

Figure 16.6: Pressure shell model.

The representative section is split into circular arcs. The radius of each arc is then used to calculate the required pressure thickness.

The required pressure thickness for each arc is calculated using the thin-walled pressure relation

$$t_{\text{req,pressure}} = \max\left(\frac{\Delta p R}{\sigma_{\text{allow}}}, t_{\min}\right),$$

where Δp is the cabin pressure differential, R is the local radius of curvature of the arc, σ_{allow} is the allowable stress of the aluminium-lithium shell material and $t_{\min}$ is the minimum gauge thickness. In this preliminary sizing, a pressure differential of $\Delta p = 50$ kPa and a minimum gauge thickness of $t_{\min} = 1.5$ mm are used.

The pressure shell sizing results are summarised in Table 16.5. The largest required thickness is obtained for the arc with the largest radius of curvature, since the pressure stress increases with radius.

Table 16.5: Pressure shell sizing results for the representative cabin section

Arc	Radius [m]	Required thickness [mm]
Top-side arc	27.51	5.08
Top-inner arc	11.88	2.19
Bottom-inner arc	6.46	1.50
Bottom-side arc	14.39	2.65
Side-end arc	1.25	1.50

The top-side arc is critical, giving a required pressure shell thickness of 5.08 mm

16.3.7. Trapezoidal Cabin Sizing

The internal trapezoid role is to transfer pressure loads and wing reactions loads through the cabin. The model includes ceiling, floor and side wall members and two column rows. The ceiling, floor and side wall members are modelled as sandwich panels. The columns, instead, are modelled as aluminium-lithium tie members repeated along the fuselage.

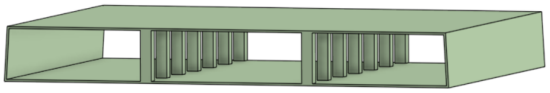

Figure 16.7: Trapezoidal cabin model

Loads The pressure loads, deriving from the intersections of different radius arcs, are resolved at the eight nodes of the trapezoid. At each node, the force is decomposed into a horizontal and vertical component in the y-z plane. The horizontal components are assigned to the ceiling and floor members while the vertical components to the side walls and columns. In addition to the pressure loads, the cabin floor load is applied to the floor members. This load represents the passenger, seat and non-structural floor masses for the selected load factor.

The wing induced shear and bending loads are then added to the model. The wing shear is applied to the side walls. The wing bending moment is split as a force couple between the upper and lower horizontal members of the trapezoid. The equivalent axial load per unit length of this bending moment is calculated as

$$N_{\text{moment}} = \frac{M_{\text{wing}}}{h_{\text{trap}} L_{\text{intro}}},$$

where M_{wing} is the total wing induced bending moment from both sides of the aircraft, h_{trap} is the vertical distance between the ceiling and floor load paths and L_{intro} is the longitudinal load introduction length. The wing induced bending moment is therefore assumed not to be applied at one single frame but spread over the longitudinal region where the wing loads enter the cabin structure.

Optimisation Once the loads are defined, the sizing routine evaluates the trapezoid and column members. Two cases are considered: only pressure loads and their combination with wing induced loads. Each member is sized for the most critical loading. The ceiling, floor and side walls members are sized as sandwich panels. Their face-sheet and core thicknesses are varied. The columns are are modelled as discrete square hollow tubes. The sizing routine varies the column spacing, the outer tube width and the wall thickness. For each candidate column, the vertical load is first obtained as a load per unit fuselage length. Since the columns are discrete, the load is calculated from the selected column spacing as

$$N_{\text{column}} = N_{\text{line}} s_{\text{column}},$$

where N_{line} is the vertical load per unit length assigned to the column line and s_{column} is the longitudinal spacing between columns.

Next, the cross-sectional area and second moment of area are calculated as

$$A = b^2 - (b-2t)^2,$$

$$I = \frac{b^4 - (b-2t)^4}{12},$$

where b is the outer width of the square tube and t is the wall thickness.

For each candidate design, the sizing routine calculates a failure margin for each relevant failure mode. The margin is defined as

$$g_i = \frac{\text{allowable}_i}{\text{applied}_i} - 1,$$

where i refers to the failure mode being checked. The numerator is the allowable stress, critical buckling load or critical instability stress for that failure mode, while the denominator is the value produced by the applied loads. If $g_i > 0$,

the member passes that check. If $g_i < 0$, the member fails. The sandwich panels are checked for face yielding, Euler buckling, face dimpling, face wrinkling and crimping. The column posts are checked for tensile and compressive yielding and Euler buckling. These checks are summarised in Table 16.6.

Table 16.6: Failure modes considered in the trapezoidal cabin sizing

Structural item	Failure mode	Purpose of check
Sandwich panels	Face yielding	Checks face-sheet stress against the material allowable
Sandwich panels	Euler buckling	Checks global buckling of the compressed member
Sandwich panels	Face dimpling	Checks local face buckling between honeycomb cells
Sandwich panels	Face wrinkling	Checks local face instability supported by the core
Sandwich panels	Crimping	Checks core-related instability of the sandwich panel
Column	Tensile yielding	Checks tensile stress against the material allowable
Column	Compressive yielding	Checks compressive stress against the material allowable, when compression occurs
Column	Euler buckling	Checks global buckling of the post, when compression occurs

For the ceiling and floor panels, vertical support members are assumed to connect the trapezoid panels to the surrounding multibubble pressure shell at frame locations. Therefore, the effective buckling length of the ceiling and floor panels is reduced. The sizing routine selects the lightest member dimensions that satisfy the proposed checks. The results of the optimisation process are shown in Table 16.7. The selected 1.00 m column spacing represents the lightest spacing found with the optimisation routine. In a later design phase, this spacing may change to better fit the cabin layout and structural integration.

Table 16.7: Trapezoidal cabin sizing results

Quantity	Value
Critical load case	LC02
Total wing-induced shear	958.15 kN
Total wing-induced bending moment	12466.69 kNm
Applied axial moment load	504.94 kN/m
Maximum selected sandwich face-sheet thickness	3.923 mm
Maximum selected sandwich core thickness	132.647 mm
Selected column/tie member spacing	1.00 m
Selected column/tie member outer width	70 mm
Selected column/tie member wall thickness	5.0 mm
Primary trapezoid mass per unit length	947.12 kg/m
Estimated primary trapezoid structure mass	18634.4 kg

16.4. Verification

To verify the Python model used for the structural analysis, several checks were implemented. First, the main aircraft inputs were printed and checked, including the main component masses, CG, fuel masses, cabin limits and wing reference locations. This was done to confirm that the structural post-processing model was using the intended values from the MDAO output. Secondly, for the fuselage and spanwise shear force and bending moment diagrams, the load application points were also printed and inspected. This included the locations of the payload, fuel, aerodynamic loads, engines, landing gear and wing load introduction points. The resulting shear force and bending moment diagrams were then checked to see whether the trends and jumps were physically reasonable. For the tank volume estimation and placement, the selected tank areas were plotted over the actual aircraft planform, as shown in Figure 16.2. This allowed the tank regions to be visually checked against the intended locations and the available aircraft geometry. The outer contour sizing was checked by confirming that the critical bending case and bending moment used in the thickness calculation matched the critical case found from the longitudinal NVM analysis. The pressure shell sizing was verified by manually calculating the required thickness of the critical arc. For the trapezoidal internal structure, the pressure reaction directions and member force signs were checked. These checks do not form a complete structural verification, but they increase confidence that the preliminary structural model was implemented consistently with the assumptions used in this chapter.

17
Performance Analysis

This chapter presents different performance characteristics measures. Firstly, the propulsion performance is outlined in Section 17.1, followed by a payload-range and mission profile in Section 17.2 and Section 17.3, respectively. The chapter ends with explaining the loading diagram and manoeuvres in Section 17.4 and Section 17.5.

17.1. Propulsion Performance

Propulsion performance is an essential part of the overall blended wing body performance, and is compiled in Table 17.1, Figure 17.1, and Figure 17.2, which summarise the propulsion performance of the preliminary design.

Table 17.1: Propulsion performance for take-off

Eng.	Segment/Constraint (OEI)	Thrust Req. kN [kN]	Per-Eng. [kN]	TOFL [m]	V_1 [m/s]	Flt Time [min]	Fuel W [kg]	Sys. M [kg]
	Takeoff Ground Roll	287.63	143.82					
	Segment 1 Climb (OEI)	258.73	129.37					
2	Segment 2 Climb (OEI)	240.37	120.19	1410	56.3	539.8	35667.38	46913.38
	Segment 3 Acc (OEI)	213.45	106.73					
	Segment 4 Climb (OEI)	201.54	100.77					
	Takeoff Ground Roll	287.63	95.88					
	Segment 1 Climb (OEI)	200.92	66.97					
3	Segment 2 Climb (OEI)	187.22	62.41	1900	57.9	540.0	44148.3	50530.80
	Segment 3 Acc (OEI)	160.09	53.36					
	Segment 4 Climb (OEI)	158.43	52.81					
	Takeoff Ground Roll	287.63	71.91					
	Segment 1 Climb (OEI)	182.67	45.67					
4	Segment 2 Climb (OEI)	172.60	43.15	2000	57.7	540.1	36790.3	52856.30
	Segment 3 Acc (OEI)	142.30	35.58					
	Segment 4 Climb (OEI)	145.13	36.28					

Figure 17.1: Design parameters summary

Design Summary Parameters
Critical Design Driver: 2-Engine Layout
Governing Segment: Take-Off Roll
Sizing Req. Total Thrust: 287.63 kN
Matched Engine: GEnX
Individual Engine Thrust: 296.00 kN
Total Fuel Weight: 35667.38 kg
Total System Weight: 46913.38 kg
Take Off Field Length: 1410 m
Decision Speed (V_1): 56.3 m/s

Figure 17.2: Fuel break-down at each stage

Segment Name	Thrust Req. [kN]	Time Req. [mins]	Fuel Burned [kg]	SFC [kg/N/s]
Taxi	41.44	30.00	2184.08	0.0000293
Take-Off	592.00	0.38	699.88	0.0000524
Transition	284.89	0.69	144.80	0.0000123
Climb 1	118.48	37.02	2453.49	0.0000093
Main Cruise	87.63	285.40	25031.66	0.0000127
Descent 1	41.44	18.02	363.08	0.0000081
Loiter	60.38	21.60	451.12	0.0000058
Final Approach	41.44	28.59	316.94	0.0000045
Go-Around	114.23	2.03	89.44	0.0000064
Divert Climb	79.61	39.15	1239.60	0.0000066
Divert Cruise	81.71	50.63	2035.54	0.0000082
Divert Desc	42.33	10.99	184.63	0.0000066
Holding Pattern	57.71	11.52	227.35	0.0000057
Final Glide	41.44	3.82	42.38	0.0000045
TOTAL MISSION		**539.83**	**35667.38**	

As can be seen from Table 17.1, the 2-engine configuration returns the most optimal system weight of 46.9 tons. The GEnx-2B engines were selected with an accompanying fuel weight of 35.7 tons, as shown in Figure 17.1. Furthermore, from the same table, it can be seen that the thrust available per engine is 296 kN while the total thrust required for the entire aircraft is only 287.63kN due to the Take-Off roll segment. This means that the aircraft would be able to perform all the mission profile segments, take-off roll and by definition the CS-25 OEI climb requirements on just one engine. This result is not random however, while it is oversizing the engines, the enegine selection was from a source of engines that have already been tested on neat SAF, which at this point is still rather limited. Thus leaving a rather large thrust gap between the Pratt & Whitney LEAP-1A engines with a maximal thrust rating of 143 kN and the General Electric GEnx-2B with a maximal thrust rating of 296 kN. Unfortunately the LEAP-1A engines were too weak to pass the thrust requirement with an acceptable safety margin, and produced too large of a system weight increase in the triple engine case, due to the higher overall fuel consumption. Currently, the weight gap between the LEAP-1A and GEnx-2B engines is almost 2.5 tons, thus as a future recommendation, it is advised to find an engine to bridge this gap between the power and weight parameters of these two engines for a further optimised propulsion system.

As a cause of this large thrust availability, it can be seen from Figure 17.1 that the Take-Off Field Length, even with a

safety margin of 1.2 is still rather short at 1410 meters, compared to TOFL of about 2000-2600 meters for aircraft in the same MTOW category.

17.2. Payload-Range Diagram

Another way to analyse the performance of an aircraft is with the help of a payload range diagram. It shows all the feasible distances that can be flown by the aircraft depending on the level of payload and fuel. Figure 17.3 shows the payload range diagram for the POGA.

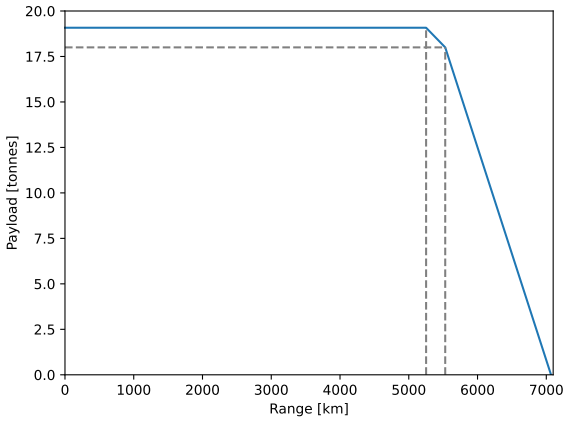

Figure 17.3: Payload-Range Diagram

This payload range diagram was constructed based on an unpublished book by Vos [59]. From this graph it can be seen that the range at the design payload is 5530 km. Increasing the mass to the total budgeted mass decreases the range slightly to 5252 km. The ferry range, however, is 7068 km. This means the aircraft can be transferred between continents without needing a refuelling stop.

17.3. Mission Profile

The aircraft follows a commercial passenger mission profile as shown in Figure 17.4. The profile is based on the mission range requirements and follows the main mission and reserve mission logic used in [4]. The main mission represents the normal flight operation, while the reserve mission is added for cases where the aircraft cannot complete the planned landing and has to continue to an alternate airport. The main and reserve mission segments are connected for completeness

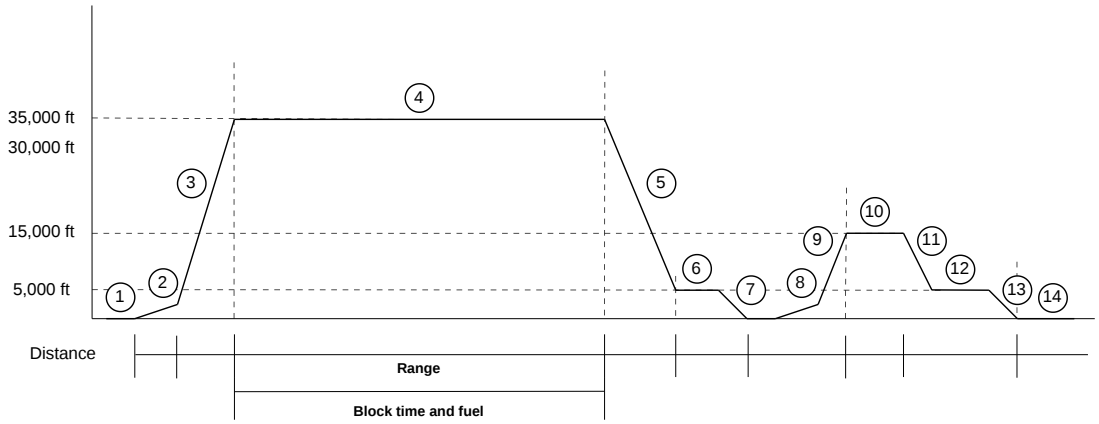

Figure 17.4: Mission profile according to the requirements [4]

The numbered phases in Figure 17.4 are summarised in Table 17.2. The first part represents the main mission with a stepped cruise. The second part represents the reserve mission with landing at the diversion airport. The operational and logistical flow of the aircraft is also illustrated in Figure 3.1.

The main mission follows the standard commercial transport mission profile described in [4]. It starts with taxi-out and take-off, followed by climb and cruise. A stepped cruise represents the increase in cruise altitude as aircraft mass reduces during flight. This could reduce the drag and improve efficiency. After the cruise segment, the aircraft descends, and performs the approach and landing at the planned destination airport. This part presents the normal operation without major delays, weather diversion or other abnormal events.

The reserve mission is included after the destination landing attempt. This is followed by the reverse mission logic, where the reserve mission contains a missed approach, climb to diversion cruise altitude, cruise, descent, holding, approach and landing [4]. In the design, the reserve part is represented by a 450 km diversion to the alternate airport and a 45-minute holding segment. For fuel-sizing purposes, this is converted into an equivalent reserve distance. This

considers realistic operational cases such as missed approach, wind shear, traffic congestion, weather deviation and final holding [60]. However, for long-haul flights, diversion airport availability should be further assessed case by case.

Table 17.2: Mission profile phase description

No.	Phase	Mission part
1	Taxi-out and enter runway	Main mission
2	Take-off and initial climb to 1,500 ft	Main mission
3	Climb to cruise altitude	Main mission
4	Stepped cruise at 35,000 ft	Main mission
5	Descent from cruise altitude	Main mission
6	Approach segment at low altitude	Main mission
7	Final approach / landing attempt	Main mission
8	Go-around and climb to 1,500 ft	Reserve mission
9	Climb to diversion cruise altitude	Reserve mission
10	Diversion cruise at 15,000 ft	Reserve mission
11	Descent from diversion altitude	Reserve mission
12	Holding / loiter at 5,000 ft	Reserve mission
13	Final approach	Reserve mission
14	Landing and taxi-in at alternate airport	Reserve mission

The range values in Figure 17.4 are selected based on the mission requirements and operational fuel allowance. The core of the mission is the 5,530 km design range, this is combined with a standard climb segment and a conservative 500 km descent allowance. This is included because flights are not always flown as a simple straight descent. They can include instrument approach procedure (IAP), arrival routing, altitude constraints, sequencing and vectoring before final approach [61]. Therefore, the mission profile gives a more realistic operating case than using cruise range only.

The mission profile is used as the basis for the O&L analysis, which is explained in Chapter 20. During the normal mission, the main checked are runway length, taxiway and stand compatibility, cruise range, approach speed, Bio-SAF replenishment, turnaround time, and maintenance access[1]. During the reserve mission, the main checks are diversion range, holding fuel, etc. As a result, route planning is not determined by range alone. Planned stopover operation also depends on traffic rights, airport availability, Bio-SAF availability, turnaround feasibility and airline network strategy. Direct flights can be used where the route is within the aircraft range, while longer missions can be supported by planned intermediate stops within the 24-hour requirement [62].

17.4. Loading Diagram

The loading diagram depicted in Figure 17.5 is the visual representation of the concept described in Section 14.3 with the two boarding strategies: front-to-back and back-to-front.

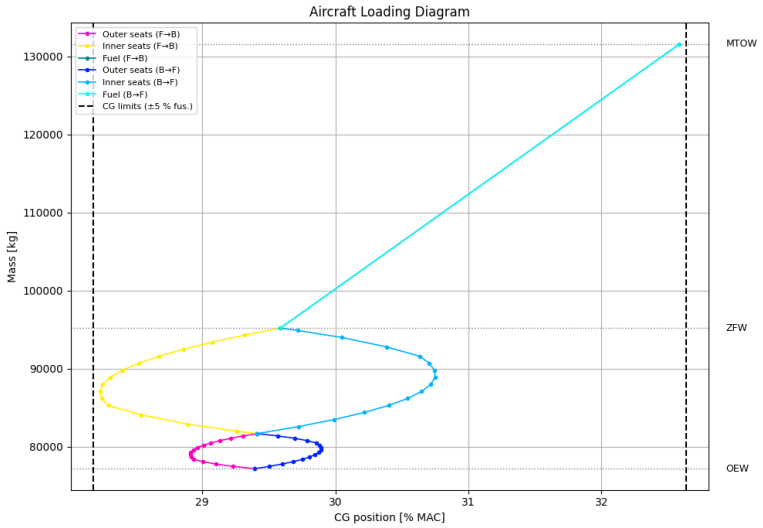

Figure 17.5: Loading Diagram

17.5. Manoeuvres

Figure 17.6 shows the V-n manoeuvre envelope at 35 000 ft ISA. The positive stall boundary grows as V^2 from the left, capped at +2.5 g by the CS-25.337 structural limit, with their intersection defining the manoeuvre speed $V_A = 287$ kt, below which the aircraft cannot structurally overstress regardless of pilot input. The negative stall boundary mirrors this

[1] URL `https://www.koreheadset.com/blogs/blog/7-phases-of-flight-understanding-every-stage-in-the-sky` [Cited 20/05/2026]

behaviour on the lower side, capped at -1.0 g, with the envelope closing at the dive speed $V_D = 1.25\,V_C$. The sustained turn boundary reflects the thrust limit, rising steeply at low speeds where induced drag dominates, peaking near V_A, and then falling as parasite drag increases. Where it lies below the stall boundary, thrust is the binding constraint.

Figure 17.7 shows the sustained turn rate as a function of airspeed. On the one hand, at low speeds, turn rate is stall-limited: the aircraft cannot bank steeply enough without losing lift. On the other hand, at high speeds, it is thrust-limited: the drag in a banked turn exceeds available thrust. The peak of $\dot{\psi} = 7.91$ deg/s at 305 kt represents the best sustained turn condition, where the two constraints are simultaneously closest to binding.

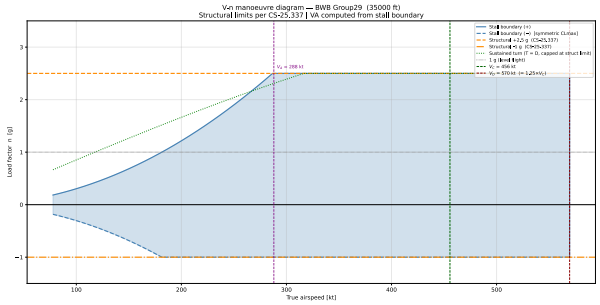

Figure 17.6: V-n manoeuvre envelope at 35,000 ft ISA.

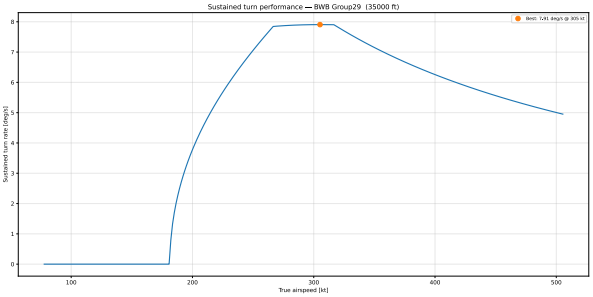

Figure 17.7: Sustained turn rate as a function of airspeed at 35,000 ft ISA.

18
Verification and Validation

Verification confirms that the design meets its stated requirements, while validation ensures that the right requirements were set in the first place. This chapter presents both activities. In Section 18.1, verification of all verifiable system requirements against their means of compliance is outlined, followed by a validation of the overall design approach in Section 18.2. The chapter ends with a sensitivity analysis in Section 18.3 to assess how key planform design variables influence aerodynamic performance, providing confidence in the robustness of the baseline design.

18.1. Verification

Each component of the OpenMDAO model has been individually verified through subsystem testing as explained in each individual methodology chapter. Furthermore, each requirement set as verifiable in Chapter 4 has been verified according to their means of compliance and the a description of their verification can be seen in Table 18.2. However the most important requirements, set out by the key stakeholders, also known as the investors are shown separately to showcase how the design complies with the main requirements of this project, this can be seen in Table 18.1.

Table 18.1: Key Stakeholder Requirement Compliance

SH-REQ-	Key Stakeholder Requirement	MoC	Achieved
8.01	The aircraft shall have a minimum flight range of 3000 km.	2	5530km
8.02	The aircraft shall be capable of covering 6000 km within 24 hours.	2	16000km
8.03	The aircraft shall accommodate a minimum of 120 passengers in business configuration.	1	120 passenger business class configuration.
8.04	Conditions at aircraft level that can lead to a catastrophic event shall be identified	3	See Risk Analysis Table 24.1.
8.05	The fuel shall not be petroleum-derived	0	Bio-SAF used as energy carrier.
8.06	The aircraft should minimise the use of petroleum derived materials	1	Aluminium, lithium based primary structure.
8.07	The first flight shall take place by 2031.	1	See Figure 25.2 Gantt Chart.
8.08	The aircraft shall be operable by 2035.	1	See Figure 25.2 Gantt Chart.
8.09	The maximum development cost shall be no more than 50 billion euros.	2	€29 billion required for development as detailed in Section 21.3.2.

Table 18.2: System Compliance Matrix

Requirement	Verified	MoC	Description of Verification
MS-REQ-2.2 (SH-REQ-1.12)	Yes	2	Computed direct operating costs for the selected concept and compared them to present programmes to confirm compliance with the stakeholder cost target.
MS-REQ-2.3 (SH-REQ-2.10)	Yes	2	Overall programme cost and acquisition cost derived using the cost analysis; results checked against stakeholder requirement SH-REQ-2.10.
MS-REQ-2.6 (SH-REQ-8.08)	Yes	2	Cost analysis produced a development budget estimate; upper bound found to be 28 billion EUR, within the stakeholder limit SH-REQ-8.08.
MS-REQ-3.1 (SH-REQ-8.07)	Yes	1	Project phasing and milestones described in the project logic diagram; timeline judged feasible to reach the stated entry-into-service goal.
MS-REQ-3.2 (SH-REQ-1.02)	Yes	1	System engineering process and design loop documented in the project logic diagram; demonstrates that the required design process can be followed.
MS-REQ-3.3 (SH-REQ-1.05)	Yes	1	Turnaround time computed from the operational concept; resulting value is 95 minutes and satisfies the stakeholder requirement.
MS-REQ-4.01 (SH-REQ-8.07) (SH-REQ-8.09)	Yes	3	Technical risk register and risk maps developed; high-consequence risks identified and mitigation actions defined in the risk assessment.
MS-REQ-4.02 (SH-REQ-1.02) (TR-06)	Yes	1	SAF selected as a certified drop-in fuel; compatibility with existing fuel infrastructure and engines justified using regulatory and OEM information.
MS-REQ-4.03 (SH-REQ-8.04)	Yes	1	A functional hazard assessment (FHA) was performed to identify failure conditions and their severities, supporting the safety requirement.
MS-REQ-4.08 (Risk Analysis)	Yes	1	An OpenMDAO-based multidisciplinary model was implemented (Chapter 6), providing coupled analysis capability and reducing integration risk.
MS-REQ-4.09 (Risk Analysis)	Yes	1	Concept selection conducted via a structured trade-off with weighted criteria; methodology and results documented in the trade-off chapter.

Requirement	Verified	MoC	Description of Verification
MS-REQ-5.1 (SH-REQ-1.04) (SH-REQ-8.03)	Yes	1	Cabin configuration and payload assumptions described in Chapter 11; shows that the required passenger configuration and payload can be accommodated.
MS-REQ-5.2 (SH-REQ-8.01)	Yes	2	Mission performance analysis gives a design range of 5 530 km, exceeding the minimum range requirement SH-REQ-8.01.
MS-REQ-5.3 (SH-REQ-8.02)	Yes	1,2	Mission profile including diversion computed at about 9 h per leg; with 95 min turnaround this yields ~19.6 h within 24 h and at least 8 280 km covered.
MS-REQ-5.4 (SH-REQ-1.16)	Yes	2	Fuel burn per passenger-kilometre computed; resulting value is 0.038 kg/pax-km for 120-seat business and 0.018 kg/pax-km for 250-seat economy.
MS-REQ-5.5 (SH-REQ-3.14)	Yes	2	Take-off field length (TOFL) estimated from performance analysis; result is about 850 m, comfortably below the stakeholder limit.
MS-REQ-6.1 (SH-REQ-3.02) (SH-REQ-3.04) (SH-REQ-3.05) (SH-REQ-3.11)	Yes	1	Airport compatibility, gate, and ground-operations analysis documented in Chapter 18.4; concept shown to meet the required airport and ground handling constraints.
MS-REQ-6.2 (SH-REQ-1.03) (SH-REQ-3.01)	Yes	2	Final planform gives a wingspan of 64.9 m; this satisfies the span requirement linked to airport code and gate compatibility.
MS-REQ-7.09 (SH-REQ-1.17)	Yes	2	Diversion and abnormal-operation cases analysed in Chapter 18.8; aircraft shown to handle diversion, fuel-supply, and abnormal landing scenarios in line with the requirement.
MS-REQ-7.14 (SH-REQ-4.02)	Yes	1	Fuel jettison/ejector locations defined near the wing tips in the fuel system diagram; supports safe fuel dumping behaviour per the stakeholder requirement.
MS-REQ-9.1 (SH-REQ-1.01) (SH-REQ-8.05)	Yes	0	Energy source defined as 100% SAF; this is non-petroleum derived and directly satisfies the non-kerosene fuel requirement.
MS-REQ-9.2 (SH-REQ-8.06)	Yes	1	Material selection strategy defined so that, once the concept is chosen, non-petroleum-based materials are preferred wherever feasible, minimising petroleum-derived structural materials.
MS-REQ-9.3 (SH-REQ-9.01)	Yes	0,2	Life-cycle emissions assessment uses SAF LCA values (e.g. FT bio-SAF with ~86% reduction) and mission fuel burn to show net-zero or strongly reduced CO_2 per stakeholder requirement.
MS-REQ-9.4 (SH-REQ-1.16)	Yes	2	Average 3 150 g CO_2 per kg SAF and a fuel use of 0.04 kg/pax-km combined to compute CO_2 per passenger-kilometre and check against the target.
MS-REQ-9.6 (SH-REQ-9.04)	Yes	1	Material sustainability strategy documented in Chapter 20.3; shows increasing sustainable material share over time.
MS-REQ-9.7 (SH-REQ-9.03) (Lifecycle Analysis)	Yes	1	Life Cycle Assessment (LCA) presented in Chapter 20.5; evaluates cradle-to-grave impacts and confirms alignment with lifecycle sustainability goals.
MS-REQ-12.6 (SH-REQ-8.08)	Yes	1	Programme timeline and scalability discussed in Chapter 21.1.6; demonstrates that production ramp-up and fleet size targets are feasible.
AL-REQ-1.1	Yes	2	Verified in the structures chapter, where the relevant structural sizing and checks are presented.
AL-REQ-1.2	Yes	2	Verified in the structures chapter; analysis shows the corresponding structural requirement is met.
AL-REQ-2.1	Yes	1	Satisfied by the stability and control analysis described in Chapter 14.
AL-REQ-2.2	Yes	2	Quantitatively shown in Chapter 14, stability analysis using eigenvalue and derivative calculations.
AL-REQ-2.3	Yes	2	Verified by the lateral-directional stability and handling qualities results in Chapter 14.
AL-REQ-2.4	Yes	2	Met according to additional stability metrics reported in Chapter 14.
AL-REQ-3.1	Yes	2	Supported by aerodynamic coefficients and performance data in the aerodynamic analysis chapter.
AL-REQ-3.2	Yes	2	Confirmed by further aerodynamic performance results (e.g. drag breakdown, L/D) in the aerodynamic analysis chapter.
AL-REQ-4.1	Yes	2	Take-off field length computed as 1 410 m; this value satisfies the associated stakeholder take-off requirement.
AL-REQ-4.2	Yes	2	Since the landing distance is shorter than the computed take-off distance, the landing performance requirement is also satisfied.
AL-REQ-4.3	Yes	2	Crosswind capability analysis shows acceptable operation in crosswinds up to 20 kt.
AL-REQ-4.4	Yes	0	Geometric data show wingspan 64.9 m and gear span within airport limits, fulfilling airport compatibility constraints.

Requirement	Verified	MoC	Description of Verification
AL-REQ-5.1	Yes	2	Climb performance calculation indicates the aircraft reaches Mach 0.79 in about 38.5 minutes, meeting the climb requirement.
AL-REQ-5.3	Yes	2	Cruise and climb performance further confirms that the required mission and altitude profiles can be achieved.
AL-REQ-6.1	Yes	2	Fuel-system and volume analysis show that more than 35 000 kg of fuel can be stored in the tanks, exceeding the minimum needed.
AL-REQ-7.3	Yes	2	Turnaround analysis yields a turnaround time of exactly 95 minutes, in line with the operational requirement.
AL-REQ-8.3	Yes	2	Electrical power budget indicates at least 1 000 kW of installed electrical power, satisfying the system demand.
AL-REQ-8.5	Yes	2	Cabin pressurisation analysis shows cabin altitude is limited to 8 000 ft at cruise.
AL-REQ-10.4	Yes	1	Crew complement defined as 4 pilots and 12 cabin crew; this satisfies regulatory and service requirements.
AL-REQ-10.5	Yes	2	Payload and mass budgets allocate exactly 9 000 kg to cargo, satisfying the cargo-mass requirement.
AL-REQ-10.7	Yes	1	Associated operational or cabin requirement confirmed qualitatively in the relevant chapter (e.g. crew rest and layouts).
AL-REQ-10.9	Yes	2	Wingspan from final geometry is 64.9 m, which is the exact maximum width allowed.
AF-REQ-2.3	Yes	2	The roll control authority margin has been computed and confirms the airframe has a positive restoring roll moment.
AF-REQ-3.2	Yes	2	Satisfied by the stability and control analysis described in Chapter 14.
AF-REQ-5.1	Yes	1	Main wingspars provide loadpath to the fuselage.
AF-REQ-6.1	Yes	2	Tested by Power and Propulsion module code, and aerodynamic analysis code.
AF-REQ-7.6	Yes	2	See SM-REQ-1.11 verification
AF-REQ-8.2	Yes	2	Tip over angle is 15.4
AF-REQ-11.1	Yes	2	The corresponding cabin differential pressure is applied to the representative multi-bubble shell geometry and the required shell thickness is sized such that the allowable stress of the selected shell material is not exceeded
AF-REQ-12.4	Yes	2	The engine mass is included as an inertial load contribution in the longitudinal moment analysis. The maximum resulting longitudinal bending stress is used to size the required outer-contour thickness.
AF-REQ-12.5	Yes	2	The fuel masses from the two tank regions are included as inertial load contributions in the longitudinal and spanwise bending moment analysis. The maximum resulting longitudinal bending stress is used to size the required outer-contour thickness and the maximum resulting lateral bending stress is used to size the internal trapezoidal structure.
AF-REQ-12.6	Yes	2	The fuel masses from the two tank regions are included as inertial load contributions in the spanwise shear force analysis. The maximum resulting shear stress is then used to size the internal trapezoidal structure.
AF-REQ-13.11	Yes	1	Current type A doors are able to support the rate.
AF-REQ-13.3	Yes	1	With 4 type A and 2 ventral, the requirement is fulfilled through equipment qualification and comparison to similar aircraft and analysis
AF-REQ-15.2	Yes	1	Geometry based off requirement, see Section 9.2 for further information.
AF-REQ-15.3	Yes	2	Current cabin dimension has a volume of 808.5 m^3
AF-REQ-15.5	Yes	2	Maximum available space in airframe is 66 m^3, this has been sized to 45.5 m^3.
AF-REQ-16.1	Yes	2	The wingspan is 64.9 metres.
AF-REQ-16.2	Yes	2	The height is 9.0 metres.
AF-REQ-16.3	Yes	2	The length is 27.6 metres.
AF-REQ-16.4	Yes	2	The sill height is 4.5 metres.
AF-REQ-16.5	Yes	2	The outer main gear wheel span is 6.85 metres.
DO-REQ-1	Yes	1	Valid space for 4 type A doors for passenger boarding and servicing. Valid space for forward and afterward cargo doors.
DO-REQ-2	Yes	0	Valid space for 4 type A doors.
DO-REQ-3	Yes	2	The passenger door sill height with 4.5 m from the ground ensuring compatibility with passenger boarding equipments.
LG-REQ-5	Yes	2	The tip back angle is more than 15 degrees with the OMGWS of 6.85 metres.
LG-REQ-7	Yes	9	The compatibility with airport GSE has been checked.
FR-REQ-3	Yes	1	Enough volume is available for crew, passenger and cargo.
FR-REQ-4	Yes	2	Enough cabin volume is available for 120 passenger under business class seating configuration and level of service.
FR-REQ-5	Yes	1	4 type A doors and 2 ventral exits create sufficient evacuation paths.
FR-REQ-6	Yes	2	The aircraft has a passenger seat pitch of 160 cm for support and comfort for the intended flight duration.
FR-REQ-7	Yes	2	The aircraft has a 51 cm cabin aisle space and access for normal passenger movement during flight.

Requirement	Verified	MoC	Description of Verification
FR-REQ-8	Yes	1	The aircraft has accessible, functional, and sufficient passenger facilities, including lavatories, galleys, etc.
FR-REQ-9	Yes	1	Enough space is available to provide individual passenger entertainment systems.
LS-REQ-1	Yes	2	Rudder planform defined in the lifting-surface geometry; integrated wetted area computed and confirmed $\approx 12.6\ \mathrm{m}^2$.
LS-REQ-2	Yes	2	Outer elevon span and chord set in the wing planform; control-surface area calculation gives $\approx 3.9\ \mathrm{m}^2$.
LS-REQ-3	Yes	2	Middle elevon geometry implemented; area obtained from planform discretisation matches $25.05\ \mathrm{m}^2$ within modelling tolerance.
LS-REQ-4	Yes	2	Inner elevon dimensions defined in the BWB layout; computed control-surface area is $\approx 45.1\ \mathrm{m}^2$.
LS-REQ-5	Yes	2	Tip chord is 2.2 meters, however the winglet root width is 3.5 meters. This is solved by extending the winglet behind the wing tip chord and including a smooth transition.
LS-REQ-6	Yes	2	Cruise lift coefficient from AVL combined with reference area and cruise dynamic pressure; resulting lift equals aircraft weight at cruise, matching 1 186 419.55 N.
LS-REQ-7	No	2	Landing C_L and approach speed analysed; trend shows adequate low-speed lift, but detailed high-lift configuration and exact lift value not fully verified.
LS-REQ-8	Yes	2	Clean-wing AVL analysis with drag build-up corrections gives cruise $L/D \approx 17.3$; this exceeds the 16.3 L/D of the Airbus A320 reference.
LS-REQ-9	Yes	2	Planform and cabin layout include four door cut-outs sized to type-A dimensions along the lifting-surface centrebody.
LS-REQ-10	Yes	2	Cabin and lower-fuselage geometry include two ventral exits with the specified dimensions in the trailing cabin section.
LS-REQ-11	Yes	1,2	Enough space available below the cabin is the middle bubble for cargo storage.
SM-REQ-1.1	Yes	2	Longitudinal beam model with AVL aerodynamic loads; outer contour sized so bending stresses stay below allowables for limit/ultimate cases.
SM-REQ-1.2	Yes	2	Beam model including payload, fuel, engine and gear loads; resulting shear/bending stresses in primary members checked against allowables.
SM-REQ-2.1	Yes	2	Critical aerodynamic load cases applied to fuselage; outer contour thickness chosen so combined bending stresses remain below material allowable.
SM-REQ-4.1	Yes	2	Shear and bending diagrams generated for LC01–LC04; sized outer contour carries these envelopes without exceeding stress or stability limits.
SM-REQ-5.1	Yes	2	Wing-root shear and bending loads applied in trapezoidal cabin model; member dimensions chosen with positive failure margins.
SM-REQ-6.1	Yes	2	Multi-bubble pressure shell sized per arc using thin-shell formulas; required thicknesses satisfy stress allowables under differential pressure.
SM-REQ-7.1	Yes	2	Pressurisation reactions resolved at nodes, applied in trapezoid model; strength and stability checks give positive margins for all members.
SM-REQ-8.1	Yes	2	Passenger and seat inertial loads modelled on cabin floor; sandwich panels and columns sized to pass strength and buckling checks.
SM-REQ-8.2	Yes	2	Cargo and systems loads included in same framework; floor and sidewall members sized for combined pressure/wing loads retain positive margins.
SM-REQ-9.1	Yes	2	Outer-wing and transition tank geometry defined; computed fuel volume in volume budget and fuel layout meets mission fuel plus margin.
SM-REQ-10.1	Yes	2	Multi-bubble shell, trapezoid and outer contour provide parallel load paths; concept checked qualitatively against fail-safe intent.
SM-REQ-11.1	Yes	0	Qualitatively justified by choosing Al-Li, sandwich panels and conventional composite practices compatible with established aerospace processes.
SM-REQ-11.2	Yes	0	Qualitatively justified by partitioning the BWB into sub-assemblies and estimating realistic prototype manufacturing, assembly and integration durations.
PP-REQ-1.1	Yes	1	Wing box integrated load-bearing design; shielded from the environment. The additional fuel thermal management system keeps SAF within the allowable temperature.
PP-REQ-1.4	Yes	1	Fuel quantity, pressure, and temperature sensors are employed in the wing tank to monitor critical parameters; see Figure 11.2 for reference.
PP-REQ-1.6	Yes	1	Fuel distribution is managed by centrifugal and injector pumps, heat exchangers, and filters; see Figure 11.2 for reference.
PP-REQ-1.7	Yes	1	Done by centrifugal and injector pumps; see Figure 11.2 for reference.
PP-REQ-1.8	Yes	1	Standard refuelling components used as per commercial aircraft industry standards.
PP-REQ-1.10	Yes	1	Fuel quantity and pressure sensors installed; see Figure 11.2 for reference.
PP-REQ-1.11	Yes	1	Main power sources are engines; backup sources include APU, batteries, and RATs (Ram Air Turbine).
PP-REQ-1.13	Yes	4	Heat exchangers, pumps, and vents maintain temperature within ranges described by the fuel storage subsystem.

Requirement	Verified	MoC	Description of Verification
PP-REQ-2.1	Yes	2	Thrust sized per CS-25 and TOFL expectations; 296 kN per engine chosen, satisfying TOFL requirement of 1410 meters.
PP-REQ-2.2	Yes	0, 2	Two VFSGs are employed per engine, each generating 250 kW (1000 kW total electrical generation); this exceeds the required value.
PP-REQ-2.6	Yes	1, 2	Required 884 kW; system provides 1000 kW, providing a 13% power reserve.
PP-REQ-2.8	Yes	2	Calculated overall efficiency of 0.47% during cruise.
PP-REQ-3.2	Yes	1	See Figure 19.1.
PP-REQ-3.3	Yes	1	APU, batteries, and RAT employed; see Figure 19.1.
PP-REQ-3.4	Yes	1	Independent data buses; hydraulic lines feature multiple independent circuits.
PP-REQ-3.5	Yes	1	Independent lines separated by physical space to ensure redundancy.
PP-REQ-6.2	Yes	2	Resultant weight fraction is 27%.
ES-REQ-2	Yes	2	Fuel tanks sized for maximum capacity of 35,560 kg; see Section 16.3.1.
ED-REQ-8	Yes	1	Cross-feed connections between tanks allow fuel balancing and transfer in case of malfunction; see Figure 11.2.
EN-REQ-1	Yes	9	Genx-2B engines utilised, each with 296 kN SLS thrust (manufacturer test data).
EN-REQ-2	Yes	9	787-series VFSGs used (250 kW each); two per engine provide 1000 kW total, per EASA data sheets.
EN-REQ-3	Yes	9	Genx-2B verified for 100% SAF operation by General Electric.
EN-REQ-6	Yes	2	TSFC of 12.7 mg/Ns achieved during cruise.
FC-REQ-1.1	Yes	2	AVL yields $x_{np} = 13.60\,\text{m}$, giving $K_n = +4.83\%$ MAC at forward CG (stable) and $K_n = -11.39\%$ MAC at aft CG (unstable), managed by FBW/SAS. See Section 14.6.
FC-REQ-1.2	Yes	2	Ganged elevon trim solved via Equation 14.18, yielding $\delta_{e,\text{trim}} = -26.48^\circ$ at loiter, within the $\pm 30^\circ$ limit. See Section 14.6.
FC-REQ-1.3	Yes	2	CG computed as $x_{cg,\text{OEW}} = 14.12\,\text{m}$, $x_{cg,\text{ZFW}} = 14.17\,\text{m}$, $x_{cg,\text{MTOW}} = 14.86\,\text{m}$; all boarding sequences remain within 13.8–14.6 m. See Section 14.3.
FC-REQ-2.1	Yes	2	AVL yields $C_{n_\beta} \approx 0.00067\,\text{rad}^{-1} > 0$, satisfying the requirement. Magnitude is weak due to absence of a vertical tail; SAS augmentation required. See Subsection 14.10.2.
FC-REQ-2.2	Yes	2	$C_{\ell_\beta} < 0$ confirmed from AVL derivatives, consistent with stabilising dihedral effect. See Subsection 14.10.4.
FC-REQ-2.3	Yes	2	Spiral confirmed unstable via Equation 14.48 ($C_{\ell_\beta} C_{n_r} - C_{n_\beta} C_{\ell_r} = 0.598$). Eigenvalue gives $t_2 = 0.74\,\text{s}$, attributed to AVL divergence error. See Subsection 14.10.1.
FC-REQ-3.1	Yes	2	All 1000 flight points fail $\zeta\omega_n \geq 0.15\,\text{rad/s}$; 25.5% fail $\zeta \geq 0.08$, driven by weak weathercock stability. Substantial SAS augmentation required. See Subsection 14.10.2.
FC-REQ-3.2	Yes	2	Points up to 9 km remain within ICAO acceptable limits; points at 12 km enter the unacceptable zone. FBW augmentation required. See Subsection 14.9.2.
FC-REQ-3.3	Yes	2	τ_R remains below 1.0 s at both approach ($V_{app} = 85.4\,\text{kt}$) and cruise ($M = 0.79$) conditions, satisfying Level 1 MIL-SPEC ($\tau_R \leq 1.4\,\text{s}$) without augmentation. See Subsection 14.10.3.
FC-REQ-4.1	Yes	2	τ_R remains below 1.0 s across all 1000 evaluated flight points, satisfying Level 1 MIL-SPEC ($\tau_R \leq 1.4\,\text{s}$) without augmentation. See Subsection 14.10.3.
FC-REQ-4.2	Yes	2	Configuration 1 selected as provisional baseline, maximising roll moment arm via outermost elevon placement. Quantitative margins pending resolved AVL derivatives. See Subsection 14.13.3 and Table 14.6.
FC-REQ-5.1	Yes	2	V-n envelope bounded by stall, structural limits of $+2.5\,g$ and $-1.0\,g$ per CS-25.337, and sustained turn boundary. See Subsection 14.12.4.
FC-REQ-5.2	Yes	1	Holding turn yields $n = 1.10\,g$, $\dot{\psi} = 1.67^\circ/\text{s}$, $R = 5.40\,\text{km}$ under ISA still-air conditions, satisfying $\leq 25^\circ$ bank and $\leq 3^\circ/\text{s}$ rate. See Subsection 14.12.3.

18.2. Validation

Validation itself takes place through multiply steps, there is the validation of the code itself, or at least each module of the code, which can be seen under each chapter in Chapter 7. Furthermore there exists the validation of each requirement, due to the fact that there are over 400 requirements in the whole system engineering process, of which over 150 were verifiable, the description of the validation of each requirement and how the TBDs were filled in would extend the papers length to an unacceptable amount. All the requirements have been checked by the key stakeholders and generally speaking the TBDs were filled in from calculations made using the processes described in Chapter 7, from the EASA Certification Specifications, or from general industry benchmarks and reference aircraft parameters [9].

18.3. Sensitivity Analysis

To assess the robustness of the baseline design and identify which planform variables most strongly drive aerodynamic performance, a sensitivity analysis is conducted on the outer wing geometry.

18.3.1. Objective and Scope

The objective of the sensitivity analysis is to quantify how key planform design variables influence the final design of the BWB, particularly its aerodynamic performance at cruise, with a focus on the total lift-to-drag ratio, total drag

coefficient, and pitching moment coefficient. The analysis considers the aspect ratio of the outer wing, taper ratio, transition width between the central body and outer wing, and streamwise position of the outer wing leading edge as geometric drivers of the outer wing.

All sensitivities are evaluated at a fixed cruise angle of attack of $\alpha_{cr} = 2.31°$, Mach number $M = 0.79$, and cruise altitude $h = 10,668\,\text{m}$. The aerodynamic response is computed with an AeroSandbox vortex-lattice model on the geometry generated by the OpenMDAO wing planform component.

It should be noted that the aerodynamic analysis in the OpenMDAO model was performed using AVL, which is similar but different still to the vortex-lattice model embedded in AeroSandbox. AeroSandbox was favoured for use in the sensitivity analysis due to computation time in AVL being significantly more than AeroSandbox. Additionally, in Figure 15.7, it is shown that AeroSandbox improves the aerodynamic performance of the aircraft which could offset the results from this sensitivity analysis. However, since a sensitivity analysis is more interested in the relationships between parameters and the general trends of both AVL and AeroSandbox VLM are similar, as shown in Figure 15.7, it was deemed suitable for use in the sensitivity analysis.

18.3.2. Methodology

Geometry-Aerodynamics Workflow

1. For each design point, the `WingPlanform` OpenMDAO component is used to compute a consistent outer-wing geometry from the inputs (AR, λ, w_{trans}, x_{root}). This yields the reference area S_{ref}, span b, outer-wing chord distribution ($c_{root,ow}$, c_{tip}), and sweep angles, while still respecting the imposed $b \leq 65\,\text{m}$ constraint.
2. The resulting planform is passed on to an AeroSandbox vortex-lattice model, which evaluates the 3D aerodynamic coefficients at the fixed cruise operating point. From these the following aerodynamic parameters can be computed:
   - Lift coefficient C_L
   - Induced drag coefficient $C_{D,i}$
   - Total drag coefficient $C_{D,tot} = C_{D,i} + C_{D,0} + C_{D,wave} + C_{D,eng}$
   - Pitching moment coefficient C_m
   - Induced and total lift-to-drag ratios, $L/D_i = C_L/C_{D,i}$ and $L/D = C_L/C_{D,tot}$

   Here $C_{D,0}$, $C_{D,wave}$, and $C_{D,eng}$ are modelled as fixed profile drag, a Mach-dependent wave drag term, and a small engine-installation increment respectively.

Latin Hypercube Sampling

To explore the design space, a Latin hypercube sample (LHS) of size $N = 60$ is drawn over uniform ranges for the four design variables:

- $AR \in [19, 23]$
- $\lambda \in [0.30, 0.50]$
- $w_{trans} \in [3.0, 7.0]\,\text{m}$
- $x_{root} \in [1.5, 3.5]\,\text{m}$

For each LHS point the geometry-aerodynamic workflow above is executed, and the resulting inputs and outputs are stored, which provides a global view of how L/D and related quantities vary over a physically plausible design region.

Local Derivatives: Central Finite Differences

To obtain local information near the current baseline design, central finite differences on the same four design variables is performed.

- Baseline: $(AR_0, \lambda_0, w_{trans,0}, x_{root,0}) = (21.0, 0.40, 5.0\,\text{m}, 2.5\,\text{m})$.
- Steps: $\Delta AR = 0.25, \Delta\lambda = 0.01, \Delta w_{trans} = 0.10\,\text{m}, \Delta x_{root} = 0.05\,\text{m}$

For each variable x, the response f is evaluated at $x_0 \pm \Delta x$ (holding the others fixed), and the derivative is thus approximated with Equation 18.1.

$$\frac{\partial f}{\partial x} \approx \frac{f(x_0 + \Delta x) - f(x_0 - \Delta x)}{2\Delta x} \tag{18.1}$$

To compare sensitivities across variables and metrics, a normalised sensitivity can be computed using Equation 18.2.

$$S_{f,x}^{\text{norm}} = \frac{\partial f}{\partial x} \cdot \frac{x_0}{f_0} \tag{18.2}$$

This can be interpreted as a fractional change in f per fractional change in x at the baseline point.

18.3.3. Results

After filtering out a small number of clearly non-physical VLM solutions, the remaining samples show consistent, smooth trends in C_L, $C_{D,tot}$, and lift-to-drag ratio L/D across the considered variation of aspect ratio, taper ratio, transition width, and outer-wing root x-position.

Global trends from Latin hypercube sampling
The LHS data shows that all designs considered for this exploration achieve a lift coefficient $C_L \approx 0.34$–0.36 at the fixed $\alpha_{cr} = 2.31°$, with induced drag coefficients around $C_{D,i} \approx 0.007$ and total drag coefficients $C_{D,tot} \approx 0.018$–0.021. This leads to the expected total lift-to-drag ratios in the range $L/D \approx 17$–18 for the parameter combinations considered.

Across the 60 LHS sampled designs, variations in the outer-wing AR and taper ratio λ produce small changes in C_L at fixed α_{cr}. These variations do, however, clearly affect drag and therefore L/D. Additionally, designs with marginally higher AR and moderate λ tend to be at the upper end of the observed L/D range, where lower AR move towards the lower end. This matches the intuition that high aspect ratio wings are more aerodynamically efficient.

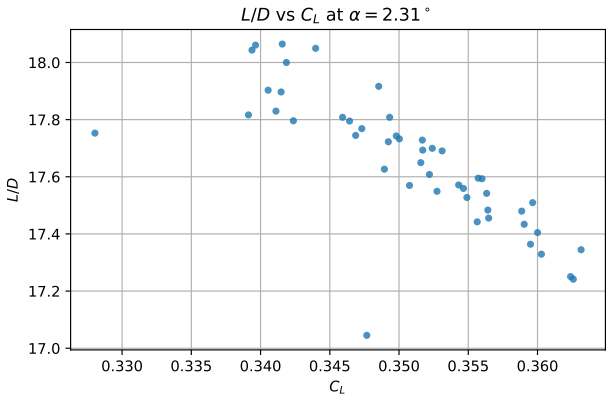

Figure 18.1: Lift-to-drag ratio against lift coefficient for LHS sampled designs at $\alpha_{cr} = 2.31°$

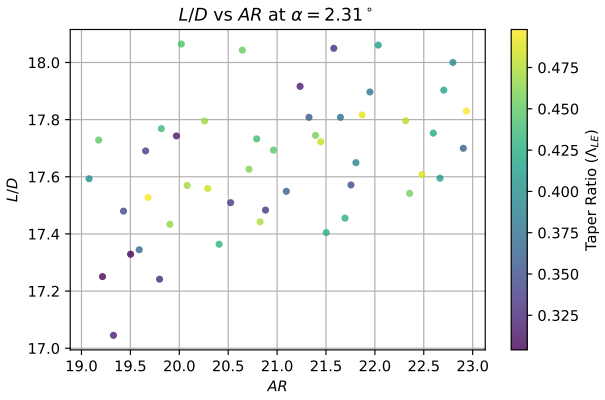

Figure 18.2: Lift-to-drag ratio against aspect ratio for LHS sampled designs at $\alpha_{cr} = 2.31°$

Figure 18.1 and Figure 18.2 show a cloud of design points which is consistent with the fact that the aircraft is span-limited and evaluated at a fixed angle of attack rather than at each geometry's optimal C_L.

Local sensitivities at the baseline design
The finite-difference results around the baseline design quantify the relative influence of each design variable, using Equation 18.2

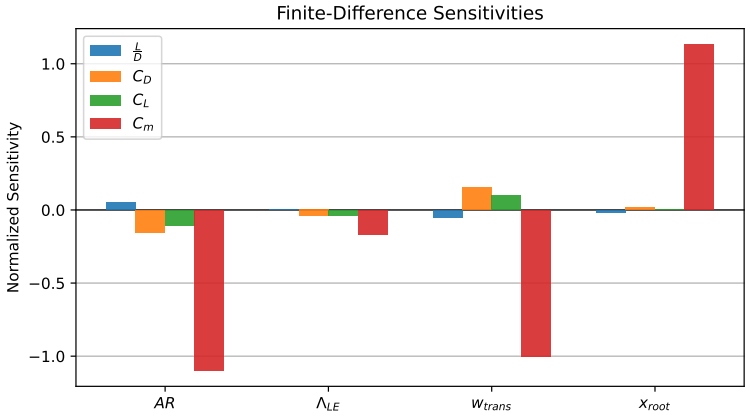

Figure 18.3: Bar chart showing finite-difference sensitivities of aerodynamic analysis

.

Aspect Ratio AR. From Figure 18.3, it can be seen that increasing AR slightly reduces both C_D and C_L at fixed α_{cr}. It decreases the drag more than the lift and so the normalised sensitivity of L/D with respect to AR is slightly positive ($S^{norm}_{L/D,AR} \approx 0.05$). The wingspan is constrained by the maximum wingspan and so increasing AR redistributes the wing area which means that AR is not as dominant as an aerodynamic design lever as it would be in an unconstrained wing design problem.

Taper Ratio λ The taper ratio has the least influence on aerodynamic parameters, as seen in Figure 18.3. Increasing λ decreases both C_L and C_D almost equally and so λ has no practical effect on the L/D. This reflects a consequence of using AVL, or VLM in general, as it neglects the effect of shockwaves at high Mach numbers. As such, the λ in our case does not affect the cruise efficiency.

Transition width w_{trans}. The transition width between the central body and outer wing has a mixed influence. Increasing w_{trans} slightly increases both C_L and $C_{D,\text{tot}}$ and results in a small negative normalized sensitivity for L/D ($S^{\text{norm}}_{L/D,dy} \approx -0.05$), indicating that making the transition region wider is locally bad for efficiency. The magnitude of these sensitivities remains small compared to those of the geometric parameters that directly set chord and thickness,

so w_{trans} can be viewed as a secondary shaping parameter. In the design of this BWB, w_{trans} was mainly used to accomodate for fuel storage.

Root position x_{root}. Varying the outer-wing root x-position at fixed α_{cr} has a very small effect on C_L and L/D (normalized sensitivities close to zero), but a relatively large effect on pitching moment. This confirms that, in the current configuration, x_{root} is primarily a trim and balance lever rather than a performance lever. Intuitively, this also makes sense and is thus an additional step of validation.

Overall, the normalized sensitivity bar plot shows that bars associated with L/D and $C_{D,\text{tot}}$ are small in magnitude for all four variables, while bars for C_m are notably higher for variables that move area fore or aft (especially AR and x_{root}). This pattern supports the interpretation that the chosen baseline is already in a relatively flat region of the local L/D landscape, and that further aerodynamic improvements within the current constraints will be incremental rather than transformative. This builds confidence that the design is, at least, near a local optimum.

Implications for design
Taken together, the LHS trends and local sensitivities suggest that, within the allowed design space and at the fixed cruise angle of attack, all four planform variables have relatively small local impact on L/D compared to the absolute drag level. This is largely because the BWB is span-limited and evaluated at a non-optimised α, so induced-drag reductions are partially masked by the fixed drag build-up.

Aspect ratio and taper ratio remain the most relevant aerodynamic levers, but near the baseline their effect on L/D is small. They are as important for structural and integration trade-offs as for aerodynamic performance. In contrast, transition width and root position are best used as tuning parameters since they matter for For the purposes of the present DSE, these results support keeping the current baseline geometry near its present AR and λ and focusing design effort on higher-leverage disciplines (e.g. structures, systems, and energy management), while using dy_{trans} and x_{root} mainly for local refinement and trimming for stability.

19
Aircraft System Characteristics

With the preliminary design established, this chapter details the key characteristics of the aircraft's systems and their interactions. The electrical power budget is presented in Section 19.1 to confirm sufficient power generation across all flight phases, followed by hardware, software, and data handling block diagrams that together capture the full system architecture of the aircraft, which are presented in Section 19.2, Section 19.3 and Section 19.4, respectively.

In Section 2.1, the available system and subsystems have been defined, however now that the preliminary design has been developed, the interactions between the systems and subsystems can be closer looked at. Figure 19.1 shows how the available subsystems interact through physical, electrical, data and mechanical power connections. It can be seen that the two key subsystem components are the Power Distribution System ensuring each system gets the right amount electrical energy, the power required for each subsystem has been calculated based on first order estimations by Voth et al. fitted to the current aircraft geometry [12]. Furthermore the Command & Data Handling Subsystems connects all the logical flow of the aircraft in order to ensure the pilots inputs are processed as intended and that all the safety and back-up procedures are operational.

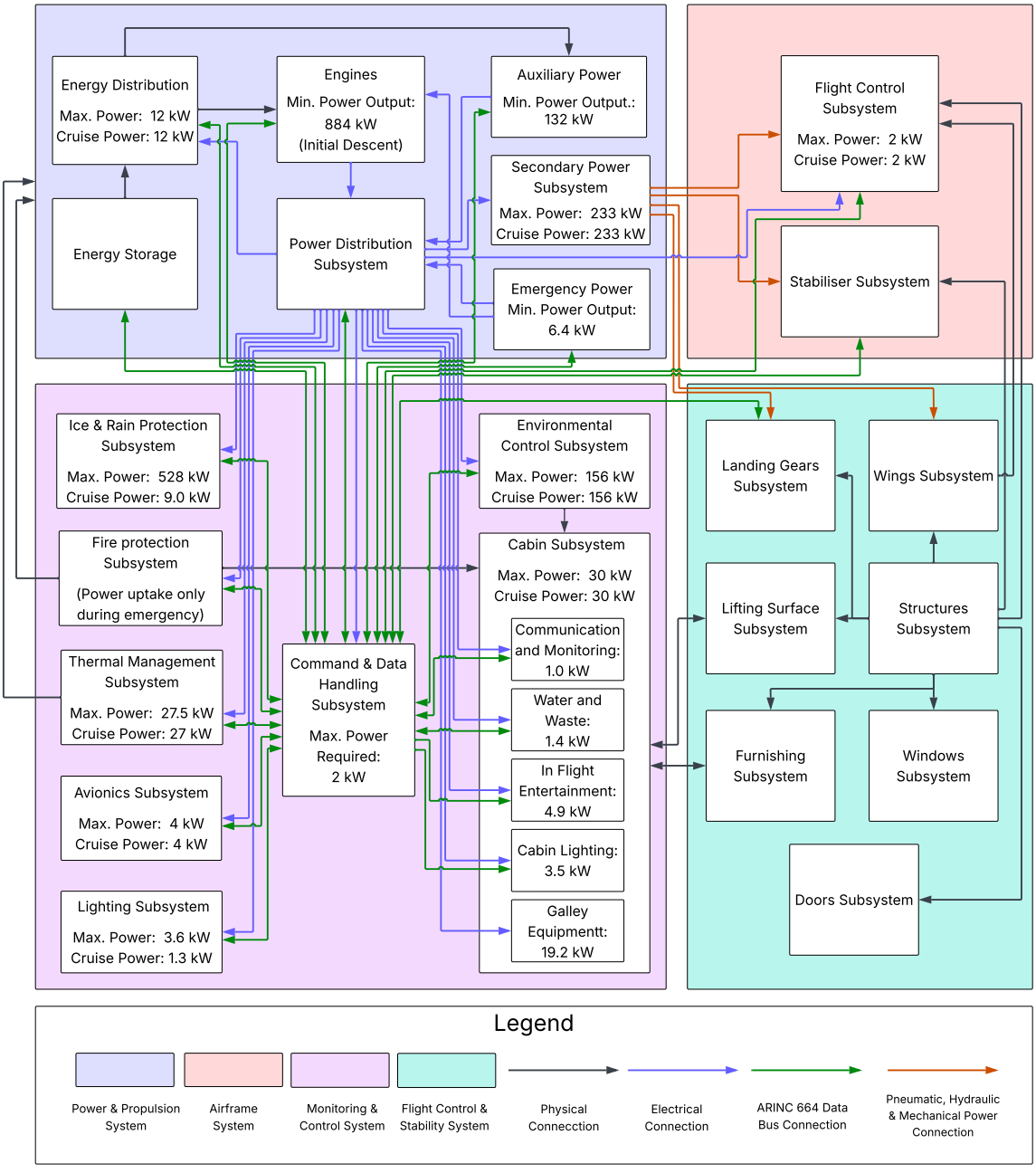

Figure 19.1: Aircraft System and Subsystems Interaction (including Electrical) Block, Power Calculations Based on [12]

19.1. Electrical Power Budget

The electrical power budget accounts for all onboard subsystems, quantifying their individual power demands and the margins applied to ensure reliable operation. Power estimates are derived from first-order models fitted to the current aircraft geometry, and the total demand is compared against the available generation capacity from the engines, APU, and emergency systems.

Table 19.1: Preliminary electrical power budget breakdown including margins and excluded propulsive power.

Subsystem	Baseline Budgeted Power [kW]	Calculated Power [kW]	Margin [%]	Budgeted Power [kW]
Total needed power	**374**	**998.1**	**–**	**1183.9**
Environmental Conditioning	–	156.0	15	179.4
Galley Equipment	–	19.2	15	22.1
Energy Distribution	–	12.0	15	13.8
Flight Control	–	2.0	15	2.3
Ice and rain protection	–	528.0	15	607.2
Internal lighting	–	3.5	15	4.0
External lighting	–	3.6	15	4.1
Water and Waste	–	1.4	5	1.5
In Flight Entertainment	–	4.9	0	4.9
Avionics	–	4.0	0	4.0
Command & Data Handling	–	2.0	15	2.3
Thermal Management	–	27.5	15	31.6
Communication and Monitoring	–	1.0	15	1.2
Secondary Power	–	233	15	268.0
Total Generated Power	**–**	**1132**	**–**	**1132**
Engines	–	1000	–	1000
APU	–	132	–	132
Emergency	–	6.4		6.4
Net Power	**374**	**133.9**	**–**	**-51.9**

From this Table 19.1, it might seem like there is not enough to power the full aircraft once margins have been applied, however, this is not the case as in reality not all the systems are going to operating at peak power at the same time. For example the ECS will be drawing most of its power during the cruise, whilst at altitude, whereas the Ice and Rain protection draws most of its power during taxiing, climb, and descent [12]. Taking this division into account, the aircraft does still have enough power when the margins are applied.
From Table 19.1, it can also be seen that the original budgeted power was three times lower than the current budgeted power. This can attributed, due to neglecting the fact that not all system are turned on at the same time, as it was simply assumed that the total generated power would always equal the total needed power of all systems turned on. There was also less depth for the electrical systems as the mission was not even in the conceptual design stage.

The margins itself have been selected to be at 15% for most of the subsystems. This is, according to Voth et al., to ensure that the systems will work 99% of the time [12]. However, for the avionics and the in flight entertainment system these margins have not been taken, simply because in the formulae for their power requirements they already have implicit margins of 8% and 15% respectively [12]. The margin for water and waste is also smaller as the equation for this model used power consumption of industry used, modern boilers, that is why this margin seemed feasible to reduce.

19.2. Hardware Block Diagram

Figure 19.2 decomposes the aircraft into its physical subsystems, spanning the lifting surface, centrebody, propulsion, fuel system, power, avionics, communications, thermal control, and command and data handling. Connections are typed by physical medium, distinguishing structural load paths, electrical lines, discrete control signals, telemetry, and pneumatic or mechanical power, with a criticality overlay identifying the safety-critical loop through the FCC to the elevon actuators and yaw control surfaces.

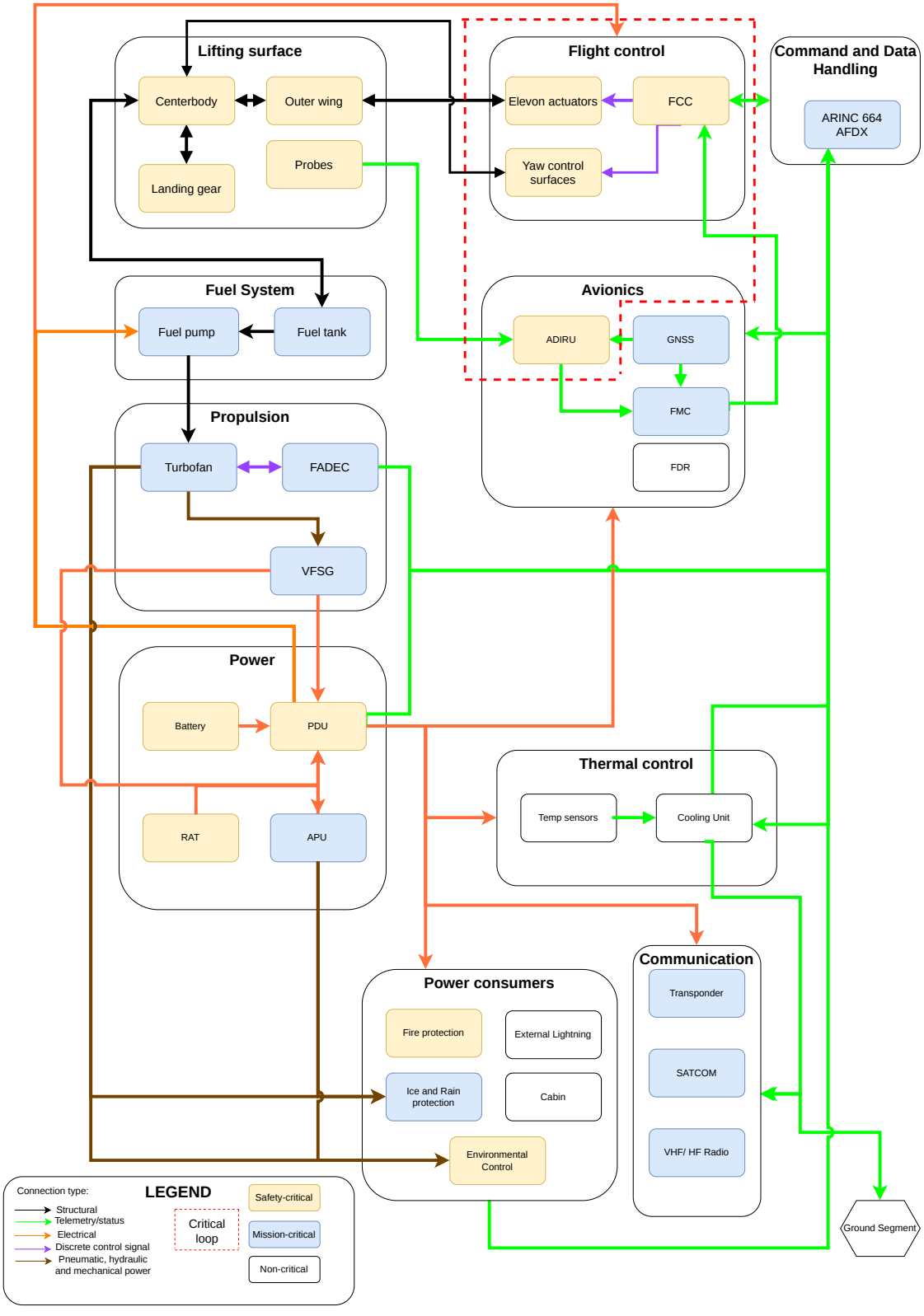

Figure 19.2: Hardware block diagram of the POGA.

19.3. Software Block Diagram

Figure 19.3 maps the software architecture across six functional domains: flight control, propulsion, power, fuel system, avionics, and thermal control, each decomposed into its constituent software modules. Data and control signal flows connect these modules through a central system manager, with the ground segment shown as an external interface.

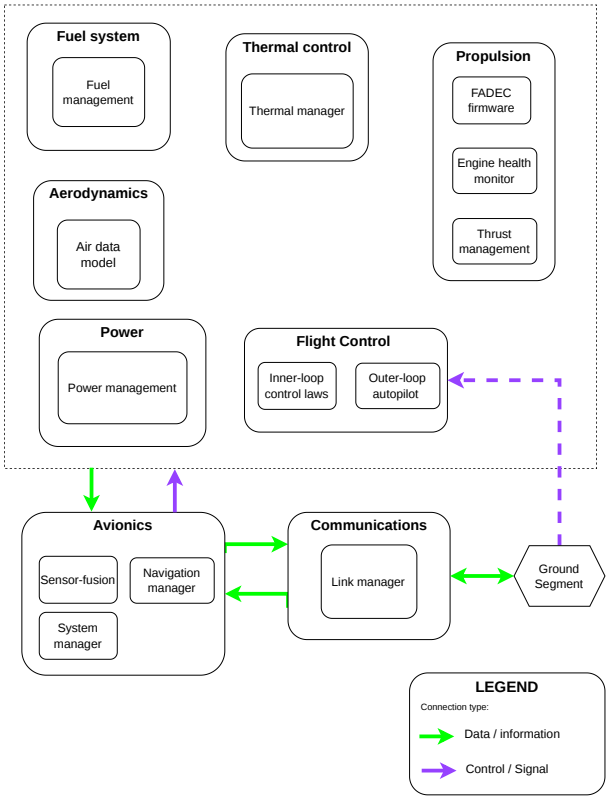

Figure 19.3: Software block diagram of the POGA.

19.4. Data Handling Block Diagram

Next to hardware and software, data handling is also considered in the shape of a block diagram. This block diagram is presented below, in Figure 19.4.

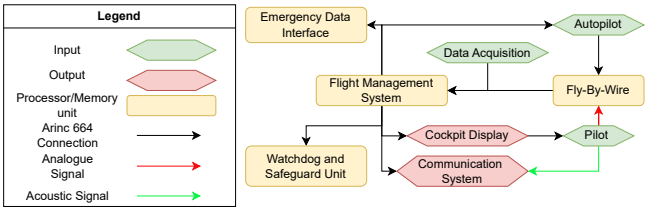

Figure 19.4: Data Handling Block Diagram

From the block diagram it can be seen that there are multiple inputs and outputs for the data system. The most important are the Data Acquisition and the pilot. The data acquisition branch consists of all the sensors of the aircraft that measure the flight conditions, such as a pitot static tube or camera's to monitor engine health. This second option is further explored in Section 20.9. The pilot will also send data to the fly-by-wire system and the communication system. This will be done through an analogue or acoustic signal respectively. These are transported nearly instantly. The other signals are made with Arinc 664 connections, which will send data with a speed of 1 Gbps. The emergency data interface contains the data storage for if there is an emergency. It is also known as the black box. The watchdog and safeguard unit make sure that the system keeps operating as intended. They will monitor the system behaviour, and will make sure they switch to an alternative system once one of the redundant systems does not function properly.

20

Operations and Logistic Concept Description

The POGA is a bio-SAF fuelled BWB configuration aircraft with above-body high-bypass turbofan propulsion. This chapter describes the operations and logistics (O&L) concept, covering all aspects required to confirm that the aircraft can be realistically operated within the existing intercontinental civil aviation network by 2035. The purpose and scope are introduced in Section 20.1, followed by the general concept of operations in Section 20.2 and the representative route strategy in Section 20.3. Airport compatibility, including approach speed, aircraft dimensions, GSE feasibility, and ground integration, is examined in Section 20.4. The Bio-SAF supply, storage, and refuelling concept are described in Section 20.5. Maintenance and inspection challenges specific to the BWB configuration are discussed in Section 20.6, and passenger and crew operation specifications are given in Section 20.7. Finally, diversion and abnormal operations are addressed in Section 20.8 and Section 20.9, respectively.

20.1. Purpose and Scope

This chapter assesses the operations and logistic concept for the POGA. It checks whether the aircraft can be operated, refuelled, turned around, maintained, and integrated into the existing intercontinental civil aviation operation network by 2035. The main operational and logistical aspects considered in this chapter are airport compatibility, GSE compatibility, turnaround feasibility, Bio-SAF logistics, passenger and crew operation, maintenance, and diversion or abnormal operations.

The aircraft should be compatible with the required airports and infrastructure. Some airport-side adaptations may be needed, but should remain limited and efficient. The nominal turnaround flow is defined and assessed for a 95-minute under full-servicing operation conditions. During the turnaround, passenger handling, baggage loading, catering preparation, cleaning, refuelling, and basic maintenance checks need to be performed in parallel.

The availability and handling of Bio-SAF are also considered, since the fuel must be supplied, stored and refuelled with high reliability. Due to the selected energy source and the wide BWB cabin layout, the aircraft must also be able to handle diversion cases and abnormal operations. Therefore, this O&L chapter describes how the aircraft is expected to operate on a daily basis, together with the main limitation, assumptions and requirements.

20.2. Concept of Operations

As mentioned before, the aircraft is intended to operate as an intercontinental passenger aircraft within a hub-based airline network. The operational concept is based on direct flights and planned intermediate technical stops. The typical one-leg mission range is 5,530 km, while the aircraft is required to provide 24 h coverage of 16,000 km. This allows current long-haul intercontinental routes to be replaced by a sequence of shorter flight legs, instead of relying on one continuous kerosene-based long-haul flight [63]. The aircraft is also able to operate transatlantic flights with two representative routes shown in Figure 20.1[1].

Table 20.1: Airport compatibility design classification

Classification system	Target classification
ICAO / EASA aerodrome reference code	Code 4E [64]
FAA Airplane Design Group (ADG)	ADG V [28]
Aircraft approach category	Category D [28]

The operation considers major international airports where Bio-SAF supply is available or can be realistically introduced. As shown in Table 20.1, the aircraft is designed to be compatible with Code 4E airports according to the ICAO / EASA aerodrome reference code [64]. It also falls within FAA Airplane Design Group V and aircraft approach Category D [28]. This keeps the aircraft comparable to existing wide-body aircraft with regard to airport compatibility. The aircraft is also able to join the existing air traffic control network with a cruise speed of 0.79 Mach at FL350.

The aircraft operation concept differs from traditional transfer flights. Instead of passengers changing aircraft at an intermediate airport, the flight is split into shorter technical legs. At the intermediate airport, only the required ground servicing and Bio-SAF refuelling are performed. The 120 passengers, under business-class cabin conditions, remain on board during the refuelling stop where allowed by the airport and operational procedures. Therefore, the main operational concept can be summarised as long-range premium passenger transport without the use of kerosene.

20.3. Representative Route Operation

The selected concept has a design range of 5,530 km, approximately 2,985 nautical miles. This range is not sufficient for most direct intercontinental flights, but it allows long-haul operation with intermediate technical stops. For these operations, the second freedom of the air is relevant, allowing a non-traffic stop to refuel[2]. This simplifies the

[1] URL `https://jettly.com/post/transatlantic-planes` [Cited 10/06/2026]

[2] URL `https://www.icao.int/introduction` [Cited 19/06/2026]

coordination between operators, authorities and governments. However, this might increase the traffic demand at some intermediate airports.

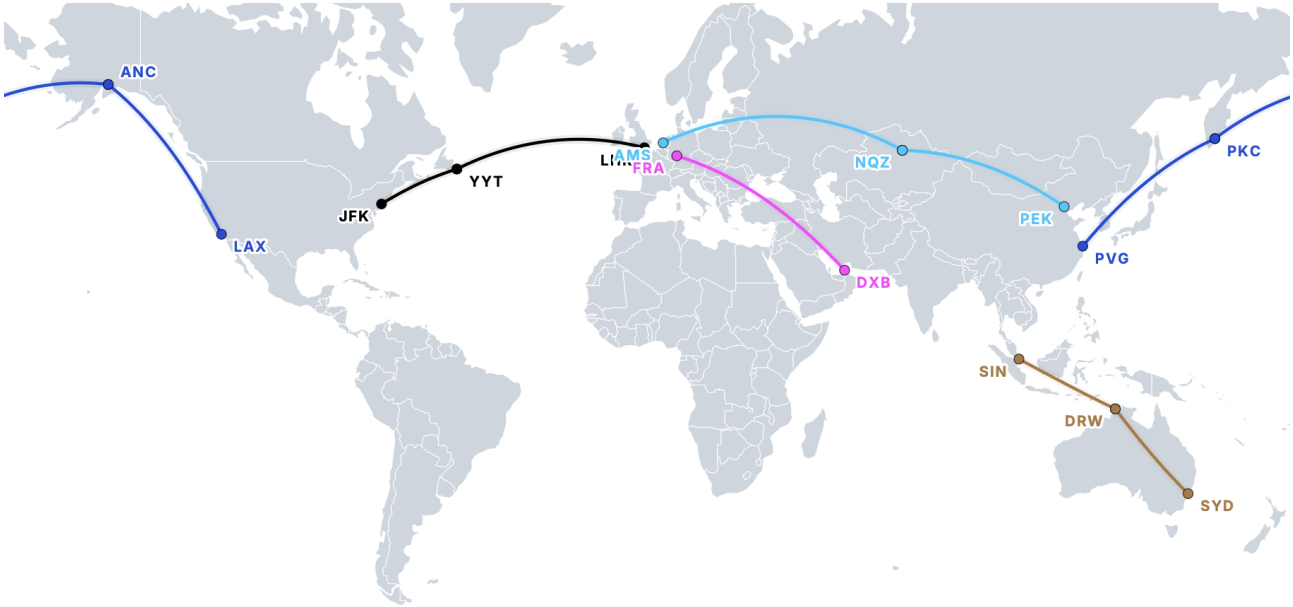

Figure 20.1: Representative Routes

Several representative routes are selected and analysed. They are intended to show how the aircraft could operate in different premium passenger markets. The selected routes are based on city pairs worldwide with strong business and first-class demand[3]. Table 20.2 lists five examples with the departure and destination airports, their intermediate stops, leg range and total range.

Table 20.2: Representative routes and leg distances

Route	From	To	Leg range [km]
PVG–PKC–ANC–LAX	Shanghai Pudong, China	Petropavlovsk-Kamchatsky, Russia	3825
	Petropavlovsk-Kamchatsky, Russia	Anchorage, USA	3141
	Anchorage, USA	Los Angeles, USA	3770
		Total	**10736**
LHR–YYT–JFK	London Heathrow, UK	St. John's, Canada	3716
	St. John's, Canada	New York JFK, USA	1841
		Total	**5557**
AMS–NQZ–PEK	Amsterdam, Netherlands	Astana, Kazakhstan	4435
	Astana, Kazakhstan	Beijing Capital, China	3654
		Total	**8089**
FRA–DXB	Frankfurt, Germany	Dubai, UAE	4843
		Total	**4843**
SIN–DRW–SYD	Singapore	Darwin, Australia	3339
	Darwin, Australia	Sydney, Australia	3155
		Total	**6494**

The routes are used to represent cases for a wider region. For example, LHR–YYT–JFK represents transatlantic operation between Western Europe and the east coast of North America. Similarly, AMS–NQZ–PEK is used to represent Europe–East Asia operation with an intermediate technical stop. The FRA–DXB route is an example of a direct mission with route length within the 5,530 km design range.

For longer intercontinental routes, the mission is divided into two or more flight legs. The intermediate airports are selected such that each leg remains within the cruise range. They are also considered operationally with available diversion airports. The relatively short take-off field length performance of 1,410 m increases the number of airports that can be considered for the intermediate stops.

The PVG–PKC–ANC–LAX route represents an ultra-long-haul flight with two intermediate stops. This shows that the aircraft is capable of serving very long-distance markets, although not using direct flights. The LHR–YYT–JFK route also shows one limitation of the transatlantic operation. Compared with other routes, there are fewer suitable diversion

[3]URL `https://www.flightroutes.com/most-popular-flights-business-first-class` [Cited 18/06/2026]

airports across the North Atlantic. As a result, airport availability and diversion planning become more important operational constraints. The other routes are less constrained in this aspect, because more diversion airports are available along the route.

20.4. Airport Compatibility and Ground Operations

Airport compatibility has a direct effect on the aircraft's commercial viability. The aircraft should be able to use major existing airports without requiring widespread infrastructure changes. Therefore, ICAO Annex 14, FAA AC 150/5300, and aircraft airport-planning references are used as the main compatibility basis [64, 65]. These references are used to check the main airport compatibility items, including aircraft size, runway and taxiway requirements, stand compatibility, rescue and firefighting category, and pavement loading.

Based on the current design parameters, the aircraft remains within Code 4E airport limits, with a maximum wingspan of 64.9 m. The maximum tail height is 9.0 m, which is determined by the tail or winglet height. A take-off field length of 1,410 m under sea-level ISA conditions is achieved[4]. The BWB configuration makes the outer main gear wheel span (OMGWS), rescue and firefighting category, evacuation, and stand compatibility important. The aircraft has an OMGWS of 6.85 m to maintain compatibility with existing taxiways and stands. During detailed design, pavement loading should be checked using the ACN/PCN concept[12]. The indicated threshold speed is 165 kts, which is below 166 kts and therefore supports approach-category compatibility.

Emergency evacuation is another BWB-specific operational constraint. The aircraft must be capable of evacuating all passengers and crew within 90 seconds during certification demonstration [66]. Existing studies show that very large BWB aircraft can have evacuation bottlenecks [67]. However, for a 120-passenger BWB, the problem is expected to be more manageable and can be assessed in more detail in the next design phase [68]. Details regarding abnormal conditions are discussed in Section 20.8.

20.4.1. Typical Ramp Layout

The ground-operation study in this section shows that the aircraft can remain compatible with existing airport ground infrastructure. The main GSE items considered are included in Table 20.3. The GSE layout includes the aircraft footprint and layout of the GSE. The full servicing turnaround sequence is discussed in Subsection 20.4.2.

Table 20.3: Ground Service Equipment (GSE)

Abbreviation	Ground Service Equipment
AC	Air Conditioning Unit
AS	Air Start Unit
BULK	Bulk Train
CAT	Catering Truck
CB	Conveyor Belt
CLEAN	Cleaning Truck
FUEL	Fuel Hydrant Dispenser or Tanker
GPU	Ground Power Unit
LDCL	Lower Deck Cargo Loader
LV	Lavatory Vehicle
PBB	Passenger Boarding Bridge
PS	Passenger Stairs
TOW	Tow Tractor
ULD	ULD Train
WV	Potable Water Vehicle

Current study shows that the BWB aircraft has high compatibility with existing infrastructure [69]. The hub condition assumes the aircraft under base operation scenario with full service available and enough support from the operator.

The layout follows the presentation style used in aircraft airport-planning manuals. The Airbus A320 Aircraft Characteristics Airport and Maintenance Planning document is used as a reference for the ramp-layout convention [70]. The Airbus layout is used as a reference for how typical GSE arrangements are presented and what GSE should be included. It should be noted that ramp layouts depend on the operator, airport, stand type, and local safety rules, the arrangement shown here should be treated as a representative servicing layout only.

The aircraft is a long-haul intercontinental passenger aircraft with lower-deck luggage storage. Therefore, both passenger-service equipment and baggage-service equipment are included.

The typical ramp layout under hub condition is shown in Figure 20.2. The purpose of this layout is to identify the ground-support vehicles required during a full-servicing turnaround and to check whether the servicing concept remains realistic. The aircraft footprint together with the GSE positions and service interfaces is included to support a detailed stand-clearance check.

The GSE list is given in Table 20.3. The GSE items are shown in Figure 20.2. The open-apron and terminal-gate cases are expected to use a similar equipment set, but the exact vehicle positions could vary. One advantage of the above-body engine installation is that the engine intake safety zone may be reduced compared with conventional below-wing engines. The detailed sequence for the servicing activities is shown in Figure 20.3.

20.4.2. Turnaround procedure

Turnaround time is an important operational driver because it affects daily aircraft utilisation and airport slot use. Current heavy aircraft can require around two hours for full servicing, depending on airport and operator procedures [16]. For the POGA, a normal hub turnaround target of 95 minutes is adopted, based on the servicing sequence shown in Figure 20.3[5].

[4] URL https://www.stantec.com/en/ideas/topic/mobility/how-long-is-an-airport-s-runway [Cited 28/04/2026]

[12] URL https://skybrary.aero/articles/pavement-classification-number-pcn [Cited 28/04/2026]

[5] URL https://ansperformance.eu/economics/cba/standard-inputs/latest/chapters/turnaround_time.html [Cited 24/06/2026]

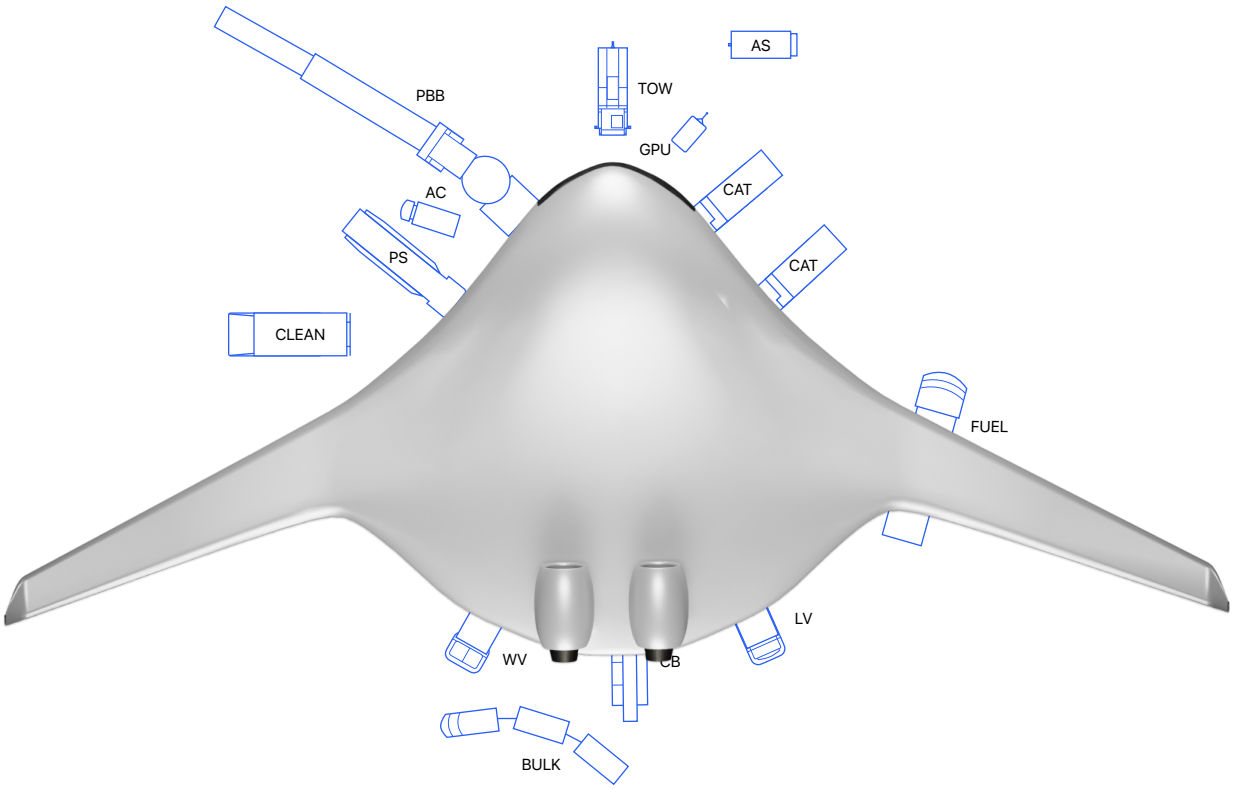

Figure 20.2: Typical Ramp Layout [70]

The normal hub condition assumes parallel servicing. The aircraft cargo-door and service-panel locations are arranged to reduce blockage between these tasks. If blockage occurs, or if the tasks have to be performed more sequentially, the turnaround time can increase significantly[6].

For the aircraft, Bio-SAF and high-bypass turbofan propulsion allow the refuelling process to remain broadly similar to conventional liquid-fuel aircraft [71]. However, the BWB layout, above-body engine installation, and load-bearing fuel tanks may affect stand access, inspection procedure, ground-support positioning, and servicing sequence [72].

The representative turnaround chart includes aircraft arrival and stand positioning, passenger disembarkation, baggage unloading, post-flight inspection, cleaning and catering, Bio-SAF refuelling, baggage loading, passenger boarding, final headcount, and dispatch release [16]. The chart also separates GSE setup/removal time, activity time, and critical-path activities. And the total turnaround time is mainly driven by the activities that cannot be shortened.

For the O&L, the positioning and removal of the GSE items are assumed to require a minimum of 5 minutes. This accounts for the unfamiliar BWB geometry and the need for more careful positioning around service doors. Catering-truck connection and removal are assumed to take 10 min. A similar assumption is applied for cargo-handling equipment, because the cargo-door geometry is different from conventional. For the load-bearing fuel tanks, the fuel-truck connection and removal are also assumed to take 10 min.

Under the hub turnaround case, refuelling is performed after passengers disembarkation and is completed before passenger boarding. For intermediate technical stops, passengers may remain on board if allowed by airport procedures and safety regulations, but this requires a separate operational assessment. In the hub case shown here, Door 2L is removed after boarding is completed, while the front passenger boarding bridge remains connected until the cabin is fully ready for door closure. The final passenger count is also completed before dispatch and front door closure.

[6] URL `https://aertecsolutions.com/en/blog/what-is-ground-handling-3/` [Cited 29/06/2026]

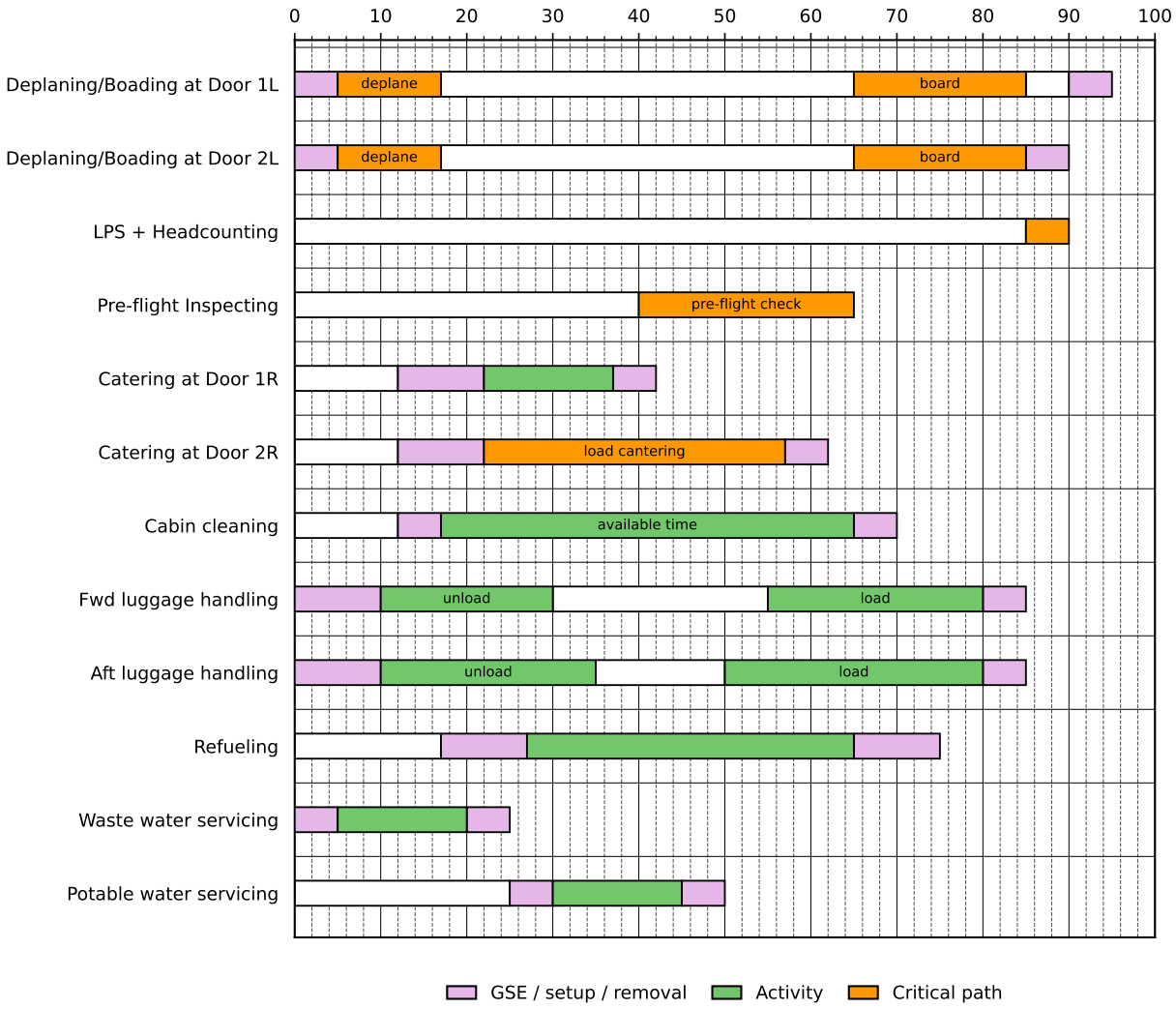

Figure 20.3: Representative full servicing turnaround time chart, adapted from [65]

The critical path has a strong effect on the final turnaround time. In Figure 20.3, the main critical-path activities are passenger handling, catering, boarding, final headcount, and dispatch preparation. The per-flight inspection differs from a TAW aircraft and is discussed further in Section 20.6.

20.5. Bio-SAF Logistics and Refuelling

SAF is defined as an alternative fuel made from non-petroleum feedstocks, aimed at reducing the environmental impact of air transportation[7]. Bio-SAF is selected as the energy carrier for this aircraft. From an operational point of view, this is favourable because it remains a liquid fuel which is closer to current Jet A operations than hydrogen or battery propulsion.

SAF is already used in commercial aviation, but the current global production volume is still low. IATA expects global SAF production to reach approximately 2.4 million tons in 2026. This represents about 0.8% of total annual jet fuel consumption[8]. Longer-term predictions also indicate that SAF production capacity could increase significantly towards 2030 [73]. This strongly supports the POGA daily operation, but does not remove the supply risk for regular airline operation.

As shown in Figure 20.4, the ReFuelEU Aviation Regulation requires the minimum SAF share supplied at Union airports to increase from 2% in 2025 to 35% in 2035 when the aircraft enters service. This shows that SAF supply is not only a technical assumption, but also supported by regulation.

SAF can be blended upstream and delivered through existing fuel terminals, pipelines and hydrant systems. Therefore, the airport refuelling operations can remain broadly similar to current kerosene-based operations[9]. This also means no major changes in stand layout, refuelling equipment procedures due to the fuel type.

[7] URL `https://afdc.energy.gov/fuels/sustainable-aviation-fuel` [Cited 12/06/2026]

[8] URL `https://www.iata.org/en/pressroom/2026-releases/06-06-saf-production-volumes-still-disappointing/` [Cited 15/06/2026]

[9] URL `https://afdc.energy.gov/fuels/sustainable-aviation-fuel` [Cited 20/05/2026]

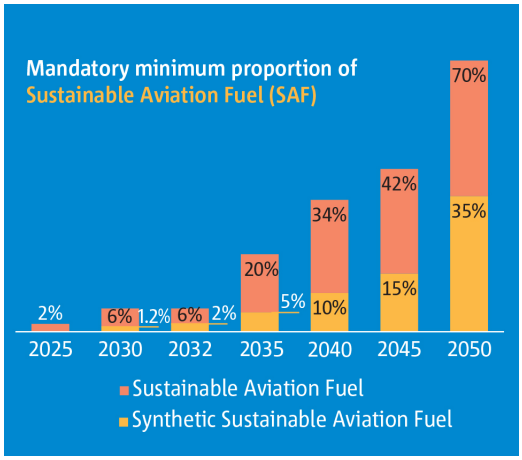

Figure 20.4: Mandatory minimum proportion of SAF under ReFuelEU Aviation[10]

The main operational challenge is therefore not basic airport compatibility, but supply scalability. Large-scale bio-SAF operation depends on sustainable feedstock availability, feedstock collection and transport, production capacity, fuel certification, and the blending limit of different production pathways. Current SAF blend limits depend on the American Society for Testing and Materials, ASTM-approved production pathway and the production method [74].

As mentioned in Section 20.3, the airline would need to select routes where bio-SAF supply is available or can be contracted in advance. This is especially important for planned intermediate technical stops, because the aircraft depends on reliable fuel availability at both hub airports and stopover airports. The intermediate airports may not be international hubs, so the scalability also needs to be considered carefully.

20.6. Maintenance and Inspection

The above-body engines require operational adjustments compared with the conventional TAW below-wing configuration. Since the engines are less accessible from ground level, direct visual inspection may require additional access equipment. As a result, an on-board camera inspection system is proposed. A 360-degree camera system capable of providing live images of the engine is used to support flight crew awareness[11].

The camera system has to be certified and included in the aircraft maintenance and inspection procedure in order to be used to support dispatch and physical visual inspection. The live image should be available to engineers during ground operation and to flight crew during flight operation. During ground operation, the system should be able to operate using auxiliary power unit (APU) or external ground power. This allows the engines to be checked before engine start and during turnaround without main engines operating.

A physical visual inspection should still be carried out before the first flight of each operating day. This should include the top of the engine. This daily inspection is important because the camera system should support the inspection process but not fully replace the walk-around and engine-area check unless specially approved. If the camera system detects damage, leakage, foreign object damage (FOD), any fault message, a direct inspection should be performed using access stairs, mobile platforms or maintenance stands. Special GSE are required in this case.

Regarding the camera system, the Minimum Equipment List (MEL) treatment also has to be defined carefully [75]. Dispatch with the system inoperative may be possible if the required physical inspection can still be completed. For this concept, the camera system is treated as an inspection-support system with a clear manual inspection backup.

The aircraft has load-bearing fuel tanks which require special inspection and additional maintenance considerations. The tanks are part of the load-carrying structure and therefore experience both fuel and structural loads. The detailed design should include sensors for leak detection, pressure and strain monitoring, and possible structural-health monitoring. This is because damage or degradation in the tank structure can affect both fuel containment and structural integrity.

Routine inspection of the tank system should be included in line maintenance and A-check procedures through external visual checks, leak checks, sensor checks. Full internal tank inspection may be performed during A-check and requires special safety procedures. Furthermore, a thorough internal inspection should be carried out during deeper maintenance checks. This should also perform whenever triggered by leakage, abnormal sensor data, heavy landing or maintenance findings.

20.7. Passenger and Crew Operation

The aircraft is designed to carry 120 passengers on board in a business-class cabin configuration. Each passenger seat has a width of 66 cm and a pitch of 185 cm. The seats are assumed to recline to 180 degrees. Six lavatories are uniformly distributed along the cabin as illustrated in Figure 13.1, and the galley area is sized to support the required business-class level of service.

A higher-density economy configuration is also possible as a cabin layout option. The aircraft could carry up to 250 passengers while the required performance is still satisfied. The existing functional areas, including galleys, lavatories, aisles, and service areas, should be checked for this higher passenger number during the detailed design phase. The 120-passenger business-class cabin is used as the baseline configuration, while the 250-passenger economy layout is treated as a possible alternative configuration.

Crew operation is considered for both flight crew and cabin crew. The number of crew is important for cabin layout,

[10] URL `https://www.easa.europa.eu/en/domains/environment/eaer/sustainable-aviation-fuels/saf-policy-actions#refueleu-aviation` [Cited 15/06/2026]

[11] URL `https://blog.parker.com/us/en/aag_grp/Fixed-Cameras-to-360-Vision-Aircraft-Situational-Awareness-is-Evolving.html` [Cited 16/06/2026]

crew seats, crew rest, emergency operation, and service quality. Details are summarised in Table 20.4.

Table 20.4: Number of flight and cabin crew

Operation case	Flight crew	Cabin crew
Legal minimum, 120 passengers	2 pilots[a]	3 cabin crew[b]
Legal minimum, 250 passengers	2 pilots[a]	5 cabin crew[b]
Long-duty operation[c]	3–4 pilots	12 cabin crew

[a] The minimum flight crew is assumed to be two pilots for this long-haul commercial transport aircraft [76].
[b] Based on one cabin crew member for every 50, or fraction of 50, passenger seats installed on the same deck of the aircraft to be operated [77].
[c] Number of flight crew with in-flight rest or crew change at the intermediate stop, cabin crew with crew rest and business class service

For flight crew planning, EASA limits the operation mainly by the flight duty period (FDP). The FDP starts when the crew reports for duty and ends after the aircraft is parked. Therefore, the planned flight time must leave enough margin for reporting, pre-flight preparation, turnaround, and post-flight duties.

For normal sector operation, two pilots are assumed. For longer duties, the operation can either use a crew change at the intermediate technical stop or use augmented flight crew with approved in-flight rest. The crew rest area has enough space for Class 1 rest facilities. According to CS FTL.1.205, with one additional flight crew member, the maximum FDP can be extended up to 16 h. In the specific long-sector case with two additional flight crew members, this may be increased to 18 h if the FDP includes one sector longer than 9 h and a maximum of two sectors [76].

For cabin crew planning, the legal minimum follows ORO.CC.100. For an aircraft carrying more than 19 passenger seats, one cabin crew member is required for every 50 passengers, or fraction of 50 passengers, installed on the same deck [77]. For the 120-passenger baseline cabin, the legal minimum is therefore 3 cabin crew. For the 250-passenger economy configuration, the legal minimum becomes 5 cabin crew.

However, the legal minimum is not sufficient for the intended business-class operation. The aircraft is designed as a premium intercontinental passenger aircraft, with a design service assumption of one cabin crew member per 10 passengers is used. This gives 12 cabin crew for the 120-passenger business-class configuration. The exact number may vary by airline and route. The current number is used as planning value for cabin layout and crew accommodation study.

20.8. Diversion and Abnormal Operations

Diversion and abnormal operating cases are included to check whether the aircraft remains operationally realistic outside the nominal mission. The aircraft should not only be able to complete the planned route, but should also be able to handle cases such as weather diversion, technical delay, rejected take-off, emergency return, fuel-supply disruption, and abnormal landing cases. ICAO Annex 6 is relevant for this part because the aircraft must be practical for airline operation, including dispatch control, reserve fuel policy, maintenance reliability and diversion capability [60].

Table 20.5: Diversion and abnormal operation considerations

Case	Operational concern
Diversion or emergency return[12]	The aircraft may require inspection, emergency service, passenger handling, or maintenance support at an unplanned airport.
Rejected take-off[13]	Brake, tyre, engine, and fuel-system checks may be required before the aircraft can be dispatched again. Firefighting and rescue service may be required.
Hard landing or high structural load[14]	The BWB structure and load-bearing tanks may require additional inspection after hard landing, over-speed, special load cases.
Emergency evacuation	The BWB cabin layout must evacuate all passengers and crew within 90 seconds time. The wide cabin requires further verification as discussed in Subsection 20.8.1.
Rescue and firefighting category	The BWB geometry may create an interpretation issue for fuselage width. The final operation should be agreed with the certification authority and operator.

Aforementioned, the use of Bio-SAF allows the aircraft to follow a largely conventional liquid-fuel operation logic. This is beneficial for diversion planning, because the aircraft can in principle use existing airport refuelling systems if certified Bio-SAF or suitable blended fuel is available. However, Bio-SAF availability still vary between airports, especially during early operation. Therefore, longer missions that require planned intermediate stops would need more conservative fuel planning, or pre-arranged fuel supply.

For routes with limited alternate-airport coverage, such as transatlantic routes in Figure 20.1, diversion planning becomes more important. The aircraft must be able to reach a suitable alternate airport and then operate from that airport after landing. Diversion airports should provide sufficient runway length and airport compatibility, passenger handling capability. The load-bearing fuel tanks also require safe inspection access after hard landing, rejected take-off, abnormal structural loading, or fuel leak indication[15].

[15] URL `https://www.ivw.uni-kl.de/en/projects/hyfive` [Cited 21/06/2026]

20.8.1. Emergency Evacuation

Emergency evacuation is an important operational scenario for the BWB cabin. The aircraft must be able to evacuate all passengers and crew within 90 seconds during the certification demonstration [66]. This requirement is especially important for a non-conventional cabin, because the passenger distribution, aisle layout, exit location, and exit capacity are different from a TAW aircraft.

The BWB layout may also give an evacuation benefit. In a conventional single-aisle aircraft, some passengers can be many rows away from the nearest exit. The Ascent1000 study shows the same idea for a small single-deck BWB: passengers are closer to the exits and fewer rows need to be crossed before reaching an exit [68]. The same logic is used for the selected POGA cabin. The cabin layout in Figure 13.1 has seven aisles and several exit routes distributed around the cabin. This reduces the number of rows between the most remote passenger and the nearest exit. It also reduces the risk that one blocked aisle or one slow passenger stops the full cabin flow. Compared with a long single-aisle layout, the BWB cabin can therefore have better passenger distribution during both boarding and emergency egress. The Type A doors also provide an evacuation benefit.

However, this advantage should be further studied. The final evacuation performance depends on actual exit size, exit location, slide arrangement, passenger routing, cabin crew position, emergency lighting, and the behaviour of passengers during evacuation. For this reason, the current O&L study treats the BWB evacuation concept as promising, but still requiring dedicated evacuation simulation and certification demonstration in the detailed design phase.

20.8.2. Rescue and Firefighting Compatibility

Rescue and firefighting (RFF) compatibility is another important issue for the BWB. ICAO aerodrome rescue and firefighting category is normally based on aircraft overall length and maximum fuselage width. For a conventional aircraft, the fuselage width is clear. For a BWB, this is less direct because the cabin is spread over a wide lifting body with a tapered oval section instead of a circular fuselage.

Therefore, the current design should not simply use the full cabin or wing-body span as the fuselage width without further interpretation. A possible approach is to define an equivalent fuselage or occupied-body width for the pressurised passenger cabin. This should be agreed with the certification authority and the airport operator. If the full BWB body width is used directly, the aircraft may require a higher rescue and firefighting category than expected for a Code 4E aircraft. If an equivalent passenger-cabin width is accepted, the airport compatibility result may be less restrictive.

At this stage, rescue and firefighting compatibility is treated as a certification-interface risk only. Therefore, the RFF category requires further authority discussion once the final cabin width, exit arrangement, passenger capacity, fuel quantity, and rescue-access concept are frozen.

20.9. Implication for Operations and Logistic

The operations and logistics concept description shows that the aircraft is able to join the existing international civil aviation network. Minor new GSE for maintenance may be required for the current design, while the aircraft keeps a high compatibility with existing airport infrastructures. Regarding the fuel type, Bio-SAF availability and production support the aircraft's entry into service in 2035. Bio-SAF can share similar infrastructure with current jet fuel. However, the scalability of Bio-SAF remains risky.

Several design implications follow from the BWB configuration. Some inspections are less accessible with the above-body engine. The design includes camera systems and additional sensors for maintenance and inspection. This also affects the aircraft system layout and electrical power budget during the detailed design phase.

The cabin is designed for 120 passengers with business class level of service. The cabin shape, door locations, crew rest areas, luggage storage areas are all considered together. They directly affect boarding, evacuation, and ground handling. Overall, no major operational issues are found. The key points that need to be carried forward are Bio-SAF scalability and the certification of the new configuration. Further recommendations can be found in Chapter 26.

Part IV: Further Analysis

21
Business Analysis

In this chapter, the business case of the chosen design will be analysed to investigate the feasibility of the proposed aircraft from the market and financial perspectives, as well as identify the key aspects that may affect these. The target market will be discussed in Section 21.1. Next, the product's position and its share in the future market will be estimated in Section 21.2 in order to obtain an expected number of aircraft deliveries. Since the preliminary design with all its characteristics has been done, an accurate cost estimation can be conducted in Section 21.3. Finally the return on investment and sales are provided in Section 21.4.

21.1. Target Market

The market analysis establishes the commercial, regulatory, and competitive context in which the POGA must succeed. The Baseline Report conducted this analysis at the mission level, before a concept was selected [19]. With the BWB and 100 % bio-SAF concept now fixed, the analysis can be sharpened to reflect the specific position this design occupies in the 2035 market environment.

Commercial aviation is being progressively priced out of petroleum. The ReFuelEU Aviation regulation, in force since January 2025, mandates a rising sustainable aviation fuel share at all EU airport, rising from 6 % in 2030 to 70 % by 2050, with a sub-mandate for synthetic e-fuels reaching 35 % by 2050[1]. The EU Emissions Trading System (ETS) moves to full auctioning for aviation from 2026, and Carbon Offsetting and Reduction Scheme for International Aviation (CORSIA) Phase 2 obligations apply from 2027[2]. Together, these frameworks impose a growing, compounding carbon cost on every petroleum-based flight operating from or connecting to EU airports, a cost that tightens throughout the 30-year service life of any conventional aircraft entering service in 2035. Only an aircraft operating on 100% non-petroleum fuel eliminates this carbon liability entirely.

The POGA is positioned to exploit exactly this regulatory gap. By operating on 100 % bio-SAF, it carries no petroleum-fuel carbon liability under EU ETS, requires no CORSIA offsetting, and satisfies the full ReFuelEU mandate in its most future form. Both Airbus and Boeing have committed to certifying their entire commercial fleets for 100 % SAF operation by 2030, so a conventional tube-and-wing aircraft entering service in 2035 on 100 % bio-SAF would also eliminate its petroleum-fuel carbon liability under the same frameworks[3]. This design's commercial differentiator is therefore the combination of that regulatory compliance together with the aerodynamic efficiency of the BWB configuration: a cruise lift to drag ratio of 19.4 outperforms the 16-19 range typical of conventional tube-and-wing widebodies.

Finally, the 120-seat all business class configuration is a design choice that reinforces the business case, proven by recent demand data that shows that a premium cabin is undergoing a shift. In Q4 2025, Delta Airlines reported that premium cabin revenue exceeded economy revenue for the first time in the carrier's history, with business class revenue growing 9 % year-on-year while main cabin revenue fell 7 %[4]. Additionally, long-haul business class tickets typically are 2 to 5 times more expensive than an economy fare[5]. This means that an all business class cabin will generate far more revenue per flight than an equivalent economy configuration, which also directly will offset the bio-SAF cost premium. Lastly, the sustainability case for this premium cabin choice is surprisingly strong. Under the ICAO Carbon Emissions Calculator methodology and UK DEFRA 2023 greenhouse gas reporting conversion factors, a business class seat is worth 2.9-3 times the CO_2 of an economy seat on the same flight, due to a greater area per seat. A further structural demand driver comes from corporate sustainability regulation. Under the Corporate Sustainability Reporting Directive (CSRD), Scope 3 greenhouse gas emissions, which include business travel under Category 6, are mandatory to report for all in-scope companies[6]. Under the UK DEFRA 2023 greenhouse gas reporting conversion factors , a business class seat generates approximately 2.9 to 3.0 times the CO2-equivalent emissions of an economy seat on the same flight, due to the greater floor area per seat[7]. This makes premium corporate travel a disproportionate and legally reportable Scope 3 liability. An aircraft operating on 100% bio-SAF eliminates the petroleum-fuel component of that liability entirely, making the POGA the only aircraft able to offer certified zero-petroleum-fuel intercontinental business class travel to corporate clients on a global business travel market.

21.2. Business Case

The business case evaluates the commercial opportunity presented by the POGA and its ability to generate a positive return on the €50 billion development investment over its production and service life.

[1] URL https://transport.ec.europa.eu/transport-modes/air/environment/refueleu-aviation_en [Cited 17/06/2026]
[2] URL https://www.icao.int/CORSIA[Cited 17/06/2026]
[3] URL https://www.airbus.com/en/innovation/energy-transition/our-commitment-to-saf [Cited 17/06/2026]
[4] URL https://onemileatatime.com/news/delta-premium-cabin-revenue-exceeds-economy-revenue/ [Cited 17/06/2026]
[5] URL https://travel-dealz.com/blog/business-class-upcharge/[Cited 17/06/2026]
[6] URL https://www.businesstravelnewseurope.com/Sustainable-travel/2024/CSRD-Ready-for-reporting[Cited 17/06/2026]
[7] URL https://www.gov.uk/government/publications/greenhouse-gas-reporting-conversion-factors-2023 [Cited 17/06/2026]

21.2.1. Market Size

Three market tiers are defined. The total addressable market (TAM) establishes the aggregate premium seat demand globally. The serviceable addressable market (SAM) narrows this to routes within the aircraft's mission capability where all-business-class demand is commercially viable. The serviceable obtainable market (SOM) is the realistically capturable share given EIS timing, ramp constraints, and competitive dynamics.

TAM

As of 2026, no commercially equivalent non-petroleum intercontinental all-business-class blended wing airliner exists or has a firm entry-into-service commitment. In 2025, The International Air Transport Association (IATA) has released the latest edition of the World Air Transport Statistics (WATS) with comprehensive statistical data for 2024[8]. From that report, a key finding was that the international premium class travel grew by 11.8 %, outpacing growth in global economy travel of 11.5%. Furthermore, the total number of international premium-class travellers in 2024 was 116.9 million (6% of total international passengers). Before the COVID crisis, which disrupted the premium class market, it accounted for approximately 7% of revenue passenger kilometres (RPK), but consistently generated around 20% of total airlines revenue in the period of 2011-2019[9]. It is since the first quarter of 2024 that this market seems to be getting back on track since COVID. As shown in figures 21.1 and 21.2, this ratio has returned to pre-pandemic levels since Q1 2024. Europe is the largest absolute market at 39.3 million international premium passengers, the Middle East records the highest premium share at 14.7% of all passengers, and Asia-Pacific is the fastest-growing region at 22.8% year-on year growth.

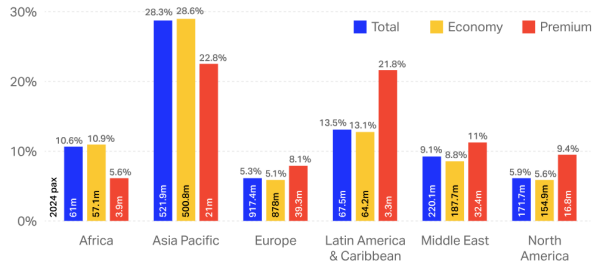

Figure 21.1: Regional passenger traffic growth and 2024 passengers numbers by cabin class.

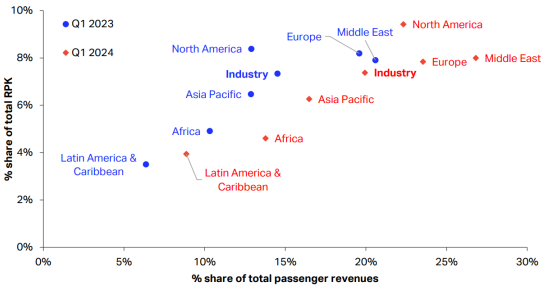

Figure 21.2: Premium total traffic performed by full-service carriers, by airline region of registration.

Applying a conservative long-run compound annual growth rate (CAGR) of 4.0%, consistent with the Boeing CMO 2025 projection of 4.2% total RPK growth through 2044, and deliberately below the post-COVID 2024 outturn of 11.8% to reflect normal conditions[10]. At this rate, international premium passengers are projected to reach approximately 180 million by 2035 and 394 million by 2055, as summarised in Table 21.1.

Table 21.1: International premium class passenger projections at 4.0% CAGR.

Year	Premium passengers (M)	Growth vs. 2024
2024 (actual)	116.9	—
2030	147.8	+26%
2035 (EIS)	179.9	+54%
2045	266.4	+128%
2055	394.7	+238%

SAM

The SAM cannot be derived directly from the TAM by applying a passenger share, because premium class traffic data at individual route level is not publicly available. Instead, the SAM is defined through a three-step route screening of the global scheduled network.

The first filter is range compatibility. The aircraft serves routes up to 5530 km direct at full payload, or up to 16000 km within a 24-hour window via one planned intermediate technical stop, as described in Section 17.3. Using the premium corridor data from the TAM, the main qualifying corridors are Europe to Middle East (3,500 to 5,500 km, covering pairs such as London-Dubai or Amsterdam-Doha), Europe to North America (5,000 to 6,000 km, and intra-Asia Pacific routes between major business hubs such as Singapore and Tokyo or Hong Kong.

The second filter is premium hub-to-hub character. Not all routes within the range band have sufficient business class passengers to support a dedicated all-business class product. Routes connecting recognised business hubs with documented high-yield demand are retained, point-to-point leisure routes are excluded even if they fall within range.

The third filter is operator viability. A route qualifies only if at least two full-service carriers operate it, confirming that the market is deep enough for a dedicated premium aircraft rather than reliant on a single carrier commitment.

[8] URL https://www.iata.org/en/pressroom/2025-releases/2025-08-04-01/ [Cited 12/06/2026]

[9] URL https://www.iata.org/en/iata-repository/publications/economic-reports/premium-traffic-and-revenue-are-back-on-track/ [Cited 12/06/2026]

[10] URL https://www.boeing.com/content/dam/boeing/boeingdotcom/market/assets/downloads/2025-commercial-market-outlook.pdf?update=1225 [Cited 12/06/2026]

Applying these three filters to the global network gives an estimated 20 to 30 qualifying route pairs. This is an order-of-magnitude estimate: precise route-level premium class load data is not publicly available, so the exact count depends on where the threshold is drawn on the second and third filters. The range is intentionally broad to capture this uncertainty.

The total SAM fleet size is estimated by multiplying the number of qualifying routes by two scenario-dependent assumptions: the number of aircraft an operator dedicates to each route, and the number of operators per route that adopt the all-business class product. The aircraft per carrier assumption is grounded in the operating model of existing all-business class operators: La Compagnie currently operates 2 aircraft across 3 routes, equivalent to approximately 1 to 2 aircraft per active route depending on service frequency[11]. A single aircraft supports 3 to 4 weekly rotations, two aircraft enable daily service with a maintenance spare available for scheduled checks. The pessimistic scenario therefore assumes 1 aircraft per carrier per route, while the optimistic scenario assumes 2, consistent with a full daily operation. The number of carriers per route and the total route count remain scenario assumptions, as detailed in Table 21.2.

Table 21.2: SAM fleet size estimation by scenario.

Scenario	Routes	Aircraft per carrier	Carriers per route	Fleet size
Pessimistic	20	1.0	1	20
Base	25	1.5	2	75
Optimistic	30	2.0	3	180

SOM

The SOM is the share of the SAM fleet that the aircraft can realistically capture over its production life from 2035 to 2055. As of the entry into service date, no certified competing product exists in this market position: no established manufacturer has announced a non-petroleum intercontinental all-business class aircraft. This first-to-market position, combined with the regulatory tailwind from the ReFuelEU mandate and EU ETS described in Section 21.1, supports a high initial capture rate. A market share of 100% of the all-business class fleet on qualifying routes is considered realistic for the initial production period.

21.3. Cost Analysis and Budget

The cost analysis covers the full life-cycle cost of the POGA: from research and development, through acquisition, operation, and disposal. The methodology follows the combined Raymer and Roskam cost breakdown, adapted for the novel characteristics of the design, specifically the BWB configuration, the above-body high-bypass turbofan propulsion, the load-bearing fuel tank structure, and 100% bio-SAF (FT gasification pathway) operation [23, 25]. All cost figures are computed using converged inputs (W_e = 77190 kg, MTOW = 130857 kg).

21.3.1. Cost Breakdown Structure

The life-cycle cost is decomposed into four categories: RDT&E, acquisition, operating, and disposal following Raymer and Roskam as illustrated in Figure 21.3 [23, 25].

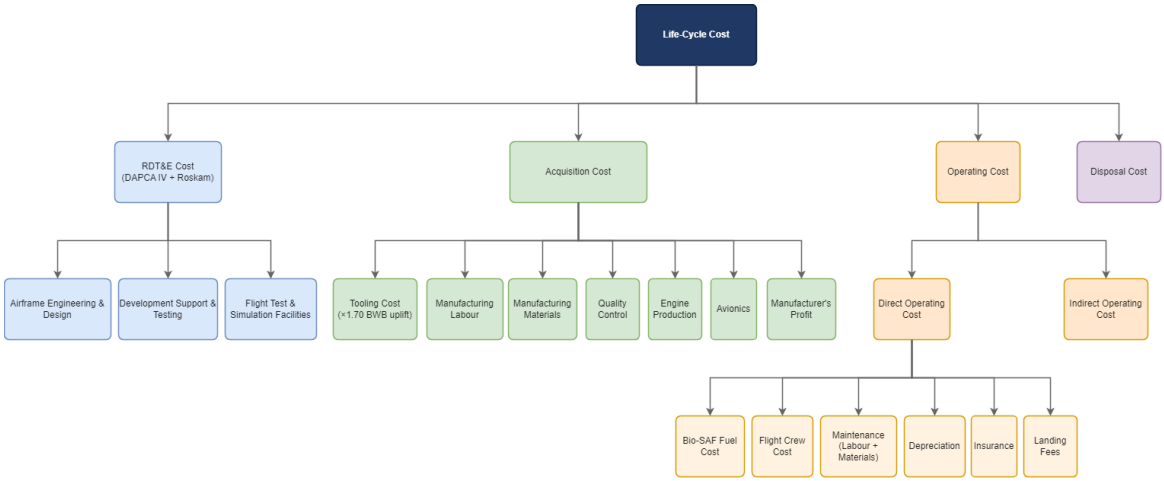

Figure 21.3: Cost breakdown structure diagram.

Two design-specific cost drivers differentiate this structure from a conventional widebody. First, the BWB geometry requires special tooling for the non-cylindrical centrebody panels and load-bearing fuel tank skins. A tooling uplift factor $f_{\text{BWB}} = 1.70$ is applied to the DAPCA IV tooling term, consistent with the complexity for large composite BWB structures [24]. Second, the fuel cost is driven by FT bio-SAF rather than Jet-A kerosene, making it the dominant operating cost sensitivity driver.

21.3.2. Development and Production Cost

The development and production cost is estimated using the DAPCA IV model with three corrections applied consistently across all delivery scenarios: a technology novelty factor $f_{\text{tech}} = 1.5$, a BWB tooling uplift $f_{\text{BWB}} = 1.70$, and a CPI

[11] URL `https://www.planespotters.net/airline/La-Compagnie` [Cited 17/06/2026]

inflation correction $f_{\text{CPI}} = 2.57$ converting 1999 US dollars to 2025 euros[12].

The DAPCA IV model estimates the man-hours required for engineering (H_E), tooling (H_T), manufacturing (H_M), and quality control (H_Q), as functions of the operating empty weight W_e (in lb), the maximum level speed V (in knots), and the number of aircraft produced in a five-year period N. These are defined in Equations (21.1)-(21.4):

$$H_E = 4.86\, W_e^{0.777}\, V^{0.894}\, N^{0.163} \tag{21.1}$$

$$H_T = 5.99\, W_e^{0.777}\, V^{0.696}\, N^{0.263} \tag{21.2}$$

$$H_M = 7.37\, W_e^{0.820}\, V^{0.484}\, N^{0.641} \tag{21.3}$$

$$H_Q = 0.076\, H_M \tag{21.4}$$

where the quality control factor of 0.076 applies for aircraft with high-fraction advanced composite structures, following Raymer [25]. The associated cost terms for development support (C_D), flight testing (C_F), and manufacturing materials (C_M) are:

$$C_D = 45.42\, W_e^{0.630}\, V^{1.3} \tag{21.5}$$

$$C_F = 1408.7\, W_e^{0.325}\, V^{0.822}\, F_T^{0.606} \tag{21.6}$$

$$C_M = 22.1\, W_e^{0.921}\, V^{0.621}\, N^{0.799} \tag{21.7}$$

where F_T is the number of flight-test aircraft. The total invested cost C_{inv} is then:

$$C_{\text{inv}} = f_{\text{tech}} \cdot f_{\text{CPI}} \cdot \Big(H_E R_E + f_{\text{BWB}} H_T R_T + H_M R_M + H_Q R_Q + C_D + C_F + C_M + C_{\text{eng}} N_{\text{eng}} + C_{\text{avionics}} \Big) \tag{21.8}$$

where R_E, R_T, R_M, R_Q are the hourly labour rates for engineering, tooling, manufacturing, and quality control respectively (in 1999 USD, converted via f_{CPI}), C_{eng} is the unit engine cost (GEnx-2B67B, €34 M at 2035 list price), N_{eng} is the total number of engines procured across the production run, and C_{avionics} is taken as €4.5 M per aircraft based on market estimates for an advanced glass cockpit and cabin management system of this class.

Table 21.3 presents the development and production cost breakdown for the reference base scenario ($N = 75$ total deliveries over the 20-year programme). All values are computed using the converged inputs: $W_e = 77190$ kg (OEW), $V = 522$ kts (sea-level equivalent of Mach 0.79), $N_{\text{pp}} = 3$ flight-test aircraft. The RDT&E subtotal must remain within the €50 B development budget[19]. The table also includes a comparison to the original estimated cost analysis from the baseline report [19]. In addition to this margins have been added to the base scenario, to get the most probable costs and account for cost growth later on in the programme.

Table 21.3: DAPCA IV cost breakdown by delivery scenario. All values in 2035 euros.

Cost component	Pessimistic (20)	Base (75)	Optimistic (180)	Baseline Budget	Margin	New Budget
Engineering labour	€8189 M	€10158 M	€11716 M	€30000 M	35%	€13713 M
Tooling ($\times f_{\text{BWB}}$)	€6862 M	€9715 M	€12230 M	€1350 M	35%	€13115 M
Development support	€1180 M	€1180 M	€1180 M	€13000 M	35%	€1593 M
Flight test	€176 M	€176 M	€176 M	€7000 M	35%	€238 M
RDT&E subtotal	€16407 M	€21228 M	€25301 M	€51350 M	–	€28659 M
Manufacturing labour	€5695 M	€13287 M	€23288 M	€4133 M	25%	€16609 M
Quality control	€433 M	€1010 M	€1770 M	€743 M	25%	€1263 M
Manufacturing materials	€2987 M	€8589 M	€17286 M	€1680 M	25%	€10736 M
Engines (all aircraft)	€1360 M	€5100 M	€12240 M	–	5%	€5355 M
Avionics (all aircraft)	€90 M	€338 M	€810 M	€1688 M	5%	€355 M
Production subtotal	€10565 M	€28322 M	€55394 M	€8244 M	–	€34318M
Total programme	**€26971 M**	**€49551 M**	**€80696 M**	**€59594 M**	–	**€62977 M**

The discrepancies between the baseline budget and the current budget can be attributed to several factors. Firstly, there was still a lot of uncertainty regarding the design at that stage, especially with regards to technologies being used. That is why larger margins were imposed, ranging from 40-75%. The tooling was also at the time not considered a part of the RDT&E costs, while it was considered a part of RDT&E at this point.
The margins have also shrunk since the baseline report. Mainly due to the use of the DAPCA IV model, this offered a more certain cost estimate. It is however not perfect, and that is why a 35% margin has been taken for the RDT&E stage and a 25% margin for the development stage. This is in accordance with a paper written by Shen et al [78]. The engines and avionics got smaller margin 5% however, as these two systems were based upon more recent and accurate cost values. Even with the inclusion of these margins, the RDT&E costs remains within the allocated €50 billion with an extra €21 billion buffer.

[12] URL `https://www.in2013dollars.com/europe/inflation/1999?endYear=2035&amount=100&future_pct=0.03` [Cited 11/06/2026]

21.3.3. Market Price

The market price per aircraft is computed by applying a manufacturer's profit margin to the unit acquisition cost, following Raymer [25]. The following equation is used:

$$P_{\text{market}} = \frac{C_{\text{inv}}}{N_{\text{sold}}} \cdot (1 + m) \tag{21.9}$$

where N_{sold} is the total number of aircraft delivered over the programme life and $m = 0.25$. The per-unit cost and selling prices by delivery scenarios are presented in Table 21.4.

Table 21.4: Per-unit cost and selling price by delivery scenario. All values in 2035 euros.

	Pessimistic (20)	Base (75)	Optimistic (180)	Budgeted Base (75)
Amortised RDT&E per unit	€820.3 M	€283.0 M	€140.6 M	€382.1 M
Production cost per unit	€528.2 M	€377.6 M	€307.7 M	€457.6 M
Unit acquisition cost	€1348.6 M	€660.7 M	€448.3 M	€839.7 M
Selling price (+25%)	€1685.7 M	€825.8 M	€560.4 M	€1049.6 M

The selling price ranges from €560 M to €1686 M across scenarios. This is substantially above conventional widebody list prices, which benefit from production runs of several hundred to over a thousand units. At the base scenario, the amortised RDT&E alone accounts for €283 M per aircraft, representing 43% of the unit acquisition cost. This is a direct consequence of the niche market size and is expected for a first-of-type programme with high development complexity. The commercial justification from the operator perspective is addressed in the next paragraph.

21.3.4. Operating Cost

The direct operating cost (DOC) is estimated using the Raymer method for a reference mission of 4140 km at Mach 0.79 and 35000 ft, giving a block fuel of 25905 kg and a block time of 7.05 hr from the converged propulsion mission profile [25].

The key cost components are defined as follows.

Bio-SAF fuel cost

The fuel cost per block hour is:

$$C_{\text{fuel}} = \frac{\dot{m}_f \cdot d_{\text{nom}} \cdot P_{\text{SAF}}}{t_{\text{block}}} \tag{21.10}$$

where $\dot{m}_f$ is the fuel mass flow per kilometre(kg/km), d_{nom} is the nominal mission distance (km), P_{SAF} is the bio-SAF price (€/kg), and t_{block} is the block time in hours. The FT bio-SAF price is taken as €2.0 /kg as an upper bound at 2035 [79].

Crew cost

The 16-crew flight deck cost per block hour, consisting of 4 pilots and 12 cabin crew, follows the Raymer formulation [25]:

$$C_{\text{crew}} = 54 \cdot V_c \cdot \left(\frac{W_{\text{MTOW}}}{10^5}\right)^{0.3} + 122 \tag{21.11}$$

where V_c is the cruise speed in knots and W_{MTOW} is the maximum take-off weight in lb.

Maintenance cost

Given the novel BWB structural arrangement, the constrained access to above-body engines, and the load-bearing tank inspection requirements, an elevated maintenance man-hours per flight hour (MMH/FH) factor in the range of 12-15 is anticipated, at the upper end of the Raymer range for aircraft with complex composite structures and non-standard configurations[25]. Total maintenance cost per block hour is the sum of labour and materials:

$$C_{\text{maint}} = \text{MMH/FH} \cdot R_{\text{maint}} + 3.3 \cdot \frac{C_a}{10^6} + 10.2 + 58 \cdot \frac{C_e}{10^6} - 19 \cdot N_e \tag{21.12}$$

where R_{maint} is the maintenance labour rate (€/hr), C_a is the aircraft cost less engines (€), C_e is the engine unit cost (€), and N_e is the number of engines.

Depreciation, insurance, and landing fees

Depreciation assumes a residual value of 10 % of unit acquisition cost over a 25-year service life[25]. Insurance is estimated at 1 % of annual operating cost. Landing fees are taken as 33 % of fuel cost per flight following Raymer[25].

Taking all this components into consideration, Table 21.5 presents the DOC breakdown. The DOC can be computed in two relevant metrics: euros / block hour and cents / available seat kilometre.

Table 21.5: DOC breakdown for the reference 4140 km mission. Scenario-dependent components reflect the selling price of each delivery scenario. All values in 2035 euros per block hour.

DOC component	Pessimistic (20)	Base (75)	Optimistic (180)	Margin	Budgeted Base
Bio-SAF fuel (€2.00/kg)	€7349	€7349	€7349	5%	€7716
Flight crew (4 pilots + 12 cabin)	€457	€457	€457	5%	€480
Maintenance	€2100	€2100	€2100	5%	€2205
Depreciation (10% residual, 25 yr)	€17339	€8494	€5764	–	€10795
Insurance	€2408	€1180	€801	–	€1500
Fees and charges	€1525	€1525	€1525	5%	€1601
Total DOC [€/BH]	**€31178**	**€21105**	**€17996**	–	**€24297**
DOC [cents/ASK]	44.26	29.96	25.55	–	34.50

The dominant cost driver in the pessimistic scenario is depreciation, which at €17339/BH accounts for 56% of total DOC and reflects the high unit acquisition cost at low production volume. In the base scenario depreciation falls to 40% as the selling price decreases with higher volume. Fuel represents 35% of base DOC at €7349/BH. The DOC per available seat kilometre of 29.96 cents/ASK at the base scenario is high relative to conventional mixed-class widebodies, which typically operate at 8 to 15 cents/ASK, but the correct comparison is against the revenue per available seat kilometre. Long-haul all-business class yields are typically 2 to 5 times the economy equivalent, which places the achievable revenue per ASK well above the DOC across all three scenarios.

The budgeted case has also been carried through from Table 21.3. Relatively low margins were set for the operating cost as the Raymer method was seen for this specific facet. On test case showed that Raymer had a rough error of 5% [80]. The values for depreciation and insurance did not get an extra margin as these are based on the unit price of the aircraft, which already included earlier margins.

21.4. Sales Estimation

The sales estimation consolidates the delivery forecast and cost analysis into a set of programme-level financial metrics. Three quantities are computed for each scenario: the return on investment (ROI), the break-even delivery count N_{BE}, and the production rate. The ROI is defined as the programme profit as a fraction of the total invested cost:

$$\text{ROI} = \frac{P_{\text{sell}} \cdot N_{\text{sold}} - C_{\text{inv}}}{C_{\text{inv}}} \times 100\% \tag{21.13}$$

where P_{sell} is the selling price per aircraft from Subsection 21.3.3, N_{sold} is the total number of deliveries, and C_{inv} is the total programme cost from Table 21.3. Since P_{sell} is defined as $1.25 \times C_{\text{inv}}/N_{\text{sold}}$ by the fixed 25% margin, substituting into Equation 21.13 gives ROI = 25% identically across all scenarios. The ROI is therefore not an output of the analysis but a consequence of how the selling price is set. The more meaningful programme metrics are the break-even count and the production rate.

The break-even delivery count N_{BE} is the number of aircraft at which cumulative revenue recovers the full programme cost. Since each additional unit sold beyond the RDT&E recovery point contributes a margin of $P_{\text{sell}} - C_{\text{unit}}$, where C_{unit} is the per-unit production cost from Table 21.4, the break-even condition gives:

$$N_{BE} = \frac{C_{\text{RDT\&E}}}{P_{\text{sell}} - C_{\text{unit}}} \tag{21.14}$$

For the base scenario this gives $N_{BE} = 21228/(825.8 - 377.6) = 47$ units. The production rate is simply the total delivery count divided by the 20-year programme duration from 2035 to 2055.

The total programme revenue is computed as $P_{\text{sell}} \times N_{\text{sold}}$ and the programme profit as the difference between revenue and total programme cost. For the base scenario: 75 x €825.8 M = €61935 M revenue against €49551 M invested cost, yielding a programme profit of €12384 M. Table 21.6 presents the full results for all three scenarios.

Table 21.6: Programme economics summary by delivery scenario. All monetary values in 2025 euros.

Parameter	Pessimistic (20)	Base (75)	Optimistic (180)	Budgeted Base (75)
Total programme cost (C_{inv})	€26971 M	€49551 M	€80696 M	€62977 M
Selling price per aircraft (P_{sell})	€1685.7 M	€825.8 M	€560.4 M	€1049.6 M
Total programme revenue ($P_{\text{sell}} \cdot N$)	€33714 M	€61935 M	€100872 M	€78720 M
Programme profit	€6743 M	€12384 M	€20176 M	€15743 M
Return on investment	25%	25%	25%	25%
Break-even count N_{BE}	14 units	47 units	100 units	49 units
Production rate	1.0 ac/yr	3.8 ac/yr	9.0 ac/yr	3.8 ac/yr

In the base scenario the programme recovers its full cost after 47 deliveries, well within the 75-unit market forecast, leaving a margin of 28 units before the market ceiling is reached. The pessimistic scenario breaks even at only 14 units, which means the programme remains financially viable even if market uptake is extremely slow. The production rate of 3.8 aircraft/yr in the base scenario is low relative to conventional widebody programmes but is consistent with the niche all-business class market established in Subsection 21.2.1 and comparable to other low-volume premium

aircraft programmes. The absolute programme profit grows from €6743 M in the pessimistic case to €20176 M in the optimistic case, reflecting the strong operating leverage of recovering fixed RDT&E costs over a larger delivery base. In the additional budgeted case, there will €3 billion more profit, but the amount of aircraft that should be sold is increased. Keeping the production rate intact, it means that there will be an additional six to seven month period before the break-even count is reached.

21.5. SWOT Analysis

Having established the development, production, and operating cost structure in Section 21.3 and the delivery and revenue outlook in the preceding section, this final section synthesises the mission's overall competitive position. Table 21.7 presents the SWOT analysis of the selected 100% bio-SAF BWB configuration, updated from the mission-level analysis of the Baseline Report to reflect the now-converged design, cost, and competitive landscape.

Table 21.7: SWOT analysis of the post-oil global airliner, 100% bio-SAF BWB configuration.

	Helpful	**Harmful**
Internal Origin	**Strengths:** - Blended wing body configuration achieves a cruise L/D of 19.4, outperforming the efficiency of a comparable tube-and-wing widebody, directly reducing bio-SAF fuel burn and operating cost per business seat - 100 percent bio-SAF (Fischer-Tropsch pathway) avoids the cryogenic tankage, novel certification basis and airport infrastructure overhaul that a hydrogen-fuelled concept would require, placing the design on a substantially higher TRL and lower risk certification path while still eliminating petroleum-derived fuel entirely - There is not a lot of competition on the market, only two airlines with all-business seats aircraft controlling a fleet of 2 aircraft. There is a lot of potential to control this growing sector. - The all-business-class 120-seat cabin generates higher revenue per flight than an equivalent economy configuration, directly offsetting the bio-SAF cost premium over conventional kerosene operation	**Weaknesses:** - No airframer heritage: certification, supplier and industrial capability to be built - Ambitious schedule: 5 years from baseline to first flight - Low-volume, premium-niche production run (20-180 aircraft over 20 years) drives a high non-recurring cost burden per unit. The resulting acquisition cost of € 826 M (base case) sits well above comparable widebodies such as the A320neo (€ 113 M), requiring the all-business revenue model to justify the premium[13]. - Primary structure uses conventional carbon fibre and conventional epoxy rather than bio-based alternatives, since bio-epoxy and bio-acrylonitrile carbon fibre combinations remain below the TRL gate for primary structures. The petroleum-derived materials reduction promised by the mission is therefore not realised in the airframe at entry into service, only through a later retrofitting strategy as bio-based materials mature.
External Origin	**Opportunities:** - Escalating regulatory cost stack on kerosene operations (ReFuelEU, EU ETS, CORSIA Phase 2) - Maturing EU lifecycle frameworks (CSRD, EU Taxonomy) extend pressure to airframe materials, and CSRD Scope 3 reporting obligations make premium-cabin travel a disproportionate, legally reportable liability for corporate customers, a market this aircraft directly addresses - Fleet replacement wave 2028-2040: a substantial share of the global fleet's projected growth to 49,210 aircraft by 2044 will replace ageing widebodies within the mission's first decade[3]. - Airbus ZEROe reset (Feb 2025) removes the only hydrogen-based intercontinental competitor, while JetZero's Z4 and Natilus' Horizon EVO are emerging BWB competitors targeting the 150-250 seat economy or mixed-class segment, leaving the 120-seat all-business niche uncontested[4].	**Threats:** - Existing aircraft retrofitted to burn SAF already satisfy near-term regulation without a new airframe purchase. Since bio-SAF alone is not a unique differentiator, the commercial case rests entirely on the BWB efficiency and revenue-model advantages[5]. - JetZero and Natilus are progressing faster on BWB certification timelines in similar segments, which could shift regulator and supplier familiarity toward their configurations rather than this mission's[6].

The analysis indicates that the mission's commercial position remains structurally favourable, now reinforced by a converged design and cost basis rather than the qualitative projections of the Baseline Report. The aerodynamic and certification advantages of the chosen configuration are concrete and quantified, but they are counterbalanced by a unit cost and break-even point (€826 M and 47 of 75 deliveries, base case) that leave limited commercial margin for schedule slip or production-volume shortfall.

22
Sustainable Development Strategy

Sustainability is defined by the United Nations Brundtland Commission as "meeting the needs of the present without compromising the ability of future generations to meet their own needs" [81]. The main idea behind a POGA is to enhance sustainability by reducing the use of fossil fuels and atmospheric emissions. However, designing and developing this aircraft requires more aspects of sustainability to be taken into account. Therefore, this chapter evaluates sustainability through technical requirements, material sustainability, and a lifecycle assessment.

This chapter starts by defining the key requirements and quantitive indicators in Section 22.1, followed by Section 22.2, which outlines how sustainability is integrated in the design. Bio-SAF and material sustainability is discussed in Section 22.3 and Section 22.4, respectively, followed by a retro- and forwardfitting strategy in Section 22.5. Lastly, a life cycle assessment in Section 22.6 evaluates the environmental impact of the POGA.

22.1. Sustainability Requirements and Verification

The design's sustainability is to be verified and validated by external experts for technical accuracy and Key Performance Indicators (KPI). Additionally, two top-level sustainability requirements are considered:

- **MS-REQ-9.1**: The fuel shall not be petroleum-derived.
- **MS-REQ-9.2**: The use of petroleum-derived materials in construction shall be minimised.

In order to quantify the top-level requirements, two sustainability KPIs are introduced:

- **Petroleum Fuel Share (PFS) (%)**: The percentage of total fuel consumption (by mass or energy) that is derived from petroleum-based sources. The target is to have a Petroleum Fuel Share of 0%.
- **Sustainable Material Share (SMS) (%)**: The percentage of the total structural weight composed of materials that are not derived from petroleum. The target is to maximise the Sustainable Material Share.

22.2. Sustainability Integration Across the Design

Although this chapter formalises sustainability through requirements and KPIs, sustainability is not confined to a standalone chapter of the design. The 0% PFS and maximised SMS targets propagate as binding constraints into nearly every discipline of the preliminary design, shaping decisions on aircraft architecture, propulsion sizing, structural material selection, manufacturing strategy, operational concept, and the commercial case for the aircraft. This section gives a brief overview of how those disciplines connect back to the sustainability strategy.

Aerodynamics. The selection of a BWB configuration, with an aerodynamically optimised centrebody and outer wing, is itself a sustainability-driven decision. A higher cruise L/D ratio directly reduces the energy required per passenger-kilometre, which in turn reduces the absolute volume of bio-SAF the aircraft consumes over its mission.

Aircraft Architecture. The above-body engine placement is noise reducing, enhancing the sustainability of the aircraft [82]. The resulting under-wing space freed by relocating the engines is reallocated to load-bearing bio-SAF tank integration.

Power, Propulsion and Fuel System. The propulsion sizing is built exclusively around bio-SAF combustion characteristics, consistent with the drop-in fuel philosophy: the turbofans, fuel system, and tank integration require no modification relative to a conventional kerosene-fuelled architecture, which keeps the 0% PFS target achievable on the 2035 entry-into-service timeline rather than dependent on unproven propulsion technology.

Structures and Weight. The conventional CF/GF-epoxy material trade-off is the structural counterpart of the SMS requirement. the resulting lightweighting is credited in the Life Cycle Assessment, and the same components later become the targets of the Retro- and Forwardfitting Strategy (Section 22.5).

Operations and Logistics. Since bio-SAF is used as drop-in solution, the airport infrastructure requires no fuelling, storage, or ground-handling modifications, allowing the aircraft to integrate into existing route networks and airport operations from the outset.

Taken together, these connections show that sustainability functions less as an isolated chapter and more as a cross-cutting design driver: every other discipline either constrains, or is constrained by, the bio-SAF strategy, the material strategy, and the retrofitting roadmap detailed in the remainder of this chapter.

22.3. Bio-SAF Characteristics

This section evaluates Biological Sustainable Aviation Fuel (bio-SAF) as a primary near-term decarbonisation pathway. It critically examines the fuel's complex sustainability profile, weighing direct emission reductions against non-CO_2 climate impacts and land-use controversies. Besides, a strategic, low-risk feedstock sourcing framework was designed to meet global availability demands without compromising ecological integrity.

22.3.1. Bio-SAF Sustainability

Bio-SAF offers a compelling near-term decarbonisation pathway for aviation primarily because it functions as a drop-in fuel: it is chemically compatible with existing turbofan architectures, airport fuelling infrastructure, requiring no modifications to engines or ground systems [83]. When assessed on a well-to-wake lifecycle basis, bio-SAF can reduce CO_2 emissions by up to 80% compared to conventional jet fuel, depending on the feedstock and conversion pathway [83]. This reduction is rooted in the closed-loop biogenic carbon cycle: unlike fossil kerosene, which introduces ancient carbon into the atmosphere, the CO_2 released during combustion of bio-SAF was recently absorbed from the atmosphere by the biomass that constitutes its feedstock, yielding a substantially lower net carbon addition [84]. Beyond CO_2, bio-SAF combustion produces lower concentrations of sulphur oxides and soot particulates compared to conventional jet fuel, improving local air quality around airports and reducing particulate deposition in the upper troposphere [85].

However, the sustainability case for bio-SAF is contested on several fronts. The most significant challenge concerns the scope of the lifecycle analysis itself. Regulatory frameworks such as CORSIA and the EU Renewable Energy Directive predominantly measure the CO_2 benefit of SAF pathways while omitting the non-CO_2 climate effects of in-flight combustion. A 2025 study published in Nature Scientific Reports quantified these non-CO_2 effects (specifically nitrogen oxides (NO_x), water vapour, and contrail-cirrus formation) and found that their combined global warming impact is between two and four times the CO_2 warming effect alone [10]. When these in-flight non-CO_2 effects are included in a comprehensive well-to-wake analysis, the maximum achievable reduction in CO_2-equivalent emissions from bio-SAF drops to below 50% compared to conventional jet fuel [10, 86]. Crucially, bio-SAF has little effect on NO_x emissions, meaning that the warming contribution from ozone production and contrail formation is largely unchanged irrespective of the fuel's biogenic origin [10].

A second controversy concerns indirect land-use change (ILUC). When bio-SAF feedstock cultivation, or the diversion of waste streams previously used in food or feed markets, displaces agricultural activity onto previously uncultivated land, the associated carbon stock losses may partially or fully negate the direct lifecycle CO_2 savings. A Transport & Environment study found that, on average, biofuels can generate more CO_2 emissions than the fossil fuels they replace once ILUC is factored in [87]. A concrete illustration of these risks emerged from investigative reporting in 2025, which found that the company behind Brazil's first planned bio-SAF biorefinery, was cultivating oil palm on land embargoed by Brazil's federal environmental agency over illegal deforestation[1]. Even where palm is planted on legally degraded land, researchers note that the displacement of existing agriculture induces indirect pressure on surrounding forested areas, as cleared forest makes way for the activities pushed out by the plantation. This is precisely why virgin palm oil is excluded as a SAF feedstock under EU and UK regulations. On top of that, Energy crops and oil palms require substantial irrigation, and large-scale monoculture plantations are known to deplete local water supplies and disrupt hydrological cycles, particularly in ecologically sensitive regions [88]. Furthermore, the imprecise nature of the term "sustainable aviation fuel" has attracted regulatory scrutiny, as the label obscures significant differences in the environmental performance of individual fuel types and feedstock origins, exposing producers and operators to greenwashing risk [87].

22.3.2. Global Bio-SAF Feedstock Availability

The 2035 timeline aligns with critical global SAF blending milestones. The aircraft can operate as a "drop-in" solution without modifications to engines or infrastructure while supporting the legal frameworks, such as the ReFuelEU Aviation mandate for 20% SAF blending target by 2035 and U.S. SAF Grand Challenge, which aims to reach 3 billion gallons per year by 2030 and 35 billion gallons by 2050[2].

There are two main industry-certified pathways for producing bio-SAF: Hydroprocessed Esters and Fatty Acids (HEFA) and Fischer-Tropsch (FT) gasification. HEFA is a highly developed thermochemical process that converts lipid-rich feedstocks, such as vegetable oils, used cooking oil, and animal fats into drop-in aviation fuel through catalytic deoxygenation and hydroprocessing [89]. Due to its reliance on well-established refining technologies, it currently dominates the commercial bio-SAF market at least until 2030 [90].

FT gasification involves thermochemically converting solid carbon-rich materials, such as municipal solid waste, agricultural residues, and forestry waste, into a synthesis gas (syngas) comprising primarily carbon monoxide and hydrogen at high temperatures [91]. This syngas is subsequently cleaned and synthesised into long-chain liquid hydrocarbons via the FT catalytic process before undergoing hydrotreatment to meet precise aviation fuel specifications [89]. Although TRL of the overall process is low, it is projected that it reaches a mature state around 2035 [90].

The choice between HEFA and FT gasification has many factors [92]. HEFA has the lowest production cost and is therefore the best option for SAF based on cost alone. Conversely, FT gasification has the lowest carbon abatement cost, which is the financial expense incurred to reduce, avoid, or eliminate one metric tonne of greenhouse gas emissions. This makes FT gasification preferable for lifecycle mitigation. However, FT gasification faces significant economic challenges, including the high biomass feedstocks cost and the substantial capital costs by scaling up production [90].

For the scope of this design, maximising greenhouse gas reductions and mitigating "green-washing" is of utmost importance. Therefore, the "lowest risk" feedstocks will be prioritised, with an emphasis on domestically sourced materials with no competing uses in food or feed markets, such as agricultural and forestry residues, municipal solid waste, and domestic used cooking oil (UCO). As detailed in Table 22.1, the availability and yield of these feedstocks vary significantly by conversion pathway. Feedstocks utilising the HEFA pathway, such as UCO and domestic inedible

[1] URL https://www.climatechangenews.com/2025/06/18/brazilian-firm-behind-saf-plan-found-growing-oil-palm-on-deforested-amazon-land/ [Cited 17/06/2026]

[2] URL https://transport.ec.europa.eu/transport-modes/air/environment/refueleu-aviation_en [Cited 17/06/2026]

tallow, offer high conversion yields (0.83 kg fuel/kg feedstock) but are relatively limited in total volume, meeting only 1.3% and 0.5% of the 2035 jet fuel demand, respectively. In contrast, advanced waste and residue feedstocks utilising FT gasification have lower conversion yields (0.11–0.22 kg/kg) but offer substantially higher production potentials. Agricultural residues alone can support up to 8.18 Mt of SAF production, satisfying 14.6% of the projected 2035 demand. This is supplemented heavily by municipal solid waste (2.3–6.0%) and forestry residues (1.6–2.2%).

Table 22.1: SAF feedstock yields, conversion pathways, and production potentials

Feedstock	**Conversion pathway**	**Yield** (kg fuel/kg feedstock)	**Source**	**SAF production** (Mt)	**% 2035 jet fuel demand**
Inedible tallow (domestic)	HEFA	0.83	[93]	0.28	0.5%
Inedible tallow (imported)	HEFA	0.83	[93]	0.04	0.1%
Used cooking oil (domestic)	HEFA	0.83	[93]	0.74	1.3%
Used cooking oil (imported)	HEFA	0.83	[93]	0.95	1.7%
Tall oil pitch	HEFA	0.83	[93]	0.11	0.2%
Palm oil sludge	HEFA	0.83	[93]	0.49	0.9%
Municipal solid waste	FT gasification	0.11	[94, 95]	1.31-3.36	2.3-6.0%
Agricultural residues	FT gasification	0.19	[94, 96]	8.18	14.6%
Forestry residues	FT gasification	0.22	[94, 97]	0.91-1.21	1.6-2.2%
Crude glycerine	Alcohol-to-jet	0.50	[98, 99]	0.22	0.4%

By explicitly excluding "high-risk" inputs of uncertain origin, such as imported UCO and imported tallow, despite their combined 1.8% demand coverage, alongside animal fats, the strategy avoids penalties associated with indirect land-use change. This approach minimises regulatory scrutiny regarding fraudulent reporting and ensures a robust supply chain anchored by highly scalable, domestic FT gasification feedstocks and highly efficient, localised HEFA inputs. However, it should be noted that the bio-SAF availability remains limited relative to jet fuel. Therefore, it should be stressed that FT gasification will be utilised first. When all the feedstock for FT gasification are used, the HEFA conversion pathway will be considered for usage, capitalising on the cost-effectiveness and high conversion yields of available domestic lipid feedstocks to supplement the overall production volume and bridge the remaining supply gap without compromising sustainability standards.

22.4. Material Sustainability

Maximising the SMS is a primary KPI for the aircraft's development. However, ensuring structural integrity while meeting the timeline requires realistic and practical materials to be selected. After the trade-off, conventional CF and epoxy are selected as primary structures and for the secondary structures, conventional CF, GF and epoxy are incorporated as secondary structures. Since conventional and bio-based materials have similar material properties, the oil-derived materials are selected due to their availability in 2035. Due to the optimised strength-to-weight ratio, the empty operative mass of the aircraft is reduced, which results in less energy over the airframe's entire service life, the manufacturing footprint will be offset.

In order to still maximise the SMS, considering that the primary and secondary structures are fully petroleum-based, sustainable materials will be utilised where possible in other systems of the aircraft. The aircraft interior (including cabin sidewalls, seating structures, overhead bins, floor panels, and insulation) serves as an optimal candidate for incorporating sustainable materials. Because these interior components have to endure lower structural loads and obtain certification faster, conventional plastics and resins will be minimised for the interior architecture with priority. This is why using environmentally friendly material reduces cabin components' weight by up to 20 percent and additional CO_2 savings can be leveraged over its entire lifecycle[3]. In order to illustrate this, Rafalo has shown that flax, hemp, and bamboo can be used as fillers or reinforcements for polymer matrices [100]. While these natural fibres are highly viable reinforcements, their structural analysis identified Areca fibre combined with a low-density polyethene (LDPE) matrix as the highest-performing sustainable composite for aircraft cabin applications.

22.5. Retro- and Forwardfitting Strategy

The aviation industry faces a critical timeline paradox: delaying new aircraft programs until bio-derived composites are fully mature allows high-emission legacy fleets to remain in the skies, while launching a conventional aircraft in 2035 risks locking in static material technologies for a 30-year operational lifespan. In order to future-proof the design and continually improve the SMS over the aircraft's lifespan, a retro- and forwardfitting framework has been integrated into the technical planning. Because the 2035 entry-into-service target necessitates the initial use of conventional petroleum-derived composites for primary and secondary structures, the aircraft is engineered with a "Design for Upgradability" (DfU) philosophy. As non-oil-derived materials systematically advance in technological maturity, they will replace conventional materials on the existing fleet [101]. This approach mitigates the risk of delaying the initial deployment while ensuring the SMS continuously climbs toward 100% over the airframe's lifespan. The strategy relies on the following key pillars:

- **Modular Replacement and Standardisation**: The aircraft architecture treats structural components as interchangeable modules rather than permanent fixtures. Cabin interiors and non-load-bearing secondary structures (such as aerodynamic fairings and landing gear doors) are engineered for straightforward removal [102]. Furthermore, weight and balance variations caused by substituting conventional composites with bio-composites of differing densities are pre-calculated and accounted for within the aircraft's foundational CG envelope.

[3] URL `https://www.lufthansa-technik.com/en/aeroflax` [Cited 20/06/2026]

- **Alignment with Maintenance Schedules**: To prevent a manufacturing carbon penalty that would negatively impact the LCA, retrofitting is strictly condition-based. Rather than prematurely discarding perfectly functional components, petroleum-derived materials will only be replaced with sustainable alternatives when they sustain damage or naturally reach the end of their usable life. These replacements are synchronised with the schedule's heavy maintenance routines. Because D-checks require the aircraft to be extensively dismantled every 6 to 10 years, the first D-checks for aircraft entering service in 2035 will occur around 2041–2045[4]. This aligns perfectly with the projected availability of mature bio-materials for secondary structures.
- **Certification via Supplemental Type Certificates (STC)**: Re-certifying an entire aircraft for a material change is a major regulatory and financial bottleneck. To bypass this, the retrofitting strategy leverages the STC process [103]. This allows approved suppliers or the original equipment manufacturer (OEM) to certify specific sustainable replacement components independently. This results in faster integration of the sustainable material.
- **Reverse Logistics of Removed Parts**: A critical element of the retrofitting strategy is managing the swapped out petroleum-based parts. In alignment with the Cradle-to-Cradle approach, removed CF and GF components will bypass landfills and immediately enter the downcycling stream described in the LCA (Section 22.6), supplying non-aerospace industries with recovered fibres and maximising the circularity of the overall design.
- **Transition to Forward-Fit Production**: By 2045, as bio-derived composites achieve full technological maturity, the manufacturing baseline will shift from post-delivery retrofitting to direct factory integration, where all newly manufactured aircraft will be equipped with bio-materials from the outset. This is known as forward-fitting, which is preferred over retrofitting for multiple reasons [104]. Firstly, it eliminates the need to manufacture redundant petroleum-based parts, avoiding the carbon footprint penalty when producing components twice. Besides, current industry demand heavily favours forward-fit, as the Aircraft Electronics Association reported forward-fit sales surging by 26.2%[5]. Ultimately, this establishes the retrofitting framework as a targeted, transitional strategy designed to maximise the SMS of early-build aircraft (2035–2044) without delaying the initial program launch.

22.5.1. Fleet Size Dependency of the Retrofitting and Forward-Fitting Strategy

The retrofitting and forward-fitting framework is not fleet-size-neutral. The pace at which the fleet's SMS improves, the point at which forward-fitting becomes the manufacturing baseline, the viability of a dedicated reverse logistics stream, and the ability to secure bio-composite supply chains all scale with the number of aircraft in service. This section evaluates those dependencies across the three scenarios established: a pessimistic fleet of 20 aircraft, a base fleet of 75, and an optimistic fleet of 180.

Retrofit Cadence and Forward-Fitting Transition

The transition from condition-based retrofitting to forward-fit production is driven by the accumulation of D-checks across the in-service fleet. A single aircraft entering service in 2035 reaches its first D-check around 2041–2045. As fleet size grows, the number of D-checks occurring per year grows proportionally, creating a broadening window of retrofit activity and an earlier moment at which the aggregate demand for bio-composite replacement parts justifies reconfiguring the factory baseline.

In the pessimistic scenario, with only 20 aircraft delivered over the production life, D-checks are sparse and spread unevenly across the schedule. The volume of bio-composite parts required per year remains low and does not generate sufficient recurring demand to motivate a factory-level shift. Forward-fitting may therefore not become economically rational within the programme lifetime, and the pessimistic fleet would likely remain on a pure condition-based retrofit model throughout, with the SMS improving only incrementally as individual aircraft cycle through heavy maintenance.

In the base scenario, 75 aircraft produce a substantially denser D-check schedule. By the late 2040s, enough aircraft are simultaneously in or approaching heavy maintenance that demand for bio-composite secondary structures becomes consistent and forecastable. This is the threshold at which reconfiguring the manufacturing baseline from petroleum-derived composites to bio-composites ceases to be a disruption and becomes a cost-saving measure. The forward-fitting transition in the base scenario is therefore plausible around 2045–2048, broadly consistent with the timeline stated.

In the optimistic scenario, 180 aircraft generate a high and early D-check frequency. The density of retrofit activity in the early 2040s may be sufficient to pull the forward-fitting transition forward to approximately 2042–2045, before bio-composites have achieved full commercial maturity across all secondary structure applications. This creates a risk: committing the factory to bio-composite forward-fitting slightly ahead of full material TRL requires closer coordination with material suppliers and may necessitate a brief parallel production capability. However, it also means the optimistic fleet reaches a high SMS earlier in the programme life, improving the overall LCA performance of the delivered fleet.

Supplier Confidence and Bio-Composite Supply Chain

Securing a reliable supply of bio-derived composites at the scale and certification standard required for aerospace secondary structures depends on supplier willingness to invest in dedicated production capacity. That willingness is directly tied to the size of the committed fleet.

In the pessimistic scenario, a 20-aircraft fleet represents a very limited offtake volume. Specialist bio-composite suppliers are unlikely to invest in aerospace-grade production lines on the basis of this demand alone. The programme would therefore be dependent on suppliers already serving other customers, with limited ability to negotiate delivery priority, pricing, or material specifications. This does not make retrofitting impossible, but it does mean the programme

[4] URL `https://gfa.aero/blog/aviation-updates/types-of-aviation-maintenance-checks` [Cited 20/06/2026]

[5] URL `https://www.ainonline.com/aviation-news/aerospace/2023-11-06/retrofit-avionics-market-grows-modestly-forward-fit-sales` [Cited 29/06/2026]

is a price-taker rather than a market shaper, and supply disruptions would have an outsized impact on the retrofit schedule.

The base scenario, with 75 aircraft, represents a more credible anchor customer. At this scale, a long-term offtake agreement with a bio-composite supplier becomes a realistic negotiating position, potentially supporting supplier investment in the dedicated capacity needed to meet aerospace certification timelines. This aligns the base scenario with the broader SAF feedstock strategy described in Subsection 22.3.1, where domestically sourced, scalable feedstocks are prioritised: the same logic applies to structural materials, where volume commitment de-risks the supplier's position.

The optimistic scenario, with 180 aircraft, generates sufficient demand to support multiple competing bio-composite suppliers. This introduces redundancy into the supply chain and creates pricing leverage, reducing the per-unit cost of bio-composite components over time. It also allows the programme to influence material qualification standards, potentially accelerating the certification of novel bio-derived composites for secondary structures by co-funding supplier qualification campaigns.

Reverse Logistics and the Downcycling Stream

As petroleum-derived CF and GF components are removed during D-checks and replaced with bio-composite equivalents, they enter the downcycling stream described in Section 22.6. The viability of that stream depends on the volume of material flowing through it.

In the pessimistic scenario, the annual volume of removed CF and GF parts is too low to sustain a dedicated internal downcycling operation. Running a proprietary recovery and fibre processing facility at this scale would be economically irrational and would likely produce a net carbon penalty relative to outsourcing. The pessimistic fleet should therefore partner with established aerospace recyclers, such as those already processing end-of-life composite structures from conventional widebody programmes, and supply removed components directly into their existing fibre recovery streams. This avoids landfill disposal while avoiding the overhead of a purpose-built facility, though it gives the programme less control over the destination and verified use of recovered fibres.

In the base scenario, the volume of removed material grows to a level where a structured partnership with a dedicated recycler becomes viable on preferential terms. Rather than simply supplying into a third-party stream, the programme can negotiate traceability and reporting commitments, allowing the downcycling credit in the LCA to be substantiated with verified end-use data rather than estimated displacement factors.

In the optimistic scenario, the volume of removed CF and GF parts across 180 aircraft is sufficient to support a dedicated reverse logistics arrangement, as many cycling through their first D-check simultaneously in the early-to-mid 2040s. This can be co-developed with aerostructures partners such as those identified in Chapter 23. At this scale, it becomes feasible to pre-negotiate fibre recovery contracts that guarantee aerospace-grade traceability and supply recovered material to specific downstream industries, strengthening the circularity argument at the centre of the LCA.

Across all three scenarios, the core retrofitting philosophy remains unchanged: condition-based replacement synchronised with D-checks, modular component design, and a planned transition to forward-fitting as bio-composites mature. What changes with fleet size is the pace, the leverage, and the logistics. A pessimistic fleet executes the same strategy more slowly, with less supply chain influence and a reliance on external recycling partners. An optimistic fleet accelerates the forward-fitting transition, shapes the bio-composite supply market, and enables a more controlled and traceable reverse logistics operation. Fleet size is therefore not merely a commercial variable: it is a direct determinant of how effectively the sustainability strategy performs in practice.

22.6. Life Cycle Assessment

To evaluate the environmental impact of the POGA, a Life Cycle Assessment (LCA) is conducted using a Cradle-to-Cradle approach. This boundary ensures that the aircraft is not only assessed on its operational footprint but also on the sustainability of its raw materials and the feasibility of returning those materials to the industrial cycle at the end of its service life. For this assessment, the functional unit is defined as equivalent CO_2 emissions per megajoule of the bio-SAF consumed (gCO_2eq/MJ). While the aircraft adheres to a 0% PFS requirement by utilising only bio-SAF, it is critical to track the gCO_2eq/MJ to account for the comprehensive lifecycle footprint [105]. Bio-SAF still produces biogenic tailpipe emissions during flight, and its production footprint, including agriculture, harvesting, refinement, and distribution, must be quantified to calculate the true net-emissions reduction [106]. The assessment is divided into the four stages identified in Figure 22.1.

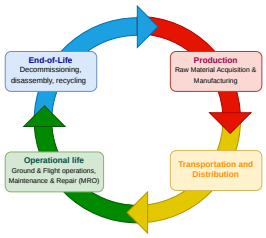

Figure 22.1: LCA framework for the POGA, illustrating the transition from raw material acquisition to end-of-life circularity [107].

Phase 1: Raw Material Acquisition and Manufacturing

In alignment with the SMS, this phase focuses on the "embodied carbon" of the aircraft. Because advanced bio-based materials possess material properties equivalent to conventional composites, petroleum-derived materials for primary and secondary structures are selected for the 2035 timeline. While these conventional materials carry a significant initial manufacturing footprint, their high strength-to-weight ratio significantly lowers the aircraft's OEM. This lightweighting offsets the initial manufacturing footprint by radically reducing energy demand over the airframe's lifespan.

From a feedstock efficiency perspective, producing 1 kg of jet fuel requires 10.36 kg of raw material via the FT pathway and 4.36 kg via HEFA, reflecting the significantly higher conversion losses associated with FT synthesis [108]. This material intensity must be factored into the upstream agricultural and logistics footprint tracked in this phase. Furthermore, LCA analysis of these pathways using the Danish EDIP environmental assessment method reveals that CO_2 emissions are heavily front-loaded: the production stage alone accounts for up to 89.12% of lifecycle emissions, while agricultural and usage-stage emissions contribute only 8.41% and 2.46%, respectively [108]. To actively suppress the embodied carbon during Phase 1, the aircraft interior incorporates lightweight bio-composites, which possess a vastly superior environmental production profile compared to conventional aviation plastics.

Phase 2: Transportation and Distribution

This phase accounts for the logistics required to move structural precursors, interior bio-materials, and the continuous supply of bio-SAF. The LCA strategy aims to minimise the transportation miles of heavy aircraft subsystems to the Final Assembly Line while continuously tracking the well-to-tank transportation carbon footprint of these various agricultural and waste feedstocks as they move from origin to refinery to airport.

Phase 3: Operational Life

The operational phase is where the 0% PFS is realised. By pairing a highly aerodynamic BWB with High Bypass Turbofans running on bio-SAF, the direct CO_2 emissions during flight are mitigated. The analysis here accounts for:

- **Energy Conversion Efficiency:** The efficiency of the turbofans in converting the bio-SAF into thrust over the life of the engine, accounting for specific fuel consumption (SFC) degradation over time.
- **Maintenance and Retrofitting:** The LCA heavily credits the scheduled phase-in of sustainable materials. As advanced non-oil-derived components reach commercial maturity (e.g., TRL 8+ by 2039–2041), conventional composite secondary structures will be systematically swapped for sustainable equivalents during heavy maintenance (D-checks). This creates a dynamic LCA that improves mid-lifecycle. The inclusion of the MRO phase is important, as it contributes heavily to cumulative climate impact through material replacement [109].

Phase 4: End-of-Life (EoL) and Circularity

Consistent with the Cradle-to-Cradle philosophy, the EoL phase is treated as a "beginning" for new products. The POGA is designed for disassembly, allowing high-value materials, such as titanium, aluminium, and rare-earth magnets from electric motors, to be recovered. This circularity credits the aircraft with "avoided emissions", effectively lowering the total gCO_2/PKM by reducing the need for material extraction in future industrial cycles.

While the modular, bio-based cabin interiors are organically processed or directly recycled, the conventional CF, GF, and epoxy structures present a unique challenge. EoL processing relies on advanced recycling techniques (solvolysis or pyrolysis) to recover high-value CF and GF [110]. However, since these thermal and chemical processes shorten fibre length and degrade the matrix interface, the recovered materials lose the structural integrity required for aerospace load-bearing applications [111, 112]. Instead of reusing it for new aircraft, they are downcycled into other industries with lower structural thresholds, e.g. automotive manufacturing [113]. This downcycling framework justifies the initial selection of conventional composites. It credits the aircraft's LCA with avoided emissions, which effectively lowers the total gCO_2/MJ footprint by displacing the need for virgin material extraction in those subsequent industrial sectors.

23
Manufacturing, Assembly and Integration

A significant aspect of aircraft design is the manufacturing, assembly and integration. This chapter outlines a preliminary plan on how this is approached for the POGA. First, the assumptions are introduced in Section 23.1, followed by Section 23.2 and Section 23.2, which outlines which parts will be manufactured and the manufacturing processes. Selecting the supplier for production together with timeline and scalability is discussed in Section 23.4 and Section 23.5, respectively.

23.1. Assumptions and Scope

In order to plan the production, integration and assembly process, assumptions have to be made at this stage.

1. **Systems will be bought off the shelf:** This assumption was made as some systems are not specifically designed for the aircraft, which means they can be bought of the shelf. Assuming that they are immediately ready for use
2. **Systems will be immediately bought and ready for use:** This neglects the waiting time for some of the more high demand components, but this can be disregarded as sufficient safety margins have been taken in the timeline for the assembly and integration stages.
3. **Suppliers are ready to sell:** In reality, some suppliers may refuse to cooperate with a company developing a novel aircraft solution due to their current market position. As this project is largely a feasibility study, this will be ignored at the current moment.
4. **Steady supply of materials:** It is assumed that all chosen materials are available at the start of the manufacturing process.

In order to construct the Manufacturing, Assembly and Integration (MAI) plan at the preliminary design stage, these assumptions are necessary; however, to ensure they do not stray too far from reality, related future risks to be monitored in later project phases are established in Chapter 24, specifically FR-23.

Due to the novelty of the BWB configuration, the production plan deliberately focuses on the BWB structure, which is the most distinctive and element compared to conventional TAW designs. The scope covers supply, machining, forming and assembly of the primary metallic structure for the BWB centrebody, multi-bubble pressure shell, aerodynamic outer shell, wingbox and outer wings, plus the composite control surfaces and trapezoid interior liners. Systems and propulsion are represented only as pre-assembled shipsets (engines, fuel and energy hardware, avionics, electrical harnesses, ECS and cabin monuments) delivered by specialised suppliers and integrated at Leonardo, ensuring the MAI plan remains tractable while still demonstrating a realistic industrial path to a complete airframe.

23.2. Production Parts Breakdown

The prototype structural scope is limited to the primary fuselage (BWB centrebody), wing primary structure and aerodynamic movables. At the highest level, two main assemblies are distinguished: the fuselage assembly and the wing assembly.

Fuselage assembly (BWB centrebody).

- **Outer BWB contour shell:** large Al–Li skins, frames and stringers forming the airfoil-shaped, largely oval external contour.
- **Three-bubble pressure shell module:** three pressurised Al–Li bubbles, including skins, frames, floor decks and two rows of Al–Li columns.
- **Centrebody structure:** floor beams, local frames and wingbox interface structure that tie the outer contour and pressure module together.
- **Trapezoid interior liners:** non-load-bearing sandwich sidewall and ceiling panels defining the cabin interior shape.

Wing assembly.

- **Wingbox (integral tank):** upper and lower Al–Li wing skins, front and rear spars and ribs, configured as an integral SAF fuel tank.
- **Outer wing panels and winglets:** structural outer wing sections and winglets without high-lift devices.
- **Movables:** composite inboard and outboard elevons, rear fuselage elevons and winglet rudders, supplied as complete control-surface assemblies.

23.3. Manufacturing Processes

Primary metallic structure is manufactured from Airware 2198–T8 Al–Li sheet, plate and extrusions. Plate is cut and 5-axis CNC machined into skins, spars, frames, ribs, floor beams and columns, followed by stretch-forming or roll-forming to obtain the required curvature for large fuselage and wing panels. Conventional drilling, reaming and countersinking operations are used to prepare mechanical joints.

Fuselage shells and pressure modules are assembled in dedicated jigs by mechanically fastening skins to frames and stringers using rivets and bolts, with local sealant application where required. The three-bubble pressure module is subsequently pressure-tested at module level to verify integrity before integration into the centrebody.

The wingbox is assembled from machined skins, spars and ribs in a wing jig and sealed as an integral fuel tank using standard tank-sealing practices. Outer wing panels and winglets are built up in similar jigs and attached to the wingbox. Non-destructive inspections (visual, ultrasonic and dimensional checks) are applied at sub-assembly and final-assembly level.

Interior trapezoid panels are manufactured as phenolic/glass skins bonded to Nomex/phenolic honeycomb cores and are trimmed and drilled before installation as non-load-bearing liners. Composite movables (elevons and winglet rudders) are produced using CFRP prepreg lay-up and curing, followed by machining of edges and installation of metallic fittings; they are then mounted to the wing and rear fuselage using standard hinge and actuator interfaces.

23.4. Supplier Choice

To keep the MAI plan realistic, each major structural package is assigned to an established European aerostructures supplier with proven experience in similar components. A three-tier structure is adopted. Tier–3 suppliers provide Airware 2198–T8 Al–Li stock and interior sandwich panels. A Tier–2 machining hub converts this stock into machined and formed kits for fuselage and wing parts. Tier–1 aerostructures integrators assemble the outer BWB shell, the three-bubble pressure module, the wingbox and wings, and perform centrebody and wing–body integration.

An Al–Li 2198–T8 product such as Airware is sourced from Constellium's aerospace mills, which already supply fuselage and wing skins for current civil aircraft, making this a credible material and supplier choice. voestalpine BÖHLER in Austria acts as a central European machining hub, providing 5-axis machining and forming of large structural parts and benefitting from good rail connections between France, Germany, Italy and Spain. It has to be recognised that this is somewhat of a bottleneck, as one company produces all metallic parts, in case voestalpine Böhler Aerospace does not have efficient capacities, MT Aerospace in Germany could fill a similar function. Premium AEROTEC, Aernnova and Leonardo have long histories in metallic fuselage shells, fuselage sections and wing structures respectively, while Euro-Composites supplies certified interior sandwich panels. Composite control surfaces are allocated to Aernnova, which already designs and manufactures a range of rudders, flaps and spoilers for commercial aircraft.

Table 23.1: Key structural suppliers and roles for the prototype

Company	Role	Tier
Constellium	Airware 2198–T8 Al–Li stock	3
Euro-Composites	Interior sandwich panels	3
voestalpine Böhler Aerospace	Fuselage and wing machining	2
Premium AEROTEC	Outer BWB contour shell	1
Aernnova	Pressure shell, columns, movables	1
Leonardo Aerostructures	Wingbox, wings, interior, integration	1

In order to provide a good visual overview both supplier distribution together with the required manufacturing processes presented in Section 23.3, this allocation is illustrative rather than prescriptive, its purpose is to demonstrate that credible European suppliers exist for each major work package. A visual time ordered sequence of manufacturing step by supplier is presented in Figure 23.1.

23.5. Timeline and Scalability

For the prototype stage, key structural suppliers can be grouped into the same Tier system as in Section 23.4. For aerospace aluminium plate and extrusions, industrial guides report lead times from $\mathcal{O}(10)$ days for standard stock up to $\mathcal{O}(3–8)$ weeks for made-to-order plate, with heavily loaded hard-alloy extrusions occasionally extending to many months[1,2]. Prototype procurement of specialised Al–Li stock can therefore be taken as "weeks to a few months" in order of magnitude.

For composite prepregs and sandwich panels, aerospace production scheduling references indicate that certified composite prepregs and exotic alloys carry procurement lead times of $\mathcal{O}(20–52)$ weeks, reflecting the need to trigger orders far in advance of planned build starts[3]. Prototype-specific panels that require new qualification or non-standard lay-ups can therefore be conservatively assumed to have lead times of "several months" between design freeze and delivery, rather than weeks.

For machining and forming of primary structure in prototype quantities, aerospace CNC suppliers indicate that complex first-off parts carry lead times that include not only machining but also First Article Inspection (FAI) close-

[1] URL https://rscalu.com/aluminum-plate-lead-time-guide/[Cited 12/06/2026]
[2] URL https://profileprecisionextrusions.com/aerospace-aluminum-alloys-and-lead-times/[Cited 12/06/2026]
[3] URL https://usersolutions.com/blog/aerospace-defense-scheduling[Cited 12/06/2026]

out and outsourced special processes such as heat treatment, anodising, and non-destructive testing[4]. End-to-end, a production-equivalent prototype with full FAI documentation, the standard required for flight-critical structure, typically requires on the order of 21–45 days at a single supplier, with additional time for process qualification and supply-chain coordination on a new design[5]. An order-of-magnitude range of 3–5 months for critical machined kits is therefore representative for a new design once supplier qualification and design iteration are included. At Tier-1 level, public information on aerostructure suppliers such as Premium AEROTEC shows that, in mature programmes, facilities are dimensioned for several to dozens of shipsets per month, whereas early phases typically deliver only a few shipsets per year while tooling and qualification are completed[6,7]. For a first prototype, each major integrated assembly (e.g. outer shell, pressure shell, wingbox) can thus be conservatively assigned a lead time of several months from frozen design to flight-ready article.

Combining these contributions, a conservative order-of-magnitude estimate for the full prototype manufacturing, assembly, and integration sequence is $\mathcal{O}$(6–12 months) from material availability to a flight-ready aircraft, once detailed design is frozen.

In serial production, both lead times and man-hours per unit are expected to decrease markedly. Industry reports show that automation and standardised routes can reduce lead times for parts that initially required months down to weeks, as demonstrated by recent transitions in aerospace supply chains[8]. Empirical learning-curve studies for aerospace manufacturing trace back to Wright's foundational observation that every doubling of cumulative aircraft output reduces direct labour by approximately 20 %, corresponding to an 80 % learning curve[9]. Subsequent empirical studies of jet fighter and commercial aircraft programmes confirm typical learning rates in the 80–85 % range, implying a 15–20 % reduction in direct worker-hours per unit each time cumulative output doubles[10]. Under such behaviour, the effective MAI time per aircraft in a stabilised low-rate production line can be expected to contract towards $\mathcal{O}$(1–3 months) per shipset, with individual supplier lead times approaching the lower ends of the bands quoted above. The prototype thus defines a conservative upper bound on calendar time, while subsequent prototypes and low-rate initial production units systematically move towards shorter, more stable lead times as processes, supply chains, and designs are stabilised.

[4] URL https://le-creator.com/blog/aerospace-machining/[Cited 12/06/2026]

[5] URL https://www.avalon.aero/cnc-machining/from-prototype-to-flight-ready-scaling-aerospace-cnc-machining-production/[Cited 12/06/2026]

[6] URL https://www.flightglobal.com/ila-premium-aerotec-gears-up-to-meet-the-demands-of-parent-airbus/113124.article[Cited 12/06/2026]

[7] URL https://www.aero-mag.com/kuka-robotics-premium-aerotec-automated-assembly-system[Cited 12/06/2026]

[8] URL https://www.precisionaviationgroup.com/company-news/how-the-aerospace-supply-chain-is-evolving/[Cited 12/06/2026]

[9] URL https://www.semanticscholar.org/paper/Factors-affecting-the-cost-of-airplanes-Wright/45552fa9afba0c33f4a24cbc40e0b044938442cb[Cited 12/06/2026]

[10] URL https://journals.plos.org/plosone/article?id=10.1371/journal.pone.0185364[Cited 12/06/2026]

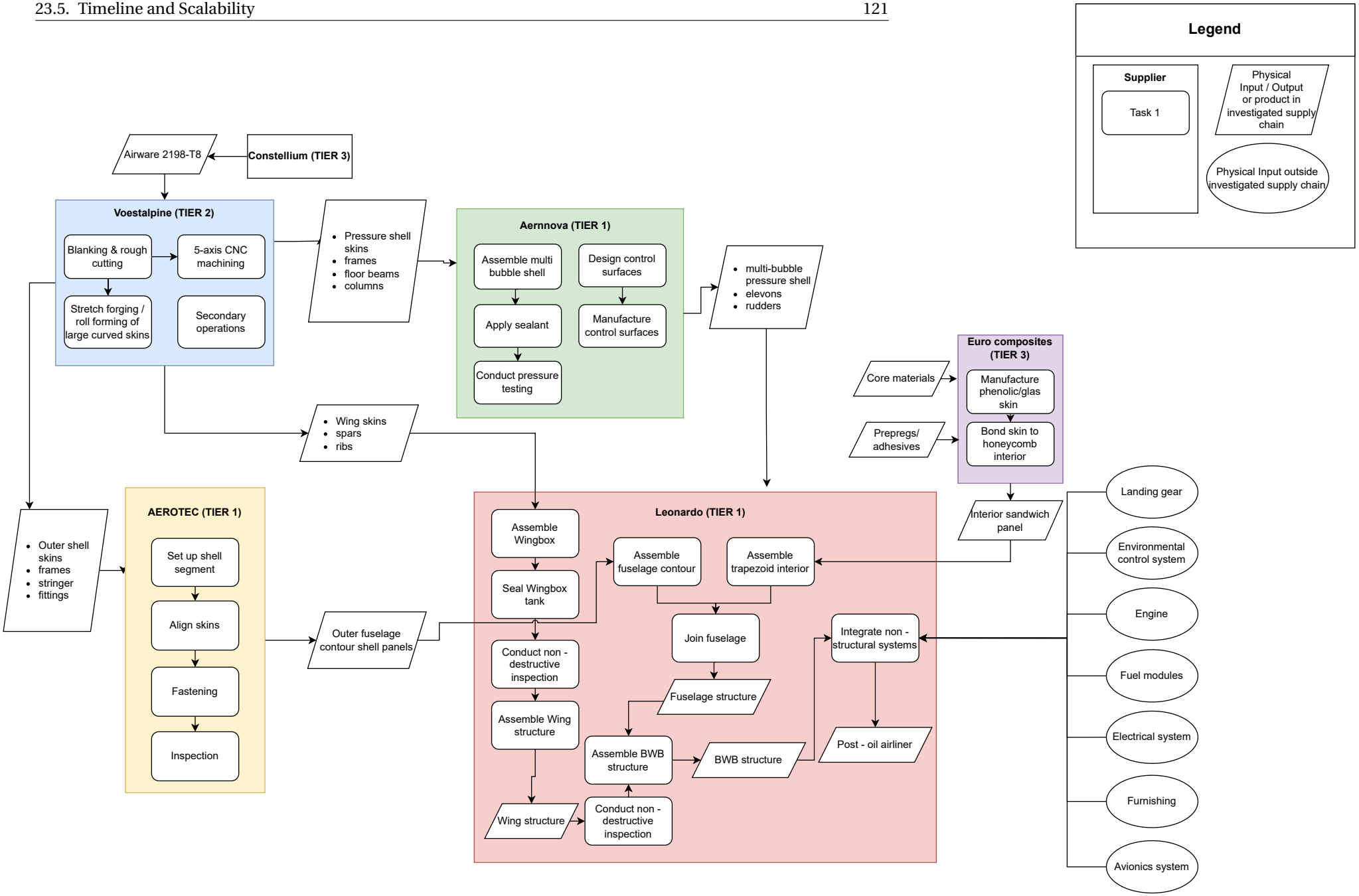

Figure 23.1: Production plan

24
Future Risks and RAMS Monitoring

After the preliminary design concept has been introduced, new risks appears that should be evaluated in the next design phases. This chapter starts with discussing the reliability, availability, maintainability and safety characteristics in Section 24.1, followed by Section 24.2, which outlines the future risks. These are mitigated in Section 24.3, from which the risk related requirements are derived in Section 24.4.

24.1. RAMS Characteristics

To assess the robustness of the selected concept and to structure the technical risk analysis, the RAMS characteristics are evaluated for the preliminary aircraft design. This design introduces specific reliability, availability, maintainability and safety challenges, which are used as the starting point for the risk identification in Section 24.2.

24.1.1. Reliability

Reliability denotes a product or system's ability to perform its intended function without failure [114]. For the selected concept, reliability is strongly linked to flight control, avionics and command and data handling. The BWB is not naturally stable and strongly depends on reliable control laws, sensors and data paths. Reliability is also linked to the fuel and propulsion system. The fuel system needs reliable pressure, temperature and purity control before the fuel reaches the engines to prevent engine failure. Therefore, the reliability focus should be on redundancy and fault detection, especially for critical systems.

24.1.2. Availability

Availability is defined as the ability of a system to remain in, or be returned to, an operable state [114]. For this concept, availability is mainly affected by maintenance access bio-SAF supply and supplier availability. The load-bearing fuel tanks may affect availability because leakage and fatigue inspection checks could keep the aircraft out of service for longer. Bio-SAF supply also affects availability since the aircraft can operate on the planned routes only if suitable fuel is available at the chosen airports. Finally, supplier availability affect the development and production schedule, especially with regard to the main structural components. Therefore, the availability focus should be on inspection access, fuel logistics and early supplier coordination.

24.1.3. Maintainability

Maintainability evaluates the ease, safety and efficiency with which maintenance actions can be performed [114]. For this concept maintainability is mainly driven by inspection and maintenance access for integrated fuel tanks, pressure shell, door and exit areas and above body engines. The load bearing fuel tanks act as both fuel storage and structural components. Therefore, leakage, fatigue and sealing issues need regular maintenance checks. The multibubble pressure shell may require specific inspection around the bubble junctions. Doors and emergency exits also affect maintainability, as their frames, seals and surrounding structure need to remain accessible for inspection. Above body engines may also be harder to access, so maintenance procedures should be developed early. Therefore, maintainability should focus on clear inspection routes, access panels, sensors monitoring and maintenance procedures that avoid major disassembly.

24.1.4. Safety

A system is considered safe when it does not cause unacceptable harm to people, the environment, or other assets during its life cycle [114]. For this concept, the main safety considerations are pressure shell integrity, crashworthiness, evacuation, fire protection and certification. The pressure shell needs to be analysed and tested in more detail to demonstrate it can safely withstand the cabin pressure, especially around the the multibubble junctions. Crashworthiness and evacuation also need further investigation, because the wide centrebody BWB differ from a conventional TAW aircraft. Fire protection is also another important aspect, since the fuel tanks are integrated into the primary structure. Therefore, safety should focus on pressure shell integrity, evacuation, fire protection and certifiction planning.

24.2. Future Risks

Starting from the RAMS characteristics presented above, the main technical risks for the next project phases are identified. The risks are listed in Table 24.1, where they are evaluated using the likelihood (L), consequence (C) and detectability (D) scales defined in Section 6.1. For each risk, the first L/C/D score represents the estimated risk level at the end of the DSE phase, before the proposed future mitigation actions are implemented. The second score represents the expected residual risk after these mitigation actions are applied.

In the register, the colour of the L/C/D cell represents the severity of the pre-mitigation risk based on the combination of the likelihood and consequence, as shown in the the risk maps, in Figure 24.1. The table first presents risks specific to the airframe, power and propulsion, monitoring and control and flight control and stability subsystems. Aircraft level and integration risks are presented at the end, since they affect multiple subsystems and project areas simultaneously.

Table 24.1: Subsystem level future technical risks

ID	Subsystem / interface	RAMS driver	Future risk	L/C/D before → after	Future mitigation / contingency
Airframe subsystema					
FR-01	Structures	Safety / Reliability	The final 3D pressure vessel geometry could lead to high local stress concentrations at the junctions between the pressure bubbles, which are not analysed in the current preliminary shell sizing.	3/4/3 → 2/4/2	**Mitigation:** In the next design phase, analyse the bubble junctions with a local 3D FEM model. Identify the critical junction radii, local thickness requirements and fatigue sensitive areas before the geometry is frozen. **Contingency:** If the local stresses are too high, add reinforcement rings or local pillars around the intersection, increase the local shell thickness or revise the layout of the pressure bubbles.
FR-02	Structures	Safety	The lower BWB centrebody structure may not provide sufficient controlled crash energy absorption, leading to excessive load transfer in the cabin.	3/4/3 → 2/4/2	**Mitigation:** Perform a crashworthiness and emergency-landing load analysis of the lower centrebody structure. **Contingency:** If energy absorption is not sufficient, add crushable structural elements, revise the cargo bay arrangement or reinforce the cabin-floor support structure.
FR-03	Doors	Safety / Maintainability	Passenger doors and emergency exits may be difficult to integrate in the final BWB geometry, having to pass through both the oval outer contour and the multibubble pressure shell. This could create issues with access, sealing and local reinforcement, especially near the wing transition area.	3/4/3 → 2/4/2	**Mitigation:** In the next design phase, check the passenger doors and emergency exits in the 3D model, verifying the access path, frames integration and required sealing and local reinforcement. **Contingency:** If an exit location is not feasible, relocate the exit and update the evacuation layout accordingly.
FR-04	Lifting surface	Reliability / Safety	The current aerodynamic analysis, mainly based on AVL with drag corrections, may not fully capture viscous, thickness and transonic effects around the BWB geometry. This could affect the predicted drag, cruise performance, lift distribution and control surface sizing.	4/3/3 → 2/3/2	**Mitigation:** Create a CAD model of the final geometry and validate the aerodynamic performance using CFD. **Contingency:** If the CFD results differ significantly, update the airfoil shape, cruise Mach number or control surface sizing.
FR-05	Windows	Safety / Maintainability	The current design does not define a window arrangement. If windows are added in later design phases, their integration through the oval outer contour and multibubble pressure shell may create local stress concentrations, pressure containment and maintenance challenges. In addition, the limited number and location of windows may reduce cabin lighting and passenger orientation, especially during an emergency evacuation.	3/2/3 → 1/2/2	**Mitigation:** Assess the possibility of structural windows integration in the final 3D geometry. Check the required local reinforcement, pressure sealing and inspection access and verify the cabin lighting and passenger orientation accordingly. **Contingency:** If windows are not feasible, use artificial lighting or virtual windows displays to support cabin lighting and passenger orientation.
FR-06	Landing gear	Reliability / Availability	The final landing gear position was only selected at preliminary level and the retracted landing gear volume has not been checked in detail. Its final position could change affecting centrebody load paths, ground clearance or compliance with the selected Code 4E / ADG V airport constraints.	3/3/3 → 2/3/2	**Mitigation:** Check the landing gear packaging in the final 3D geometry, including wheel volume, retraction kinematics, ground clearance and centrebody structure. In addition, check the landing and taxi loads for the gear attachments and include a backup system for extension in case the normal system fails. **Contingency:** If the gear does not fit or creates structural issues, move the gear, adapt the local structure or update the airport compatibility assumptions.
FR-07	Furnishings	Safety / Maintainability	The final cabin interior layout, including galleys, lavatories, crew rest areas and cabin equipment, may affect evacuation routes, mass distribution or maintenance access.	2/3/2 → 1/3/1	**Mitigation:** Verify compliance with evacuation standard. **Contingency:** If requirements are not met, review the cabin design and modify seat rail layout, seat spacing, seat pitch, lavatory geometry and aisle layout to ensure proper evacuation flow, accessibility, safety and weight distribution
Power and propulsion subsystems					
FR-08	Energy storage	Maintain -ability / Safety	The integrated load bearing fuel tanks may require more complex sealing, access and monitoring than assumed. Since the tanks are part of the primary structure, leakage, impact damage or fatigue could affect both fuel storage and structural integrity.	3/3/3 → 2/3/2	**Mitigation:** In the next design phase, define the tank sealing, access panels, leak detection and structural-health monitoring in more detail. **Contingency:** If the tanks are too difficult to inspect or seal, change the tank layout, add more access points or separate the most critical tank and structural parts.
FR-09	Energy storage	Safety / Reliability	Ullage overpressure, underpressure or fuel evaporation in the unpressurised fuel tank could lead to fuel vapour reaching its lower flammability limit. In addition, sloshing of fuel could create flight instability and exert additional loads on the fuel-tank structural components.	2/4/3 → 1/4/2	**Mitigation:** Use pressure sensors and vent lines in case of ullage overpressure or underpressure and fuel temperature sensors and heaters in case the fuel temperature falls outside the acceptable range. Include fuel-tank ullage inerting through nitrogen-enriched air and design ribs and lightening holes to reduce sloshing and optimise fuel flow. **Contingency:** If overpressure cannot be controlled, use the emergency fuel dump procedure, flight crew alerting through EICAS/ECAM and structural pressure-relief devices as passive last-resort protection.

ID	Subsystem / interface	RAMS driver	Future risk	Current L/C/D	Future mitigation / contingency
FR-10	Energy distribution	Safety / Maintainability	Incorrect conditioning of fuel purity, temperature or pressure prior to engine injection could reduce engine efficiency and may lead to engine flameout or failure.	2/4/3 → 1/4/2	**Mitigation:** Use multiple independent fuel lines with filters, pressure sensors with feedback to pressure regulation, and heat exchange for thermal regulation. Include fuel cross-feed lines in case of fuel quantity imbalance between the left and right tanks, and backup and segregated fuel pumps and fuel lines in case of pump, valve or piping failure. **Contingency:** If fuel conditioning failure causes flameout, use the engine relight procedure, cross-feed from the opposite tank or line to bypass the degraded conditioning path and the crew checklist for single-engine operation and diversion under OEI conditions.
FR-11	Engine	Availability / Reliability	An engine fire could lead to engine failure and the possibility of the fire spreading to the structure and fuel tanks, resulting in catastrophic failure.	2/4/3 → 1/4/2	**Mitigation:** Include an engine fire-protection system that cuts off fuel supply, hydraulic fluid and bleed air, and discharges fire-extinguishing agent within the engine. Ensure that all performance and thrust calculations are checked for OEI conditions to support safety and CS-25 compliance. **Contingency:** If one engine or generator is lost, use the cross-tie bus architecture between the engine and APU VFSG architecture to prioritise electrical distribution to key systems.
FR-12	Secondary / Emergency power	Safety / Reliability	Loss or degradation of the main and backup power supply could lead to partial or total failure of flight controls, landing gear extension or retraction, thrust reversers, trim controls, pumps, gearboxes, pressurisation, air conditioning or anti-ice systems. These failures could have severe consequences, especially for the inherently unstable BWB configuration.	3/4/3 → 2/4/2	**Mitigation:** Use multiple power-transmitting lines and sources, including RATs for electrical and hydraulic power generation, the APU in case the failure is caused by engine failure, and other electrical redundancies such as batteries and cross-tie buses allowing load sharing. **Contingency:** If primary and backup generation are lost, use automatic load shedding to prioritise flight controls and essential avionics, and keep the aircraft controllable through degraded flight-control laws until emergency power is restored.
Monitoring and control subsystems					
FR-13	Ice and rain protection	Safety / Reliability	If the ice and rain protection system is not sized correctly, ice could build up on exposed probes or control surfaces, and heavy rain could affect external sensors. This could give unreliable flight data or reduce control response in bad weather conditions.	2/3/3 → 1/3/2	**Mitigation:**Identify the sensors, probes and surfaces that need ice and rain protection and size the protection system for the selected operating conditions. **Contingency:** If reliability is still not sufficient, add sensor redundancy or revise the sensor, probe and protected-surface placement.
FR-14	Fire protection subsystem	Safety	The fire detection and suppression system for the above-body engines, fuel lines and integrated fuel-tank structure is not defined in detail yet. If the isolation and suppression are not sufficient, an engine or fuel-system fire could spread to the structure or tanks.	3/4/4 → 2/4/2	**Mitigation:** Define the fire zones, detection sensors, suppression system and redundancy requirements. **Contingency:** If the fire risk remains too high, increase the separation from the engines, add shielding, move critical equipment or add extra fire protection.
FR-15	Thermal management	Reliability / Availability	Thermal loads from avionics, electrical systems, cabin systems and above-body engines may be higher than assumed. This could cause overheating of critical equipment.	3/3/3 → 2/3/2	**Mitigation:** Perform detailed thermal-load sizing for normal and abnormal cases. **Contingency:** If the cooling capacity is not sufficient, increase the cooling system, improve heat rejection or move some equipment.
FR-16	Avionics	Reliability / Availability	The avionics architecture, redundancy level and verification plan of the fly-by-wire system are not defined in detail yet. This could increase the complexity of the safety-critical avionics and the certification effort.	3/4/3 → 2/4/2	**Mitigation:** Define the avionics architecture, redundancy level and verification plan for the safety-critical functions. **Contingency:** If the architecture becomes too complex, separate the safety-critical and non-critical functions more clearly or simplify the avionics architecture.
FR-17	Command and data handling	Reliability / Safety	The command and data handling system may become more complex than assumed because it has to connect fly-by-wire, sensors, monitoring systems and other subsystems. If the data paths are not defined clearly, safety-critical data could be delayed or lost.	3/3/3 → 2/3/2	**Mitigation:** Define the data architecture and the safety-critical communication paths early. **Contingency:** If the integration becomes too complex, separate the safety-critical and non-critical data functions more clearly and add redundancy to the critical data paths.
FR-18	Cabin subsystem	Safety / Maintainability	The wide BWB cabin may not meet evacuation requirements once passenger flow, aisle congestion, exit accessibility, slide arrangement and emergency lighting are checked in detail.	3/4/3 → 2/4/2	**Mitigation:** Perform a dedicated evacuation and passenger flow simulation, including exit locations, slides, cabin crew positions and emergency lighting. **Contingency:** If the evacuation requirement is not met, revise the aisle layout, exit distribution or cabin arrangement.
FR-19	External lighting	Safety / Maintainability	The BWB shape may make external lighting placement more difficult. Some lights may not have the required visibility or may be difficult to access for maintenance	2/2/2 → 1/2/1	**Mitigation:** Check external lighting visibility and maintenance access during the detailed layout design. **Contingency:** If the visibility is not sufficient, move the lights or add additional lighting units.
Flight control and stability subsystems					

ID	Subsystem / interface	RAMS driver	Future risk	Current L/C/D	Future mitigation / contingency
FR-20	Flight control subsystem	Safety / Reliability	The stability and control characteristics are not confirmed with enough confidence yet. The current aerodynamic derivatives are based on preliminary methods, so the required control authority and fly-by-wire behaviour may still change in later analyses.	3/4/3 → 2/4/2	**Mitigation:** Repeat the stability and control analysis with higher-fidelity aerodynamic methods over the full CG range and flight envelope. **Contingency:** If the control authority is not sufficient, revise the control-surface sizing, CG limits, flight-control logic or operating limits.
FR-21	Stabilisers subsystem	Safety / Reliability	Split-drag rudders were selected for lateral and directional control, but their final effectiveness still needs to be confirmed with higher-fidelity analysis. If they are not sufficient, the stabilisation concept may need to be changed or compared again with alternatives such as a V-tail.	3/3/3 → 2/3/2	**Mitigation:** Perform a detailed yaw-control and lateral-stability analysis, including OEI, actuator loads and failure cases. **Contingency:** If the selected concept is not sufficient, increase the control-surface effectiveness or reconsider another stabiliser concept.
Aircraft-level and integration risks					
FR-22	Aircraft-level certification	Safety / Reliability	The certification basis for the BWB may be difficult to define because several parts of the aircraft do not follow a conventional tube-and-wing layout. This includes the pressure shell, evacuation layout, flight-control system and rescue and fire-fighting category.	3/4/3 → 2/4/2	**Mitigation:** Start certification discussions early and link the novel BWB features to the applicable CS-25 requirements and possible special conditions. **Contingency:** If certification issues become critical, update the layout, verification plan or operational assumptions before design freeze.
FR-23	MAI / supplier availability	Availability / Maintainability	The MAI plan depends on several selected European suppliers for the BWB shell, pressure module, wingbox and metallic parts. If supplier capacity or availability is lower than assumed, the prototype build could be delayed or the supplier split may need to change.	3/3/2 → 2/3/1	**Mitigation:** Confirm supplier availability and production capacity early, especially for the metallic parts and pressure-module work. Define backup suppliers for the main bottleneck areas. **Contingency:** If one supplier cannot support the schedule, move part of the work to a backup supplier, split the work differently or update the assembly schedule.
FR-24	MDAO / design tools	Reliability	The final design may still depend strongly on the assumptions used in the preliminary models. Since OpenMDAO links the aerodynamic, mass, propulsion and stability models, an error in one model could affect the final sizing and performance results.	3/3/3 → 2/3/2	**Mitigation:** Check the MDAO results with independent calculations, CAD geometry checks, CFD, higher-fidelity simulations and sensitivity studies. **Contingency:** If large differences are found, update the affected models and repeat the sizing or performance analyses.
FR-25	Bio-SAF supply / fuel logistics	Availability	Bio-SAF availability or cost may be worse than assumed on some routes. Since the aircraft uses Bio-SAF, the first routes should be chosen based on airports where the fuel is available or can be arranged in advance.	3/3/2 → 2/3/1	**Mitigation:** Check Bio-SAF availability at the hub and stopover airports and arrange fuel supply early. **Contingency:** If the fuel supply is not sufficient, limit the first route network, add technical stops or use other certified Bio-SAF suppliers.

Mitigation actions and contingency measures affect the post-mitigation likelihood, consequence and detectability scores. In general, design analyses and early testing reduce risk likelihood, contingency measures reduce risk consequence and monitoring and inspections improve detectability.

24.3. Pre- and Post- Mitigation Risk Maps and Monitoring Approach

Based on the evaluation of the future risks described in Table 24.1, the pre-mitigation and post-mitigation risk maps in Figure 24.1 and Figure 24.2 are obtained. The pre-mitigation map shows several risks clustered in the probable/critical or probable/catastrophic regions. The highest risks are related to the pressure shell, crashworthiness, doors and emergency exits integration, emergency power, fire protection, avionics, evacuation, flight control and certification. Their mitigations should therefore be the focus of the next design phase.

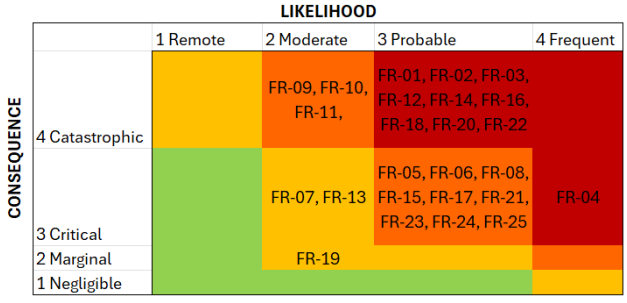

Figure 24.1: Pre-mitigation technical risk map

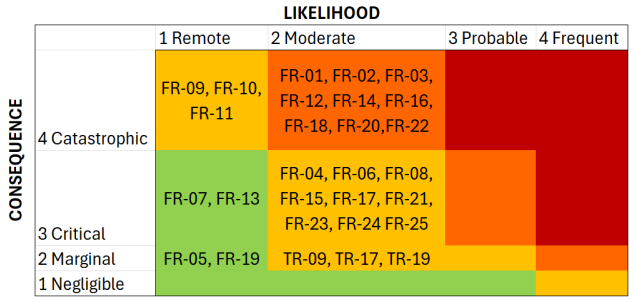

Figure 24.2: Post-mitigation technical risk map

After mitigation, several risks shift towards lower likelihood, as shown in the post-mitigation map. However, several risks still still have catastrophic consequences after mitigation, especially FR-01, FR-02, FR-03, FR-12, FR-14, FR-16, FR-18, FR-20 and FR-22. These risks mainly concern structural integrity, emergency access and evacuation, power and fire safety, avionics, flight control and certification. Therefore, they should should be monitored carefully in the next design phases.

Many of risks identified concern interactions between subsystems, rather than one subsystem alone. The pressure shell affects the doors positioning and the evacuation layout. The flight-control risks are linked to the aerodynamic

assumptions, avionics and emergency power. The fuel-tank and fire-protection risks are also linked, because the tanks are part of the primary structure. For this reason, the risk register should be updated whenever one of these linked design areas changes.

In the future design phases, the risk register should be used as a monitoring tool at each major design iteration. First, the mitigation actions from Table 24.1 should be implemented for the most critical pre-mitigation risks. The risk map should then be updated accordingly. If any risk do not reduce as expected or moves back to an unacceptable region, the corresponding contingency action should be activated before the design is frozen.

24.4. Risk Derived Requirements

Requirements are derived for risks that remain most relevant for the future design work. These are shown in Table 24.2,

Table 24.2: Technical risk-derived requirements

RSK-REQ	Related risk	Risk requirement
01	FR-01	The pressure vessel bubble junctions shall be checked with a local 3D finite-element model before the pressure-shell geometry is frozen. The analysis shall identify the critical local stresses, required local thicknesses and fatigue-sensitive areas.
02	FR-02	The lower BWB centrebody and cabin floor support structure shall be checked for the selected crash and emergency-landing load cases. The analysis shall show whether the structure can limit excessive load transfer into the cabin.
03	FR-03	Passenger doors and emergency exits shall be checked in the final 3D BWB geometry for access path, frame integration, sealing and required local reinforcement.
04	FR-04	The final BWB aerodynamic geometry shall be checked with a higher-fidelity aerodynamic method before the aerodynamic shape and control-surface sizing are frozen. The check shall include drag, lift distribution, cruise performance and control-surface effectiveness.
05	FR-08	The load-bearing fuel tanks shall include defined sealing, inspection access, leak detection and structural-health monitoring provisions for leakage, fatigue and local damage.
06	FR-09	The fuel-storage system shall include ullage pressure control, fuel-temperature monitoring, ullage inerting and anti-sloshing features for the selected tank operating conditions.
07	FR-10	The fuel-distribution system shall provide pressure, temperature and purity control before engine injection, with monitoring of the relevant fuel-transfer conditions.
08	FR-11 / FR-14	The engine and fuel-system fire-protection layout shall define the fire zones, detection sensors, suppression provisions, fuel shut-off logic and isolation of critical fluids.
09	FR-12	The emergency and backup power architecture shall be checked for continued supply to essential flight-control and avionics functions after loss or degradation of one main power source.
10	FR-16 / FR-17	The avionics and command and data handling architecture shall define the redundancy level, safety-critical data paths and fault-monitoring provisions for flight-control and monitoring functions.
11	FR-18	The cabin and emergency-exit layout shall be verified with a dedicated evacuation or passenger-flow simulation for the selected passenger and crew configuration.
12	FR-20 / FR-21	The flight-control and stabiliser concept shall be reassessed with higher-fidelity aerodynamic methods over the full CG range and flight envelope, including OEI yaw-control cases, actuator loads and relevant failure cases.
13	FR-22	The certification basis for the main BWB-specific features shall be reviewed with the relevant certification authority and linked to the applicable CS-25 requirements or special conditions before design freeze.
14	FR-23	Supplier availability and production capacity shall be confirmed for the main structural components, including the BWB shell, pressure module, wingbox and metallic parts. Backup suppliers shall be identified for the main bottleneck items.
15	FR-24	The MDAO results shall be checked against independent calculations, CAD geometry checks, higher-fidelity simulations and sensitivity studies before they are used to freeze major sizing decisions.
16	FR-25	Bio-SAF availability shall be checked for the selected hub and stopover airports before the initial operational route network is fixed.

25
Project Design and Development Logic

This chapter outlines the post–DSE design and development logic for the POGA up to entry into commercial service in 2035. The future tasks are divided into two distinct phases, the first phase after DSE and seventh in the current project phase framework: **Industrial level design** which lasts until the first test flight milestone and the second phase after DSE, and eighth phase in the project logic: **Certification and service introduction** last until entry to service.

The sequence is presented in more detail in Figure 25.1 and describes the transition from the DSE preliminary design to an industrially viable aircraft programme, including prototype manufacture, ground and flight testing, type certification, route proving and cooperation with operators. A time estimate for all tasks is presented in Figure 25.2.

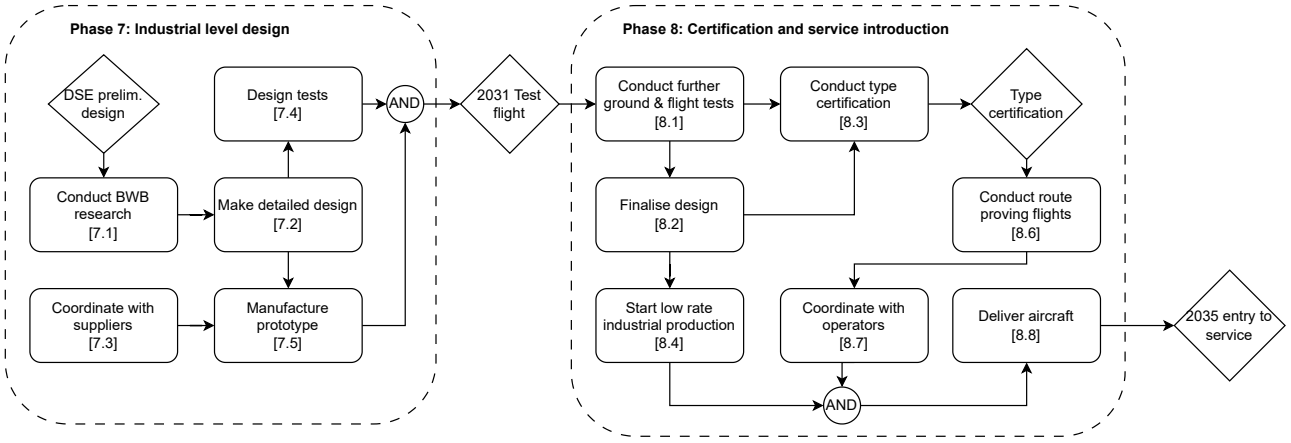

Figure 25.1: Post–DSE design and development logic for the POGA.

25.1. From DSE Preliminary Design to Detailed Design

At the end of the DSE, a preliminary BWB configuration and subsystem architecture are delivered at preliminary design level, which is the design outlined in this report. This configuration is used as the starting point for the industrial-level design phase.

Although the DSE outcome provides a coherent BWB layout, many empirical methods and certification practices in current industry are still calibrated to conventional tube-and-wing aircraft. As a result, the next step towards an operational design is to conduct further research on BWBs over a period of roughly one year, specifically on:

- Structural and loads estimation for non-cylindrical pressure vessels and integrated wing–fuselage structures;
- Lateral stability of BWB aircraft;
- Control surface sizing methods of BWB aircraft;
- BWB aircraft mass estimation methods;
- Airfoil optimization methods for BWB;
- Advanced drag reduction methods for BWB aircraft ;
- systems layout, evacuation, maintenance access and certification aspects that differ from tube-and-wing baselines.

The outcome of this activity is an updated set of analysis tools and design guidelines suitable for a BWB at CS-25 level. These tools then serve as the means through which the detailed design can be created. In this detailed design phase, with a duration of approximately one year, the structural concept is frozen at drawing level, system architectures and interfaces are finalised, and industrialisation planning is carried out in cooperation with key suppliers and operators. In parallel, coordination with suppliers starts shortly after the BWB research starts and continues up to the completion of the detailed design to prepare tooling, qualification and manufacturing routes for the prototype and for later series production.

25.2. Prototype Manufacture and Initial Test Campaign

Once the detailed design is mature enough, long-lead items are released and the first flight-test article is built in the Manufacture prototype step. This phase is expected to take about one year, matching the upper bound of the prototype manufacturing estimate from Chapter 23. The prototype is configured as a test aircraft with added instrumentation and provisions for later modifications, following the MAI plan in Chapter 23.

In parallel, the Design tests activity prepares the ground and flight test programme. It defines test objectives, selects outstanding Methods of Compliance (MoC) not yet specified in Section 18.1, sets instrumentation requirements, and

plans envelope-expansion and performance tests. The result is an integrated test plan linking each test to certification items and design verification objectives.

Completion of prototype build, basic ground tests and regulatory readiness leads to the 2031 test flight milestone, marking first flight of the prototype.

25.3. Ground and Flight Testing, Design Finalisation

After first flight, the development enters a cycle of testing and design refinement. The Conduct further ground & flight tests step lasts about four years and covers structural, systems and performance testing. Ground activities include system integration, environmental tests and any required static or fatigue follow-up, while flight tests explore the operational envelope, handling qualities, performance, failure modes and noise.

Test results feed into Finalise design, where discrepancies between prediction and measurement are resolved through local design changes, software updates or revised operating limitations. Once the necessary changes have been verified and validated, the configuration is frozen for production. This finalisation, together with Low-Rate Initial Production (LRIP), takes about one and a half years and marks the start of low-rate series manufacture while certification is still ongoing.

25.4. Type Certification and Route Proving

In parallel with testing and LRIP, the Conduct type certification activity runs for several years. It covers the certification basis, special conditions for BWB-specific features, compliance demonstrations and the supporting documentation for the authorities. The Type certification milestone represents issue of the Type Certificate once all requirements are met.

After certification, the aircraft enters route proving flights for a few months. These flights use representative long-haul missions with airline crews to validate procedures, turnaround, maintenance concepts, dispatch reliability and airport compatibility.

25.5. Operator Cooperation and Entry into Service

The final phase is captured by Operator cooperation and the 2035 entry to service milestone. Over roughly one to one-and-a-half years, the manufacturer and launch airlines prepare crew training, maintenance procedures, spares provisioning, manuals and fleet introduction planning.

Once customer aircraft are delivered, crews are trained and all approvals are in place, the aircraft enters commercial operation. This is represented by the 2035 entry to service diamond, consistent with the requirement that the aircraft shall be operable by 2035. From then on, continuous improvement and retrofit activities continue through the fleet life.

25.6. Post DSE GANTT chart

Figure 25.2 summarises the explicit post DSE timeline used for this project. BWB research and supplier coordination start in mid 2026, followed by about one and a half years of detailed design. Prototype manufacturing and test preparation run from spring 2029 to late 2030, leading to first flight in September 2030, ahead of the 2031 requirement. The main test campaign then runs from late 2030 to late 2034, overlapping with type certification, design finalisation and LRIP. Type certification is targeted for late 2034, after which route proving and intensified operator cooperation continue up to mid 2035. Entry into service is scheduled around May 2035, satisfying the requirement that the aircraft shall be operable by 2035.

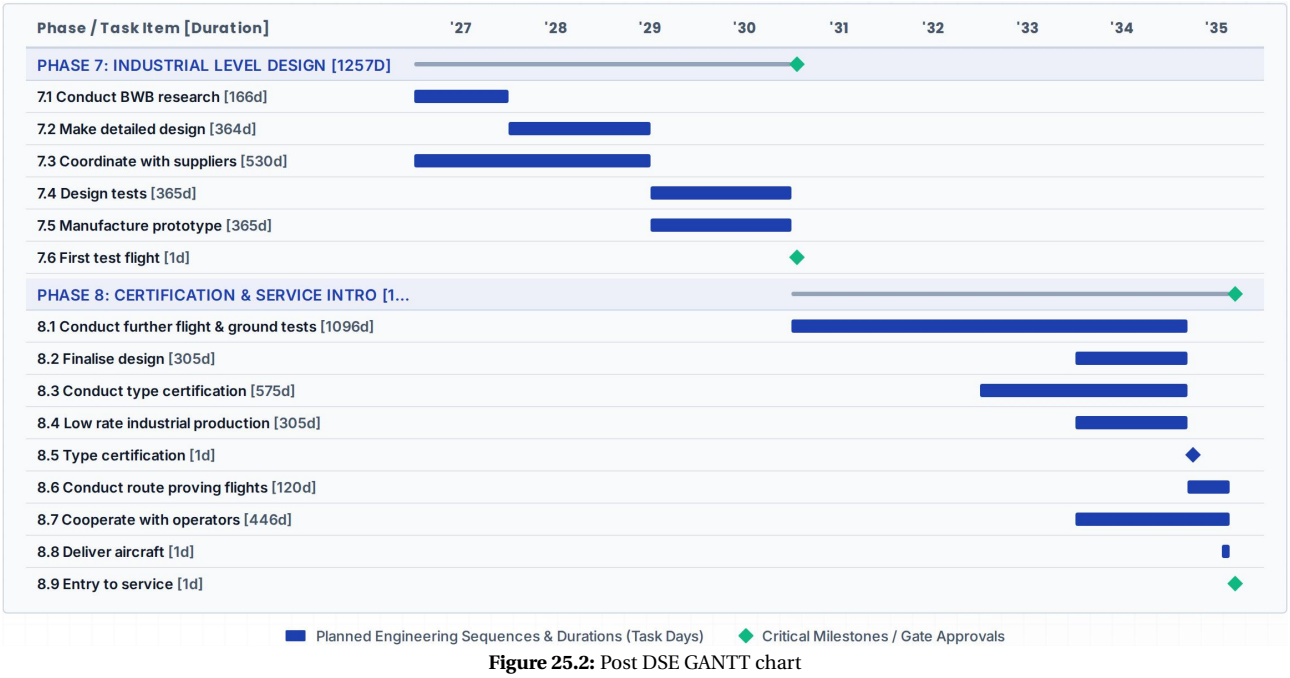

Figure 25.2: Post DSE GANTT chart

26
Recommendations

This chapter outlines the key recommendations for the continued development of the BWB aircraft, addressing the limitations encountered during this phase of the project. The recommendations are categorised by discipline to guide future design iterations. Section 26.1 discusses operations and logistics, focusing on turnaround validation and airport compatibility. Next, Section 26.2 and Section 26.3 highlight the need for higher-fidelity analysis to validate control surface sizing, dynamic stability, and aerodynamic profiles. Section 26.4 addresses engine selection and the acquisition of accurate efficiency data, while Section 26.5 outlines necessary refinements to the 3D structural model and multibubble pressure shell. Finally, Section 26.6 reflects on the OpenMDAO framework and proposes improvements to the automated optimisation tool.

26.1. Operations & Logistics

The O&L has discussed the aircraft operational aspect with current design choices. However, several recommendations should be highlighted due to limitation of DSE project. This should not change the overall operational concept, but to further verify the airport, maintenance, evacuation and fuel-supply interfaces.

The turnaround concept should be validated with a more detailed GSE layout, especially around passenger boarding, baggage service, catering, cleaning, refuelling and technical inspection. The current 95 minute turnaround target should be kept but further verification, validation and optimization should be carried. Bio-SAF logistics should be treated as a route-planning constraint which heavily depend on the industry development. Since the aircraft depends fully on non-petroleum fuel, future route selection should also confirmed Bio-SAF availability at the airports.

The maintenance concept should be developed further for the above-body engines and load-bearing fuel tanks. The camera-based engine inspection system should be detailed designed and certified. Access platforms or dedicated maintenance stands should also be defined with specified dimensions. For the load-bearing tanks, leak detection, pressure monitoring and structural-health monitoring should be further studied.

The cabin comfort including possible interior lighting system as a replacement of the windows may be considered. Also, the emergency operation concept requires dedicated verification. The wide BWB cabin and multiple aisles can support boarding and evacuation, but the 90 second requirement should be simulated and demonstrated. The final exit locations, slide arrangement, cabin crew positions and emergency lighting should be adjusted.

The rescue and firefighting category should be discussed with certification authorities and airport operators, because the equivalent fuselage width of a BWB is very different comparing to the conventional tube-and-wing aircraft as mentioned in Section 20.8.

Last but not least, the cockpit arrangement should also be further considered in the next design phase. In the current design, the cockpit is mainly modelled as an extended airfoil section at the centre of the aircraft. This is not detailed enough for later aircraft development. The cockpit layout needs to be studied together with the pilot seating position, flight deck arrangement, crew access, emergency escape and the connection between the cockpit and the main cabin structure. Due to the BWB configuration, the cockpit shape will also affect the local aerodynamic performance and should be optimised. Another important aspect is pilot visibility. The view during take-off, landing and high angle of attack conditions should be checked carefully, since the wide nose and blended body shape may limit the downward and side field of view.

26.2. Stability & Control

The stability and control analysis discussed the stability characteristics and control surfaces required to meet certification requirements. However, several recommendations should be highlighted due to limitation of the DSE project.

Due to the low confidence in the computed values derived from AVL, no numerical comparison for control surface sizing were presented. It is recommended to address this limitation in future work by re-running AVL with reduced deflection amplitudes and cross-checking with a higher-fidelity method. Additionally, the absence of trustworthy control and stability analysis means that the aircraft's dynamic stability modes and overall handling qualities could not be definitively verified. Future iterations must prioritise obtaining accurate aerodynamic derivatives across the full flight envelope to validate the provisional baseline, so that the control surfaces can be sized using high-fidelity methods.

For lateral stability, a configuration with split-drag rudders were selected, which meets the OEI requirement. For future research, it is recommended to analyse other configurations for lateral stability, such as a V-tail.

Furthermore, a sensitivity analysis of the stability and control characteristics is recommended for future work. The current analysis is performed at a few representative operating points, such as cruise, loiter and approach, with fixed mass properties. A systematic sensitivity analysis should map how the dynamic mode eigenvalues, static margin and control authority margins vary across the mass states, CG and flight envelope. In particular the variation of the Dutch roll damping and phugoid stability should be quantified, as these are known to be sensitive parameters for the BWB [4].

Due to the inherent instability of the BWB and immense usage of FBW and SAS, it is of utmost important that pilot's receive training on how the controllability and stability of a BWB functions, as they deviate significantly from TAW configurations. Further research should explore what the training should entail in detail.

26.3. Aerodynamics

First recommendation is to make a greater work on airfoil optimisation for the body part. The performance shall be increased even with small reference area penalty. There should be found a compromise which would lead to better overall performance.

Second, connected to the first point, if the airfoil with high thickness to chord ratio is inevitable to fit the cabin, it is recommended to explore the lower Mach numbers. Higher t/c lead to the formation of shock waves and thus higher drag, flying on the lower Mach number would be a solution to that.

Third, while AVL is an essential program for basic aerodynamic analysis, it is recommended to create the CAD model and perform a computation fluid dynamics analysis. This would give an insights into the nuances that AVL cant include and would give a higher overall accuracy.

26.4. Power & Propulsion

Based on the extent of the current preliminary design within the Power & Propulsion itself, the main recommendation is to identify engines within the range of 143 and 296 kN with high efficiencies (over 40% for overall efficiency during cruise), and have them tested on neat SAF to ensure compatibility as previously discussed in Section 17.1. As the current LEAP-1A and GEnx-2B provide too large of a sea level static thrust gap and hence a weight gap of almost two and a half tons. This can lead to system weight reductions of up to two tons, or possibly even more if the engines bridging this gap provide higher efficiencies than the current GEnx-2B that is used by the current aircraft.

As an additional note that caused difficulties as described in Section 11.3. The fact that engine efficiency parameters are proprietary manufacture information, the calculation of the specific fuel consumption gets a little more complicated, as gas turbine efficiency relations have to be used as detailed in Section 11.2, these equations use variables that are more commonly available to the public however are not as reliable as efficiency metrics would be from the manufacturer itself. Therefore a proper partnership (in the scope of this DSE project) with the engine manufacturer itself in order to gain access to the actual data would increase accuracy of the performance calculations resulting a more adequate propulsion system sizing and hence aircraft sizing.

26.5. Structures

There are several aspects of the structural analysis that can be refined in the next design phases. First, a three dimensional model of the full centrebody structure should be developed. This is especially important for the multibbuble pressure shell, where the bubble junctions, pressure end caps and local geomtric transitions need to be investigated to verify that the shell can withstand cabin pressurisation. In the current structural analysis, a simplified cross section is used for preliminary sizing, which does not capture all the stress concentrations.

The internal columns distribution should also be checked against the cabin layout. In the current model, these members are sized for structural loads but their interaction with cabin and access requirements has not been fully assessed.

Finally, the multibubble layout should also be investigated together with the cargo layout. In the current model, the cargo is fitted in the large central bubble, since the side bubbles do not provide enough space. Future work should therefore investigate alternative bubble arrangements, for example different bubble radii or a larger number of bubbles. This should be analysed carefully, since additional bubbles may improve packaging but would also introduce extra columns and structural complexity.

26.6. Overall Design Methodology Reflection

The design tool that was created for this BWB design in OpenMDAO was mostly successful, but it must be noted that the initial aim of automatically optimising the design through this framework was not able to be executed. As such, if this project were to be extended it would recommended to rework some components of the tool so that it is compatible with the MDAO optimisation. Particularly, the propulsion sizing component at the moment uses a database of existing engines to select for the design. The consequence of this is that OpenMDAO sees a stepwise change in propulsion parameters, which breaks the optimiser. Instead, it would likely be better if the performance sizing component only calculates the minimum values required for the design and then an engine is selected post-optimisation.

Additionally, there is quite some uncertainty due to the fact that the verification process used is not very extensive. To build more confidence in this tool, and take this design further, it would also be recommended to rebuild components around unit tests to ensure that their functionality is correct and so the entire model is more robust.

Finally, the tool is built specifically for BWB aircraft with a geometry particularly built for this design. This unfortunately means that to validate this model is difficult, especially when considering that there are not that many existing BWB aircraft. The recommendation would be to figure out how to use reference aircraft as test cases in the model, to ensure that all parameters can be validated, or to adapt the aircraft geometry build-up such that any aircraft can be input into the model and its performance characteristics can be found reliably.

27
Conclusion

The mission of this project is to establish a feasible design for the "Post Oil Global Airliner" with no kerosene fuel and minimisation of oil-based materials during the material selection. This report presents a preliminary design of the Blended Wing Body with 120 passengers and minimal range of 3,000 km.

Establishment of the design was done through the iteration of each module to achieve the final design. Starting with cabin, fuselage and wing planform, the goals of these modules are to generate basic geometry. The aerodynamic module, with the help of AVL, compute basic aerodynamic performance for the geometry. The Power and Propulsion module compute the required thrust and sizing of the engines, as well as the number of them. The mass module, containing Class I and Class II mass estimation, are dealing with the mass convergence and stability and controllability calculate the basic derivatives for the iterations. All of those modules are connected by the MDAO to find the most optimal preliminary design.

The final design consist of fuselage with reference area of 598 m^2, with the total wingspan of 64.9 m. The maximum take-off weight converged to 131554 kg. To accommodate such a high surface area and maximum take-off weight, 2 engines GEnx type 2B67B are added, with the usage of Sustainable Aviation Fuel (SAF). The SAF is located in the wings with the help of load bearing tanks. With this design, the range design are achieved with the high safety margin, specifically 5,530 km of range in one flight, and 16,000 km of range in 24 hours. The achieved L/D of 17.84 makes the design competitive with airliner of similar passenger amount and range.

In conclusion, the Post-oil Global Airliner preliminary design demonstrates that a blended wing body configuration powered by bio-based Fischer-Tropsch SAF is technically feasible, commercially viable, operationally feasible, and achievable within the stated programme timeline. The converged design satisfies the primary range, payload, and fuel requirements while meeting Code 4E airport compatibility. The most significant open design items, longitudinal pitch instability, pressure-shell junction stress distribution, and control surface authority under degraded conditions, have been formally captured in the risk register with defined mitigation actions, and form the primary input to the recommended next design phase. The team is confident that the preliminary design established in this report provides a coherent and defensible baseline from which a full detailed design programme can proceed.

Bibliography

[1] Lee, D. S., Fahey, D. W., Skowron, A., Allen, M. R., Burkhardt, U., Chen, Q., Doherty, S. J., Freeman, S., Forster, P. M., Fuglestvedt, J., Gettelman, A., De León, R. R., Lim, L. L., Lund, M. T., Millar, R. J., Owen, B., Penner, J. E., Pitari, G., Prather, M. J., Sausen, R., and Wilcox, L. J., "The contribution of global aviation to anthropogenic climate forcing for 2000 to 2018," Atmospheric Environment, Vol. 244, 2021, p. 117834. doi: 10.1016/J.ATMOSENV.2020.117834, URL https://www.sciencedirect.com/science/article/pii/S1352231020305689.

[2] International Civil Aviation Organization, "Resolution A41-21: Consolidated statement of continuing ICAO policies and practices related to environmental protection — Climate change," , Oct. 2022. URL https://www.icao.int/sites/default/files/Resolution_A41-21_Climate_change.pdf, adopted at the 41st Session of the ICAO Assembly.

[3] Gray, J. S., Hwang, J. T., Martins, J. R. R. A., Moore, K. T., and Naylor, B. A., "OpenMDAO: An Open-Source Framework for Multidisciplinary Design, Analysis, and Optimization," Structural and Multidisciplinary Optimization, 2019. In Press.

[4] Okonkwo, P. P. C., "Conceptual Design Methodology for Blended Wing Body Aircraft," Phd thesis, Cranfield University, May 2016.

[5] {van Dommelen}, J., and Vos, R., "Conceptual Design and Analysis of Blended-Wing Body Aircraft," Journal of Aerospace Engineering, Vol. 228, No. 13, 2014, pp. 2452–2474. doi: 10.1177/0954410013518696.

[6] Howe, D., "Blended wing body airframe mass prediction," Proceedings of the Institution of Mechanical Engineers, Part G: Journal of Aerospace Engineering, Vol. 215, No. 6, 2001, pp. 319–331. doi: 10.1243/0954410011533329, URL https://doi.org/10.1243/0954410011533329.

[7] Howe, D., Aircraft Conceptual Design Synthesis, Professional Engineering Publishing, 2000.

[8] Roskam, J., Airplane Design. Part 5. Component weight estimation, DAR Corporation, 2019.

[9] European Aviation Safety Agency, "Certification Specifications for Large Aeroplanes CS-25," , 9 2007.

[10] Yin, F., et al., "A comprehensive well-to-wake climate impact assessment of sustainable aviation fuel," Scientific Reports, 2025. doi: 10.1038/s41598-025-13445-x, URL https://www.nature.com/articles/s41598-025-13445-x.

[11] Raymer, D., "Enhancing aircraft conceptual design using multidisciplinary optimization /," , 01 2002.

[12] Voth, V., Lübbe, S. M., and Bertram, O., "Estimating Aircraft Power Requirements: A Study of Electrical Power Demand Across Various Aircraft Models and Flight Phases," Aerospace, Vol. 11, No. 12, 2024. doi: 10.3390/aerospace11120958, URL https://www.mdpi.com/2226-4310/11/12/958.

[13] Chevron, "Chevron Global Aviation Aviation Fuels Technical Review," , 2006. URL www.chevronglobalaviation.com/ga/ga_operational.asp.

[14] Keiser, D., Schnoor, L. H., Pupkes, B., and Freitag, M., "Life cycle assessment in aviation: A systematic literature review of applications, methodological approaches and challenges," Journal of Air Transport Management, Vol. 110, 2023, p. 102418. doi: https://doi.org/10.1016/j.jairtraman.2023.102418, URL https://www.sciencedirect.com/science/article/pii/S0969699723000613.

[15] Federal Aviation Administration Flight Standards Service Regulatory Support Division, "FEDERAL AVIATION ADMINISTRATION JOINT AIRCRAFT SYSTEM/COMPONENT CODE TABLE AND DEFINITIONS," , 10 2008.

[16] V Chan, W. K., Zacharewicz, G., Mustafee, N., Wainer, G., San Antonio Aeronautical Management, A., Juan, A. A., Fonseca Casas, P., and Guimarans, D., "USING SIMULATION TO ESTIMATE CRITICAL PATHS AND SURVIVAL FUNCTIONS IN AIRCRAFT TURNAROUND PROCESSES," Proceedings of the 2017 Winter Simulation Conference, 2017. URL http://www.eurocontrol.int.

[17] McCausland, R., "Hydrogen for aviation A future decarbonization solution for air travel?" , 2025.

[18] European Aviation Safety Agency, "EASA Certification Roadmap on H2-International Workshop 2024 On-site event Event Materials Documents EASA Certification Roadmap on H2 Workshop-Presentations," , 2024.

[19] Behán, A. K., Boekema, F., Kao, W.-J., Kort, C., Malacarne, G., Gonzalez, L. M., Robinson, A., Savchenko, A., Wehsely, I., and Xu, Y., "Baseline Report: Post-oil Global Airliner," , 2026.

[20] Ciampa, P. D., Prakasha, P. S., Torrigiani, F., Walther, J.-N., Lefebvre, T., Bartoli, N., Timmermans, H., Vecchia, P. D., Stingo, L., Rajpal, D., van Gent, I., Rocca, G. L., Fioriti, M., Cerino, G., Maierl, R., Charbonnier, D., Jungo, A., Aigner, B., Anisimov, K., Mirzoyan, A., and Voskuijl, M., Streamlining Cross-Organizational Aircraft Development: Results from the AGILE Project, AIAA, 2019. doi: 10.2514/6.2019-3454, URL https://arc.aiaa.org/doi/abs/10.2514/6.2019-3454.

[21] Lambe, A. B., and Martins, J. R. R. A., "Extensions to the Design Structure Matrix for the Description of Multidisciplinary Design, Analysis, and Optimization Processes," Structural and Multidisciplinary Optimization, Vol. 46, 2012, pp. 273–284. doi: 10.1007/s00158-012-0763-y.

[22] Drela, M., and Youngren, H., AVL User Primer, Massachusetts Institute of Technology, Department of Aeronautics and Astronautics, 2014. URL https://web.mit.edu/drela/Public/web/avl/, version 3.32.

[23] Roskam, J., Airplane Design Part VIII: Airplane Cost Estimation: Design, Development, Manufacturing and Operating, DARcorporation, 1990.

[24] Liebeck, R. H., "Design of the Blended Wing Body Subsonic Transport," Journal of Aircraft, Vol. 41, No. 1, 2004, pp. 10–15. doi: 10.2514/1.9084.

[25] Raymer, D. P., Aircraft Design: A Conceptual Approach, 6th ed., American Institute of Aeronautics and Astronautics, Reston, VA, 2018.

[26] Brown, M., and Vos, R., "Conceptual design and evaluation of blended-wing-body aircraft," AIAA Aerospace Sciences Meeting, 2018, 2018. doi: 10.2514/6.2018-0522.

[27] Whitcomb, R. T., "Review of NASA supercritical airfoils," , 1974. URL https://ntrs.nasa.gov/citations/19740024976.

[28] Airbus SAS, "ICAO / EASA Aerodrome Reference Code, FAA Airplane Design Group and Aircraft Approach Category for Airbus Aircraft," , Jul. 2020. Issue 4.0, Airport Operations.

[29] Mulyanto, T., and Nurhakim, M. L. I., "Conceptual Design of Blended Wing Body Business Jet Aircraft," Journal of KONES Powertrain and Transport, Vol. 20, No. 4, 2013, pp. 299–306. doi: 10.5604/12314005.1137620.

[30] Budziak, K., "Aerodynamic Analysis with Athena Vortex Lattice (AVL)," , September 2015.

[31] Scholz, D., "13 Drag Prediction," , jan 2026. URL https://www.fzt.haw-hamburg.de/pers/Scholz/HOOU/AircraftDesign_13_Drag.pdf, aircraft Design Lecture Notes.

[32] Jenkinson, L. R., Simpkin, P., and Rhodes, D., Civil Jet Aircraft Design, American Institute of Aeronautics and Astronautics, Reston, VA, 1999.

[33] Chai, P. R., and Wilhite, A. W., "Quantifying the Effects of Model Uncertainty on Design Mass Margin in Advanced Earth-to-Orbit Launch Vehicles," AIAA SPACE 2010 Conference & Exposition, 2010.

[34] Etkin, B., and Reid, L. D., Dynamics of Flight: Stability and Control, 3rd ed., John Wiley & Sons, Inc., New York, 1996. URL https://aerocastle.wordpress.com/wp-content/uploads/2012/04/dynamics_of_flight_by_etkins.pdf.

[35] Nelson, R. C., Flight Stability and Automatic Control, 2nd ed., WCB/McGraw-Hill, Boston, Massachusetts, 1998.

[36] Nguyen, L. T., Ogburn, M. E., Gilbert, W. P., Kibler, K. S., Brown, P. W., and Deal, P. L., "Simulator study of stall/post-stall characteristics of a fighter airplane with relaxed longitudinal static stability," , December 1979. NASA-TP-1538, Report No. 19800005879.

[37] WANG, L., ZHANG, N., LIU, H., and YUE, T., "Stability characteristics and airworthiness requirements of blended wing body aircraft with podded engines," Chinese Journal of Aeronautics, Vol. 35, No. 6, 2022, pp. 77–86. doi: https://doi.org/10.1016/j.cja.2021.09.002, URL https://www.sciencedirect.com/science/article/pii/S1000936121003125.

[38] Cook, M. V., Flight Dynamics Principles: A Linear Systems Approach to Aircraft Stability and Control, 3rd ed., Butterworth-Heinemann, Oxford, UK, 2013.

[39] Vos, R., and van Dommelen, J., "A Conceptual Design and Optimization Method for Blended-Wing-Body Aircraft," 53rd AIAA/ASME/ASCE/AHS/ASC Structures, Structural Dynamics and Materials Conference, American Institute of Aeronautics and Astronautics, 2012. doi: 10.2514/6.2012-1756, URL https://resolver.tudelft.nl/uuid:56dd842b-1e8b-4845-908b-ed1e6c5ae171.

[40] Denieul, Y., Bordeneuve, J., Alazard, D., Toussaint, C., and Taquin, G., "Multicontrol Surface Optimization for Blended Wing–Body Under Handling Quality Constraints," Journal of Aircraft, Vol. 55, No. 2, 2018, pp. 638–651. doi: 10.2514/1.C034268.

[41] in 't Veld, A., "Lateral Stability and Control in Steady Flight," , 2026.

[42] Torenbeek, E., Synthesis of Subsonic Airplane Design, Kluwer Academic Publishers, 1982.

[43] Neubacher, C., "Flight Dynamic Investigations of a Blended Wing Body Aircraft," , October 2008. Examiner: Prof. Dr.-Ing. Dieter Scholz, MSME.

[44] Denieul, Y., "Preliminary Design of Control Surfaces and Laws for Unconventional Aircraft Configurations," Doctoral thesis, Institut Supérieur de l'Aéronautique et de l'Espace (ISAE), Toulouse, France, December 2016. URL https://hal.science/tel-01482103, nNT: 2016ISAE0034, HAL Id: tel-01482103.

[45] Sedhain, B. K., Dhungana, B., Paudel, S., Bhattarai, D., Dhakal, R., Gautam, S., Sedai, A., and Dhakal, R., "Design and Analysis of Blended Wing Body Aircraft for Stability," Proceedings of the International Conference on Mechanical Engineering and Applications, Springer, 2023, pp. 885–891. doi: 10.1007/978-981-99-2342-7_84.

[46] Merino Martínez, R., "Design and Analysis of the Control and Stability of a Blended Wing Body Aircraft," Master's Thesis, Royal Institute of Technology (KTH), Stockholm, Sweden, May 2014. Supervisor: Arthur Rizzi. Joint program with Universidad Politécnica de Madrid.

[47] Mulder, J. A., van Staveren, W. H. J. J., van der Vaart, J. C., de Weerdt, E., de Visser, C. C., in 't Veld, A. C., and Mooij, E., "AE3202 Flight Dynamics Lecture Notes," , March 2013.

[48] Oliviero, F., "AE3211-I Systems Engineering and Aerospace Design: Lecture 9 - Design for Lateral-directional aspects, Design for ground operations, Use of SE for aircraft design," Lecture Slides, March 2024.

[49] Anderson, J. D., Introduction to Flight, 8th ed., McGraw-Hill Education, New York, NY, 2015.

[50] International Civil Aviation Organization (ICAO), Aircraft Operations - Procedures for Air Navigation Services (PANS-OPS), Volume I – Flight Procedures, Montreal, Canada, sixth edition ed., 11 2018. Incorporates all amendments approved prior to 29 August 2018.

[51] Roskam, J., Airplane Flight Dynamics and Automatic Flight Control Systems (Part I), Roskam Aviation and Engineering Corporation, Lawrence, Kansas, 1979.

[52] Humphreys-Jennings, C., Lappas, I., and Sovar, D. M., "Conceptual Design, Flying, and Handling Qualities Assessment of a Blended Wing Body (BWB) Aircraft by Using an Engineering Flight Simulator," Aerospace, Vol. 7, No. 5, 2020. doi: 10.3390/aerospace7050051, URL https://www.mdpi.com/2226-4310/7/5/51.

[53] Abbott, I. H., and von Doenhoff, A. E., Theory of Wing Sections: Including a Summary of Airfoil Data, Dover Publications, New York, 1959.

[54] Wildschek, A., "Flight Dynamics and Control Related Challenges for Design of a Commercial Blended Wing Body Aircraft," AIAA Guidance, Navigation, and Control Conference, American Institute of Aeronautics and Astronautics, National Harbor, Maryland, 2014, p. 0599. doi: 10.2514/6.2014-0599.

[55] Brar, R., "Design of a Blended Wing Body Aircraft," , 2014. Pp. 61, 73.

[56] The Boeing Company, "747-8 Airplane Characteristics for Airport Planning," , August 2023. Content Owner: Boeing Commercial Airplanes.

[57] Martínez-Val, R., Pérez, E., and Palacín, J. F., "Historical evolution of air transport productivity and efficiency," 43rd AIAA Aerospace Sciences Meeting and Exhibit, Reno, NV, 2005.

[58] Deiler, C., and Fezans, N., "Modeling of the A320 Landing Gear Drag During Their Extension and Retraction," AIAA Paper 2025-1250, 2025.

[59] Vos, R., "Airplane Design and Analysis," , 2025. (To be published).

[60] International Civil Aviation Organization, Annex 6 to the Convention on International Civil Aviation: Operation of Aircraft, International Civil Aviation Organization, Montréal, Quebec, Canada, eleventh edition ed., Jul. 2018. International Standards and Recommended Practices.

[61] Erzberger, H., McLean, J. D., and Barman, J. F., "Fixed-Range Optimum Trajectories for Short-Haul Aircraft," , Dec. 1975.

[62] Proesmans, P.-J., "Sustainable Aviation and Future Technologies," , 2025. Lecture slides for 3501-25 Air Transportation.

[63] Bernardo, V., and Fageda, X., "Globalization, long-haul flights and inter-city connections," Economics of Transportation, Vol. 19, 2019, p. 100122. doi: 10.1016/j.ecotra.2019.100122.

[64] International Civil Aviation Organization, Annex 14 to the Convention on International Civil Aviation: Aerodromes, International Civil Aviation Organization, Montréal, Quebec, Canada, eighth edition ed., Jul. 2018. International Standards and Recommended Practices.

[65] Airbus S.A.S., A350 Aircraft Characteristics: Airport and Maintenance Planning, Airbus S.A.S., Blagnac Cedex, France, revision no. 12 ed., 2024. Issue: Nov. 01, 2016; revised Apr. 01, 2024.

[66] Butcher, N. J., Barnett, J. C., and Buckland, T., "Emergency Evacuation of Commercial Passenger Aeroplanes," , Jun. 2020. A specialist paper prepared by the Flight Operations Group of the Royal Aeronautical Society.

[67] Xie, J., Huang, B., Wang, X., Li, P., and Chen, K., "Emergency Evacuation Assessment of Blended-Wing-Body Aircraft Based on Dynamic Risk Model: A Comparative Study," Proceedings of the Institution of Mechanical Engineers, Part G: Journal of Aerospace Engineering, Vol. 240, No. 5, 2026, pp. 772–786. doi: 10.1177/09544100251401056.

[68] Page, M. A., Smetak, E. J., and Yang, S. L., "Single-Aisle Airliner Disruption with a Single-Deck Blended-Wing-Body," 31st Congress of the International Council of the Aeronautical Sciences, ICAS, 2018.

[69] Zhang, Y., Cao, K., Zhou, Q., Cui, B., Li, D., and Zhang, B., "Economic efficiency and airport compatibility analysis of blended wing body civil aircraft configurations," Aerospace Science and Technology, Vol. 168, 2026, p. 111291. doi: 10.1016/j.ast.2025.111291.

[70] Airbus S.A.S., A320 Aircraft Characteristics: Airport and Maintenance Planning, Airbus S.A.S., Blagnac Cedex, France, 2024. Issue: Sep. 30, 1985; Revision No. 44: Jun. 01, 2024.

[71] International Air Transport Association (IATA), "Net Zero 2050: Sustainable Aviation Fuels (SAF) Fact Sheet," , December 2025. URL https://www.iata.org/flynetzero, fly Net Zero Initiative.

[72] Skleznev, A. A., "Overview of Existing Designs for Load-Bearing Fuel Tanks," 19th International Conference "Aviation and Cosmonautics" (AviaSpace-2020): Abstracts, Publishing House "Pero", Moscow, Russia, 2020, pp. 791–792. Conference abstract, Moscow Aviation Institute.

[73] International Air Transport Association, "SAF & Net Zero Updates," Media briefing presentation, IATA Annual General Meeting and World Air Transport Summit, 2026. Presented by Marie Owens Thomsen, Hemant Mistry, and Preeti Jain.

[74] Cathcart, J., Humphrey, J., Kirk, T., Rosas, J., Sadler, J., and Wu, Y., "Fueling Up Sustainable Aviation: A Roadmap for SAF in the Rocky Mountain Region – Colorado, New Mexico, Utah, and Wyoming," , Jun. 2024. URL https://rmi.org/fueling-up-sustainable-aviation/, accessed 20 May 2026.

[75] European Union Aviation Safety Agency, "Easy Access Rules for Master Minimum Equipment List (EAR for CS-MMEL)," , 2024. URL https://www.easa.europa.eu/en/document-library/easy-access-rules/easy-access-rules-master-minimum-equipment-list-ear-cs-mmel.

[76] European Union Aviation Safety Agency, "Easy Access Rules for Air Operations: Regulation (EU) No 965/2012, CS FTL.1.205 Flight Duty Period," , 2026. URL https://www.easa.europa.eu/en/document-library/easy-access-rules/easy-access-rules-air-operations, revision 24, March 2026; Annex III Part-ORO, Subpart FTL; CS FTL.1.205.

[77] European Union Aviation Safety Agency, "Easy Access Rules for Air Operations (Regulation (EU) No 965/2012)," , Mar. 2026. URL https://www.easa.europa.eu/en/document-library/easy-access-rules/online-publications/easy-access-rules-air-operations, revision 24, March 2026; see Annex III Part-ORO, ORO.CC.100 Number and composition of cabin crew.

[78] Shen, A. W., Guo, J. L., and Wang, Z. J., "Analysis of the influence of advanced materials for aerospace products R&D and manufacturing cost," IOP Conference Series: Materials Science and Engineering, Vol. 103, No. 1, 2015, p. 012004. doi: 10.1088/1757-899X/103/1/012004, URL https://doi.org/10.1088/1757-899X/103/1/012004.

[79] Dossow, M., Eyberg, V., Dieterich, V., Bastek, S., Spliethoff, H., and Fendt, S., "Techno-economic assessment of electrification options to produce sustainable aviation fuel via biomass gasification and Fischer–Tropsch synthesis," Energy Conversion and Management, Vol. 345, 2025, p. 120344. doi: 10.1016/j.enconman.2025.120344.

[80] Lammering, T., Franz, K., Risse, K., Hoernschemeyer, R., and Stumpf, E., Aircraft Cost Model for Preliminary Design Synthesis, Institute of Aeronautics and Astronautics, 2012. doi: 10.2514/6.2012-686, URL https://arc.aiaa.org/doi/abs/10.2514/6.2012-686.

[81] United Nations, "Report of the World Commission on Environment and Development: Our Common Future Towards Sustainable Development 2. Part II. Common Challenges Population and Human Resources 4," , 1987.

[82] Lepot, I., Leborgne, M., Schnell, R., Yin, J., Delattre, G., Falissard, F., and Talbotec, J., "Aero-mechanical optimization of a contra-rotating open rotor and assessment of its aerodynamic and acoustic characteristics," Proceedings of the Institution of Mechanical Engineers, Part A: Journal of Power and Energy, Vol. 225, No. 7, 2011, pp. 850–863. doi: 10.1177/0957650911413695, URL https://doi.org/10.1177/0957650911413695.

[83] Airbus, "What is sustainable aviation fuel?" , 2024. URL https://www.airbus.com/en/innovation/energy-transition/our-commitment-to-saf/sustainable-aviation-fuels, cited 17 June 2026.

[84] CarbonClick, "How does SAF reduce emissions? Exploring its benefits," , 2024. URL https://www.carbonclick.com/news-views/how-does-saf-reduce-emissions-exploring-its-benefits, cited 17 June 2026.

[85] Everglades University, "Why Sustainable Aviation Fuel (SAF) is the Future of Aviation," , May 2026. URL https://www.evergladesuniversity.edu/blog/why-sustainable-aviation-fuel-is-critical-for-aviation/, cited 17 June 2026.

[86] TU Delft, "Researchers TU Delft: include non-CO2 climate effects to calculate the real impact of SAF," , August 2025. URL https://www.tudelft.nl/en/2025/lr/researchers-tu-delft-include-non-co2-climate-effects-to-calculate-the-real-impact-of-saf, cited 17 June 2026.

[87] InfluenceMap, "Sustainable Aviation Fuel Investor Briefing," , January 2026. URL https://influencemap.org/briefing/Sustainable-Aviation-Fuel-Investor-Briefing-35413, cited 17 June 2026.

[88] Vasilakou, K., Nimmegeers, P., Billen, P., and Van Passel, S., "Prospective water scarcity footprint under climate change applied to bio-based sustainable aviation fuel production pathways," iScience, Vol. 29, No. 4, 2026, p. 115435. doi: https://doi.org/10.1016/j.isci.2026.115435, URL https://www.sciencedirect.com/science/article/pii/S2589004226008102.

[89] Shahabuddin, M., Alam, M. T., Krishna, B. B., Bhaskar, T., and Perkins, G., "A review on the production of renewable aviation fuels from the gasification of biomass and residual wastes," Bioresource Technology, Vol. 312, 2020, p. 123596. doi: https://doi.org/10.1016/j.biortech.2020.123596, URL https://www.sciencedirect.com/science/article/pii/S0960852420308683.

[90] Maghzian, A., and (John) Saddler, J., "Which processes to making biojet/Sustainable Aviation Fuel (SAF) are likely to supplement the predominant, HEFA/lipid-to-biojet production route?" Bioresource Technology, Vol. 441, 2026, p. 133631. doi: https://doi.org/10.1016/j.biortech.2025.133631, URL https://www.sciencedirect.com/science/article/pii/S0960852425015986.

[91] Sahir, A. H., Zhang, Y., Tan, E. C. D., and Tao, L., "Understanding the role of Fischer–Tropsch reaction kinetics in techno-economic analysis for co-conversion of natural gas and biomass to liquid transportation fuels," Biofuels, Bioproducts and Biorefining, Vol. 13, No. 5, 2019, pp. 1306–1320. doi: https://doi.org/10.1002/bbb.2035, URL https://scijournals.onlinelibrary.wiley.com/doi/abs/10.1002/bbb.2035.

[92] He, S., Dong, K., Hou, M., Song, H., Zhu, T., Li, A., and Jiang, C., "Fueling the future: A comparative analysis of sustainable aviation fuel pathways," Transport Policy, Vol. 174, 2025, p. 103843. doi: https://doi.org/10.1016/j.tranpol.2025.103843, URL https://www.sciencedirect.com/science/article/pii/S0967070X25003865.

[93] Brandt, K., et al., "Hydroprocessed Esters and Fatty Acids Techno-Economic Analysis v2.2," , 2021. doi: 10.7273/000001460.

[94] Lee, U., et al., "Life Cycle Analysis of Gasification and Fischer-Tropsch Conversion of Municipal Solid Waste for Transportation Fuel Production," Journal of Cleaner Production, Vol. 382, 2023, p. 135114. doi: 10.1016/j.jclepro.2022.135114.

[95] IEA Bioenergy, "Municipal Solid Waste and Its Role in Sustainability," , September 2003. URL https://www.ieabioenergy.com/wp-content/uploads/2013/10/40_IEAPositionPaperMSW.pdf, [cited 22 May 2026].

[96] Tumuluru, J. S., "Comparison of Chemical Composition and Energy Property of Torrefied Switchgrass and Corn Stover," Frontiers in Energy Research, Vol. 3, 2015. doi: 10.3389/fenrg.2015.00046.

[97] Krajnc, N., Wood Fuels Handbook, Food and Agriculture Organization of the United Nations, 2015.

[98] Bauer, F., and Hulteberg, C., "Isobutanol from Glycerine – A Techno-Economic Evaluation of a New Biofuel Production Process," Applied Energy, Vol. 122, 2014, pp. 261–268. doi: 10.1016/j.apenergy.2014.02.037.

[99] Geleynse, S., et al., "The Alcohol-to-Jet Conversion Pathway for Drop-In Biofuels: Techno-Economic Evaluation," ChemSusChem, Vol. 11, No. 21, 2018, pp. 3728–3741. doi: 10.1002/cssc.201801690.

[100] Rifada, P. R., Mochamad, A., Haris, S., Muhammad Oktaviano Putra, H., and M. Saddam, A., "Green Polymer Composites for Aerospace Engineering Applications : A Review," Proceeding of International Conference on Artificial Intelligence, Navigation, Engineering, and Aviation Technology (ICANEAT), Vol. 1, 2024, pp. 129–133. doi: 10.61306/icaneat.v1i1.217.

[101] Aziz, N., Wahab, D., Ramli, R., and Azhari, C., "Modelling and optimisation of upgradability in the design of multiple life cycle products: a critical review," Journal of Cleaner Production, Vol. 112, 2016, pp. 282–290. doi: https://doi.org/10.1016/j.jclepro.2015.08.076, URL https://www.sciencedirect.com/science/article/pii/S0959652615011671.

[102] Bachmann, J., Yi, X., Gong, H., et al., "Outlook on ecologically improved composites for aviation interior and secondary structures," CEAS Aeronautical Journal, Vol. 9, 2018, pp. 533–543. doi: 10.1007/s13272-018-0298-z, URL https://doi.org/10.1007/s13272-018-0298-z.

[103] Federal Aviation Administration, "Advisory Circular 21-40: Application Guide for Obtaining a Supplemental Type Certificate," , 1998. URL https://www.faa.gov/documentLibrary/media/Advisory_Circular/AC21-40.pdf, provides the legal framework for certifying modular structural replacements without OEM recertification.

[104] FDC, NDConsult, CSIR, and ECORYS, "EGNOS Aviation CBA for AFI," Presentation at the ESESA Aviation Workshop, Oct. 2010. ESESA is a project co-funded by the EU 7th FP and South Africa.

[105] de Jong, S., Antonissen, K., Hoefnagels, R., Lonza, L., Wang, M., Faaij, A., and Junginger, M., "Life-cycle analysis of greenhouse gas emissions from renewable jet fuel production," Biotechnology for Biofuels, Vol. 10, 2017. doi: 10.1186/s13068-017-0739-7, URL https://doi.org/10.1186/s13068-017-0739-7.

[106] Prussi, M., Lee, U., Wang, M., Malina, R., Valin, H., Taheripour, F., Velarde, C., Staples, M. D., Lonza, L., and Hileman, J. I., "CORSIA: The first internationally adopted approach to calculate life-cycle GHG emissions for aviation fuels," Renewable and Sustainable Energy Reviews, Vol. 150, 2021, p. 111398. doi: 10.1016/j.rser.2021.111398, URL https://doi.org/10.1016/j.rser.2021.111398.

[107] Brusseau, M., "Chapter 32 - Sustainable Development and Other Solutions to Pollution and Global Change," Environmental and Pollution Science (Third Edition), edited by M. L. Brusseau, I. L. Pepper, and C. P. Gerba, Academic Press, 2019, third edition ed., pp. 585–603. doi: https://doi.org/10.1016/B978-0-12-814719-1.00032-X, URL https://www.sciencedirect.com/science/article/pii/B978012814719100032X.

[108] Wu, J., Li, H., and Li, J., "Environmental and economic evaluation of sustainable aviation fuels based on the FT-HEFA route," Journal of Physics: Conference Series, Vol. 3159, 2025, p. 012043. doi: 10.1088/1742-6596/3159/1/012043.

[109] Rahn, A., Dahlmann, K., Linke, F., Kühlen, M., Sprecher, B., Dransfeld, C., and Wende, G., "Quantifying climate impacts of flight operations: A discrete-event life cycle assessment approach," Transportation Research Part D: Transport and Environment, Vol. 141, 2025. doi: 10.1016/j.trd.2025.104646.

[110] Kooduvalli, K., Unser, J., Ozcan, S., and Vaidya, U. K., "Embodied energy in pyrolysis and solvolysis approaches to recycling for carbon fiber-epoxy reinforced composite waste streams," Recycling, Vol. 7, No. 1, 2022, p. 6. doi: 10.3390/recycling7010006.

[111] Semitekolos, D., Terzopoulou, S., Zecchi, S., Marinis, D., Farsari, E., Amanatides, E., Sajdak, M., Sobek, S., Smok, W., Tański, T., Werle, S., Tagliaferro, A., and Charitidis, C., "Performance restoration of chemically recycled carbon fibres through surface modification with sizing," Polymers, Vol. 17, No. 1, 2024, p. 33. doi: 10.3390/polym17010033.

[112] Butenegro, J. A., Bahrami, M., Martínez, M. Á., and Abenojar, J., "Reuse of carbon fibers and a mechanically recycled CFRP as rod-like fillers for new composites: Optimization and process development," Processes, Vol. 11, No. 2, 2023, p. 366. doi: 10.3390/pr11020366.

[113] Scaffaro, R., Di Bartolo, A., and Dintcheva, N. T., "Matrix and filler recycling of carbon and glass fiber-reinforced polymer composites: A review," Polymers, Vol. 13, No. 21, 2021, p. 3817. doi: 10.3390/polym13213817.

[114] RAMS-group at Department of Production and Quality Engineering, "System safety Reliability, Availability, Maintainability, Safety-the RAMS-group at Department of Production and Quality Engineering," , 2025.